NASA Technical Memorandum 4073

Near-Field Testing of the 15-Meter Hoop-Column Antenna

Lyle C. Schroeder, Richard R. Adams,
M. C. Bailey, W. Keith Belvin,
David H. Butler, and Thomas G. Campbell
Langley Research Center
Hampton, Virginia

National Aeronautics and
Space Administration
Office of Management
Scientific and Technical
Information Division

1989

Contents

Nomenclature

A,B,C,D	pillow regions
AAFE	Advanced Applications Flight Experiment
ASA-100	film speed
ATS	Advanced Technology Satellite
Autoset	automatic video-scanning monocomparator used in STARS
Az	angle used to define hoop planarity (table 5)
a	x and y coordinate distance to quad-aperture vertex
adj.	adjusted
BFP	best-fit paraboloid
BW	beam width
CDR	critical design review
CRT	cathode-ray tube
$\mathbf{c}$	vector of 96 control cable length changes
$\mathbf{c}_a$	vector of 96 compensating cable adjustments
co or cross	measured radiation polarizations
D	diameter of antenna aperture
$+D$, $-D$	diagonal radiation patterns at 45° from Y-axis (figs. 67 and 68)
DC	direct current
E-, H-planes	planes of EM radiation
EM	electromagnetic
El	elevation
ecc.	eccentricity
FFT	fast-Fourier transform
f	focal length of aperture
$f/45$,$f/32$	photographic stops
freq	frequency
G	gain of antenna
$G0i$	surface control cord (fig. 17(a))
GSI	Geodetics Services, Inc.
H pol, V pol	horizontal and vertical polarization
Harris	Harris Corporation, Melbourne, Florida
$\mathbf{I}$	influence coefficient matrix
illum	illumination
JPL	Jet Propulsion Laboratory
K	coefficient of elasticity
LSA	Large Scale Antenna

LaRC	Langley Research Center
MC	metric camera
MMA	Martin Marietta Corporation, Denver Aerospace Division, Denver, Colorado
meas	measured or measurement
NASA	National Aeronautics and Space Administration
NFTL	Near-Field Test Laboratory
O.D.	outside diameter
Pillows I	set of 960 targets located in the center of each mesh element
Pillows II	dense set of 645 targets in quadrant 4 gores
pol	polarization
pos	position
Quad	quadrant
R	correlation coefficient
RF	radio frequency
Radial	radial boundary between gores (see table 12)
r	radial coordinate (in X-Y plane)
rms	root mean square
rss	root sum square
SLR	single lens reflex
STARS	Simultaneous Triangulation and Resection System
$\mathbf{s}$	vertical displacement of 888 surface targets (vector)
$\mathbf{s}_e$	vertical reflector surface error vector
spec	specifications
Theod	theodolite
Tie Points I	set of 888 primary targets near intersection of radial and circumferential cords
Tie Points II	set of 888 secondary targets within a few inches of Tie Points I
x, y, z	Cartesian coordinate system (see fig. 9)
x_L, y_L	axis of movement of antenna positioner
x_o, y_o, z_o	coordinates of vertex (see fig. 31)
y	coordinates of aperture of EM studies (fig. 56)
β	angle of divergence (fig. 22)
γ	angle of incidence (fig. 22)
ϵ	surface rms roughness, in.
η	aperture efficiency
θ	azimuthal coordinate in X-Y plane
λ	wavelength

σ	standard deviation
ϕ, θ	pointing direction of feeds (table 10)

Subscripts:

i	ideal
m	measured

1. Introduction

The development of large, self-deployable antennas has been a major technology thrust for the NASA Large Space Systems Technology Program for the past two decades. The need for larger aperture antennas evolved from the requirements for increased resolution for remote sensing and greater signal-to-noise ratios for applications such as cellular satellite communications, very long baseline interferometers (VLBI), and space-based radar systems. Examples of some of the deployable antenna concept programs NASA has funded are illustrated in figures 1 through 3 and are described herein.

A reflector concept developed by the Lockheed Missiles and Space Company, Sunnyvale, California, for the Jet Propulsion Laboratory utilizes flexible metallic composite rib elements which unwrap in deployment from a central spool and provide a stable surface from which to mount a mesh reflecting surface (fig. 1(a) and ref. 1). A three-gore section ($\approx 20°$ sector) of a 55-m-diameter model of this wrap rib antenna (fig. 2(a)) was constructed to demonstrate the feasibility of this technique. A 9-m antenna of this design was launched in 1973 on the ATS-6 satellite. A concept of the General Dynamics Corporation, Convair Division, San Diego, California, used a rigid tetrahedral truss base upon which an elaborate design of cord ties shaped a reflector surface (fig. 1(b) and ref. 2). A model of this antenna with a 5-m aperture was constructed (fig. 2(b)), and its surface characteristics and antenna pattern were measured in the Near-Field Test Laboratory at the Martin Marietta Corporation, Denver Aerospace Division (MMA), Denver, Colorado (ref. 3), for NASA. The box truss concept developed by MMA uses modular cubes which deploy from a configuration of parallel rod elements to form the structure upon which a mesh surface is contoured (fig. 1(c) and ref. 4). A model of this box truss antenna with a 5-m ($\approx$15-ft) square reflector constructed for an offset feed is shown in figure 2(c).

The hoop-column antenna, another large-scale antenna concept, which originated in the early 1970's under the Advanced Applications Flight Experiment (AAFE) Program (fig. 3), has been under continuous development by Langley Research Center and the Harris Corporation, Melbourne, Florida. This concept utilizes a deployable structure composed of a hoop around an axial column which is stiffened by cables from the column ends to the hoop. This structure supports and contours an RF reflective mesh surface. Performance analyses of a 100-m-diameter hoop-column antenna system design (fig. 4) for advanced communications applications showed that such a system was feasible and had many structural advantages (ref. 5). In a subsequent contract with Harris, a 50-m-diameter model of four gores (a 30° sector) of this hoop-column antenna system, including the surface mesh, was built to demonstrate the fabrication feasibility and surface configuration control capability. (See fig. 5 and ref. 6.) The 50-m surface verification model was also used to measure pillow shape (ref. 7). The RF performance characteristics of a solid quad-aperture reflector surface in the presence of quartz cables were determined theoretically and experimentally (ref. 8). These activities demonstrated that a hoop-column antenna with a precision reflector surface was technically feasible for advanced microwave utilization; therefore this antenna is the subject of this report.

A 15-m-diameter deployable model of the hoop-column antenna (fig. 6) was built (1983–1985) under the direction of LaRC by Harris. This model used a "build-to dimension" design philosophy, and its development was undertaken to verify the adequacy of the design concept to achieve the dimensional tolerances necessary for acceptable electromagnetic performance for frequencies in the microwave range (ref. 9). A further goal was to test and verify structural and mechanical performance predictions.

The 15-m model of the hoop-column antenna was tested at the NFTL in 1985 to measure its electromagnetic performance at frequencies of 2.225, 2.27, 4.26, 7.73, and 11.6 GHz. The reflector was configured as four separate offset-fed parabolic apertures, and only one aperture was fed during a given test. The detailed measurement results of this test program are given in references 10, 11, and 12. The present report describes these near-field tests, the test plans and rationale, and a summary of results. Preliminary selected results of near-field tests and structural dynamics tests have been previously reported in reference 13.

In support of the near-field EM tests, an assessment was made of deployment activities and measurements of the surface figure and feed locations. Methods were also developed and employed to adjust the reflector surface to conform more closely to the design paraboloid shape.

2. Antenna Description

The 15-m-diameter hoop-column antenna is a scale model of a 100-m point design (ref. 9). The diameter of this scale model was chosen as the largest that could be tested in existing RF ground facilities. This diameter also conveniently fits in the 16-m thermal-vacuum sphere at the Langley Structural Dynamics Research Laboratory.

The primary structural elements of this antenna design are a telescoping column, which deploys from a central hub, and a hoop consisting of 24 articulating segments which fold and nest parallel to the axis of the column around the central hub in the stowed position. Both the hoop and the column are composed primarily of laminated graphite-epoxy material. Figure 7 shows the antenna as it progresses from stowed to deployed configurations. In the stowed configuration, the antenna fits into a package 2.7 m long by 0.9 m in diameter.

Deployment is driven by electric motors on the column and at hinge joints on the hoop. As these motors extend the column and open the hoop, cords emanating from each hoop joint to the upper and lower masts are drawn from spools into position. The lower cords are made of graphite, whereas the upper cords are made of quartz because of the need for low conductivity and RF transparency. The length of the cords in conjunction with the manufacturing precision and thermal stability of the materials of the hoop and column structures provides a stable, reproducible, cable-stiffened structure upon which the mesh reflector and feed are attached.

The reflector surface is a gold-plated molybdenum mesh material which has been shaped and stitched to a network of cord elements. (See fig. 8 and ref. 9 for details.) This reflector surface is attached at the hoop joints and at the lower part of the center hub and is shaped by 24 cord trusses and a network of front cord elements which support and contour the reflective mesh surface. Each cord truss has four rear control cords which can be adjusted in length to allow some surface adjustment capability (figs. 8 and 9). These surface and control cords are made of multifiber, unidirectional graphite material, which has a high stiffness and a low coefficient of thermal expansion to provide a stable foundation for the mesh surface.

The antenna mesh and control cord lengths have been designed so that each quadrant of the antenna surface comprised a portion of a separate offset-fed parabola (quad-aperture) in the "cup-up" attitude in a $1g$ environment, as shown in figure 9. The equation of the design paraboloid of these apertures is

$$z = \frac{a^2}{2f} + \frac{r^2}{4f} - \frac{ar(\sin\theta + \cos\theta)}{2f} \qquad (2.1)$$

where $a = 14.69891$ in., $f = 366.85$ in., and $\theta = 0°$ at the radial boundary between the first and fourth quadrant. The plan view of figure 9 shows the antenna from the top. In this drawing and in equation (2.1), the four design paraboloids have vertices at $x = y = \pm a$, and $z = 0$. The antenna vertical axis is along the Z-axis, with $z = 0$ at the vertex location.

In this report, the quadrants are labeled following the conventional right-hand coordinate system as shown in figure 9. In reference 9, a different convention was used in which the quadrants were labeled in order of increasing hoop numbers. The reader is cautioned to exercise care when comparing results from this report and other reports.

The feeds for this antenna were designed to directly illuminate only one quadrant. The feeds used are shown in figure 10. The feeds were mounted on a mast with a bracket which allowed adjustment of the feeds in three dimensions to the required position over the illuminated quadrant. The feed was also manually adjustable in rotation.

3. Test Program

3.1. Objectives

The major objective of the near-field tests was to assess the RF performance of the 15-m quad-aperture hoop-column antenna at frequencies ranging from approximately 2 to 12 GHz. Secondary objectives included (1) obtaining valid near- and far-field radiation patterns, (2) performance validation of feed designs for this antenna, (3) evaluation of surface characteristics by using optical measurements and best-fit algorithms, (4) verification of optimum location of the antenna feeds for a rough reflector surface, and (5) adjustment of the surface to achieve a more precise reflector shape and resulting antenna patterns.

The plan for assessing the RF performance of the antenna is shown in figure 11. Keys to the performance assessment are the reflector surface conformance data and the near-field antenna pattern measurements. With these data and the analyses discussed in the following sections, it was possible to compare the predicted surface configuration with the actual configuration, to correct gross distortions, and to compare predicted with measured antenna electromagnetic patterns.

3.2. Test Facility and Parameter Rationale

3.2.1. Facility. The selection of a facility to demonstrate the performance of the hoop-column system as an antenna was based on the following rationale. The large antenna aperture with a microwave frequency of operation precluded the use of a far-field range. Additionally, the adverse environmental effects on the fragile antenna mesh ruled out an outdoor facility. Indoor facilities with glass domes or windows would allow small angle scans by

the methods of star tracking, but even for these limited scans, extensive observation periods would be required. Therefore, the best option for testing the electromagnetic performance of this antenna was to use the near-field facility at MMA. This facility provides a large high bay area (fig. 12) with environmental control and is instrumented with precision calibrated positioning table and scanning RF probes. A description of this facility and system errors for this antenna/near-field test is given in reference 10. This facility is capable of measuring near-field antenna patterns over a 78- by 78-foot area at frequencies from 1 to 18 GHz. This test area provides enough space to erect a 15-m-diameter model of the hoop-column antenna and the counterbalance apparatus necessary to deploy an antenna in a $1g$ environment (as opposed to $0g$ in space). Additionally, a 16-m thermal-vacuum facility at LaRC was available for structural dynamics testing.

3.2.2. RF frequencies for testing. The frequency range for testing the antenna was based on electromagnetic performance for the anticipated surface distortion level and the antenna aperture. The rationale is presented in figure 13, where antenna gain for a roughened surface based on Ruze theory (ref. 14) is plotted as a function of the diameter-to-wavelength ratio. Since the antenna was composed of four parabolic apertures, the effective aperture diameter D was about 6 m. In this figure, the line for a smooth (perfect) reflector is given as a limiting case. For frequencies of interest, plots of the gain characteristics for a range of rms surface roughness values are shown.

For the predicted design surface tolerances of 0.069 in., the antenna will depart about 6 dB from ideal starting at a frequency of approximately 12 GHz. However, for actual rms surface roughness levels of 0.150 in. measured at Harris just prior to these tests, the reflector gain was predicted to be near ideal at frequencies below about 4 GHz, to show measurable losses at 6–8 GHz, and to show significant degradation at higher frequencies. It was therefore determined that frequencies of approximately 2, 4, 8, and 12 GHz were appropriate for these tests. Feeds designed for this purpose are discussed in section 8. The LaRC feeds were designed to provide linearly polarized feed radiation to a single aperture. Circularly polarized feeds at 2.225 GHz were provided by JPL for testing but are not discussed herein.

3.2.3. Antenna pattern parameters. The fundamental pattern measurements desired were the main beam of the antenna plus the first few side lobes. (See table 1 for measurement goals.) These properties were measured by taking co- and cross-polarization patterns with the reflector feed location optimized experimentally. (See fig. 9.) The radial gore structure and the surface roughness, as well as reflections from adjacent apertures, were expected to affect the side lobes. An analysis described in reference 10 determined that patterns out to 25° from the peak lobe were desirable.

Additional tests were desired at selected frequencies with the feed moved off the focal point to produce a scanned beam. These tests were designed to demonstrate multiple beam interleaving feasibility. JPL also designed a feed at 2.225 GHz for use in these pattern studies, these tests are reviewed in reference 9 and are not discussed herein.

3.3. Test Program Schedule and Activities

The sequence of activities at the MMA near-field facility is shown in figure 14, and the conditions for each of the tests are given in table 2. The activities began with the deployment of the antenna and initial alignment and dynamics studies. Near the end of this period, May 16, 1985, the first metric camera measurements of the surface (discussed in section 5) were conducted. On May 24, the surface was adjusted to reduce the overall surface roughness. The surface adjustment model and activities are discussed in section 6. After this surface adjustment, shortened near-field phase scans at 7.73 GHz showed that one surface adjustment cord had been inadvertently missed, resulting in an approximately 0.2-in. upward bulge in quad-aperture 4. This assessment was confirmed by the results of metric camera measurements taken May 25. A second adjustment of the missed cord and nine other cords was done on May 31. Immediately after this adjustment, near-field phase scans showed significantly reduced surface distortions; therefore, the tests could begin. The near-field phase assessments of reduced surface distortion were verified by metric camera data but not until after the completion of the first set of 7.73- and 11.6-GHz tests (tests 1–4).

Tests at 2.27 GHz (tests 5–7) were completed on June 20, and tests with the JPL feed (tests 8–11) were completed on July 2. Prior to the initiation of the 4.26-GHz tests, a metric camera surface measurement was performed on July 8 to verify that the surface rms distortion was in reasonable agreement with the preceding measurement. The 4.26-GHz series (tests 12–17) consisted of beam interleaving from opposite quad-apertures but no cross-polarization measurements. The completion of these tests on July 23 finished the initial pattern study of this antenna and feeds.

On July 24, the 7.73-GHz feed was reinstalled, and after one scan identical to test 1 for repeatability (test 18), the surface was readjusted with an adjustment model weighted by feed illumination intensity. A series of 7.73-GHz scans of all apertures (tests 19–24), a metric camera surface measurement on July 30, and co- and cross-polarization scans at 11.6 GHz on quad-aperture 4 (tests 25 and 26) completed the test program on August 4. During the final 2 weeks at the MMA facility, the antenna was restowed on the near-field facility turntable using the counterbalance system, and the complete system taken down and shipped back to LaRC. The following sections discuss aspects of this program in more detail.

4. Deployment and Antenna Stability

David H. Butler

4.1. Antenna Deployment Sequence

Prior to deployment, the 15-m antenna is stowed as shown in figure 7(a) in a package 2.7 m high and 0.9 m in diameter. Deployment is accomplished in three basic steps: column extension, hoop-surface deployment, and system preloading (which tensions and shapes the surface). During column extension (fig. 7(b)), the telescoping sections of the column are deployed sequentially and tensioned by a cable drive system. The tensioning process allows the column cam lock latches to actuate at the completion of column extension. The sequence is passively controlled by the latches.

The next step is deployment of the hoop and surface (figs. 7(c) and (d)). The hoop consists of 24 tubular segments that contain double hinge joints at each end to permit rotation but inhibit torsion. During deployment, the hoop segments simply rotate from vertical to horizontal orientation about an axis in the horizontal plane from the center of the hoop through the center of each hoop segment. Electrical motors drive worm gears that transmit torque at eight equally spaced hoop hinge joints and through four bar mechanisms to adjacent passive joints. The surface is deployed simultaneously with the hoop. Tensioning of the surface is accomplished by extending the column (to which the surface control cords are attached) an additional 0.4 m by means of a screw mechanism called the preload segment (fig. 15). The shaping of the surface is accomplished by the precise fabrication and assembly control of lengths of the 96 control cords attached to the surface chord truss attachment points and the lower column hub (figs. 8 and 9). Set screw adjustment of the control cord length was provided at the attachment points to allow some surface smoothness adjustment. Estimated design tolerances and the resultant expected surface error are given in table 3.

4.2. Deployment Tests and Anomalies

The deployment at the MMA near-field facility proceeded as just described, except for problems in the pedestal alignment, hoop planarity, and theodolite operation. The problems and their corrective actions are described in the following paragraphs and are shown in figures 16 through 19.

4.2.1. Pedestal alignment. During installation of the antenna on the MMA near-field test table, it was determined that holes in the antenna attachment pads did not align with the tapped holes in the pedestal legs. The attachment pads (fig. 16(a)) were also not in alignment radially and the mounting surfaces were not in a level plane. It was thought that the pedestal needed to be level to ensure vertical alignment of the column and alignment of the hoop in a horizontal plane when the antenna is subsequently deployed. It was clear that the misalignment problem occurred in the antenna attachment portion of the pedestal because the pedestal legs had been previously aligned and leveled with a precision tooling plate. This problem delayed the test schedule almost 1 week while a solution was developed and implemented.

To correct this problem the antenna was suspended over the pedestal legs, and threaded rod studs 6 in. long were inserted through the attachment pads into the tapped holes in the pedestal legs. The jacking screws at the pedestal bases were used to align the holes in the legs to the holes in the attachment pads (fig. 16(b)). The studs were repeatedly turned back and forth to assure that binding did not occur. The stowed antenna (fig. 16(b)) was lowered until one pad came in contact with a pedestal leg. Since contact between the attachment pads and the pedestal legs was at a single point, the attachment arms could have rotated about two axes and inflicted severe damage to the antenna column longerons if the fasteners had been tightened. Therefore, prior to tightening, shims (fig. 16(b)) were fabricated and inserted around each of the fasteners.

4.2.2. Column deployment and verticality. Deployment of the column and hoop was completed and the preload section partially extended until low-level tensions were observed in the hoop and surface control cords. The vertical alignment of the column was then determined to be considerably out of the maximum allowable tolerance of 0.1 in. Vertical

alignment preceded hoop levelness in order to provide the maximum buckling factor of safety. The procedure used to align the column was to suspend the deployed (but not preloaded) antenna over the pedestal and to repeat the procedure described in section 4.2.1. Suspension of the antenna was accomplished (fig. 7(d)) by adding approximately 60 lb to the upper cable stowage system counterweight and removing the antenna-pedestal interface bolts. The counterbalance weights for the hoop and lower cable stowage system were not changed. Overbalancing of the upper cable stowage system provided a suspension point above the center of gravity of the antenna and aligned the column vertically. The pedestal legs were then aligned, shimmed, and secured as noted in section 4.2.1.

After completing this procedure the column vertical misalignment was observed (using transits) to be about 0.5 in. between the upper and lower cable stowage trays (point A to point B in fig. 17(a)). Final alignment was performed with a two-theodolite system after the antenna was fully deployed and disconnected from the counterbalance system. The procedure for final alignment was to loosen the pedestal-leg turntable bolts and use the jacking screws to align the antenna. This procedure resulted in a 0.269-in. overall misalignment (0.144 in. between points A and B of fig. 17(a) and an additional 0.125-in. misalignment of the feed mast, points B and C). The resulting column angular misalignment off of the vertical axis is approximately 0.03°. These measurements were later verified with metric camera data which showed the misalignment to be 0.019° to 0.036°. For this angular misalignment, an acceptable buckling factor of safety of 4 was computed for the deployed antenna with a feed system weight of 250 lb assumed (the maximum weight for the feed system, including the feed mast during MMA testing, was 220.8 lb).

4.2.3. Hoop planarity. The hoop was not expected to be within planarity tolerances when deployed at MMA because four additional hoop drive motors had been installed at Harris without a precision adjustment of the limit switches. A precision adjustment of the additional limit switches required disassembly of the antenna, but schedule and resource considerations required that this activity be delayed until the antenna was deployed at the MMA near-field facility.

The procedure for aligning the hoop nodes in a plane involved extending the preload segment in small increments, after which the lower hoop support and the outer surface control cord (G04 in fig. 17(a)) tensions were measured to assure that overstressing of the cords did not occur. The motorized hoop joints were individually driven in a direction to adjust the G04 cord tension toward the average measured value without exceeding maximum allowable cord load limits. This iterative procedure was repeated until the preload section was fully extended. A history of the cord tensions is included in table 4.

The hoop planarity was determined after preload extension and counterbalance removal. Digital theodolite readings were taken at each of the hoop joints. A computer was used to calculate a best-fit plane through the hoop joint coordinates measured by theodolites and to determine the vertical deviation of each joint from this plane. Transformation of some of the hoop joint coordinates was necessary because the hoop joint targets are not all located at the hoop centerline (fig. 18). The transformed measurements (table 5) indicated a standard deviation of all hoop joints of 0.069 in. rms or less relative to a plane (compared with a worst-case tolerance for successful deployment of 0.100 in.). This result was better than previous attempts to align all 24 hoop hinge brackets within a plane (0.081 to 0.083 in., ref. 9).

4.2.4. Proof testing. The antenna with the feed system was not proof-tested until installation in the MMA facility because the Harris radome facility was not high enough to accommodate the feed system. The antenna column upper and lower sections had been individually proof-tested, and NASTRAN® results indicated that the buckling factor of safety of the antenna-feed system was in excess of four. The proof test consisted of placing a weight at the top of the feed mast (fig. 19). The weights were U-shaped so that they could be installed around the safety cable. Also, the weights were composed of 1/8-in-thick layers weighing about 20 lb so that they could be handled by one person. Tethers were attached to the weights until they were secured. The entire proof weight was 283 lb (including the feed mast), and the antenna gave no indications of buckling when the weights were installed. The heaviest feed configuration tested was 220 lb, including the feed mast.

4.2.5. Dynamic response testing. RF pattern measurements in a near-field facility require quick lateral translations of the antenna in small increments of approximately 1/2 wavelength of the test frequency (ref. 8). This movement could cause vibration of the feed system and surface reflector that would have a negative effect on the measured patterns and, in an extreme case, possibly cause buckling. A lateral acceleration upper limit of $0.006g$ was calculated and imposed on the antenna for safety reasons. A test was conducted at MMA in which the antenna was translated in small increments beginning with very slow but increasing rates. The

accelerations measured are given in appendix A of reference 11.

The proof test configuration was used to measure dynamic system response. Dynamic loading at the feed location was measured as a function of the input loads obtained by translating the table supporting the antenna. The table was excited in two modes for the dynamic testing: (1) movement in the same direction and (2) movement in the reverse direction. The table movement increments ranged from 0.1 to 2.6 in. for input acceleration levels from $0.0005 \times 10^{-3}g$ to $5.5 \times 10^{-3}g$ and feed deflections up to 0.03 in. The deflections were estimated by two observers viewing, through theodolites, a scale (graduated at 0.1-in. increments) that was attached to the proof test weight. (See fig. 19.) The accelerations measured at the feed location were always attenuated relative to measurements of accelerations at the input (base) and the vibratory deflections were considered negligible. The oscillations at the feed location quickly damped to an undetectable level when measured with the accelerometers.

4.2.6. Hysteresis testing. The hysteresis test was conducted to establish that the antenna could be preloaded without the counterbalance system being in place. It was believed that the hysteresis test was necessary because the system had always been preloaded while under the effects of the counterbalance system simulated $0g$ environment. The specific concern was that the hoop could "settle" with the repeated preload cycles necessary to adjust the surface and the settling would change the surface contour. The proof test configuration was also used for the hysteresis test. The test consisted of measuring the hoop elevation at hoop joints 3, 11, and 19 before the test, after removing and reapplying the preload, and after measuring the cord tensions on the antenna. The preload section was cycled three times with measurements at each cycle. Test results are recorded in table 5. These variations are within the system design tolerances, and it was concluded that the surface contour would not be adversely affected if the surface was adjusted in the uncounterbalanced state.

The final installation task was to align the antenna aperture with the facility probe system. Points A and B in figure 17(b) were located by suspending a plumb bob from the center of two RF probes located in the ceiling of the near-field antenna chamber. A transit was placed at point C and aligned along a line extending between points A and B.

The next step was to rotate the antenna into alignment with line CB. Hoop joints 10 and 22 were selected for alignment because they would establish a relationship between the center of the test quadrant (4, fig. 20) and the facility probe system. Alignment was accomplished by sighting across the G04 cord plane for hoop joints 10 and 22. The antenna is translated from the assembly area toward the test area until the edge of the joint 10 G04 cord was aligned with the vertical cross hair on the transit. The antenna was then rotated until it "appeared" that the G04 cord at hoop joint 22 was in alignment with joint 10. The word "appeared" was used because the translation and rotation procedures had to be repeated many times because the rotation also caused the G04 cord on joint 10 to move. Translation into the field of view of the transit was always toward the test area to negate any system backlash. The translation-rotation movements were repeated until no further rotational adjustment was required.

The reason for aligning by this method was to also negate the difference between the antenna centerline and the table center of rotation. Antenna-table vertical axis alignment was not required; consequently, a low priority was assigned during the installation process.

4.3. Deployment Summary

The process described was used successfully to install the antenna in the Near-Field Test Laboratory. Two improvements that would reduce the installation time and improve antenna safety would be the addition of 3-axis rotation pedestal arm adjustments and 2-axis translation adjustments at the pedestal-table interface.

5. Metric Camera Measurements

Richard R. Adams

Convergent close range photogrammetry (ref. 15) was used to precisely characterize the surface of the 15-m hoop-column antenna, its structure, and its orientation at RF testing at the MMA NFTL. The data were obtained by taking full-coverage metric camera photographs of the antenna from eight vantage points 21 ft above the hoop at 45° increments about the center of the antenna.

Three-dimensional coordinates of some 3381 retroreflective tape targets distributed over the reflector surface were obtained to an rms accuracy of about 0.007 in. by using STARS hardware and software. Additional targets on the hoop, upper and lower columns, feeds, and floor were measured for scaling and orientation purposes. Subsequent transformation of measured data to design coordinates provided an independent basis for predicting the potential RF behavior of the model and served as input

for shape-control analysis; this allowed adjustment of the reflector shape. Fully automatic precision film reading for a 3-day data turnaround significantly enhanced RF testing productivity.

5.1. Computer Simulations

Simulation studies were used to predict the potential accuracy attainable for the photogrammetric measurement. The scenario which yielded optimum measurement accuracy utilized eight full-coverage camera stations located 21 ft directly above and symmetrically distributed around the antenna hoop. For this case, with the camera configuration used and a monocomparator rms film reading accuracy of 3 μm assumed, the measurement accuracies for all targets are given in table 6. The predicted measurement accuracies for the primary surface targets satisfy a goal of 0.007 in. accuracy (10 times better than the predicted manufacturing tolerances for the antenna surface).

The effects of target size and configuration; illumination intensity, angle, and distribution; image foreshortening; and film processing variables, which were not considered by the simulator, were determined by independent computations and verified by laboratory testing prior to target fabrication and field measurements. The simulator also does not predict the effect on resulting data of object nonrigidity during the photographic session, which is shown later to be within the estimated measurement accuracy for all but the outer portion of the reflector, but is still within the 0.007-in. rms measurement accuracy required for the complete surface.

5.2. Photogrammetry Targets

For the 15-m hoop-column antenna, the density of surface targets was chosen such that targets were placed near all surface cord tie points and at the center of all pillows. This resulted in the placement of 3381 targets on the upper surface. An identical set of targets was placed on the reverse side of the mesh, opposite these targets, to allow the option of metric camera or theodolite measurement from the floor.

Figure 20 shows a schematic of the 15-m antenna (plan view), as viewed from the top. In this figure, each of the 24 gores (indicated with the letter G) and the hoop joints are numbered. The primary test aperture of the antenna (quad 4) contained three gores (shown hatched) which were more heavily targeted to allow the study of finer detail pillowing shape for each gore type.

For convenience, surface targets were divided into four groups:

(1) Tie Points I: a set of 37 targets per gore (888 targets total) near the intersection of radial and circumferential surface cords; this set was the primary set of targets used in the finite element surface analysis (see fig. 21(a))

(2) Tie Points II: a set of 888 targets within a few inches of respective Tie Points I targets, which were nearly redundant and not used in early analyses (see fig. 21(b))

(3) Pillows I: the 960 targets located in the center of each mesh element bounded by surface cords; these were used in the surface analyses with pillows (see fig. 21(c))

(4) Pillows II: a dense set of 645 targets in sections of three quad 4 gores (see fig. 21(d))

With the exception of Pillows II targets, each of the 24 gores from which the surface was assembled was identically targeted during manufacturing by using precision target placement jigs. The design x and y coordinates of the targets from these templates were used to compute the corresponding z coordinate from the equations for an ideal quad-aperture parabolic surface given in section 2. No design coordinates are available for Pillows II targets, since they were installed by hand.

The targets used on the antenna reflector were fabricated of retroreflective tape (3M Scotchlite brand high gain 7610 sheeting) to produce nearly constant image luminances over a wide range of incidence angles. (See fig. 22.) The targets for all applications except Pillows II were fabricated by using a $^{13}/_{16}$-in. hollow punch. A rub-on, flat black doughnut mask was then applied to each retroreflective tape disk, leaving a $^{3}/_{16}$-in-diameter circle in the center and a thin ring around the edge of the retroreflective tape. A 0.03-in. central black dot was also applied to allow theodolite measurements if required. Pillows II targets were 0.25-in-diameter retroreflective tape circles without the outer reflecting ring to allow distinction from other targets. Figure 23 summarizes fabrication details and the results of measurements made on the concentricity of center dots of a number of randomly selected targets after fabrication. The outer reflecting ring proved extremely useful in analysis for computer rejection of false targets caused by contamination on the film.

Targets and labels were also placed on the antenna structure, on each of the 24 hoop segments, about the upper column hub, the central hub, and the lower column hub (24-target circles). Retroreflective tape index arrows were placed at quadrant intervals on each of these target circles for identification aides.

Targets were placed in the near-field facility to provide reference points:

(1) At eight locations around the circumference of the rotating table

(2) On the floor on a 20-ft radius below the model

(3) At both ends of each of 12 steel scaling bars distributed uniformly on the floor beneath the model

(4) At two floor reference targets located by plumb line beneath each end of the RF ceiling probe track

All targets located on the floor of the facility were marked with large retroreflective tape numbers for easy identification on the camera negatives.

5.3. Metric Camera

5.3.1. Camera. The camera used to perform the photography (fig. 24) was a CRC-1 Metric Camera designed and built by Geodetic Services, Inc., for close range photogrammetry. This is a large format, microprocessor-controlled roll film camera. The removable film magazine can accommodate a 125-ft roll of 9.5-in. film (140-frame capability), and incorporates a unique projected Reseau ultra-flat vacuum platen. The camera was fitted with a calibrated micrometer focusing drum and a lens with 120 mm focal length to allow single frame coverage of the entire 15-m model from each camera station. The camera is powered by an independent 12 V DC gel cell rechargeable battery pack.

Scene illumination was provided by a strobe lamphead with a 5-in. dimpled reflector and a 1-in. lamp extender. The strobe was powered by a rechargeable battery pack set to operate at 200 W-sec. The lamphead was mounted directly to the metric camera and was located 10 in. from (and aligned with) the lens axis.

The camera was mounted on a heavy duty tripod. The front-facing leg was disconnected from the tripod column in order to allow placement of the pan-tilt tripod head directly above a corner of the safety railing of a lift platform. Heavy duty cable ties were used to secure the tripod legs to the lift platform railing and the tripod feet were bolted to the flooring of the platform for added safety and rigidity.

Kodak Technical Pan Film 2415 was selected for use in the metric camera. This is an extremely fine-grain, high-resolution film capable of being processed in accordance with user requirements.

5.3.2. Photographic procedure. For photogrammetric measurements, the optical axis of the camera lens was depressed about 50° from the horizontal at each camera station. Precise pointing was accomplished by use of a matched and boresighted 35-mm SLR viewfinder camera attached to the body of the metric camera. From simulator views, the ideal camera pointing was obtained when the lower column hub was at the frame center. Thus, frame centering was a simple matter if the camera was at the prescribed height and directly above the hoop. The lift was driven (fully extended, with camera remaining 42 ft above the floor) to each of eight stations around the antenna until all photographs were taken. A typical position is illustrated in figure 25. Since both metric camera and strobe were powered by battery packs, there was no requirement for extension cords to the camera platform.

Three photographs were taken of the antenna at each camera station:

(a) Shutter speed at 1/125 sec, 200 W-sec strobe, exposure at $f/45$

(b) Shutter speed at 1/125 sec, 200 W-sec strobe, exposure at $f/32$

(c) Shutter speed at bulb exposed for 10 sec, 200 W-sec strobe, exposure at $f/32$

A 90° roll of the magazine about the camera axis was made at each camera station to allow for complete STARS self-calibration of the camera lens.

5.3.3. Film developing. Film handling and processing were accomplished in total darkness by using a standardized film process developed by GSI for this purpose. A processing speed of about ASA-100 was attained by processing for 8 min at 68°F in Kodak HC-110 (Dil D) developer in a rewind processor. The film was then fixed for an additional 3 min. Washing time was 30 min in running water. The film was then hung by film clips to air-dry.

After drying, the film was cut into individual frames and each frame annotated as to station number and exposure conditions. This annotation supplemented the date/time and frame number data already exposed on the edge of each frame by the CRC-1 camera.

Typical metric camera photographs which illustrate the complexity of target identification are shown in figure 26, an example of a 10-sec time exposure view of the antenna to bring out the background, and figure 27, an example of a 1/125-sec exposure with the background suppressed as was used for actual mensuration.

5.4. Data Analysis

Photographs were measured with an automatic video-scanning monocomparator (STARS Autoset-1) to reduce the chance for target misidentification and the amount of time required. Autoset-1 has a resolution of 0.1 μm and an x-y accuracy setting of under 0.5 μm, about five times the accuracy attainable

manually. Furthermore, film reading is 6 to 20 times faster than could be accomplished manually.

The processing of film data is described in the flow diagram of figure 28. After mensuration of photographs from all eight stations of measurement was completed, standard STARS software was used to preprocess each image file to correct the image data for small systematic errors introduced by the monocomparator and film deformation. After preprocessing, the files were merged and a preliminary resection was run using approximate coordinates of selected well-distributed targets on the surface to update estimates of location and orientation for each camera station.

A preliminary triangulation computes the coordinates of each target measured. At this time, three circumferentially distributed targets were chosen to establish an arbitrary coordinate system for the subsequent reduction.

The bundle adjustment simultaneously triangulates the coordinates of the targets, resects the locations and orientations of the camera stations, and solves for the camera interior elements of orientation (self-calibration) in a least-squares iterative fashion. Iteration was automatically continued until convergence was attained; that is, until the difference in the rms of the triangulation residuals from two successive iterations was less than a preset value (0.1 μm).

At this point, the camera parameters, station parameters, and x, y, z coordinates of all targets and their corresponding accuracies have been generated in a coordinate system uniquely defined by the three selected control coordinates. Since the coordinates of these three points were estimates only, a rigid-body coordinate transformation was performed that consisted of three translations, three rotations, and a scale change to overlay (in a least-squares sense) a specific group of measured targets with their corresponding design locations. All transformations used Tie Points I targets only for the entire reflector surface. These transformations allowed the photogrammetry results to be specified in a system matching the antenna design coordinate system in a least-squares sense. The rigid-body transformation also provides differences for each surface target from their respective design coordinates. The differences in the z-direction were used as an indication of the roughness of the 15-m surface.

5.5. First Measurement at Harris

Prior to use with data from MMA, the Autoset-1 monocomparator, operated in the semiautomatic mode, was used to analyze a metric camera photograph set taken on March 27, 1985, at Harris. For this measurement, all targets were measured in both the semiautomatic mode and the automatic mode. This added step allowed the operator to correct target identification blunders and compensate for thermal drift experienced during slower semiautomatic operation. Each iteration of the bundle adjustment for the first measurement required the solution of over 10 000 equations for more than 3100 unknowns, and convergence was attained after three iterations. The entire process took about 4 hr per 1000-target photograph, about six times faster than could be accomplished manually, assuming proper target identification.

For this particular reduction, the added step of independent scaling was applied to the results. A final iteration of the bundle adjustment was performed with the distances between target pairs on each of 12 floor scaling bars. This test demonstrated that scaling performed during the rigid-body transformation provided nearly identical results as obtained with independent scaling. Experience has shown that independent scaling using floor bar targets may compromise the consistency of the measurement data due to the random nature of obscurations by veiling and the hoop and surface control cords. Hence, independent scaling was eliminated in subsequent measurements.

5.6. Measurements at MMA

There were five sets of metric camera photographs taken of the 15-m antenna while deployed in the Near-Field Test Laboratory.

5.6.1. First set. The measurement for the first set was made on May 16, 1985, to determine if the surface configuration was repeatable with the earlier deployment and if the surface quality was adequate for RF testing. Since no attempt was made to adjust the surface, any changes in its shape since last measured at Harris could be attributed to stowage, packaging, shipment, and redeployment. The counterbalance system was still in place but was not used to support the antenna except that the hoop was tethered between two towers to aid in reducing distortion of the surface due to rotation of the hoop (torsional mode) during the photographic session. Hoop tethering was not used for subsequent measurements with the exception of outriggers added to the rotation table to aid in torsional stabilization during testing.

The processed film was taken to GSI for mensuration using Autoset-1. Since the coordinates for all Tie Points I targets were known from the first measurements at Harris, the Autoset monocomparator

could be used in the automatic resection driveback mode to reduce the time required to complete each frame to just over an hour.

5.6.2. Second set. After the first measurement, while the hoop-counterbalance system was being removed, the surface data were analyzed and used to compute control cord adjustment lengths required to reduce the vertical deviations of the surface from the design paraboloid, using the analysis described in section 7. The second set of measurements was made on May 25, 1985, after 85 surface control cords had been adjusted in an effort to decrease the surface rms deviation relative to the design paraboloid. This time Pillows I targets were also included in the measurement, and all targets from both surface target groups were measured in a single pass for each photograph with the autoset resection driveback technique.

When these data were reviewed (see section 7), it was found that one surface control cord (radial 21, G03) was either missed or misadjusted so that a local high spot remained in a critical area of quadrant 4. As a result, this cord and nine others were identified by analysis to be 0.040 in. or greater out of tolerance and were readjusted.

5.6.3. Third set. The measurement for the third set was made on June 14, 1985, following the 10-cord adjustment. The data were analyzed in the same manner as for the second measurement. These data showed that the vertical deviation of the surface from the design paraboloid is close to the predicted 0.070-in. tolerance for quadrant 4 and, thus, was suitable for RF testing to begin.

5.6.4. Fourth set. The fourth set of measurements was made July 8, 1985, just after tests using the JPL feed and just prior to tests using the LaRC 4.26-GHz feed. Since no adjustment of the surface had been made since the last metric camera measurement and the antenna had experienced considerable dynamic excitation due to RF test scanning, this measurement was intended to provide data about the stability of the antenna surface during the RF test program.

5.6.5. Fifth set. The fifth set of measurements was made July 30, 1985, after the surface was adjusted a final time. The adjustments were calculated with the shape-control analysis as before, but this time the importance of each target was weighted in proportion to its feed illumination intensity. Near-in side lobes at 7.73 GHz were predicted to decrease significantly as a result of this adjustment.

5.7. Effect of Antenna Torsional Motion

Since the metric camera measurements were based on photographs of the surface from eight different stations, several hours elapsed between the first and final photographic measurements. During this time, the antenna was known to experience small but visible torsional movements, probably caused by air currents interacting with the large mesh surface, exciting the torsional vibration mode of the antenna system (0.077-Hz natural frequency, ref. 13).

The air conditioner was turned off during metric camera tests to minimize effects of this motion on the surface figure measurements. However, during the antenna pattern measurements (periods of several hours each) the air conditioner was left on because it was felt that the facility temperature instability would cause greater error. Antenna motion during antenna pattern tests was not visibly greater but was not measured.

To examine this effect on the accuracy of metric camera results, the rms of metric camera triangulation residuals was calculated as a function of radial distance of the target used in the data base for metric camera mensuration. The results, given in figure 29, show that errors are less than one half the average rms for all targets out to a radius of about 170 in. If the radius of the targets used is increased to 240 in., the residuals exceed the average. These results confirm that small rotation errors are affecting the accuracy of the outer targets; however, errors for the entire surface are still below the 7-mil rms estimated accuracy. Further, if much higher accuracy surface information is required for the 15-m antenna studies, the data base should be restricted by radius as defined in figure 29.

6. Analyses of Reflector Surface and Feed Location Measurements

Lyle C. Schroeder

6.1. Reflector Surface Analysis

The result of a metric camera measurement is a set of coordinates for each of the targets in a coordinate system matching the design coordinate system of the antenna in a least-squares sense. To evaluate the quality of the reflector surface, these data were processed to determine a best-fit paraboloid (BFP) for each aperture of the antenna. BFP methods are described in reference 16 and more recently in an unpublished report for NASA contract NAS3-23249 done by Harris for Lewis Research Center. The BFP computer program used to fit these data differed somewhat as described in the following paragraphs.

In testing the BFP program of reference 16, it was discovered that very small changes in the input data (corresponding to deviations from a perfect paraboloid) resulted in failure of the best-fit process. It was therefore decided to implement a two-step BFP process. First, the residuals in the direction of the paraboloid axis (z residuals) were minimized in a least-mean-squares best-fit of four degrees of freedom: translation in three dimensions of the vertex location and the paraboloid focal length. Second, to allow for rotation about the X- and Y-axes, an iterative solution was developed. With the Langley FORTRAN math library routine SDFP, iterative minimizations of the X- and Y-axis rotation angles were performed. A subroutine was created which accepts the two rotation angles as parameters, performs the coordinate transformations of the paraboloid surface data, and invokes the four-degree-of-freedom algorithm described in the first step. This subroutine returns the mean-squares error of the surface z residuals to SDFP, which attempts to find the rotation angles which minimize this error.

The z residuals were used rather than the residuals normal to the paraboloid surface in this minimization process to reduce complexity in the algorithm. Further, the long focal length-to-diameter ratio of the 15-m antenna results in very little difference in the normal and z residuals, and this approach produced results in reasonable agreement with rotation-constrained results from reference 16. With no rotation constraints, this two-step approach proved to be much more stable than the program of reference 16, but both programs showed rather large rotation angles. Large rotation angles are believed to result since the surface of a paraboloid of long focal length is nearly spherical (which is insensitive to rotation), such that the "error surface" being minimized as a function of rotation angle is relatively flat.

The analysis of the surface measurements used the BFP computer program which constrained rotation of the paraboloid axis. In addition to reasons stated above, this constraint was used because it is consistent with the experimental feed focusing procedure described later. The reflector surface deviation in the z direction was used to characterize the antenna roughness, because the z variations are much greater than those of the corresponding x and y coordinates and have a first-order effect on the analyses of sections 7 and 8, whereas the x and y coordinates were assumed negligible or of lower order importance. The z coordinate reflector surface deviation was evaluated by using the x and y coordinates and equation (2.1) at each target point in two different ways: (1) relative to the BFP and (2) relative to the design surface.

Figure 30 shows a plot of reflector surface deviation relative to the BFP. In this plot, the ideal paraboloidal surface is represented by the XY-plane in the aperture quadrant and shows a peak for each target location whose height is the relative magnitude of this difference. This plot was used as an aid to display the surface quality.

The BFP computer program also calculates vertex offset location and focal length of the BFP. Table 7 is a summary of the BFP analyses of metric camera measurements made at Harris and MMA. This table gives for each aperture the derived BFP focal length, vertex offset, and the reflector surface deviation (rms). Results are given for the complete antenna surface and for the effective surface, which excludes the outer portion of the antenna. (See section 7.) It can be seen that deviations from ideal values for the effective surface are much less than for the complete antenna surface, except those for offset values, which are of the same order. Since the feed illumination is about 15 dB less at the outer reflector portion, the effective surface rms was expected to better represent antenna performance. From table 7 and figure 31, it can be seen that after the second surface adjustment (the June 14 metric camera measurement), the reflector surface rms deviation and the focal length deviations from ideal in all four apertures have been significantly lowered. Subsequent surface rms deviations for all four apertures were quite consistent. The metric camera measurement of July 8 shows that the surface rms deviation did not significantly change when no surface adjustments were made; this valuable information shows that the surface maintains its shape during the test program. Also, the final metric camera measurement (just after the third surface adjustment) shows a small increase in focal length and vertex offset deviations and a very small decrease in the surface rms deviation; however, section 8 shows significant improvements in the antenna EM performance.

For completeness, table 8 gives the complete set of reflector surface deviation data for all Tie Points I targets of quadrant 4 aperture; these data start with the first metric camera measurement of the surface at Harris and include data from all subsequent measurements at MMA. The left-hand side of this table gives the z coordinate from the BFP analysis, and the right-hand side gives the difference between the measured and the BFP values of z. The data of table 8 are organized into regions of the gore that have similar pillow structures, as defined in the sketch. Statistics are provided for each pillow type, for the complete reflector surface, and for the effective antenna surface. These statistics are summarized in table 9. The table gives the mean and rms

deviation of the z coordinate relative to BFP for each of these pillow regions. These data show that the rms deviation increases as the radial distance of the pillow increases. The type D pillow has the largest rms deviation, possibly because the control cords do not directly attach to any boundary of this pillow. These analyses are discussed further and used extensively in the analyses of sections 7 and 8.

6.2. Feed Location Measurements

Prior to RF testing of the 15-m antenna, a method for predicting where to place the feed for a reflector with small distortions was necessary. In our initial approach to this problem, computer-generated random errors were added to z coordinates at selected points of a perfect design paraboloid. Then, unconstrained best-fit paraboloids were fit to the perturbed data sets to determine the resulting changes to the paraboloid parameters. Although the resulting surface roughness statistics were reasonable, the results shown in figure 32 predict that the actual lateral location of the focal point is significantly influenced by the way the errors are distributed on the surfaces. The vertex also varied laterally in phase with the predicted focal point location. Experiments and analyses described herein showed that this focal point prediction method using BFP does not accurately predict the optimum feed location for best RF performance and that a better method is necessary and is under study. However, in part because of this predicted focal point sensitivity, the feed location was experimentally optimized and carefully measured during these tests.

The antenna feeds were mounted to a bracket (fig. 33) with motor-driven translators in three axes so that the feed could be positioned anywhere within the travel of the translators (± 3 in. along the feed boresight axis by ± 4 in. in the other two axes). Figure 34 shows the orientation of the feed positioner on the antenna. This positioner and a manual rotation adjustment were used to move the feed as close as possible to the optimum location for each test setup.

At first, feed location measurements were made with a three-theodolite setup, with digital data outputs input to triangulation software (fig. 35). After standard theodolite calibration and setup, optical targets located on the feed systems (fig. 36) along with sufficient antenna surface targets were then measured and transformed to the antenna coordinate system by using the STARS rigid-body transformation software (ref. 15). The results of these feed measurements for the initial RF test setup (7.73 GHz, tests 1 and 2) and the corresponding offset feed location (test 3) are given in table 10. Comparison with the coordinates of the focal point of an ideal design shows lateral offsets from 0.13 to 0.31 in. and a vertical (z) offset of 0.17 in. for tests with the feed directly at the focal point (tests 1 and 2) and of 0.22 to 0.34 in. lateral and 0.34 in. axial for the first scanned feed case (test 3). The actual feed positions were set using the near-field RF test scans (discussed later), not preplanned design locations; hence, these measurements show that the reflector feed point is close to the design for an ideal paraboloid.

The results for the 4-GHz feed setup of tests 5, 6, and 7 are also given in table 10. These results again confirm that the focal point obtained by the near-field RF scan is in fair agreement with that expected for an ideal reflector, although the lateral offset errors are somewhat greater for quadrant 2.

After these measurements, one of the theodolites began to drift excessively. When attempts to correct the theodolite system failed, the feed locations were measured with a combination of techniques. When different antenna feed systems were first installed, moved, or switched to a new quad-aperture, the location was measured with the metric camera system at an elevation angle including the feed in the field of view. When the feed was adjusted between tests with the positioner only, the relative locations were measured by using the calibrated readouts of potentiometers on the feed positioner.

Table 11 gives the compiled phase center locations as determined by these various techniques. The estimated accuracy of the theodolite and metric camera measurements is given in this table. (Shown also in this table for information only is the position of the centroid of the three targets for the feed setup for the initial JPL test, test 8). For the nonscanned 4.26-GHz test and the tests derived therefrom (12, 14, and 15), the feed was placed about 5 in. farther away than from previous tests with LaRC feeds. This feed placement clearly resulted from adjustment of the feed positioner to this location as confirmed by the console readings. It is noted that for tests 15, 16, and 17, no actual feed measurements were made; however, estimates of the feed point derived by summing the relative feed positioner console offsets with the locations of earlier tests are given in the table. After test 17, feed positioner data were no longer recorded; hence, estimates of feed location are not possible for test 18.

For tests 19 through 26, metric camera feed measurements were made for all four quadrants after the final adjustment of the reflector surface. (See fig. 37.) Two comments are offered regarding these tests:

(1) The phase center z dimension is close to the ideal focal length for quadrant 4 again

(2) The lateral and axial agreements with the ideal feed location decrease in the following order: quadrant 1, 3, 4, 2

A comparison was made of the variation in the feed location relative to the reflector by plotting the data from theodolite measurements on June 5 with the metric camera measurements of July 30 for quadrant 4. It is noted that the theodolite measurements were transferred into the antenna coordinate system using sufficient antenna surface targets and the STARS software (ref. 15). Figure 38 shows the XY plan view and the ZX elevation view of these tests. The theodolites measured targets on the horn face, whereas the metric camera measured targets on the feed brackets. The orthographic projections in the plane perpendicular to the brackets show an average separation distance of these planes of 7.81 in., and based on these projections, the difference in the two measurements of the location of the phase center is less than 0.1 in. This plot demonstrates that

(1) Over the approximately 2-month test period, the feed location was very repeatable

(2) The measurement systems used for these tests yield consistent data

6.3. Near-Field Phase Focus Measurements

Predicting the proper location of the feed for a system of this scale is a demanding problem. Fortunately, the phase of the near-field measurement provides a convenient, sensitive method for determining if the feed is near the focal point. Figure 39 illustrates the near-field phase measurement across the aperture when the feed is (1) axially offset, (2) misaligned, and (3) at the focal point. These errors yield not only the characteristic traces shown, but also an estimate of the required feed adjustment. (See ref. 9.) This measurement technique provided an end-to-end method of positioning the feed optimally at the focal point for the various configurations tested at MMA.

7. Shape Control of Antenna Surface

W. Keith Belvin

The 15-m hoop-column antenna was constructed to assess the surface accuracy and EM performance attainable with build-to-design techniques (refs. 5 and 9). The predicted deviation of the surface from an ideal paraboloid due to fabrication errors was 0.069 in. rms. The predicted electromagnetic performance for such an antenna is acceptable for many communications and science applications up to a frequency of about 8 GHz. Thus in many ways, the MMA near-field tests were an assessment of whether a working antenna could be fabricated using the hoop-column design.

Figure 40 shows a contour plot of the antenna surface error in the direction of the vertical axis. These data are based on the metric camera measurement March 27, 1985, using the Tie Points I targets (fig. 21(a)) from the second antenna deployment at Harris. The average rms error of the four quadrants (relative to a best-fit parabola) was 0.119 in. for the effective surface defined in figure 41. Since surface error of this magnitude would significantly degrade the EM performance of the antenna (fig. 13), a method for reducing the surface error using the 96 control cords was developed.

7.1. Structural Modeling

The surface shape control method described herein employs finite element analysis coupled with least-squares error analysis. An analytical model was required to compute the influence of the 96 control cables on the surface shape. A finite element structural model was developed to predict the displacement of the surface at the 888 target locations which results from control cable length adjustments. (See ref. 17.) The control cable adjustments necessary to minimize the surface error were based on the finite element model influence coefficients. The Engineering Analysis Language (EAL) finite element program (ref. 18) was used for modeling. Figure 42 shows the structural elements of the analytical model of the antenna with no reflecting surface. The hoop, column, and tripod were modeled with beam elements, whereas the cables were modeled with rod elements. The stiffness effects of tension/compression loads in the members were modeled in the analysis by including the differential stiffness. (It is noted that since the cables cannot carry a compression load, cable elements are valid in tension only.) Since the antenna was designed for testing in ground facilities, gravity loading in the downward direction (fig. 42) was included in all analyses. Dynamic system identification tests prior to installation of the surface on the antenna were used to verify this model.

The model for the surface required 4592 rod elements and 2880 two-dimensional triangular membrane elements. Since each quadrant of the antenna is a separate offset paraboloid of six gores each, a basic three-gore antenna surface model (fig. 43(a)) was used and reflective symmetry was applied to produce one complete quadrant (fig. 43(b)). The entire surface was formed by consecutive rotations of the quadrant model. The merging of the surface and the hoop-column models produced a model of the complete antenna.

Static analysis of the model was performed to determine the effect of control cable adjustments on the surface shape. Using an artificial thermal strain input to the analytical model, the control cables shown in figure 44 (one gore only) were individually shortened and the resulting surface target displacements were computed. A matrix of influence coefficients for one quadrant (24 cables × 888 surface target locations) was thus assembled. Rotational symmetry was used to expand the matrix for the complete antenna surface (96 × 888). Typical displacements of the surface targets in the vertical direction (fig. 45) result from lengthening the control cables by

Radial 4, cord 1 = 1.00 in. in quadrant 1
Radial 10, cord 2 = 0.75 in. in quadrant 2
Radial 16, cord 3 = 0.50 in. in quadrant 3
Radial 22, cord 4 = 0.25 in. in quadrant 4

The effects of cable length adjustments are generally local in nature. The sensitivity of surface target locations to cable length changes is higher in outboard (near the hoop) cables than the inboard (near the hub) cables. Although the inboard cables are more nearly vertical, the outboard cables have higher sensitivity because the cable tension becomes the dominant parameter affecting the surface target displacements.

Several observations regarding the structural model and the use of the influence coefficients are needed to qualify and maintain the validity of the analysis. First, the matrix of influence coefficients is based on linear analysis, even though cable length adjustments produce changes in the differential stiffness. For small cable adjustments, the differential stiffness will remain nearly constant and linear analysis should be sufficient. Second, control cable adjustments must be limited to maintain a level of tension force sufficient to prevent cable slackening but small enough to prevent cable breakage. Third, the stretch of the control cables when the cables are adjusted (based on the antenna configuration used at Harris and MMA) has been included in this model. If different control cables are used, the influence coefficients should be adjusted to account for different levels of control cable stretch.

7.2. Surface Control Analysis

Minimization of the antenna surface error can be performed by using the control cable influence coefficient matrix $\mathbf{I}$ discussed in section 7.1. The analysis was simplified by neglecting X and Y target motions and accounting for Z motion only, since control cable adjustments produce predominately vertical (Z) motion with very small x and y coordinate changes.

The effect of the control cables on the surface is given by

$$\mathbf{I}\,\mathbf{c} = \mathbf{s} \tag{7.1}$$

where $\mathbf{c}$ is a vector of 96 control cable length changes and $\mathbf{s}$ is a vector of vertical displacements of the 888 surface targets.

To adjust for a vertical reflector surface error $\mathbf{s}_e$, a set of compensating control cable adjustments $\mathbf{c}_a$ may be computed by using least-squares error analysis of the following form:

$$\mathbf{I}^{\mathrm{T}}\,\mathbf{I}\,\mathbf{c}_a = \mathbf{I}^{\mathrm{T}}\,(-\mathbf{s}_e) \tag{7.2}$$

Equation (7.2) represents a set of 96 simultaneous equations which may be solved to obtain the best set of control cable adjustments $\mathbf{c}_a$ to minimize a given surface error $\mathbf{s}_e$.

The design paraboloidal shape is given by equation (2.1). The measured x and y coordinate values of the surface targets were substituted into this equation to obtain the ideal z coordinate z_i. Thus, the vertical surface shape error is

$$\mathbf{s}_e = z_m - z_i \tag{7.3}$$

Substituting $\mathbf{s}_e$ from equation (7.3) into equation (7.2) permits the calculation of control cable adjustments to compensate for $\mathbf{s}_e$ in a least-squares sense. The shape control analysis has been implemented in software using the FORTRAN language on CDC CYBER and DEC VAX computers. The computer program follows the flowchart of figure 46.

7.3. Results and Discussion

The analysis described in section 7.2 has been used to compute antenna control cable adjustments for three different cases. Results from these cases are presented in the form of contour plots and rms errors. The rms errors are given for the effective surface area which is the predominant portion of the surface illuminated by the electromagnetic energy. (See fig. 41.)

7.3.1. Case 1: Adjustment of 96 cables on May 25, 1985. After deployment but prior to electromagnetic testing at MMA, the surface of the antenna was measured with the use of a metric camera. The measured surface (fig. 47) indicated that significant deviations from the design paraboloidal aperture surfaces were present. The measured surface errors (as defined by eq. (7.3)) were input to the shape control analysis, and the cable adjustments were computed as given in table 12. The predicted reflector shape after adjustment (fig. 48(a)) is obtained by adding the

computed surface displacements due to cable adjustment to the measured surface errors. The predicted rms error after adjustment has an average value of 0.082 for the effective surface area.

The cable adjustments of table 12 exceeding 0.011 in. were implemented and the antenna surface shape was remeasured. (Cable adjustments below approximately 0.015 in. were not deemed practical due to limited precision of the manual adjustment procedure used in the experiment.) The measured surface error after adjustment is shown in figure 48(b). Although the contour plots of the predicted and measured surface errors show that differences still exist, the rms error levels show good agreement except for quadrant 4. Subsequent analysis showed that during the manual cable adjustments, one cable in this quadrant was inadvertently skipped (radial 21, cord 3).

7.3.2. Case 2: Adjustment of 10 cables on June 14, 1985. A second iteration to improve the antenna surface accuracy utilized a subset of the cable adjustments as shown in table 13. In addition to the cable that had been overlooked, it was decided that all control cables whose required adjustments exceeded 0.040 in. would be readjusted. The shape control algorithm was modified to permit only 10 of the 96 cables to be adjusted. (See table 14.) The predicted error contours from these 10 cable adjustments are shown in figure 49(a). After the 10 cables were experimentally adjusted, the surface shape was remeasured and found to yield the error contour of figure 49(b). The predicted and measured surface contour shapes and rms error are in good agreement.

The measured data of figure 49(b) were used to compute another iteration of 96 cable adjustments as given in table 15. These new cable adjustments were small and were not implemented since analysis predicted they would have little effect on the rms error levels.

7.3.3. Case 3: Weighted surface error cable adjustment on July 30, 1985. A final adjustment of the antenna surface control cables was computed (and subsequently implemented) by using the surface errors measured after case 2 and by using the magnitude of the electric field for the 7.73-GHz feed horn to weight the antenna surface error. (See fig. 50.) The goal of this case was to optimize adjustment of the surface errors most strongly affecting the RF performance.

Table 16 lists the 96 cable adjustments computed using the weighted surface error. From this table, the cable adjustments exceeding 0.020 in. were chosen to be adjusted. Thus, the shape control algorithm was modified to permit only 33 of the 96 cables to be adjusted. Table 17 lists the 33 cable adjustments that were experimentally performed. Although the predicted and measured surface errors in figure 51 show little change in rms error (0.076 ± 0.018 in.), both the measured and predicted antenna electromagnetic patterns for quadrant 4 showed measurable improvement. (See section 8.)

7.4. Shape Control Summary and Recommendations

The 15-m hoop-column antenna is designed to permit reflector surface shape control through adjustment of control cables. A method for shape control of the antenna based on finite element modeling coupled with least-squares error analysis has been developed. The predicted and measured surface rms error levels agree within 4 percent, and error contours show similar trends. The effective antenna surface average rms error was reduced by an average of 38 percent in two iterations of control cable adjustments. The effective surface rms surface error of the best aperture (quad 4) was reduced from 0.131 to 0.056 in.

The shape control method was based on the availability of 888 surface target measurements and the least-squares solution of 96 simultaneous equations. Follow-on studies are now underway which focus on simplifying assumptions to reduce the computational requirements. For example (ref. 19), the localized nature of surface shape distortions due to control cable adjustments should be used to reformulate the shape control algorithm such that fewer computations are required. Automation of the shape control procedure can be performed by using control cable actuators for cable adjustment and near-real-time sensors for surface target measurement. However, modifications of the shape control analysis will be required for dynamic control due to the dynamics of actuators, sensors, and antenna.

Antenna surface shape control permits compensation for fabrication, thermal, and other surface distortions and appears to be quite practical for large space antennas. The as-built and assembled surface accuracy of the 15-m hoop-column antenna indicates fabrication errors will probably be an important source of surface distortion, although the surface shaping system and the feed positioning system can be built and adjusted with great precision. Thus, future large space antennas should include the necessary hardware and software to enable on-orbit surface shape control.

8. Electromagnetic Results

M. C. Bailey

In this section, some results of the extensive testing of the hoop-column antenna are presented and compared with calculations. All the measured results are contained in references 10, 11, and 12, and only four sets of data are discussed in this section since these demonstrate the pertinent radiation characteristics of the antenna.

The antenna was tested at four frequencies of 2.27, 4.26, 7.73, and 11.6 GHz with LaRC-designed feeds and at 2.225 GHz with a JPL-designed feed. The feeds for 2.27 and 4.26 GHz were microstrip patch arrays of 19 elements and the feeds for 7.73 and 11.6 GHz were conical multimode horns. (See fig. 10.) The radiation patterns for these feeds are shown in figures 52 through 55 for the E- and H-planes. The feed patterns were measured in other planes in increments of 15°, and these measured patterns were used for interpolation purposes to determine the reflector surface illumination for calculation of antenna radiation patterns. The reflector radiation patterns were calculated by numerical integration of the aperture fields determined by geometrical optics projection of the feed patterns onto a plane normal to the axis of the paraboloid. The feed is assumed to be located at the focal point of the best-fit paraboloid. Figure 56 shows the aperture geometry for one quadrant of the reflector. In all tests shown, the feeds were linearly polarized with the E-vector geometry as shown in figure 56.

In order to establish a reference for discussion of test results, calculations were performed for a perfectly smooth paraboloid. These calculated smooth reflector patterns are shown in figures 57 through 60. The "pie-shaped" aperture results in a much lower edge illumination in the H-plane which yields a lower side lobe envelope than for the E-plane.

The actual surface of the reflector was characterized by measuring the x, y, z coordinates of optical targets placed on the mesh. (See section 5.) For radiation pattern calculations, a best-fit paraboloid is determined for the measured target data and the target residuals are used in a fifth-order bivariate polynomial interpolation for the phase of the electrical field in the aperture plane. The aperture plane projection of the target locations for quadrant 4 is shown in figure 61 and the polynomial interpolation for the residuals is plotted in figure 62 with the distortions amplified in order to be observable. The maximum value in figure 62 is +0.5 cm and the minimum value is −0.8 cm with an rms value of 0.167 cm.

The measured radiation patterns for tests 5, 12, 1, and 4 are compared in figures 63 through 66 with the calculated patterns. The general side lobe envelope agrees with the predictions, and as would be expected, the envelope of the side lobe level increases with increases in frequency relative to the smooth surface side lobe envelope of figures 57 through 60. Additional studies are being conducted in order to refine the calculations and to better understand the effects of surface distortions upon the details of side lobe structure.

Certain side lobe structures are unique to this reflector antenna configuration and are worthy of comments. In the E-plane, a side lobe occurs at about 6° from the boresight due to feed spillover illumination of the opposite quadrant (quadrant 2) of the reflector. This lobe is more distinct at the higher frequencies. At the lower frequencies, this lobe occurs nearer the main beam and causes some interference with the close-in side lobes of the primary aperture. Similar lobes occur in the diagonal planes at about 4° from boresight due to feed spillover illumination of adjacent quadrants as observed in figures 67 and 68 for the data of test 1. The position of these lobes depends upon the location of the feed relative to the focal point of the particular reflecting surface. The level of these lobes depends upon the total feed spillover onto the adjacent and opposite apertures relative to the total feed illumination of the primary aperture.

The most distinctive structure in the H-plane is two lobes symmetrically located about the main beam. These two lobes are frequency dependent both in position and in amplitude and are a result of the rippling of the surface. The spacing (in wavelengths) of the ripples determines the position of the radiation pattern lobes, and the height (in wavelengths) of the ripples determines the amplitude of the lobes. These lobes resemble "grating lobes" although the surface ripples are not truly periodic.

The highest side lobe for quadrant 4 occurs in the +45° plane at an angle of −1°. (See fig. 68.) After the final surface adjustment in which 33 of the 96 surface control cords were adjusted, this side lobe level was reduced by an additional 3.6 dB relative to peak level.

Calculated gain at each of the four frequencies was compared with measured gains, and the agreement was inconsistent. It was determined from MMA that several errors were made during the gain measurements that are still under investigation; however, the accuracy of the directivity was not significantly affected by measurement errors.

The aperture directivity for each of the four frequencies is plotted in figure 69 for quadrant 4. The

measured values were determined from the measured radiation patterns and do not include feed spillover loss. The calculated values are actually the calculated gains of the distorted reflector, including feed spillover loss but neglecting mesh transmission and feed insertion loss. Since the edge illumination of the reflector is below −14 dB, the feed spillover loss is very small and comparison of the data in figure 69 is valid. The measured and predicted directivity values agree quite well.

9. Concluding Remarks

This report documents the activities undertaken at the Martin Marietta Near-Field Test Facility from about May 1 through August 1, 1985, to measure the electromagnetic performance of the 15-m hoop-column antenna. This is the largest deployable antenna ever tested. During the test period between deployment and restowage, 26 electromagnetic tests (some with several patterns) as well as extensive mechanical alignment, static and dynamic tests, photogrammetry, and other tests were conducted. The test program was completed on schedule, with time available for additional valuable cross-polarization pattern tests.

The objectives of this test program were met to our fullest expectations as follows:

Antenna deployment was accomplished after much difficulty by on-site fabrication of brackets and shims. The column was measured to be vertical within 0.03° and the hoop to be planar within 0.07 in. In addition to antenna deployment, the antenna was successfully proof-tested with 283 lb on the feed mast. Also, with the 283 lb on the feed mast, incremental movements from 0.1 to 2.6 in. of the test facility mounting table (to simulate system dynamics during near-field testing) caused no more than 0.03 in. deflection of the antenna feed system, which quickly damped out.

Antenna RF performance was measured at 2.27, 4.26, 7.73, and 11.6 GHz (and at 2.225 GHz for a JPL feed not reported herein). High quality near- and far-field patterns were measured which showed lower than expected initial antenna performance, which improved significantly after reflector surface adjustments. Antenna performance at 11.6 GHz even showed an acceptable peak-to-first side lobe gain value of approximately 20 dB. The effects of cord ribbing and interference patterns from adjacent apertures agree well with predictions.

The antenna feeds performed as predicted in these measurements for both on-focus and scanned-beam locations. The near-field amplitude and phase measurements provided a quick and accurate method of placing the feed properly.

Surface characteristics of the antenna were measured with a metric camera to an accuracy of 0.007 in. rms for the whole antenna. The outer reflector surface accuracy was limited by effects of small torsional motion of the antenna. In addition, locations of the feed, hoop, and column were measured with good precision by a metric camera and theodolites.

Adjustment of the reflector surface was accomplished with a finite element model of all structural elements of the antenna. This model related the length of surface control cords to the location of the surface tie point targets. This model, when coupled with a least-squares error analysis, proved very accurate in optimizing the reflector surface for RF performance, even though precision of the hand adjustment was limited to about 0.015 in.

The reflector surface figure was stable between June 14 and July 30, 1985. This is significant, since during this period, many movements of the antenna and changes of the feed occurred.

The directivity values agreed quite well between measured and predicted results.

The high quality of the antenna pattern data and the achievement of the objectives of this test program are felt to be due in a large part to

A high quality fabrication of the 15-m antenna by the government and contractor team

The use of a well-designed and understood, high-precision near-field facility and a very dedicated, cooperative staff

A strong cooperative effort by government and contractor employees on-site at the facility at Martin Marietta Corporation, Denver Aerospace Division.

NASA Langley Research Center
Hampton, VA 23665-5225
March 7, 1989

References

1. Freeland, R. E.; Garcia, N. F.; and Iwamoto, H.: Wrap-Rib Antenna Technology Development. *Large Space Antenna Systems Technology—1984*, William J. Boyer, compiler, NASA CP-2368, Part 1, 1985, pp. 139–166.
2. Bush, H. G.; Herstrom, C. L.; Stein, P. A.; and Johnson, R. R.: Synchronously Deployable Tetrahedral Truss Reflector. *Large Space Antenna Systems Technology—1984*, William J. Boyer, compiler, NASA CP-2368, Part 1, 1985, pp. 237–250.
3. Kefauver, Neill; Cencich, Tom; Osborn, Jim; and Osmanski, J. T.: *Near-Field Testing of the 5-Meter Model of the Tetrahedral Truss Antenna.* NASA CR-178147, 1986.
4. Coyner, J. V.: Box Truss Development and Its Applications. *Large Space Antenna Systems Technology—1984*, William J. Boyer, compiler, NASA CP-2368, Part 1, 1985, pp. 213–233.
5. Sullivan, Marvin R.: *LSST (Hoop/Column) Maypole Antenna Development Program.* NASA CR-3558, Part 1, 1982.
6. Allen, B. B.: *50-Meter Surface Model Hoop Column Antenna—Final Report.* NASA CR-181715, 1982.
7. Sowden, R. W.: *50-Meter Hoop Column Antenna Pillow Measurements Report.* NASA CR-181716, 1983.
8. Croswell, W. F. (Editor); Vanstrum, M. D.; Schrimpf, R. J.; Taylor, R. C.; and Moye, R. L.: *Hoop/Column Antenna RF Verification Model—Volume II: Analysis and Correlation.* NASA CR-172413, 1984.
9. *Development of the 15 Meter Diameter Hoop Column Antenna—A Final Report.* NASA CR-4038, 1986.
10. Hoover, John; Kefauver, Neill; Cencich, Tom; Osborn, Jim; and Osmanski, Joe: *Near-Field Testing of the 15-Meter Model of the Hoop Column Antenna. Volume I—Final Technical Report.* NASA CR-178059, 1986.
11. Hoover, John; Kefauver, Neill; Cencich, Tom; Osborn, Jim; and Osmanski, Joe: *Near-Field Testing of the 15-Meter Model of the Hoop Column Antenna. Volume II—Near- and Far-Field Plots for the LaRC Feeds, Final Report.* NASA CR-178060, 1986.
12. Hoover, John; Kefauver, Neill; Cencich, Tom; Osborn, Jim; and Osmanski, Joe: *Near-Field Testing of the 15-Meter Model of the Hoop Column Antenna. Volume III—Near- and Far-Field Plots for the JPL Feed, Final Report.* NASA CR-178061, 1986.
13. Campbell, Thomas G.; Bailey, Marion C.; and Belvin, W. Keith: The Development of the 15-Meter Hoop Column Deployable Antenna System With Structural and Electromagnetic Performance Results. *A Collection of Technical Papers—AIAA 11th Communication Satellite Systems Conference*, Mar. 1986, pp. 444–452. (Available as AIAA-86-0667.)
14. Ruze, John: Antenna Tolerance Theory—A Review. *Proc. IEEE*, vol. 54, no. 4, Apr. 1966, pp. 633–640.
15. Brown, Duane C.: *Application of Close-Range Photogrammetry to Measurements of Structures in Orbit, Volume 2. (Appendices).* GSI Tech. Rep. No. 80-012 (Contract No. MOM7DNS-895942), Geodetic Services Inc., Sept. 15, 1980.
16. Ludwig, A., ed.: *Computer Programs for Antenna Feed System Design and Analysis. Volume I: Programs and Sample Cases.* NASA CR-84810, 1967.
17. Belvin, W. Keith; Edighoffer, Harold H.; and Herstrom, Catherine L.: Quasi-Static Shape Adjustment of a 15 Meter Diameter Space Antenna. *A Collection of Technical Papers, Part 1—AIAA/ASME/ASCE/AHS 28th Structures, Structural Dynamics and Materials Conference*, Apr. 1987, pp. 705–713. (Available as AIAA-87-0869.)
18. Whetstone, W. D.: *EISI-EAL Engineering Analysis Language Reference Manual—EISI-EAL System Level 2091.* Engineering Information Systems, Inc., July 1983.
    Volume 1: General Rules and Utility Processors.
    Volume 2: Structural Analysis—Primary Processors.
19. Grantham, William L.; Bailey, Marion C.; Belvin, Wendell K.; and Williams, Jeffrey P.: Controls-Structures-Electromagnetics Interaction Program. *NASA/DOD Control/Structures Interaction Technology—1986*, Robert L. Wright, compiler, NASA CP-2447, Part 2, 1987, pp. 701–715.

Table 1. Measurement Goals for Near-Field Testing of 15-m Hoop-Column Antenna

Near-field performance goals:	
Determine RF performance of 15-m hoop-column antenna	
Provide end-to-end RF performance verification of—	
Reflectivity of mesh	
Surface design adequacy	
Feed placement capability	
Surface stability	
Measurement goals:	
Dynamic range:	
Standard, dB	80
Experimental, dB	60
Maximum, dB	80
Boresight gain, dB	±0.25
Boresight angle, BW	±1/50
Cross-polarization level at—	
-25 dB, dB	±1
-40 dB, dB	±2
Side lobe level at—	
-25 dB, dB	±1
-40 dB, dB	±2
Planar probe truncation at—	
8 GHz, deg	±26
Other, deg	±23

Table 2. MMA Test Conditions and Sequence

Test	Test date	Freq., GHz	Feed pos	Far-field pol	Illum quad	Beam scan, BW	Scan size, data points
1	June 5	7.73	1	Co	4	0	2048 × 2048
2	June 6	7.73	1	Cross	4	0	2048 × 2048
3	June 10	7.73	11	Co	4	6	2048 × 2048
4	June 11–13	11.6	1	Co	4	0	2048 × 2048
5	June 17	2.27	1	Co	4	0	512 × 512
6	June 18	2.27	1	Cross	4	0	512 × 512
7	June 20	2.27	2	Co	2	1	512 × 512
8	June 23 to July 2	2.225	8	Cross	4	0	512 × 512
9		2.225	8	Co	4	0	512 × 512
10		2.225	2	Cross	4	2	512 × 512
11		2.225	2	Co	4	2	512 × 512
11a		2.225	4	Cross	4	1	512 × 512
11b		2.225	4	Co	4	1	512 × 512
11c		2.225	5	Cross	4	1	512 × 512
11d		2.225	5	Co	4	1	512 × 512
11e		2.225	8	Cross	4	0	*512 × 512
11f		2.225	8	Co	4	0	*512 × 512
11g		2.225	2	Cross	4	2	*512 × 512
11h		2.225	2	Co	4	2	*512 × 512
12	July 10	4.26	1	Co	4	0	1024 × 1024
13	July 12	4.26	8	Co	2	2	1024 × 1024
14	July 15	4.26	11	Co	4	6	1024 × 1024
15	July 17	4.26	1	Co	2	0	1024 × 1024
16	July 19	4.26	2	Co	2	1	1024 × 1024
17	July 23	4.26	3	Co	2	−1	1024 × 1024
18	July 24	7.73	1	Co	4	0	*512 × 512
†19	July 25	7.73	1	Co	4	0	*512 × 512
†20	July 25	7.73	1	Co	2	0	*512 × 512
†21	July 26	7.73	1	Co	3	0	*512 × 512
†22	July 26	7.73	1	Co	1	0	*512 × 512
†23	July 29	7.73	1	Cross	4	0	*512 × 512
†24	July 29	7.73	1	Co	4	0	*512 × 512
†25	Aug 2	11.6	1	Co	4	0	*1024 × 1024
†26	Aug 4	11.6	1	Cross	4	0	*1024 × 1024

*Abbreviated scans.
†After final cord adjustment.

Table 3. Design Dimensions and Tolerances

[From ref. 9]

Antenna dimensions:

Stowed	0.92 m diameter by 2.7 m high (without feed mast)
Deployed	15 m diameter by 10.0 m high (without feed mast)
Feed mast	4.57 m high (max)
Surface	
Lateral	48.8 to 234.7 in. (radius)
Vertical*	$z = \frac{a^2}{2f} + \frac{r^2}{4f} - \frac{r(\sin\theta + \cos\theta)}{2f}$

Tolerance goals:

Column	
Length	±0.100 in.
Eccentricity	±0.250 in.
Hoop	
Vertical	±0.100 in.
Radial	±0.050 in.

rss of design tolerances for reflector surface goal of 0.069 in.:

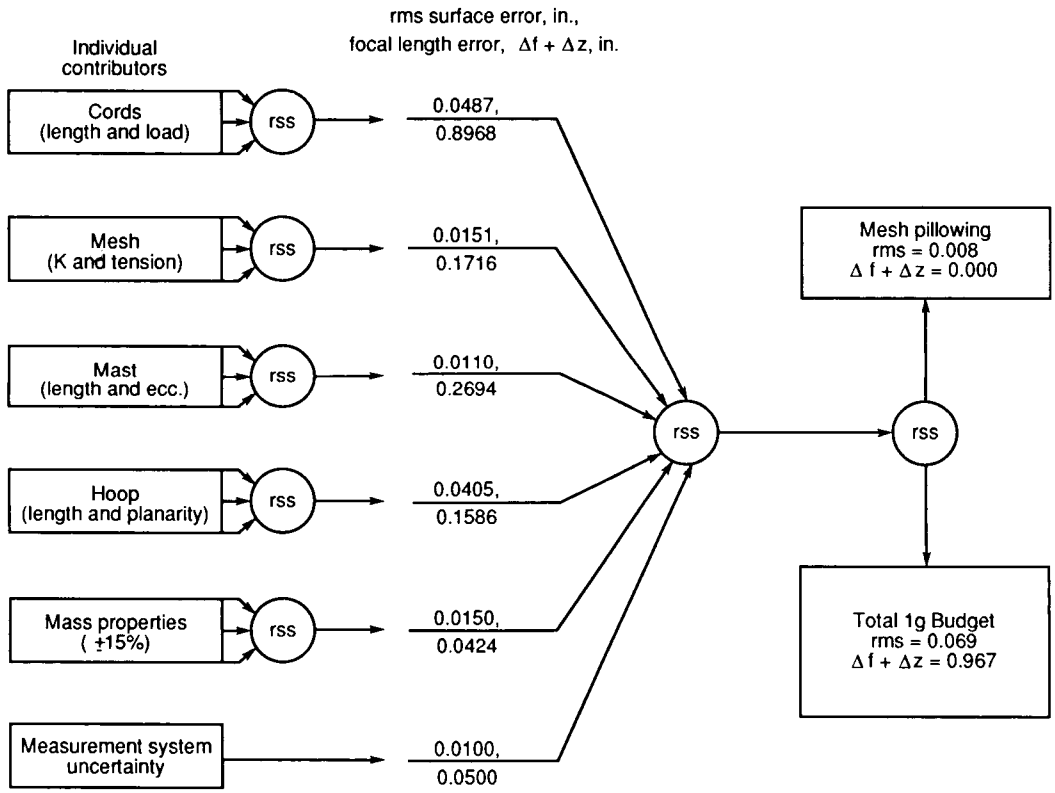

*a = 14.7 in. (distance to vertex).
f = 366.85 in. (focal length).

Table 4. Hoop Cord Tension History

Cord	Tension	Tension, lb, at—							
		5/14 9 AM	5/14 4 PM	5/14 5 PM	5/14 6 PM	5/15	5/24 8 AM	6/6 9 AM	Design spec
G01	Mean						1.46	1.45	1.33
	σ						0.11	0.08	0.042
G02	Mean						1.37	1.37	1.06
	σ						0.15	0.11	0.089
G03	Mean						1.72	1.67	1.15
	σ						0.16	0.14	0.118
G04	Mean	11.17	11.44	11.4	11.6	11.3	*9.78	11.28	11.12
	σ	1.02	1.04	1.07	1.06	1.12	0.67	0.625	0.79
Lower hoop	Mean	5.87	5.83	5.85	5.92	6.10	*4.47	5.81	13.12
	σ	1.99	1.92	1.96	1.92	2.43	1.63	2.80	0.32
Left quartz	Mean					27.5			30.15
	σ					2.7			0.34
Right quartz	Mean					27.8			30.15
	σ					2.16			0.34

*Considered anomalous.

Table 5. Hoop Theodolite Measurements

[H is height of target above floor; H_o, A, and B are coefficients of equation of derived best-fit plane]

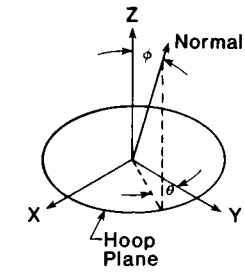

(a) Hysteresis tests, May 14, 1985

[$H = H_o + Ax + By$ is best-fit plane to targets on hoop joints 3, 11, and 19]

Event	Coefficients			H_{av}*	Normal vector	
	H_o	$A \times 10^4$	$B \times 10^4$		Az, deg	El,† deg
Before test	255.046	−4.4560	5.5349	254.855	−44.930	0.0368
First R/R‡	255.032	−3.4992	5.1125	254.859	−55.611	0.0355
After tension	255.009	−2.8161	5.3432	254.850	−55.611	0.0346
Second R/R	255.015	−3.2586	5.2124	254.847	−57.988	0.0352
After tension	255.025	−3.5752	4.9478	254.853	−54.149	0.0350
Third R/R	255.006	−3.4525	4.5981	254.844	−53.098	0.0329
After tension	255.024	−3.8747	4.6830	254.848	−50.396	0.0348

*Average H (H_{av}) fluctuation is negligible (within system accuracy).
†Hoop normal elevation (El) vector variation is negligible (within ±0.002°).
‡R/R = Release and reapply preload.

(b) Planarity tests, May 14–15, 1985

[$H = H_o + Ax + By$ is best-fit plane to targets on all 24 hoop joints]

Event	Coefficients			H_{av}	Normal vector		rms
	H_o	$A \times 10^4$	$B \times 10^4$		Az, deg	El, deg	H♯
Before adjustment	254.954	−4.7219	2.3708	254.792	−26.661	0.0303	0.064
After adjustment 10	254.945	−3.6758	2.7302	254.805	−36.603	0.0202	0.069

♯Hoop planarity is better than measurements at Harris of 0.081 − 0.083 in. rms (ref. 9).

Table 6. Predicted Metric Camera Measurement Accuracies

Target group	Number of rays	σ_x, in.	σ_y, in.	σ_z, in.
Reflector surface	8	0.0051	0.0051	0.0061
Floor	8	.0070	.0065	.0102
Upper column	3	.0062	.0065	.0048
Central hub	3	.0080	.0088	.0105
Lower column	3	.0110	.0123	.0221

Table 7. Results of BFP Analyses of Metric Camera Measurements of Antenna Surface

Meas date	Quad	Focal length, f, in.	Vertex offset			$(\Delta z)_{\text{rms}}$, in.
			x, in.	y, in.	z, in.	
Complete surface						
Ideal		366.85	0	0	0	0
3/27/85	1	369.45	−1.238	−1.202	-1.44×10^{-1}	0.156
	2	368.67	0.706	−0.801	-6.01×10^{-2}	0.164
	3	370.80	1.145	1.335	-7.47×10^{-2}	0.169
	4	368.58	−1.029	1.311	-1.88×10^{-1}	0.128
5/16/85	1	370.05	−1.264	−1.430	-2.05×10^{-1}	0.164
	2	368.72	0.730	−0.770	-8.70×10^{-2}	0.164
	3	370.37	0.729	1.312	-8.91×10^{-2}	0.174
	4	368.04	−0.809	1.096	-2.16×10^{-1}	0.161
5/25/85	1	368.15	0	0	6.85×10^{-2}	0.113
	2	369.57	0.290	−0.476	5.16×10^{-2}	0.133
	3	370.56	0.524	0.760	4.13×10^{-2}	0.129
	4	367.50	0.122	0.061	4.49×10^{-2}	0.110
6/14/85	1	367.99	0.021	−0.012	5.07×10^{-2}	0.112
	2	369.12	0.224	−0.389	4.87×10^{-2}	0.132
	3	369.96	0.432	0.492	4.93×10^{-2}	0.131
	4	368.26	−0.041	0.391	2.94×10^{-2}	0.085
7/08/85	1	368.32	−0.342	−0.018	4.70×10^{-2}	0.112
	2	369.40	0.309	−0.555	3.39×10^{-2}	0.129
	3	370.01	0.451	0.579	3.62×10^{-2}	0.126
	4	368.46	−0.108	0.457	2.31×10^{-2}	0.088
7/30/85	1	369.20	−0.550	−0.262	1.04×10^{-2}	0.114
	2	370.15	0.579	−0.767	4.23×10^{-3}	0.128
	3	371.06	0.925	0.962	1.52×10^{-2}	0.123
	4	368.99	−0.432	0.468	-6.67×10^{-4}	0.081
Effective surface						
Ideal		366.85	0	0	0	0
3/27/85	1	367.58	−1.129	−1.064	-1.89×10^{-1}	0.117
	2	366.65	0.569	−0.536	-9.39×10^{-2}	0.122
	3	369.13	1.091	1.214	-1.18×10^{-1}	0.146
	4	366.65	−0.766	1.035	-2.03×10^{-1}	0.110
5/16/85	1	367.84	−1.103	−1.249	-2.53×10^{-1}	0.120
	2	365.78	0.408	−0.310	-1.15×10^{-1}	0.110
	3	367.97	0.488	1.107	-1.31×10^{-1}	0.143
	4	365.22	−0.288	0.654	-2.19×10^{-1}	0.132
5/25/85	1	366.41	0.204	0.221	4.79×10^{-2}	0.075
	2	367.54	0.110	−0.137	3.00×10^{-2}	0.087
	3	368.58	0.367	0.536	8.43×10^{-3}	0.095
	4	365.53	0.467	−0.302	4.66×10^{-2}	0.092
6/14/85	1	366.24	0.179	0.218	3.04×10^{-2}	0.075
	2	367.02	0.028	−0.037	2.73×10^{-2}	0.085
	3	367.83	0.250	0.219	1.85×10^{-2}	0.096
	4	366.59	0.243	0.110	2.69×10^{-2}	0.061
7/08/85	1	366.62	0.003	0.209	2.44×10^{-2}	0.074
	2	367.55	0.161	−0.265	1.03×10^{-2}	0.084
	3	368.11	0.306	0.350	5.53×10^{-3}	0.094
	4	366.82	0.147	0.187	1.71×10^{-2}	0.062
7/30/85	1	367.91	−0.514	−0.135	-2.09×10^{-2}	0.076
	2	368.81	0.550	−0.577	-2.34×10^{-2}	0.088
	3	369.63	0.881	0.819	-4.83×10^{-2}	0.094
	4	367.68	−0.260	0.240	-7.17×10^{-3}	0.058

Table 8. Metric Camera Measurements of Surface Tie Points in Quad 4

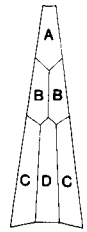

(a) Type A pillows

Target number	z location per best-fit paraboloid equation, in.						z measured − z per best-fit paraboloid equation, in.					
	Mar 27	May 16	May 25	Jun 14	Jul 08	Jul 30	Mar 27	May 16	May 25	Jun 14	Jul 08	Jul 30
2414	4.673	4.305	4.478	4.485	4.477	4.443	0.0058	0.0536	-0.0004	-0.0176	-0.0189	-0.0048
2415	3.177	2.799	2.992	2.995	2.987	2.955	0.0247	0.0295	0.0053	-0.0113	-0.0118	0.0124
2416	1.983	1.596	1.810	1.809	1.800	1.769	0.0308	0.0224	0.0128	-0.0141	-0.0131	0.0244
2417	1.160	0.766	1.000	0.993	0.984	0.953	0.0319	0.0468	0.0286	-0.0112	-0.0148	0.0184
2314	4.264	3.898	4.049	4.062	4.058	4.038	0.0703	0.0316	0.0868	0.0869	0.0851	0.0640
2315	2.840	2.464	2.639	2.646	2.641	2.621	0.0544	0.0160	0.0530	0.0536	0.0549	0.0476
2316	1.714	1.329	1.529	1.531	1.525	1.503	0.0385	0.0014	0.0100	0.0146	0.0131	0.0195
2317	0.947	0.555	0.778	0.773	0.766	0.743	-0.0080	-0.0293	-0.0660	-0.0604	-0.0590	-0.0380
2214	4.001	3.639	3.778	3.791	3.790	3.781	-0.0243	-0.0808	0.0206	0.0096	0.0055	0.0197
2215	2.608	2.233	2.399	2.407	2.405	2.394	0.0154	-0.0436	0.0381	0.0338	0.0293	0.0403
2216	1.535	1.151	1.343	1.345	1.341	1.328	0.0043	-0.0487	0.0120	0.0148	0.0114	0.0160
2217	0.819	0.428	0.645	0.641	0.635	0.618	-0.0154	-0.0573	-0.0256	-0.0153	-0.0188	-0.0211
2114	3.906	3.540	3.681	3.694	3.694	3.696	0.1233	0.1313	0.0782	-0.0131	-0.0163	-0.0243
2115	2.542	2.166	2.333	2.340	2.339	2.337	0.1372	0.1414	0.0932	0.0293	0.0283	0.0264
2116	1.481	1.095	1.289	1.291	1.287	1.280	0.0932	0.0867	0.0448	0.0144	0.0135	0.0197
2117	0.765	0.373	0.592	0.587	0.581	0.570	0.0426	0.0379	-0.0024	-0.0109	-0.0069	0.0080
2014	3.997	3.633	3.783	3.789	3.789	3.796	0.0476	0.0442	-0.0215	-0.0351	-0.0348	-0.0265
2015	2.618	2.243	2.417	2.419	2.417	2.420	0.0616	0.0549	0.0183	0.0149	0.0133	0.0204
2016	1.544	1.160	1.359	1.357	1.353	1.350	0.0340	0.0201	0.0159	0.0196	0.0181	0.0250
2017	0.823	0.432	0.655	0.647	0.641	0.632	0.0108	-0.0324	-0.0007	0.0169	0.0169	0.0242
1914	4.253	3.889	4.058	4.053	4.053	4.060	-0.0094	-0.0110	-0.0626	-0.0689	-0.0711	-0.0145
1915	2.830	2.455	2.645	2.638	2.636	2.639	-0.0207	-0.0414	-0.0602	-0.0588	-0.0582	-0.0113
1916	1.715	1.331	1.543	1.533	1.529	1.527	-0.0275	-0.0427	-0.0430	-0.0366	-0.0362	0.0049
1917	0.961	0.571	0.804	0.790	0.784	0.776	-0.0278	-0.0360	-0.0201	-0.0084	-0.0099	0.0306
1814	4.691	4.325	4.522	4.504	4.501	4.509	0.0225	0.0386	0.0300	0.0445	0.0466	0.0293
1815	3.172	2.796	3.011	2.993	2.989	2.991	0.0523	0.0259	0.0034	0.0244	0.0300	0.0139
1816	1.989	1.605	1.838	1.819	1.813	1.810	0.0538	0.0123	-0.0316	-0.0070	0.0004	-0.0191
1817	1.180	0.790	1.039	1.018	1.010	1.002	0.0230	-0.0167	-0.0871	-0.0617	-0.0598	-0.0869
Number of samples							28	28	28	28	28	28
Mean of values							0.0302	0.0127	0.0046	-0.0019	-0.0023	0.0078
Standard deviation of values							0.0423	0.0538	0.0452	0.0366	0.0364	0.0302
rms							0.0513	0.0544	0.0446	0.0360	0.0358	0.0307

Table 8. Continued

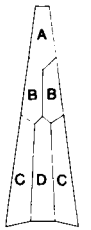

(b) Type B pillows

Target number	z location per best-fit paraboloid equation, in.						z measured − z per best-fit paraboloid equation, in.					
	Mar 27	May 16	May 25	Jun 14	Jul 08	Jul 30	Mar 27	May 16	May 25	Jun 14	Jul 08	Jul 30
2410	13.734	13.427	13.513	13.526	13.518	13.470	-0.1138	-0.0315	-0.0210	-0.0290	-0.0268	-0.0387
2411	10.996	10.670	10.779	10.792	10.784	10.740	-0.0709	0.0236	-0.0156	-0.0364	-0.0401	-0.0407
2412	8.581	8.239	8.370	8.382	8.374	8.334	-0.0404	0.0557	0.0012	-0.0163	-0.0204	-0.0170
2413	6.474	6.118	6.270	6.280	6.272	6.236	-0.0331	0.0321	-0.0410	-0.0505	-0.0527	-0.0435
2428	13.311	13.005	13.075	13.095	13.090	13.054	0.1200	0.1753	0.1808	0.1120	0.1169	0.1111
2429	10.649	10.325	10.416	10.435	10.431	10.398	0.1054	0.1593	0.1865	0.1181	0.1197	0.1030
2430	8.275	7.936	8.050	8.067	8.063	8.033	0.0850	0.1246	0.1376	0.0964	0.0968	0.0702
2431	6.192	5.836	5.974	5.987	5.982	5.954	-0.0859	-0.0649	-0.0671	-0.0503	-0.0529	-0.0708
2310	13.045	12.741	12.796	12.819	12.817	12.789	0.0064	0.0021	-0.0090	-0.0236	-0.0303	-0.0192
2311	10.395	10.074	10.151	10.173	10.170	10.147	0.0018	0.0068	0.0282	0.0150	0.0071	0.0081
2312	8.048	7.715	7.816	7.836	7.833	7.812	-0.0068	-0.0244	0.0226	0.0114	0.0084	-0.0087
2313	6.008	5.655	5.781	5.797	5.795	5.775	0.0421	0.0335	0.1008	0.0820	0.0828	0.0455
2328	12.792	12.491	12.533	12.551	12.552	12.536	-0.2692	-0.2588	-0.2194	-0.0394	-0.0331	-0.0033
2329	10.171	9.851	9.919	9.938	9.939	9.924	-0.1801	-0.2226	-0.1655	-0.0477	-0.0429	-0.0221
2330	7.841	7.504	7.596	7.615	7.614	7.601	-0.0696	-0.1060	-0.0173	0.0536	0.0614	0.0678
2331	5.807	5.456	5.574	5.590	5.589	5.576	-0.2334	-0.3026	-0.1737	-0.1436	-0.1416	-0.1280
2210	12.610	12.313	12.350	12.366	12.370	12.364	-0.1379	-0.2041	-0.2321	-0.0449	-0.0472	-0.0273
2211	9.986	9.668	9.730	9.749	9.751	9.745	-0.1112	-0.1244	-0.1155	0.0097	0.0033	0.0211
2212	7.688	7.354	7.440	7.459	7.461	7.455	-0.0901	-0.0972	-0.0469	0.0085	0.0046	0.0261
2213	5.694	5.344	5.457	5.473	5.474	5.467	-0.0355	-0.0815	0.0254	0.0153	0.0115	0.0364
2228	12.454	12.147	12.185	12.204	12.210	12.213	-0.1056	-0.0366	-0.1112	-0.0005	0.0008	-0.0287
2229	9.887	9.564	9.627	9.646	9.651	9.654	0.0019	0.0141	-0.0350	0.0167	0.0156	0.0037
2230	7.590	7.250	7.339	7.358	7.361	7.363	0.0258	0.0487	0.0475	0.0226	0.0209	0.0231
2231	5.582	5.229	5.342	5.359	5.361	5.361	-0.1647	-0.2061	-0.1163	-0.1828	-0.1832	-0.1574
2110	12.444	12.142	12.179	12.200	12.206	12.217	0.1458	0.1869	0.0794	0.0391	0.0390	-0.0321
2111	9.846	9.523	9.586	9.607	9.612	9.622	0.1723	0.2192	0.1285	0.0578	0.0551	0.0037
2112	7.554	7.215	7.304	7.324	7.327	7.335	0.1867	0.2111	0.1344	0.0402	0.0378	0.0057
2113	5.569	5.215	5.330	5.348	5.350	5.355	0.1612	0.1815	0.1183	-0.0069	-0.0098	-0.0231
2128	12.481	12.177	12.214	12.233	12.239	12.256	0.0890	0.1445	0.1673	0.0920	0.1251	0.0335
2129	9.866	9.544	9.608	9.628	9.632	9.647	0.2054	0.2227	0.2067	0.1148	0.1394	0.0652
2130	7.537	7.198	7.291	7.308	7.312	7.324	0.1996	0.2165	0.1779	0.0877	0.1007	0.0481
2131	5.594	5.242	5.361	5.375	5.377	5.387	0.1955	0.1945	0.1126	0.0309	0.0356	0.0017
2010	12.587	12.285	12.328	12.340	12.346	12.366	-0.0636	-0.0409	0.0814	0.0483	0.0652	0.0422
2011	10.019	9.700	9.770	9.782	9.786	9.804	-0.0275	-0.0239	0.0508	0.0278	0.0378	0.0269
2012	7.706	7.370	7.467	7.478	7.481	7.496	0.0151	0.0207	0.0227	-0.0047	0.0012	-0.0003

Table 8. Continued

(b) Concluded

2013	5.703	5.351	5.475	5.484	5.485	5.497	-0.0099	-0.0065	-0.0840	-0.0981	-0.0948	-0.0819
2028	12.792	12.489	12.545	12.548	12.554	12.574	-0.1735	-0.0948	-0.0288	-0.0321	-0.0272	-0.0083
2029	10.147	9.827	9.909	9.914	9.918	9.936	-0.0580	0.0062	0.0397	0.0391	0.0393	0.0736
2030	7.828	7.492	7.600	7.604	7.607	7.622	-0.0575	-0.0393	-0.0513	-0.0371	-0.0375	0.0102
2031	5.800	5.449	5.582	5.585	5.586	5.599	0.0056	0.0170	-0.0774	-0.0803	-0.0875	-0.0249
1910	13.002	12.699	12.775	12.771	12.776	12.795	0.0101	-0.0036	0.0469	0.0350	0.0398	0.0664
1911	10.355	10.035	10.135	10.132	10.137	10.154	0.0250	0.0249	0.0254	0.0140	0.0098	0.0506
1912	8.021	7.685	7.808	7.806	7.809	7.824	0.0357	0.0472	0.0020	-0.0146	-0.0202	0.0304
1913		5.635	5.780	5.778	5.779	5.791		0.0389	-0.0275	-0.0360	-0.0412	0.0248
1928	13.330	13.026	13.127	13.113	13.117	13.133	0.0836	0.0047	0.0178	0.0175	-0.0099	0.0335
1929	10.602	10.280	10.401	10.390	10.392	10.409	0.1485	0.1057	0.0932	0.0850	0.0656	0.1073
1930	8.217	7.879	8.021	8.010	8.012	8.027	0.0525	0.0254	0.0086	0.0062	-0.0068	0.0284
1931	6.170	5.817	5.980	5.970	5.970	5.981	0.0259	0.0169	-0.0300	-0.0435	-0.0553	0.0093
1810	13.657	13.352	13.478	13.452	13.454	13.471	-0.0250	-0.0247	-0.0324	-0.0063	0.0077	-0.0232
1811	10.921	10.598	10.742	10.719	10.719	10.734	0.0014	-0.0298	-0.0166	0.0113	0.0207	0.0098
1812	8.538	8.199	8.361	8.340	8.340	8.353	0.0471	0.0163	0.0362	0.0563	0.0627	0.0586
1813	6.505	6.152	6.331	6.312	6.310	6.321	-0.0521	-0.0711	-0.0404	-0.0213	-0.0136	-0.0194
				Number of samples			51	52	52	52	52	52
				Mean of values			-0.0004	0.0093	0.0097	0.0061	0.0069	0.0082
				Standard deviation of values			0.1121	0.1229	0.1011	0.0609	0.0640	0.0523
				rms			0.1110	0.1221	0.1006	0.0606	0.0638	0.0524

Table 8. Continued

(c) Type C pillows

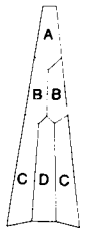

Target number	z location per best-fit paraboloid equation, in.						z measured − z per best-fit paraboloid equation, in.					
	Mar 27	May 16	May 25	Jun 14	Jul 08	Jul 30	Mar 27	May 16	May 25	Jun 14	Jul 08	Jul 30
*2401	49.331	49.268	49.168	49.162	49.120	49.003	-0.3433	-0.5369	-0.3790	-0.3761	-0.3345	-0.2047
*2402	45.427	45.334	45.249	45.248	45.210	45.103	-0.1677	-0.3023	-0.2067	-0.1742	-0.1447	-0.0579
2403	40.532	40.401	40.343	40.339	40.310	40.217	-0.0176	-0.0591	-0.0264	0.0029	0.0303	0.0581
2404	35.889	35.726	35.692	35.692	35.672	35.586	0.0127	0.0733	0.0521	0.0559	0.0630	0.0498
2405	31.497	31.301	31.291	31.295	31.278	31.204	-0.0113	0.1175	0.0596	0.0478	0.0444	-0.0151
2406	27.400	27.178	27.185	27.192	27.178	27.109	-0.0541	0.0786	0.0364	0.0247	0.0234	-0.0242
2407	23.557	23.310	23.337	23.347	23.335	23.271	-0.1303	0.0156	-0.0170	-0.0296	-0.0308	-0.0680
2408	19.999	19.729	19.775	19.787	19.777	19.718	-0.1847	-0.0463	-0.0614	-0.0753	-0.0799	-0.1023
2409	16.722	16.432	16.498	16.511	16.502	16.449	-0.1427	-0.0110	-0.0052	-0.0270	-0.0296	-0.0343
*2432	44.220	44.133	44.000	44.002	43.979	43.908	-0.1089	-0.2304	-0.1421	-0.1159	-0.0988	-0.0617
2433	39.709	39.579	39.487	39.493	39.475	39.409	-0.0408	-0.1452	-0.1201	-0.0993	-0.0878	-0.0682
2434	35.105	34.948	34.881	34.893	34.879	34.820	0.0906	0.0209	-0.0290	-0.0287	-0.0245	-0.0247
2435	30.771	30.580	30.540	30.554	30.543	30.488	0.1209	0.1208	0.0177	-0.0103	-0.0110	-0.0206
2436	26.699	26.483	26.461	26.478	26.469	26.420	0.2016	0.2242	0.1265	0.0995	0.1043	0.0860
2437	22.901	22.658	22.658	22.678	22.672	22.626	0.1511	0.1985	0.1186	0.0869	0.0857	0.0789
2438	19.370	19.105	19.126	19.148	19.143	19.102	0.0801	0.1445	0.0830	0.0326	0.0302	0.0358
2439	16.312	16.026	16.069	16.092	16.087	16.050	0.0076	0.0559	0.0005	-0.0705	-0.0699	-0.0506
*2302	44.267	44.173	44.032	44.036	44.026	43.960	-0.2355	-0.4205	-0.2711	-0.2314	-0.2346	-0.1860
*2301	48.094	48.022	47.859	47.858	47.856	47.780	-0.2986	-0.4546	-0.2453	-0.2197	-0.2402	-0.1668
2303	39.371	39.244	39.134	39.142	39.129	39.075	-0.0672	-0.2329	-0.1640	-0.1388	-0.1339	-0.1092
2304	34.773	34.617	34.531	34.543	34.534	34.486	0.0182	-0.0904	-0.0874	-0.0800	-0.0810	-0.0753
2305	30.489	30.298	30.239	30.257	30.249	30.208	0.0344	0.0013	-0.0569	-0.0761	-0.0812	-0.0946
2306	26.436	26.223	26.188	26.207	26.202	26.161	0.0357	0.0214	-0.0482	-0.0647	-0.0674	-0.0638
2307	22.668	22.428	22.415	22.437	22.432	22.396	0.0613	0.0453	-0.0149	-0.0279	-0.0329	-0.0208
2308	19.199	18.937	18.946	18.969	18.966	18.933	0.0753	0.0909	0.0375	0.0157	0.0077	0.0250
2309	15.986	15.702	15.734	15.757	15.754	15.724	0.0769	0.0664	0.0362	0.0231	0.0206	0.0529
*2332	43.364	43.261	43.106	43.119	43.113	43.077	0.0180	-0.0725	0.1235	0.1306	0.1262	0.1545
2333	38.874	38.748	38.612	38.629	38.625	38.594	0.0616	-0.0211	0.1705	0.1524	0.1476	0.1657
2334	34.326	34.175	34.056	34.078	34.075	34.048	-0.0092	-0.0725	0.1157	0.0678	0.0615	0.0725
2335	30.046	29.868	29.774	29.799	29.799	29.775	-0.2406	-0.3172	-0.1344	-0.1915	-0.1984	-0.1887
2336	26.039	25.837	25.772	25.793	25.794	25.771	-0.1759	-0.2774	-0.1469	-0.1273	-0.1274	-0.1038
2337	22.280	22.056	22.019	22.037	22.038	22.019	-0.1475	-0.2540	-0.1771	-0.0787	-0.0749	-0.0522
2338	18.793	18.548	18.538	18.554	18.556	18.539	-0.1375	-0.2680	-0.2246	-0.0453	-0.0465	-0.0169
2339	15.803	15.534	15.544	15.557	15.558	15.544	-0.2535	-0.4931	-0.3791	-0.1067	-0.1078	-0.0749
*2201	47.322	47.266	47.044	47.059	47.062	47.022	-0.4099	-0.5241	-0.2288	-0.2208	-0.2457	-0.1969

Table 8. Continued

(c) Continued

*2202	43.467	43.389	43.194	43.208	43.210	43.176	-0.2907	-0.4306	-0.1348	-0.1381	-0.1547	-0.1116
2203	38.646	38.532	38.367	38.386	38.384	38.362	-0.0076	-0.1280	0.1381	0.1115	0.1047	0.1282
2204	34.127	33.978	33.845	33.868	33.869	33.849	0.0570	-0.0479	0.1755	0.1205	0.1186	0.1327
2205	29.828	29.649	29.545	29.572	29.573	29.558	-0.0462	-0.1443	0.0546	-0.0087	-0.0145	-0.0037
2206	25.812	25.609	25.537	25.558	25.561	25.546	-0.0507	-0.1372	-0.0197	0.0028	0.0003	0.0201
2207	22.096	21.864	21.821	21.840	21.843	21.831	-0.0861	-0.1572	-0.1017	0.0068	0.0015	0.0161
2208	18.619	18.364	18.348	18.365	18.369	18.359	-0.1478	-0.2074	-0.2045	-0.0172	-0.0255	-0.0035
2209	15.475	15.197	15.209	15.224	15.227	15.219	-0.1858	-0.2472	-0.3138	-0.0490	-0.0530	-0.0270
*2232	42.867	42.770	42.581	42.595	42.599	42.582	-0.1408	-0.2223	-0.0510	-0.0663	-0.0791	-0.0536
2233	38.411	38.289	38.133	38.148	38.152	38.139	0.0195	-0.0493	0.0307	0.0157	0.0099	0.0287
2234	33.878	33.713	33.599	33.616	33.622	33.609	0.1180	0.0994	0.0669	0.0505	0.0444	0.0779
2235	29.604	29.414	29.329	29.347	29.354	29.348	0.1787	0.1833	0.0679	0.0596	0.0551	0.0843
2236	25.614	25.394	25.336	25.356	25.363	25.362	0.1155	0.1277	-0.0123	-0.0067	-0.0078	-0.0051
2237	21.910	21.667	21.633	21.653	21.660	21.663	0.0911	0.0919	-0.0499	-0.0292	-0.0276	-0.0466
2238	18.448	18.183	18.173	18.194	18.201	18.208	0.0972	0.1069	-0.0291	0.0026	0.0032	-0.0395
2239		15.178	15.191	15.212	15.219	15.227		0.0735	-0.0397	-0.0031	-0.0070	-0.0772
*2101	47.059	46.989	46.774	46.785	46.792	46.772	-0.7227	-0.8299	-0.6081	-0.6134	-0.6384	-0.6167
*2102	43.255	43.151	42.973	42.982	42.988	42.973	-0.3995	-0.4645	-0.3603	-0.3495	-0.3660	-0.3399
2103	38.452	38.311	38.174	38.184	38.191	38.183	-0.0227	-0.0140	-0.0519	-0.0523	-0.0636	-0.0465
2104	33.925	33.757	33.648	33.661	33.667	33.660	0.1738	0.2102	0.0783	0.0667	0.0525	0.0840
2105	29.644	29.454	29.375	29.389	29.395	29.395	0.2120	0.2611	0.0456	0.0434	0.0387	0.0656
2106	25.657	25.439	25.381	25.397	25.404	25.409	0.2251	0.2675	0.0744	0.0712	0.0689	0.0634
2107	21.929	21.687	21.652	21.670	21.678	21.686	0.1967	0.2259	0.0604	0.0589	0.0532	0.0221
2108	18.468	18.203	18.191	18.211	18.218	18.229	0.1685	0.2110	0.0674	0.0602	0.0600	0.0005
2109	15.328	15.042	15.054	15.075	15.082	15.094	0.1659	0.2175	0.0911	0.0819	0.0795	-0.0043
*2132	42.982	42.853	42.715	42.719	42.727	42.714	-0.1590	0.1037	-0.1293	-0.1278	-0.1487	-0.1126
2133	38.585	38.443	38.322	38.327	38.334	38.329	0.0605	0.2168	0.0235	0.0172	0.0150	0.0314
2134	33.984	33.817	33.724	33.730	33.738	33.740	0.1487	0.2558	0.0358	0.0170	0.0175	0.0255
2135	29.710	29.526	29.448	29.457	29.466	29.475	0.0921	0.0791	-0.0428	-0.0705	-0.0709	-0.0744
2136	25.679	25.467	25.411	25.422	25.429	25.443	-0.0039	0.0103	-0.0871	-0.1136	-0.0912	-0.1140
2137	21.885	21.644	21.610	21.624	21.631	21.650	-0.0348	-0.0045	-0.0261	-0.0609	-0.0336	-0.0700
2138	18.501	18.241	18.227	18.242	18.249	18.268	-0.0584	-0.0302	0.0399	0.0006	0.0288	-0.0257
2139	15.532	15.253	15.258	15.274	15.280	15.299	-0.0686	-0.0528	0.1154	0.0696	0.0989	0.0285
*2001	47.248	47.164	47.000	46.986	46.997	46.981	-0.3725	-0.4542	-0.2586	-0.2461	-0.2739	-0.2431
*2002	43.499	43.400	43.241	43.240	43.248	43.240	-0.1522	-0.2646	-0.0987	-0.0933	-0.1066	-0.0878
2003	38.678	38.531	38.420	38.419	38.429	38.427	0.0314	0.1107	0.0113	0.0062	0.0019	0.0179
2004	34.128	33.953	33.870	33.873	33.880	33.888	0.1380	0.2408	0.0824	0.0572	0.0575	0.0603
2005	29.870	29.679	29.616	29.621	29.628	29.642	0.1471	0.1707	0.0311	0.0026	0.0077	0.0079
2006	25.877	25.664	25.616	25.623	25.631	25.648	0.0664	0.0829	0.0417	0.0113	0.0197	0.0109
2007	22.120	21.883	21.855	21.864	21.871	21.891	-0.0535	-0.0418	0.0073	-0.0232	-0.0119	-0.0308
2008	18.677	18.416	18.408	18.419	18.426	18.446	-0.0933	-0.0762	0.0575	0.0220	0.0368	0.0074
2009	15.502	15.219	15.233	15.245	15.251	15.272	-0.1252	-0.1042	0.1068	0.0725	0.0935	0.0566
*2032	43.605	43.466	43.377	43.367	43.365	43.362	-0.2833	0.0493	-0.1877	-0.1617	-0.1474	-0.1377
2033	39.051	38.906	38.814	38.800	38.807	38.808	-0.1697	-0.0083	-0.0368	-0.0302	-0.0331	-0.0129
2034	34.450	34.285	34.210	34.200	34.208	34.217	-0.1663	-0.0443	-0.0072	-0.0239	-0.0423	-0.0107

Table 8. Continued

(c) Concluded

2035	30.244	30.060	29.998	29.991	29.999	30.013	-0.1788	-0.1614	-0.0107	-0.0395	-0.0731	-0.0371
2036	26.196	25.985	25.945	25.940	25.951	25.969	-0.2059	-0.1835	0.0001	-0.0302	-0.0720	-0.0348
2037	22.390	22.154	22.138	22.136	22.146	22.167	-0.1757	-0.1610	0.0310	0.0039	-0.0322	-0.0020
2038	18.901	18.641	18.650	18.650	18.659	18.679	-0.1895	-0.1508	0.0175	-0.0094	-0.0376	-0.0125
2039	15.944	15.665	15.699	15.701	15.707	15.729	-0.0865	-0.0523	0.0432	0.0263	0.0176	0.0382
*1901	48.035	47.954	47.830	47.808	47.809	47.800	-0.2711	-0.3846	-0.1840	-0.1581	-0.1792	-0.1832
*1902	44.246	44.166	44.032	44.009	44.011	44.006	-0.2650	-0.5914	-0.1532	-0.1272	-0.1422	-0.1338
1903	39.395	39.270	39.174	39.156	39.158	39.161	-0.0998	-0.2412	0.0119	0.0239	0.0199	0.0373
1904	34.810	34.652	34.583	34.563	34.572	34.579	-0.0563	-0.0982	0.0847	0.0793	0.0756	0.0957
1905	30.507	30.320	30.275	30.259	30.268	30.279	-0.1205	-0.1102	0.0480	0.0339	0.0266	0.0540
1906	26.454	26.241	26.215	26.203	26.210	26.227	-0.1849	-0.1747	0.0095	-0.0136	-0.0095	0.0060
1907	22.688	22.450	22.450	22.440	22.449	22.467	-0.2115	-0.2151	-0.0325	-0.0550	-0.0541	-0.0349
1908	19.181	18.920	18.946	18.938	18.946	18.966	-0.1380	-0.1278	-0.0022	-0.0216	-0.0355	-0.0158
1909	15.953	15.669	15.720	15.714	15.721	15.740	-0.0166	-0.0091	0.0599	0.0432	0.0399	0.0576
*1932	44.601	44.490	44.448	44.404	44.396	44.390	-0.1292	-0.2017	-0.2020	-0.1530	-0.1565	-0.1592
1933	40.135	40.003	39.971	39.925	39.923	39.925	0.0325	-0.0713	-0.0900	-0.0401	-0.0362	-0.0408
1934	35.535	35.371	35.366	35.324	35.322	35.336	0.1531	0.0725	0.0133	0.0467	0.0595	0.0471
1935	31.142	30.949	30.970	30.933	30.936	30.951	0.1512	0.1031	-0.0122	0.0154	0.0347	-0.0040
1936	26.971	26.752	26.788	26.756	26.760	26.780	0.1505	0.1137	0.0505	0.0730	0.0908	0.0492
1937	23.102	22.858	22.911	22.883	22.888	22.907	0.0972	0.0818	0.0498	0.0684	0.0771	0.0384
1938	19.588	19.322	19.393	19.368	19.373	19.393	0.0474	0.0340	0.0340	0.0483	0.0520	0.0166
1939	16.568	16.282	16.370	16.349	16.352	16.373	-0.0099	-0.0230	0.0031	0.0156	0.0123	-0.0161
*1801	49.271	49.202	49.149	49.090	49.079	49.064	-0.3630	-0.5128	-0.4098	-0.3235	-0.3467	-0.3424
*1802	45.428	45.331	45.302	45.244	45.235	45.225	-0.1691	-0.2767	-0.2620	-0.1840	-0.1967	-0.1845
1803	40.479	40.351	40.344	40.287	40.283	40.282	0.0374	-0.0456	-0.1086	-0.0430	-0.0405	-0.0488
1804	35.848	35.687	35.705	35.653	35.649	35.657	0.1394	0.0984	-0.0193	0.0282	0.0411	0.0131
1805	31.484	31.292	31.337	31.288	31.286	31.301	0.1455	0.1298	-0.0333	0.0094	0.0252	-0.0232
1806	27.345	27.128	27.189	27.145	27.146	27.162	0.1082	0.0903	-0.0346	0.0052	0.0193	-0.0296
1807	23.521	23.280	23.356	23.318	23.320	23.337	0.0983	0.0861	0.0022	0.0325	0.0443	-0.0029
1808	19.958	19.694	19.787	19.753	19.755	19.773	0.0635	0.0545	0.0047	0.0332	0.0405	-0.0044
1809	16.688	16.402	16.511	16.481	16.483	16.501	-0.0109	-0.0184	-0.0228	0.0032	0.0149	-0.0244
Complete surface:				Number of samples			110	111	111	111	111	111
				Mean of values			-0.0466	-0.0655	-0.0419	-0.0337	-0.0350	-0.0316
				Standard deviation of values			0.1649	0.2126	0.1336	0.1124	0.1160	0.1052
				rms			0.1706	0.2216	0.1395	0.1169	0.1206	0.1094
Effective surface (entries with * omitted):				Number of samples			90	91	91	91	91	91
				Mean of values			0.0015	-0.0027	-0.0029	0.0023	0.0024	-0.0009
				Standard deviation of values			0.1235	0.1508	0.0923	0.0602	0.0620	0.0593
				rms			0.1228	0.1500	0.0918	0.0599	0.0617	0.0589

Table 8. Continued

(d) Type D pillows

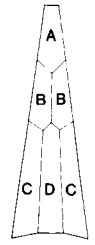

Target number	z location per best-fit paraboloid equation, in.						z measured − z per best-fit paraboloid equation, in.					
	Mar 27	May 16	May 25	Jun 14	Jul 08	Jul 30	Mar 27	May 16	May 25	Jun 14	Jul 08	Jul 30
*2420	44.622	44.529	44.426	44.420	44.396	44.309	-0.1948	-0.3148	-0.2075	-0.1806	-0.1571	-0.1106
2421	40.396	40.271	40.192	40.193	40.173	40.093	-0.1602	-0.1995	-0.1494	-0.1382	-0.1342	-0.1142
2422	35.752	35.591	35.536	35.542	35.525	35.455	0.0164	0.0605	0.0541	0.0482	0.0507	0.0236
2423	31.387	31.187	31.159	31.169	31.154	31.091	-0.0327	0.1117	0.0510	0.0326	0.0307	-0.0304
2424	27.286	27.061	27.052	27.064	27.052	26.996	-0.0337	0.1084	0.0712	0.0502	0.0503	-0.0198
2425	23.443	23.196	23.207	23.221	23.213	23.160	0.0134	0.1509	0.1305	0.1089	0.1062	0.0501
2426	19.879	19.611	19.641	19.658	19.650	19.602	-0.0233	0.1093	0.1183	0.0938	0.0923	0.0512
2427	16.604	16.315	16.365	16.383	16.376	16.332	-0.1411	-0.0134	0.0347	0.0086	0.0041	-0.0112
*2320	43.606	43.508	43.360	43.370	43.359	43.312	-0.1175	-0.2546	-0.1140	-0.0909	-0.0902	-0.0582
2321	39.418	39.295	39.170	39.182	39.173	39.130	0.0146	-0.1211	-0.0224	-0.0121	-0.0062	0.0131
2322	34.832	34.686	34.584	34.601	34.594	34.557	0.1398	0.0272	0.0680	0.0576	0.0556	0.0673
2323	30.514	30.338	30.267	30.288	30.283	30.249	0.1346	0.0687	0.0519	0.0254	0.0195	0.0393
2324	26.469	26.263	26.215	26.237	26.235	26.203	0.1495	0.0837	0.0642	0.0607	0.0589	0.0791
2325	22.690	22.459	22.434	22.457	22.455	22.427	0.0800	0.0338	0.0107	0.0318	0.0282	0.0551
2326	19.191	18.931	18.929	18.952	18.951	18.926	0.0014	-0.0414	-0.0548	-0.0135	-0.0154	0.0185
2327	15.911	15.632	15.655	15.678	15.678	15.654	-0.0864	-0.1489	-0.1603	-0.1064	-0.1062	-0.0603
*2220	42.961	42.868	42.680	42.696	42.697	42.674	0.0300	-0.0466	0.1731	0.1572	0.1509	0.1788
2221	38.803	38.685	38.521	38.538	38.539	38.523	0.0928	0.0135	0.2203	0.1853	0.1817	0.2010
2222	34.254	34.100	33.969	33.990	33.993	33.982	0.1052	0.0599	0.2226	0.1649	0.1582	0.1701
2223	29.986	29.805	29.703	29.728	29.731	29.724	-0.0441	-0.1047	0.0296	-0.0422	-0.0377	-0.0390
2224	25.970	25.762	25.689	25.710	25.714	25.707	-0.0409	-0.1174	-0.0394	-0.0312	-0.0317	-0.0201
2225	22.223	21.991	21.948	21.965	21.970	21.966	-0.0570	-0.1443	-0.1206	-0.0312	-0.0281	-0.0238
2226	18.742	18.488	18.472	18.488	18.494	18.492	-0.0747	-0.1512	-0.1777	-0.0190	-0.0171	-0.0134
2227	15.560	15.284	15.292	15.306	15.311	15.311	-0.2241	-0.3401	-0.3554	-0.1064	-0.1075	-0.1032
*2120	42.948	42.829	42.671	42.679	42.687	42.670	-0.2506	-0.1554	-0.2361	-0.2361	-0.2578	-0.2196
2121	38.823	38.676	38.549	38.558	38.565	38.556	-0.0760	0.0005	-0.1316	-0.1402	-0.1449	-0.1225
2122	34.247	34.079	33.978	33.988	33.995	33.994	0.0643	0.1253	-0.0594	-0.0711	-0.0710	-0.0538
2123	29.932	29.740	29.664	29.676	29.683	29.687	0.1109	0.1388	-0.0815	-0.0948	-0.0803	-0.0728
2124	25.882	25.666	25.613	25.627	25.635	25.644	0.0918	0.1314	-0.0788	-0.0947	-0.0812	-0.0985
2125	22.157	21.916	21.884	21.901	21.909	21.923	0.0780	0.1362	-0.0416	-0.0676	-0.0512	-0.0983
2126	18.607	18.342	18.333	18.352	18.360	18.376	0.1291	0.1889	0.0610	0.0231	0.0385	-0.0383
2127	15.483	15.200	15.212	15.232	15.239	15.255	0.0829	0.0946	0.0523	0.0114	0.0247	-0.0743
*2020	43.308	43.169	43.064	43.057	43.064	43.057	-0.1943	0.2120	-0.1121	-0.1014	-0.1056	-0.0829
2021	39.205	39.059	38.962	38.955	38.963	38.962	-0.0182	0.2592	0.0334	0.0369	0.0389	0.0534
2022	34.579	34.413	34.335	34.330	34.338	34.345	0.0681	0.2405	0.0607	0.0473	0.0525	0.0600

Table 8. Concluded

(d) Concluded

2023	30.273	30.092	30.030	30.029	30.034	30.050	-0.0371	0.0170	-0.0967	-0.1255	-0.1096	-0.1077
2024	26.178	25.972	25.927	25.928	25.933	25.953	-0.1099	-0.0731	-0.0788	-0.1054	-0.0840	-0.0898
2025	22.496	22.264	22.237	22.241	22.247	22.267	-0.1562	-0.1239	-0.0341	-0.0666	-0.0458	-0.0499
2026	18.981	18.726	18.720	18.725	18.731	18.753	-0.1779	-0.1351	0.0209	-0.0103	0.0105	-0.0007
2027	15.776	15.500	15.517	15.523	15.529	15.551	-0.2064	-0.1775	0.0495	0.0195	0.0350	0.0225
*1920	44.174	44.052	43.992	43.960	43.952	43.949	-0.1196	0.0008	-0.0936	-0.0565	-0.0536	-0.0543
1921	40.102	39.967	39.910	39.879	39.876	39.876	-0.1508	-0.1480	-0.0984	-0.0649	-0.0522	-0.0501
1922	35.519	35.361	35.321	35.290	35.295	35.301	-0.1136	-0.0775	-0.0265	-0.0178	-0.0220	-0.0109
1923	31.132	30.941	30.917	30.891	30.895	30.911	-0.1677	-0.1537	-0.0528	-0.0640	-0.0689	-0.0664
1924	26.930	26.715	26.712	26.691	26.698	26.715	-0.1841	-0.1830	-0.0497	-0.0575	-0.0924	-0.0834
1925	23.113	22.874	22.893	22.875	22.885	22.905	-0.1313	-0.1401	-0.0063	-0.0134	-0.0587	-0.0472
1926	19.532	19.269	19.310	19.294	19.301	19.322	-0.1957	-0.1800	-0.0121	-0.0189	-0.0623	-0.0456
1927	16.320	16.038	16.104	16.092	16.095	16.116	0.0192	0.0078	0.0453	0.0377	0.0226	0.0377

Complete surface:	Number of samples	48	48	48	48	48	48
	Mean of values	-0.0437	-0.0243	-0.0223	-0.0204	-0.0201	-0.0198
	Standard deviation of values	0.1141	0.1457	0.1132	0.0869	0.0860	0.0809
	rms	0.1211	0.1462	0.1142	0.0884	0.0875	0.0825
Effective surface (entries with * omitted):	Number of samples	42	42	42	42	42	42
	Mean of values	-0.0298	-0.0144	-0.0114	-0.0112	-0.0107	-0.0144
	Standard deviation of values	0.1103	0.1381	0.1056	0.0757	0.0743	0.0719
	rms	0.1130	0.1372	0.1050	0.0756	0.0742	0.0725

ALL PILLOW TYPES

Complete surface:	Number of samples	237	239	239	239	239	239
	Mean of values	-0.0270	-0.0318	-0.0213	-0.0186	-0.0191	-0.0160
	Standard deviation of values	0.1371	0.1726	0.1170	0.0925	0.0949	0.0861
	rms	0.1394	0.1752	0.1187	0.0942	0.0966	0.0873
Effective surface (entries with * omitted):	Number of samples	211	213	213	213	213	213
	Mean of values	-0.0014	-0.0001	-0.0005	0.0000	0.0003	-0.0002
	Standard deviation of values	0.1112	0.1320	0.0924	0.0612	0.0624	0.0577
	rms	0.1109	0.1317	0.0922	0.0611	0.0622	0.0576

Table 9. Reflector Surface Deviation* by Pillow Regions in Quad 4

(a) Effective surface

Meas date, 1985	Pillow region A No. of samples = 28		Pillow region B No. of samples = 52		Pillow region C No. of samples = 91		Pillow region D No. of samples = 42		Total samples = 213	
	$(\Delta z)_{mean}$, in.	$(\Delta z)_{rms}$, in.	$(\Delta z)_{mean}$, in.	$(\Delta z)_{rms}$, in.	$(\Delta z)_{mean}$, in.	$(\Delta z)_{rms}$, in.	$(\Delta z)_{mean}$, in.	$(\Delta z)_{rms}$, in.	$(\Delta z)_{mean}$, in.	$(\Delta z)_{rms}$, in.
3/27	0.030	0.051	0.000	0.111	0.002	0.123	−0.030	0.113	−0.001	0.111
5/16	0.013	0.054	0.009	0.122	−0.003	0.150	−0.014	0.137	0.000	0.132
5/25	0.005	0.045	0.010	0.101	−0.003	0.092	−0.011	0.105	−0.001	0.092
6/14	−0.002	0.036	0.006	0.061	0.002	0.060	−0.011	0.076	0.000	0.061
7/08	−0.002	0.036	0.007	0.064	0.002	0.062	−0.011	0.074	0.000	0.062
7/30	0.008	0.031	0.008	0.052	−0.001	0.059	−0.014	0.073	0.000	0.058

(b) Effective surface

Meas date, 1985	Pillow region A No. of samples = 28		Pillow region B No. of samples = 52		Pillow region C No. of samples = 111		Pillow region D No. of samples = 48		Total samples = 239	
	$(\Delta z)_{mean}$, in.	$(\Delta z)_{rms}$, in.	$(\Delta z)_{mean}$, in.	$(\Delta z)_{rms}$, in.	$(\Delta z)_{mean}$, in.	$(\Delta z)_{rms}$, in.	$(\Delta z)_{mean}$, in.	$(\Delta z)_{rms}$, in.	$(\Delta z)_{mean}$, in.	$(\Delta z)_{rms}$, in.
3/27	0.030	0.051	0.000	0.111	−0.047	0.171	−0.044	0.121	−0.027	0.139
5/16	0.013	0.054	0.009	0.122	−0.066	0.221	−0.024	0.146	−0.032	0.175
5/25	0.005	0.045	0.010	0.101	−0.042	0.140	−0.022	0.114	−0.021	0.119
6/14	−0.002	0.036	0.006	0.061	−0.034	0.117	−0.020	0.088	−0.019	0.094
7/08	−0.002	0.036	0.007	0.064	−0.035	0.121	−0.020	0.088	−0.019	0.097
7/30	0.008	0.031	0.008	0.052	−0.032	0.109	−0.020	0.082	−0.016	0.087

*Surface deviation Δz is the difference between $(\Delta z)_{meas}$ and $(\Delta z)_{rms}$ of a target location.

Table 10. Feed Phase Center Locations Measured by Theodolite and Ideal Design Paraboloid Locations

Test	Freq	Coord	Measured	Design	Comment
1 and 2	7.73	x	15.012	14.699	No scan; co and cross pol
		y	−14.565	−14.699	
		z	366.680	366.850	
		θ	21.48	21.00	
		ϕ	−44.74	−45.00	
3	7.73	x	2.546	2.324	Scanned
		y	−26.734	−27.073	
		z	366.513	366.850	
		θ	21.75	21.00	
		ϕ	36.91	36.40	
5 and 6	2.27	x	14.713	14.699	Quad 4; co and cross pol
		y	−14.730	−14.699	
		z	366.513	366.850	
		θ	21.40	21.00	
		ϕ	−45.26	−45.00	
7	2.27	x	−22.616	−21.959	Quad 2; co pol scanned
		y	8.255	7.822	
		z	365.626	366.850	
		θ	20.61	21.00	
		ϕ	133.45	135.00	

Table 11. Feed Phase Center Location Measurement Results

[NM indicates no measurement]

Test	Test data					Measurement technique		
	Date, 1985	Freq	Pol	Feed pos	Quad	Date, 1985	System	Accuracy
1	6/5	7.73	Co	1	4	6/6	Theod	
2	6/6	7.73	Cross	1	4	6/6	Theod	
3	6/10	7.73	Co	11	4	6/6	Theod	
4	6/11 13	11.60	Co	1	4	6/6	Theod	
5	6/17	2.27	Co	1A	4	6/21	Theod	
6	6/18	2.27	Cross	1A	4	6/21	Theod	
7	6/20	2.27	Co	2B	2	6/21	Theod	
8 to 11		2.225			4	7/8	MC	
12	7/10	4.26	Co	1A	4	7/9	MC	0.0100
13	7/12	4.26	Co	8B	2	(a)	(a)	(a)
14	7/15	4.26	Co	11A	4	7/9	MC	0.0100
15	7/17	4.26	Co	1A	2	(b)	(b)	(b)
16	7/19	4.26	Co	2B	2	(a)	(a)	(a)
17	7/23	4.26	Co	3B	2	(a)	(a)	(a)
18	7/24	7.73	Co	1	4	NM	NM	NM
19	7/25	7.73	Co	1	4	7/30	MC	0.0150
20	7/25	7.73	Co	1	2	7/30	MC	0.0150
21	7/26	7.73	Co	1	1	7/30	MC	0.0150
22	7/26	7.73	Co	1	3	7/30	MC	0.0150
23	7/29	7.73	Cross	1	4	7/30	MC	0.0150
24	7/29	7.73	Co	1	4	7/30	MC	0.0150
25	8/2	11.60	Co	1	4	7/30	MC	0.0150
26	8/4	11.60	Cross	1	4	7/30	MC	0.0150

Test	Feed location results								Console readings		
	Pointing angle		Feed target midpoint			Feed phase center					
	θ, deg	ϕ, deg	x	y	z	x	y	z	Δx	Δy	Δz
1	21.48	−44.74	15.012	−14.565	366.680	15.012	−14.565	366.860	0	0	0
2	21.48	−44.74	15.012	−14.565	366.680	15.012	−14.565	366.860	0	0	0
3	21.75	−36.91	2.546	−26.734	366.513	2.546	−26.734	366.513	0	0	0
4	21.40	−44.74	15.012	−14.565	366.680	15.012	−14.565	366.860	0	0	0
5	21.40	−45.26	14.713	−14.730	366.575	14.713	−14.730	366.575	0	0	0
6	21.40	−45.26	14.713	−14.730	366.575	14.713	−14.730	366.575	0	0	0
7	20.61	133.45	−15.356	15.132	365.626	−22.616	8.255	365.626	0.24	0.106	−0.65
8 to 11	20.91	−45.04	22.283	−22.903	370.940	(c)	(c)	(c)			
12	20.99	−45.26	13.708	−13.978	370.752	13.708	−13.978	370.752	0.65	−0.964	4.89
13	(a)	(a)	(a)	(a)	(a)	−22.535	21.301	371.439	−0.64	0.308	1.90
14	20.99	−45.26	13.708	−13.978	370.752	−9.101	−36.581	370.752	0.65	−0.954	4.89
15	(b)	(b)	(b)	(b)	(b)	−14.998	15.250	370.763	(b)	(b)	(b)
16	(a)	(a)	(a)	(a)	(a)	−20.131	11.249	368.176	−0.64	0.308	1.90
17	(a)	(a)	(a)	(a)	(a)	−12.361	19.015	368.176	−0.64	0.308	1.90
18									NM	NM	NM
19	21.78	−45.22	14.792	−15.142	366.366	14.792	−15.142	366.366	NM	NM	NM
20	21.50	135.23	−15.249	15.501	364.058	−15.249	15.501	364.058	NM	NM	NM
21	22.21	224.21	14.581	14.602	367.734	14.581	14.602	367.734	NM	NM	NM
22	21.30	44.96	−14.628	−14.921	365.548	−14.628	−14.921	365.548	NM	NM	NM
23	21.78	−45.22	14.792	−15.142	366.366	14.792	−15.142	366.366	NM	NM	NM
24	21.78	−45.22	14.792	−15.142	366.366	14.792	−15.142	366.366	NM	NM	NM
25	21.78	−45.22	14.792	−15.142	366.366	14.792	−15.142	366.366	NM	NM	NM
26	21.78	−45.22	14.792	−15.142	366.366	14.792	−15.142	366.366	NM	NM	NM

[a]Estimate is based on test 7 measurements of panel B plus console adjustments of test 13.

[b]Estimate is based on test 12 measurements of panel A rotated 180° with no error from quad 4 to quad 2.

[c]Data for the JPL feed tests are the centroid of targets for quad 4.

Table 12. Prediction of First Control Cable Adjustments

[96 cables]

Radial	Hoop joint	Cable adjustment,* in., for—			
		Cord 1	Cord 2	Cord 3	Cord 4
1	19	0.149	0.151	0.092	−0.035
2	18	0.142	0.080	0.022	0.034
3	17	0.160	0.089	0.026	−0.083
4	16	0.199	−0.029	−0.086	−0.004
5	15	0.196	0.069	−0.040	−0.041
6	14	0.215	0.310	0.073	−0.003
7	13	0.191	0.150	0.013	−0.060
8	12	0.270	0.047	0.009	−0.011
9	11	0.212	0.075	−0.030	−0.041
10	10	0.162	0.055	−0.014	0.017
11	9	0.161	0.058	0.020	−0.058
12	8	0.145	0.039	−0.007	−0.054
13	7	0.128	0.149	0.027	−0.036
14	6	0.178	0.048	0.042	0.059
15	5	0.159	0.069	−0.042	−0.065
16	4	−0.001	0.031	−0.069	−0.005
17	3	0.216	−0.006	0.096	−0.013
18	2	0.142	0.005	−0.076	−0.068
19	1	0.192	0.034	0.030	−0.035
20	24	0.175	0.157	0.012	−0.056
21	23	0.228	0.129	†0.192	0.014
22	22	0.143	0.043	−0.025	−0.096
23	21	0.242	0.047	0.175	−0.058
24	20	0.255	0.040	0.033	0.031

*Minus value indicates cable pull.

†Cord which was not adjusted.

Table 13. Prediction of Second Control Cable Adjustments

[96 cables]

Radial	Hoop joint	Cable adjustment,* in., for—			
		Cord 1	Cord 2	Cord 3	Cord 4
1	19	−0.026	−0.014	−0.004	−0.015
2	18	−0.024	−0.014	0.010	0.003
3	17	−0.055	−0.005	−0.003	−0.014
4	16	−0.098	0.030	0.004	0.002
5	15	−0.017	−0.068	0.005	0.008
6	14	−0.015	−0.029	−0.029	−0.004
7	13	0.002	−0.080	−0.017	−0.013
8	12	−0.019	0.053	0.004	−0.010
9	11	−0.021	−0.024	−0.008	0.003
10	10	−0.020	−0.002	−0.011	−0.005
11	9	−0.005	−0.022	−0.016	−0.022
12	8	−0.009	−0.065	−0.021	−0.001
13	7	−0.002	−0.037	−0.018	−0.008
14	6	−0.017	−0.019	−0.012	0.014
15	5	−0.006	−0.028	−0.006	−0.026
16	4	−0.034	0.010	−0.038	−0.006
17	3	−0.002	0.010	−0.042	−0.018
18	2	−0.022	−0.039	−0.019	−0.009
19	1	−0.045	−0.029	−0.031	−0.022
20	24	−0.020	−0.020	−0.011	−0.018
21	23	−0.019	−0.011	†0.222	−0.020
22	22	−0.038	−0.080	−0.032	−0.009
23	21	−0.027	−0.011	−0.034	0.009
24	20	0.010	0.026	−0.021	0.004

*Minus value indicates cable pull.

†Cord not adjusted during first control cord adjustment.

Table 14. Actual Second Control Cable Adjustments

[10 cables]

Radial	Hoop joint	Cable adjustment,* in., for—			
		Cord 1	Cord 2	Cord 3	Cord 4
1	19	0.000	0.000	0.000	0.000
2	18	0.000	0.000	0.000	0.000
3	17	−0.059	0.000	0.000	0.000
4	16	−0.084	0.000	0.000	0.000
5	15	0.000	−0.058	0.000	0.000
6	14	0.000	0.000	0.000	0.000
7	13	0.000	−0.092	0.000	0.000
8	12	0.000	0.042	0.000	0.000
9	11	0.000	0.000	0.000	0.000
10	10	0.000	0.000	0.000	0.000
11	9	0.000	0.000	0.000	0.000
12	8	0.000	−0.090	0.000	0.000
13	7	0.000	0.000	0.000	0.000
14	6	0.000	0.000	0.000	0.000
15	5	0.000	0.000	0.000	0.000
16	4	0.000	0.000	0.000	0.000
17	3	0.000	0.000	−0.069	0.000
18	2	0.000	0.000	0.000	0.000
19	1	−0.072	0.000	0.000	0.000
20	24	0.000	0.000	0.000	0.000
21	23	0.000	0.000	0.185	0.000
22	22	0.000	−0.099	0.000	0.000
23	21	0.000	0.000	0.000	0.000
24	20	0.000	0.000	0.000	0.000

*Minus value indicates cable pull.

Table 15. Prediction of Third Control Cable Adjustments

[96 cables]

Radial	Hoop joint	Cable adjustment,* in., for—			
		Cord 1	Cord 2	Cord 3	Cord 4
1	19	−0.033	−0.016	−0.009	−0.015
2	18	−0.020	−0.013	0.012	0.004
3	17	−0.003	−0.008	−0.008	−0.016
4	16	−0.014	0.032	0.003	0.002
5	15	−0.002	−0.043	0.011	0.014
6	14	−0.019	−0.017	−0.028	−0.008
7	13	0.026	−0.040	−0.016	−0.011
8	12	−0.029	0.015	0.005	−0.017
9	11	−0.009	−0.032	−0.004	0.007
10	10	−0.017	0.002	−0.013	−0.009
11	9	−0.001	−0.016	−0.012	−0.018
12	8	−0.003	0.014	−0.022	−0.005
13	7	−0.001	−0.035	−0.027	−0.017
14	6	−0.015	−0.018	−0.019	0.008
15	5	0.000	−0.028	−0.007	−0.024
16	4	−0.031	0.015	−0.037	−0.003
17	3	0.005	0.002	0.020	−0.017
18	2	−0.015	−0.029	−0.014	0.002
19	1	−0.008	−0.024	−0.028	0.022
20	24	−0.012	−0.041	−0.011	−0.017
21	23	−0.031	0.000	0.043	−0.019
22	22	−0.024	−0.012	−0.032	−0.004
23	21	−0.041	−0.006	−0.032	0.010
24	20	0.009	0.026	−0.016	0.017

*Minus value indicates cable pull.

Table 16. Prediction of Control Cable Adjustments Weighted by Feed Illumination

[96 cables]

Radial	Hoop joint	Cable adjustment,* in., for—			
		Cord 1	Cord 2	Cord 3	Cord 4
1	19	−0.043	−0.011	−0.006	−0.017
2	18	−0.026	−0.015	0.014	0.007
3	17	−0.046	−0.001	−0.007	−0.019
4	16	0.020	0.025	0.012	0.000
5	15	−0.021	−0.040	0.002	0.014
6	14	−0.043	−0.026	−0.036	0.006
7	13	0.024	−0.039	−0.037	−0.012
8	12	−0.031	0.003	−0.022	0.004
9	11	−0.009	−0.034	−0.009	0.005
10	10	−0.001	0.001	0.004	−0.016
11	9	−0.013	−0.015	−0.004	−0.026
12	8	−0.005	0.016	−0.008	−0.010
13	7	−0.003	−0.022	0.034	−0.042
14	6	−0.012	−0.014	−0.029	0.000
15	5	−0.010	−0.025	−0.005	−0.012
16	4	−0.021	0.009	−0.028	−0.019
17	3	−0.002	0.012	0.031	−0.016
18	2	−0.016	−0.039	−0.038	0.004
19	1	−0.008	−0.015	−0.019	−0.024
20	24	−0.022	−0.050	−0.001	−0.023
21	23	−0.048	0.006	0.034	−0.012
22	22	−0.021	−0.021	−0.034	−0.006
23	21	−0.043	−0.006	−0.042	0.018
24	20	0.017	0.027	−0.021	0.014

*Minus value indicates cable pull.

Table 17. Actual Weighted Control Cable Adjustments

[33 cables]

Radial	Hoop joint	Cable adjustment,* in., for—			
		Cord 1	Cord 2	Cord 3	Cord 4
1	19	−0.059	0.000	0.000	0.000
2	18	−0.040	0.000	0.000	0.000
3	17	−0.046	0.000	0.000	0.000
4	16	0.000	0.024	0.000	0.000
5	15	−0.049	0.000	0.000	0.000
6	14	−0.040	−0.022	−0.031	0.000
7	13	0.022	−0.051	−0.052	0.000
8	12	−0.026	0.000	0.000	0.000
9	11	0.000	−0.047	0.000	0.000
10	10	0.000	0.000	0.000	0.000
11	9	0.000	0.000	0.000	−0.033
12	8	0.000	0.000	0.000	0.000
13	7	0.000	−0.030	0.037	−0.045
14	6	0.000	0.000	−0.034	0.000
15	5	0.000	−0.039	0.000	0.000
16	4	0.000	0.000	−0.054	0.000
17	3	0.000	0.000	0.000	0.000
18	2	0.000	−0.040	−0.033	0.000
19	1	0.000	0.000	0.000	−0.032
20	24	−0.019	−0.054	0.000	−0.026
21	23	−0.046	0.000	0.023	0.000
22	22	−0.021	−0.025	−0.047	0.000
23	21	−0.037	0.000	0.000	0.000
24	20	0.000	0.032	0.000	0.000

*Minus value indicates cable pull.

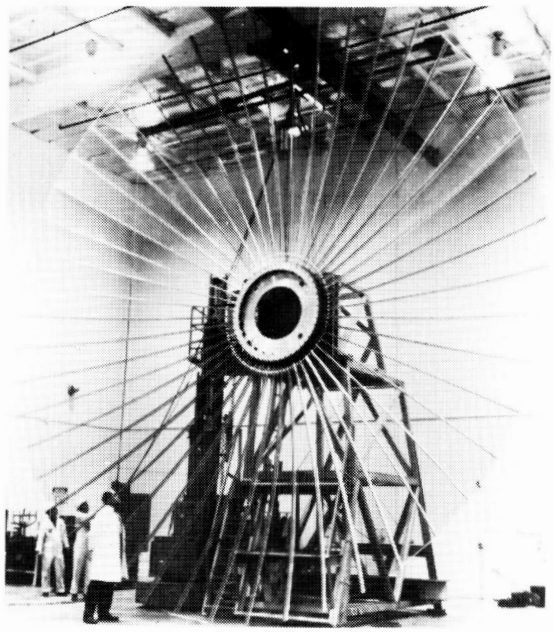

(a) Wrap rib.

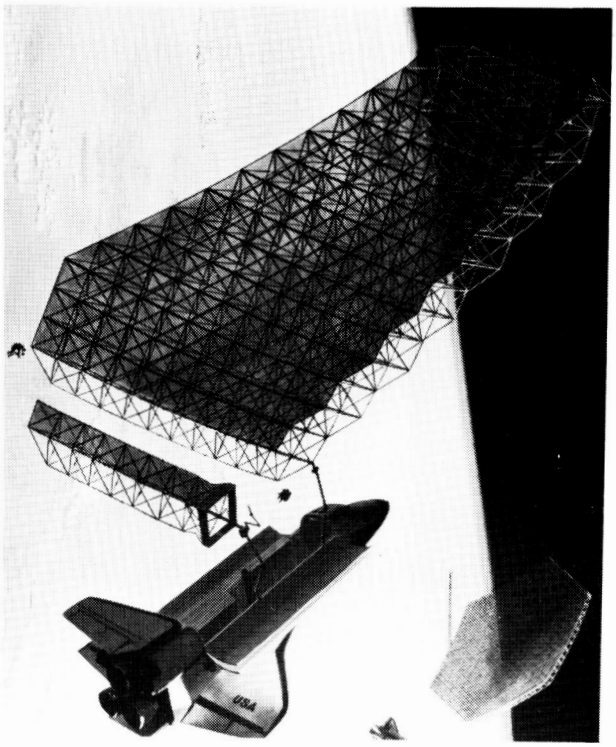

(b) Tetrahedral truss.

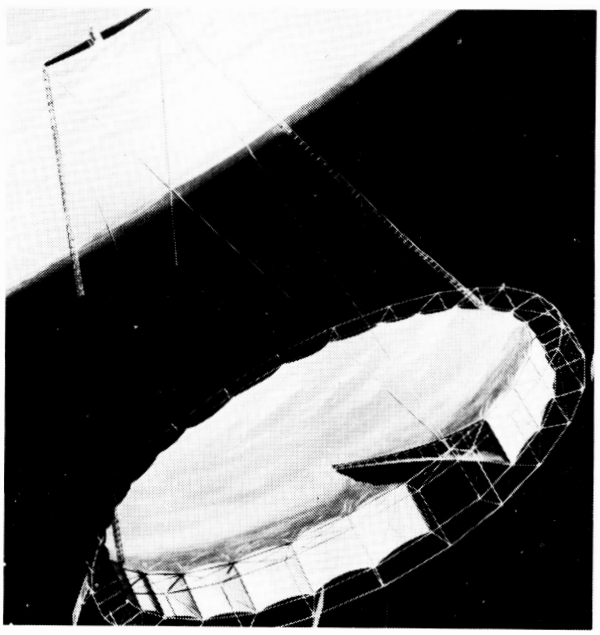

(c) Box truss.

Figure 1. Examples of some large scale deployable antenna concepts.

L-89-21

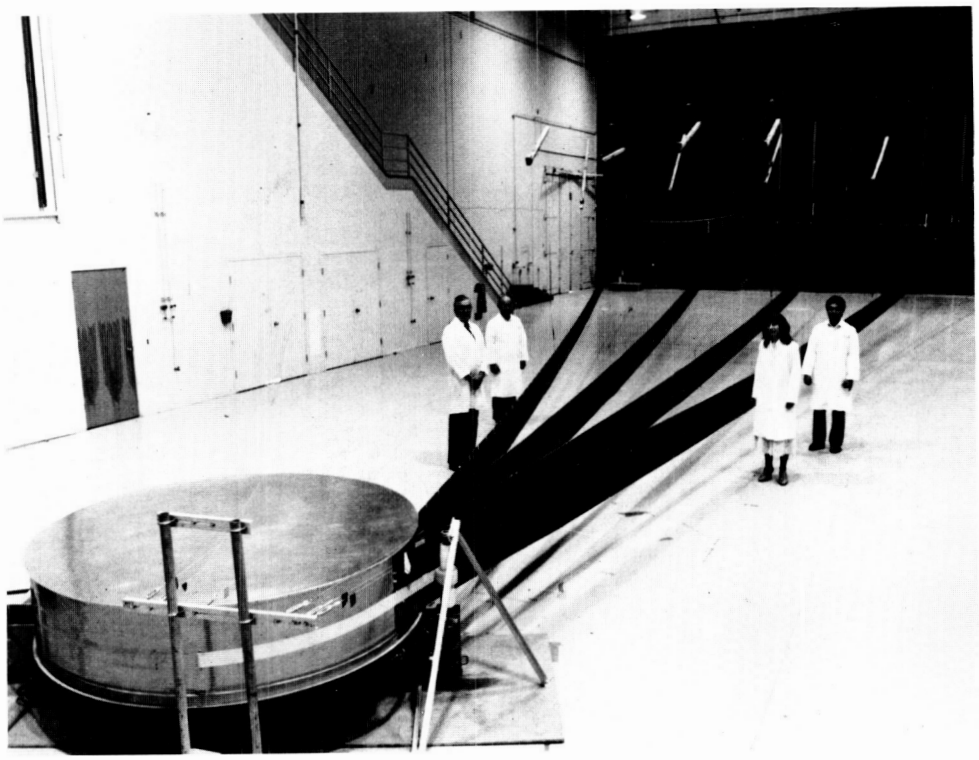

(a) Three-gore section of wrap rib.

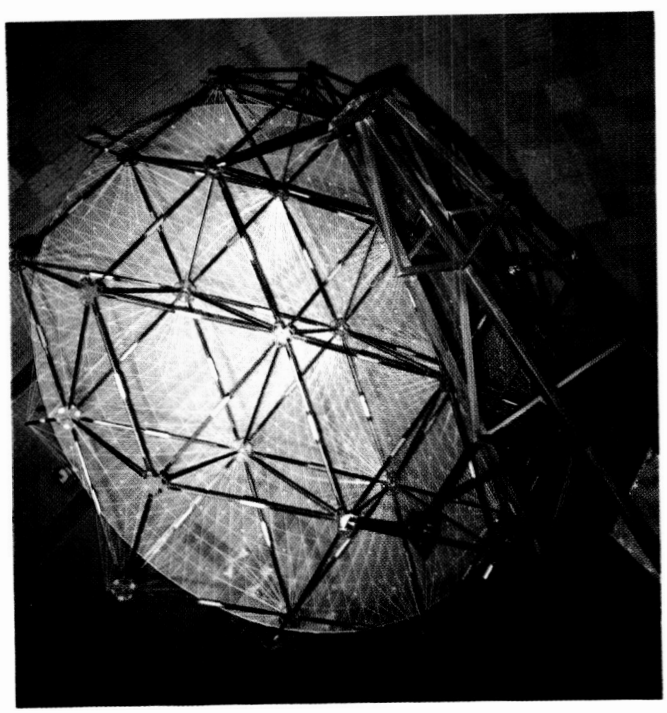

(b) 5-m model of tetrahedral truss.

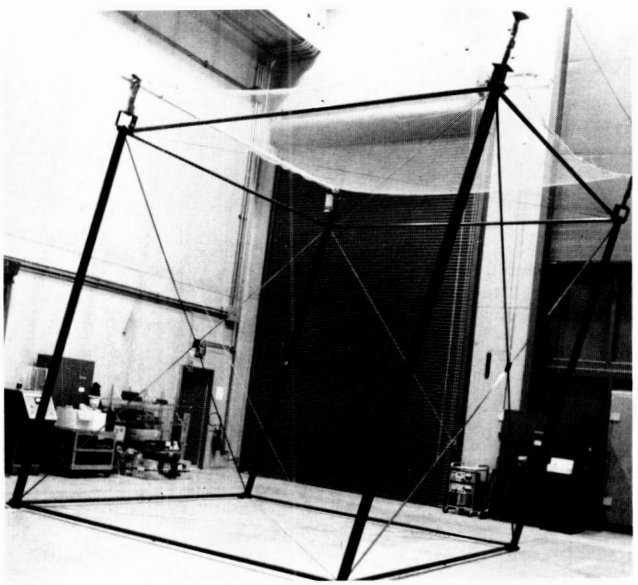

(c) 5-m model of box truss.

Figure 2. Models of some large scale deployable antenna concepts.

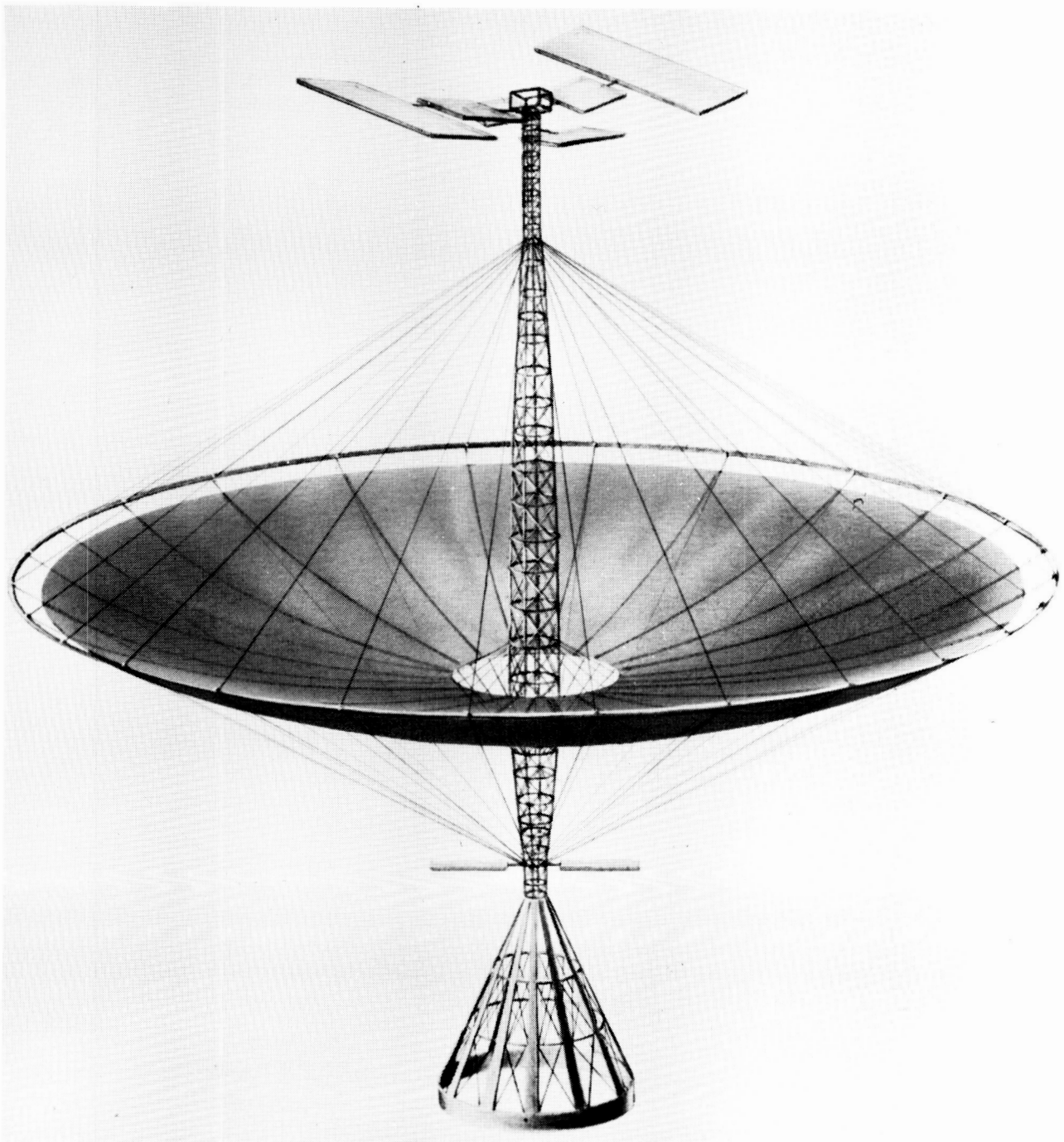

L-89-22

Figure 3. Hoop-column deployable antenna concept designed in Advanced Applications Flight Experiments Program.

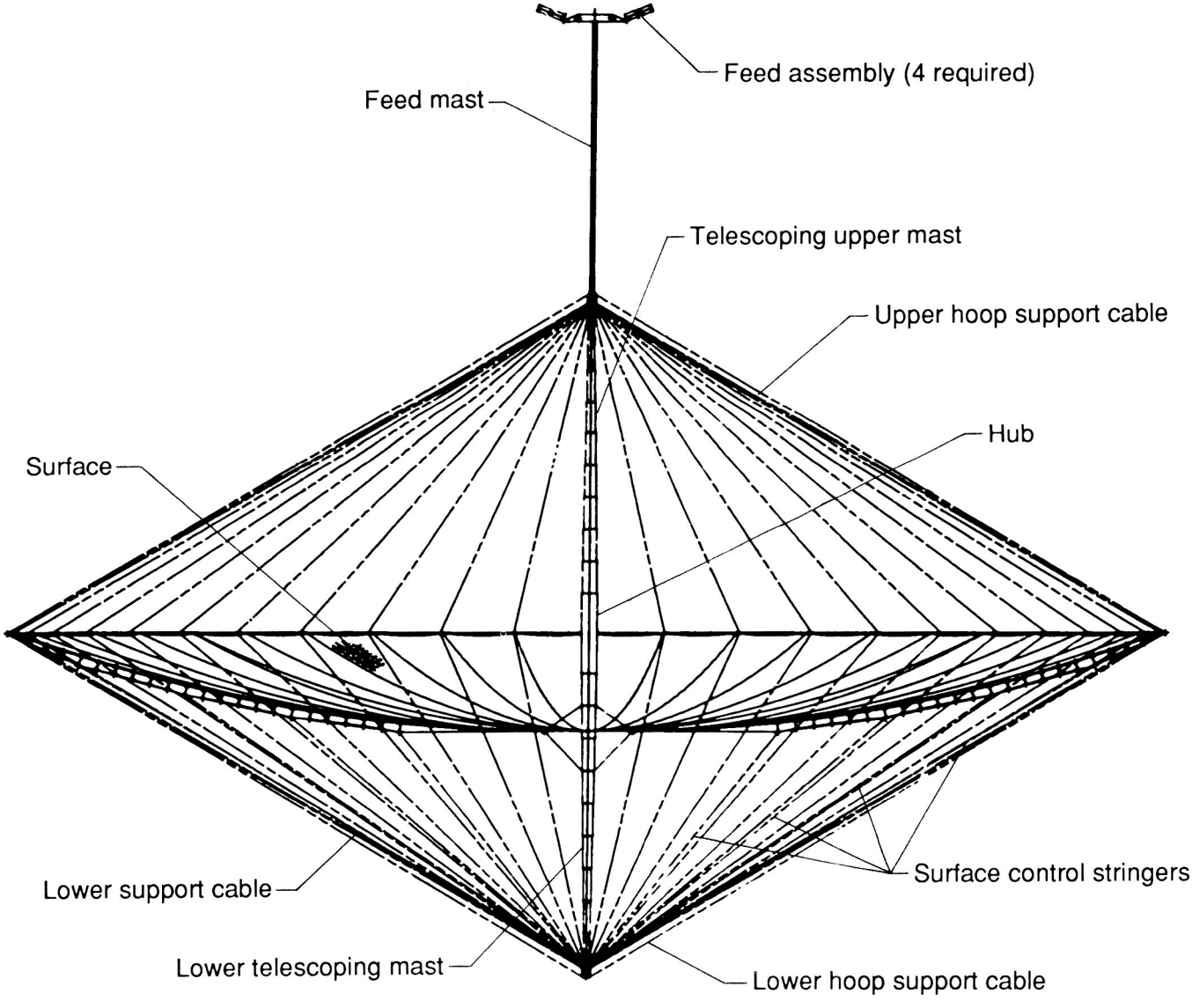

Figure 4. Design of 100-m-diameter hoop-column antenna.

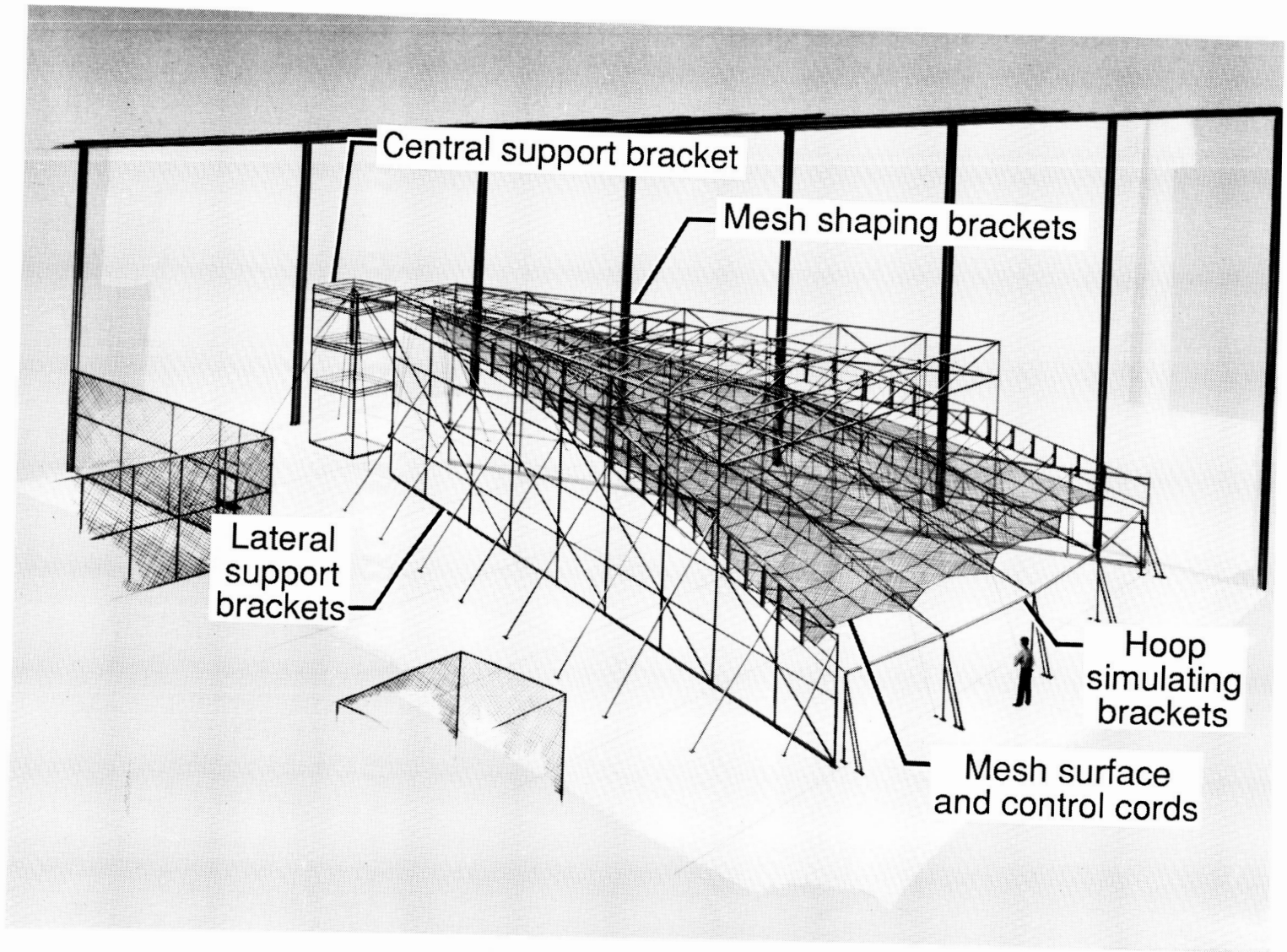

Figure 5. Hoop-column antenna model (four gores, 50-m diameter). L-89-23

L-89-24

Figure 6. Deployable 15-m model of hoop-column antenna.

ORIGINAL PAGE
COLOR PHOTOGRAPH

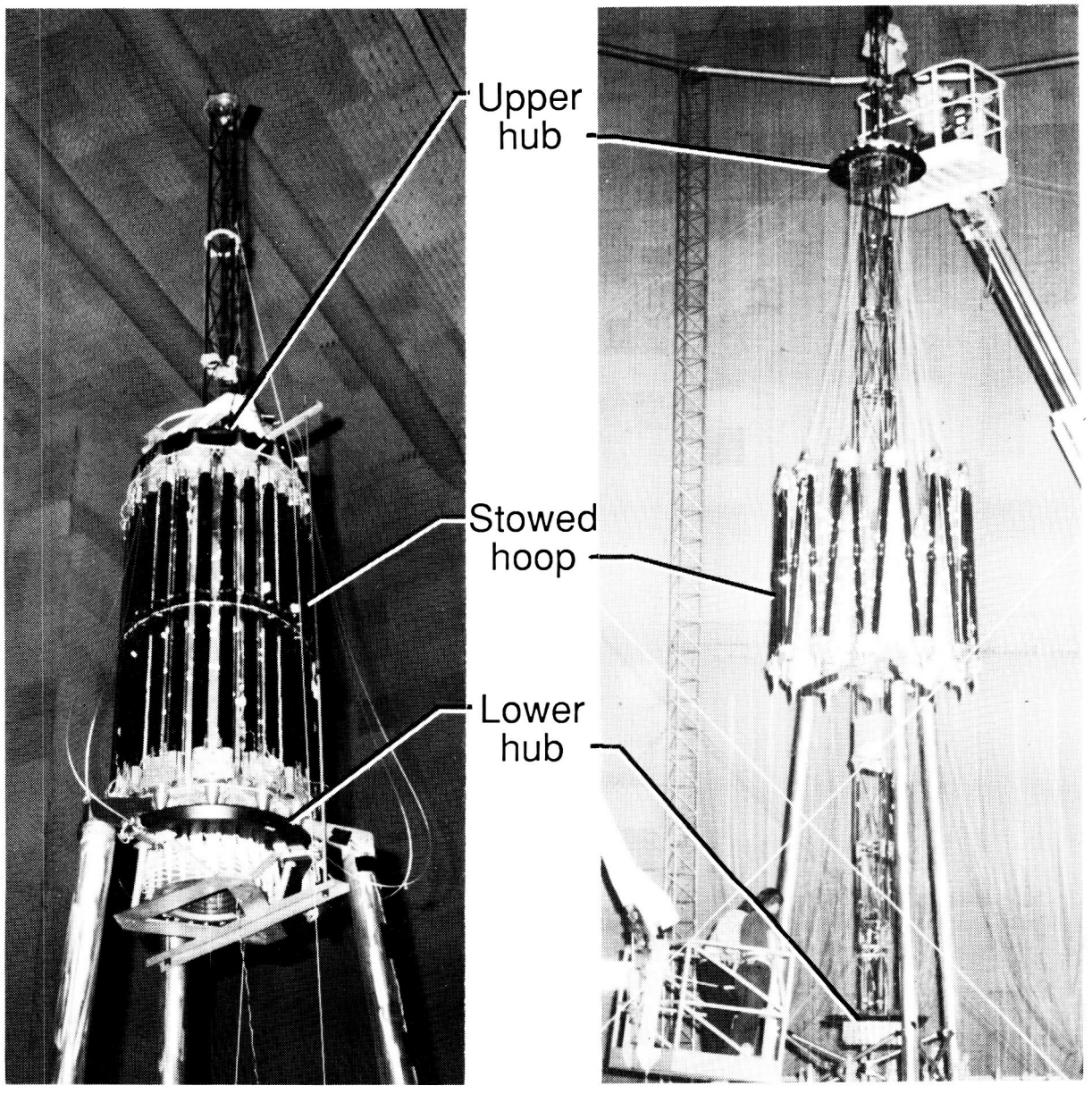

(a) Stowed configuration.

(b) Column extension.

L-89-25

Figure 7. Sequence showing deployment of 15-m hoop-column antenna.

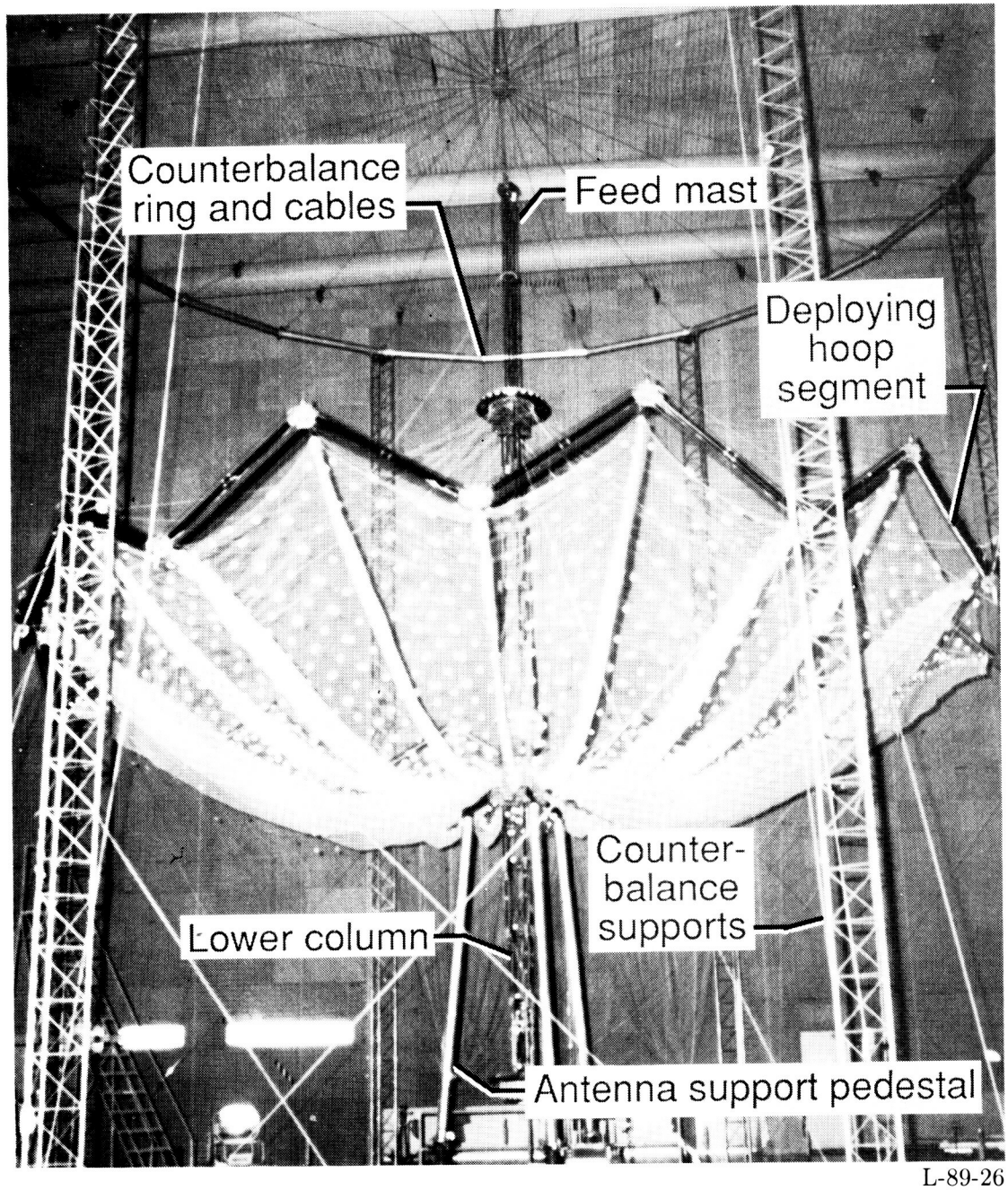

L-89-26

(c) Hoop partial deployment.

Figure 7. Continued.

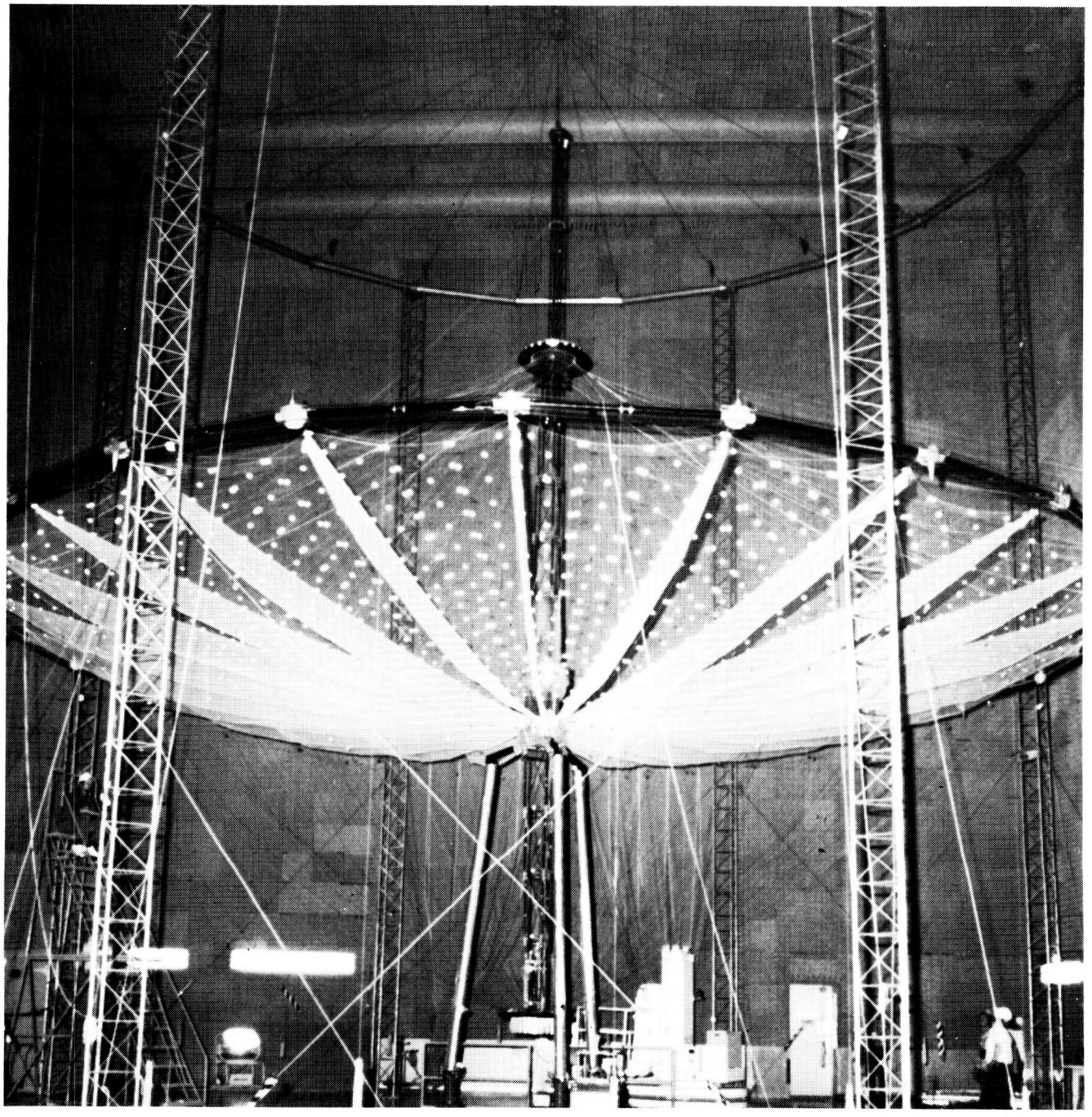

L-89-27

(d) Hoop full deployment.

Figure 7. Concluded.

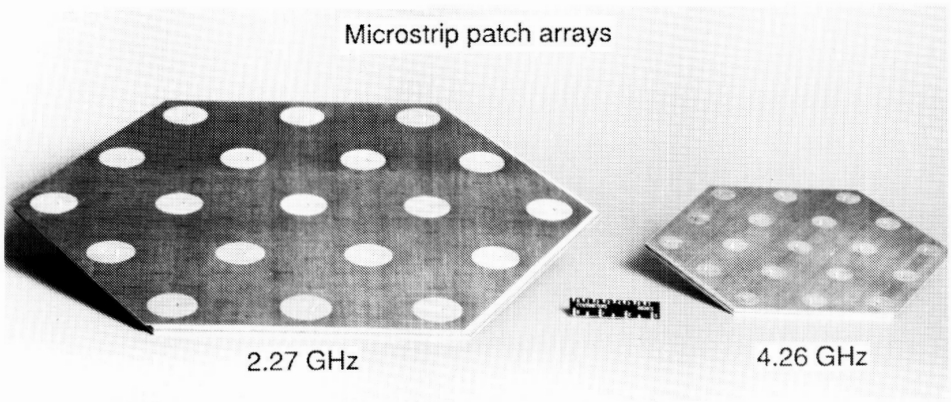

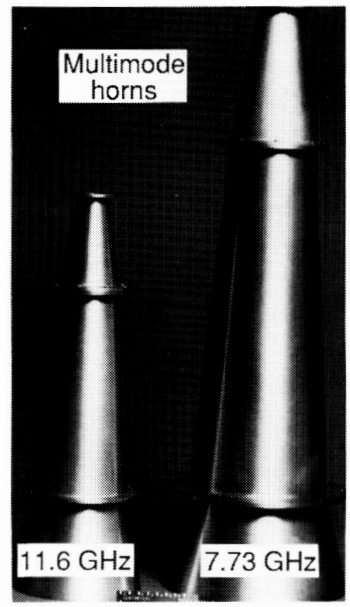

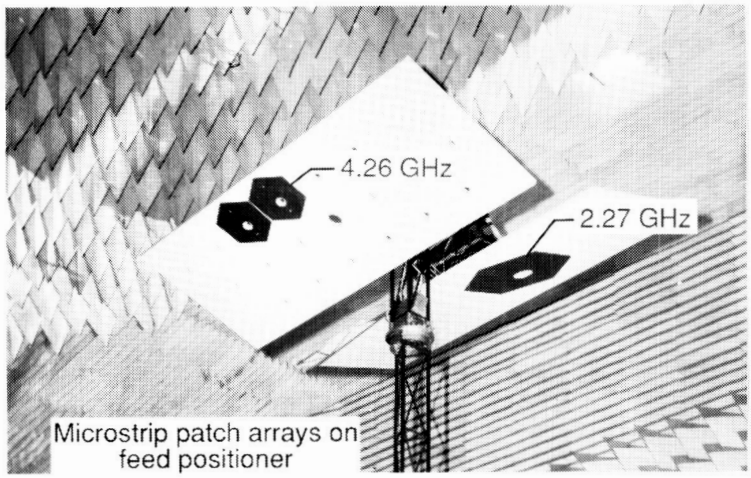

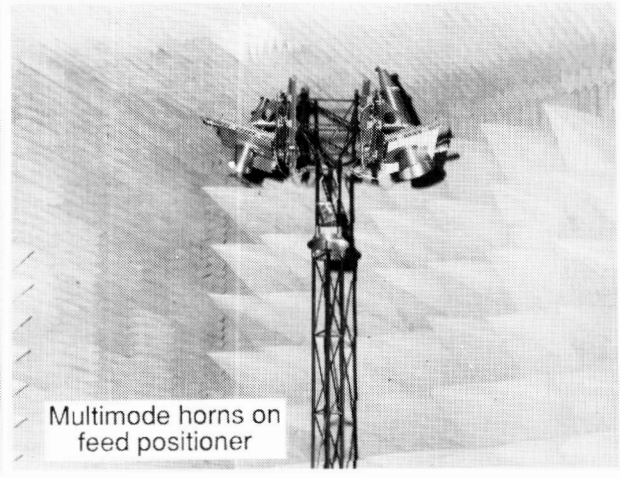

L-89-28

Figure 10. LaRC antenna feeds used for 15-m antenna.

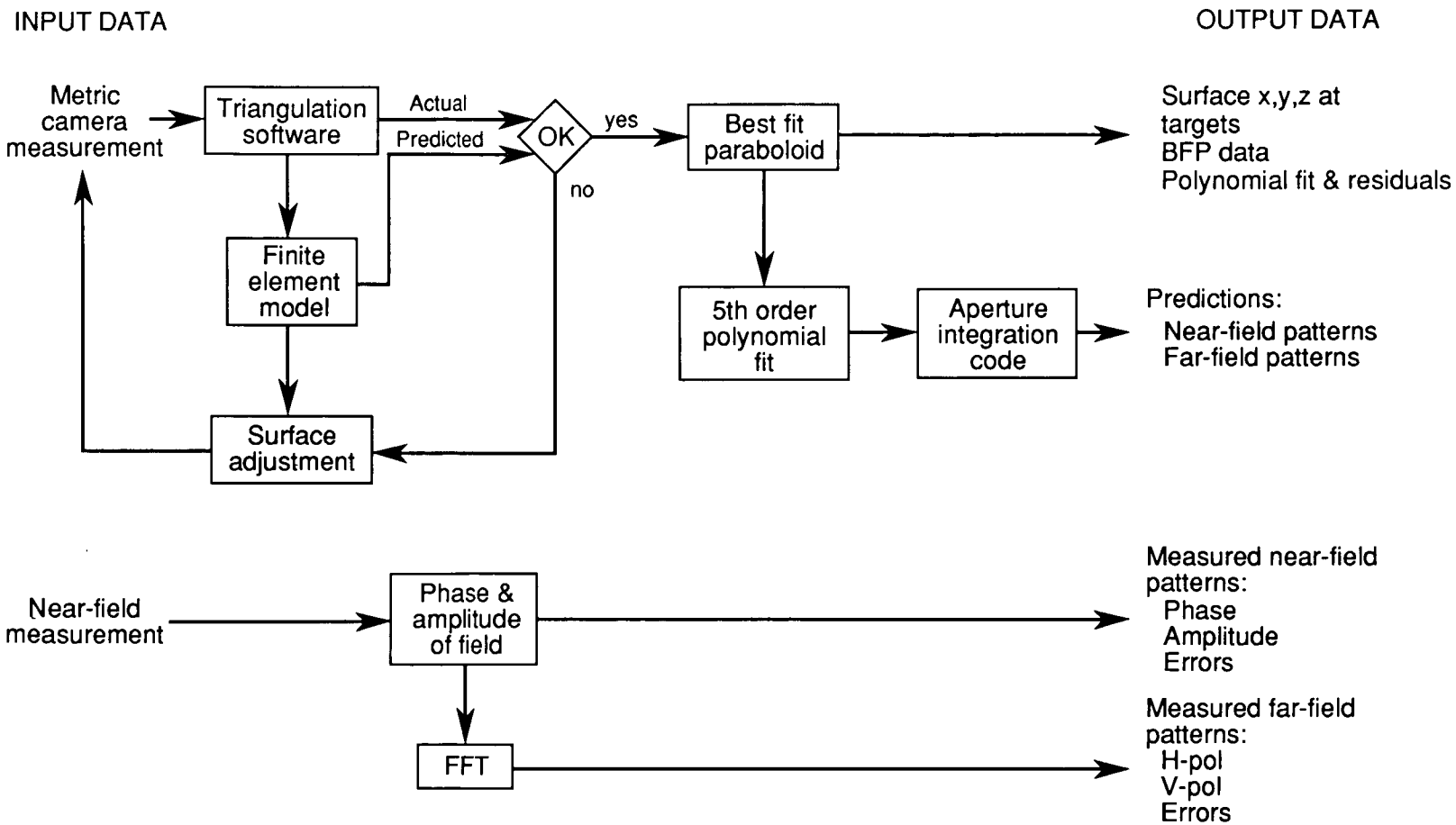

Figure 11. Plan for assessing the RF performance of 15-m hoop-column antenna.

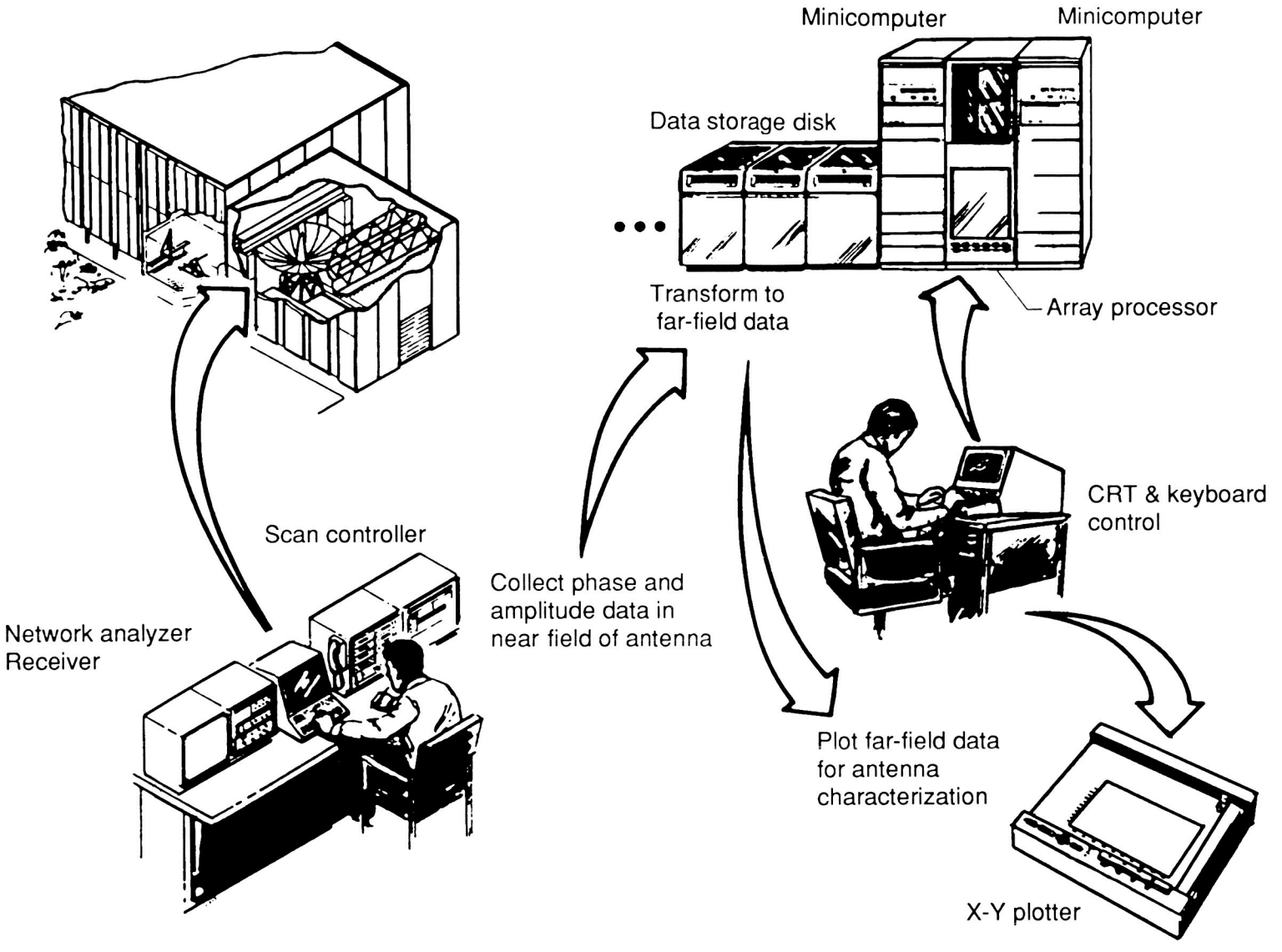

Figure 12. Near-field test facility at MMA.

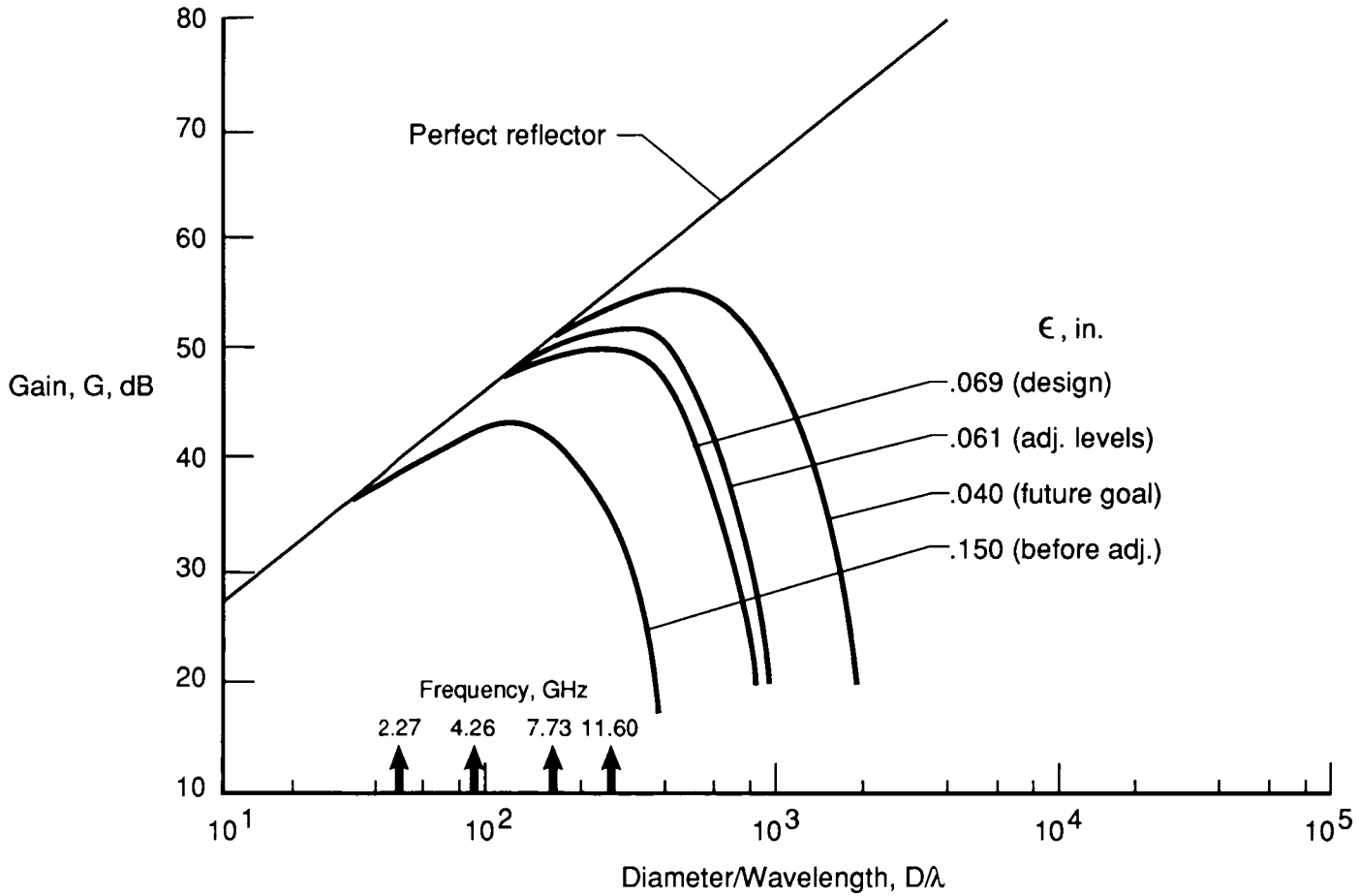

Figure 13. Rationale for frequency range for testing 15-m hoop-column antenna; $D = 6.09$ m; $\eta = 40$ percent.

15-meter hoop-column near-field tests
Schedule of activities (1985)

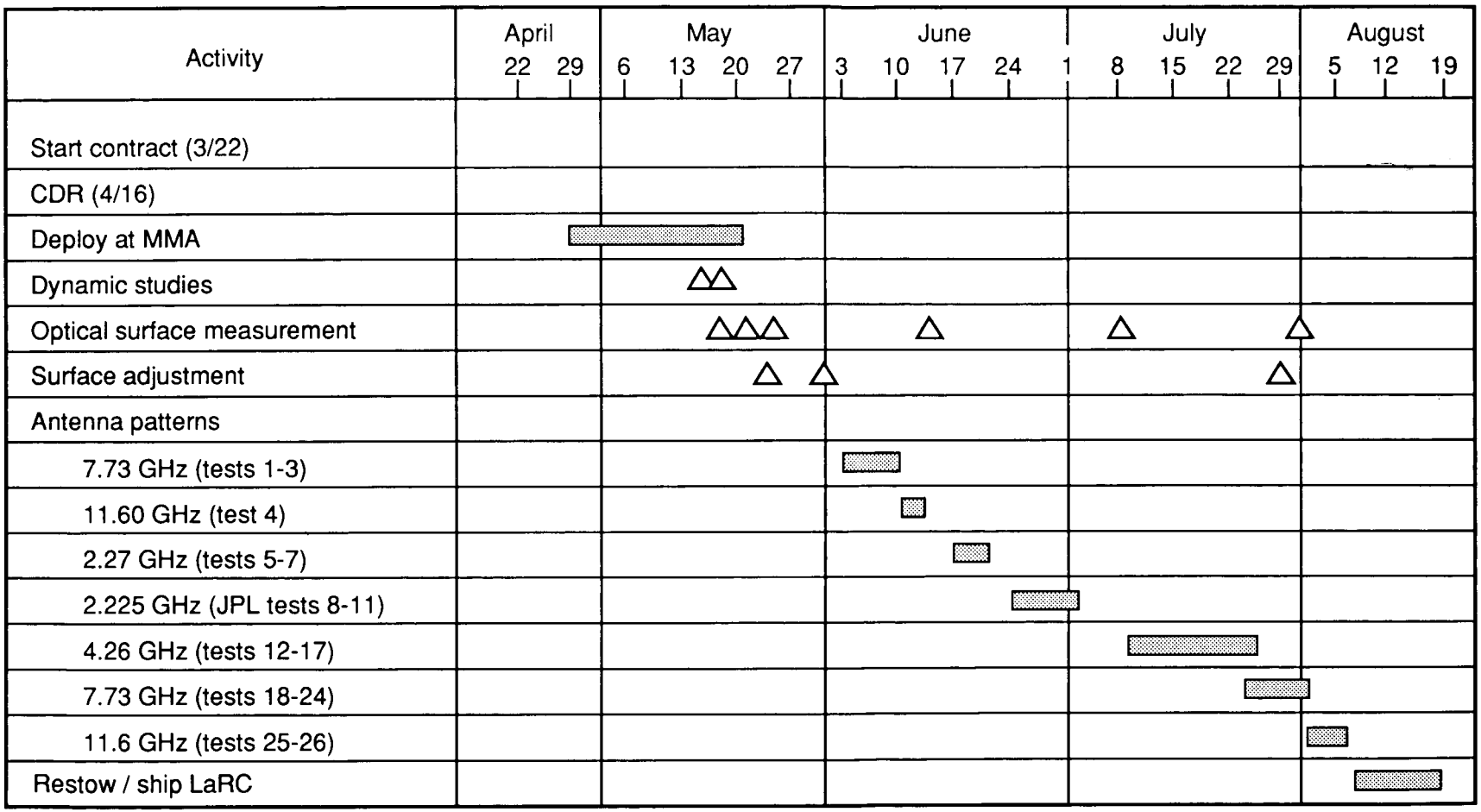

Figure 14. Sequence of activities during near-field test program of 15-m hoop-column antenna.

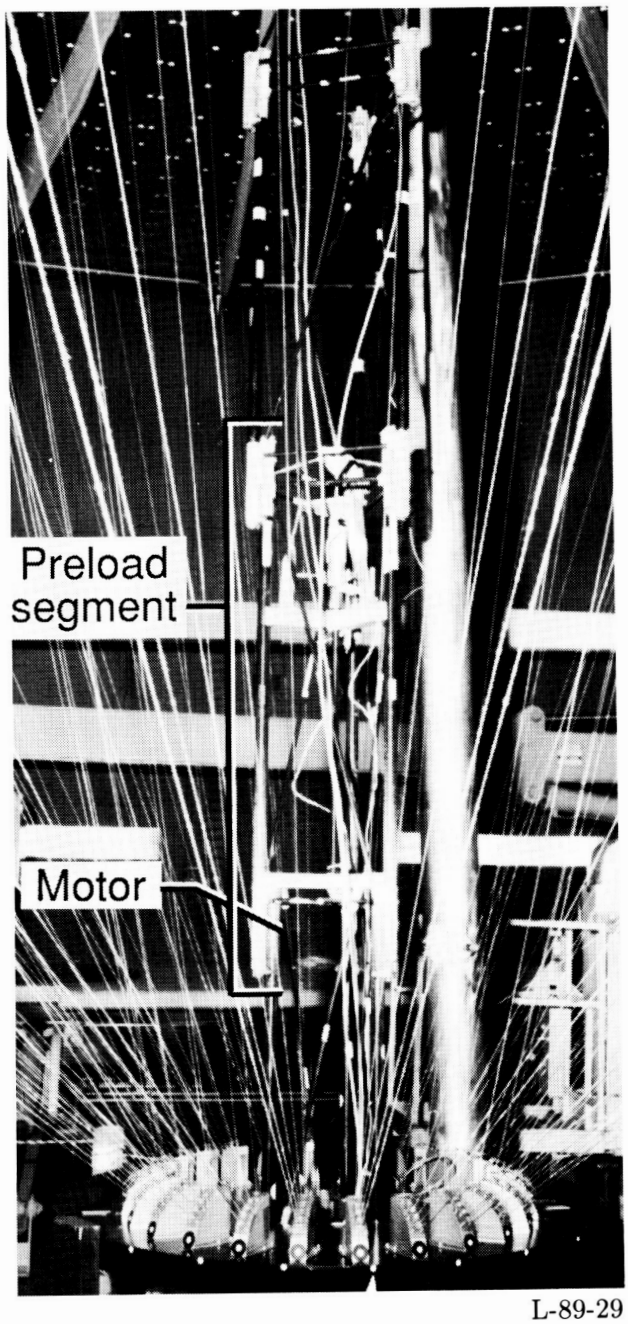

L-89-29

Figure 15. Preload segment of 15-m hoop-column antenna.

L-89-30

(a) Photograph showing misalignment.

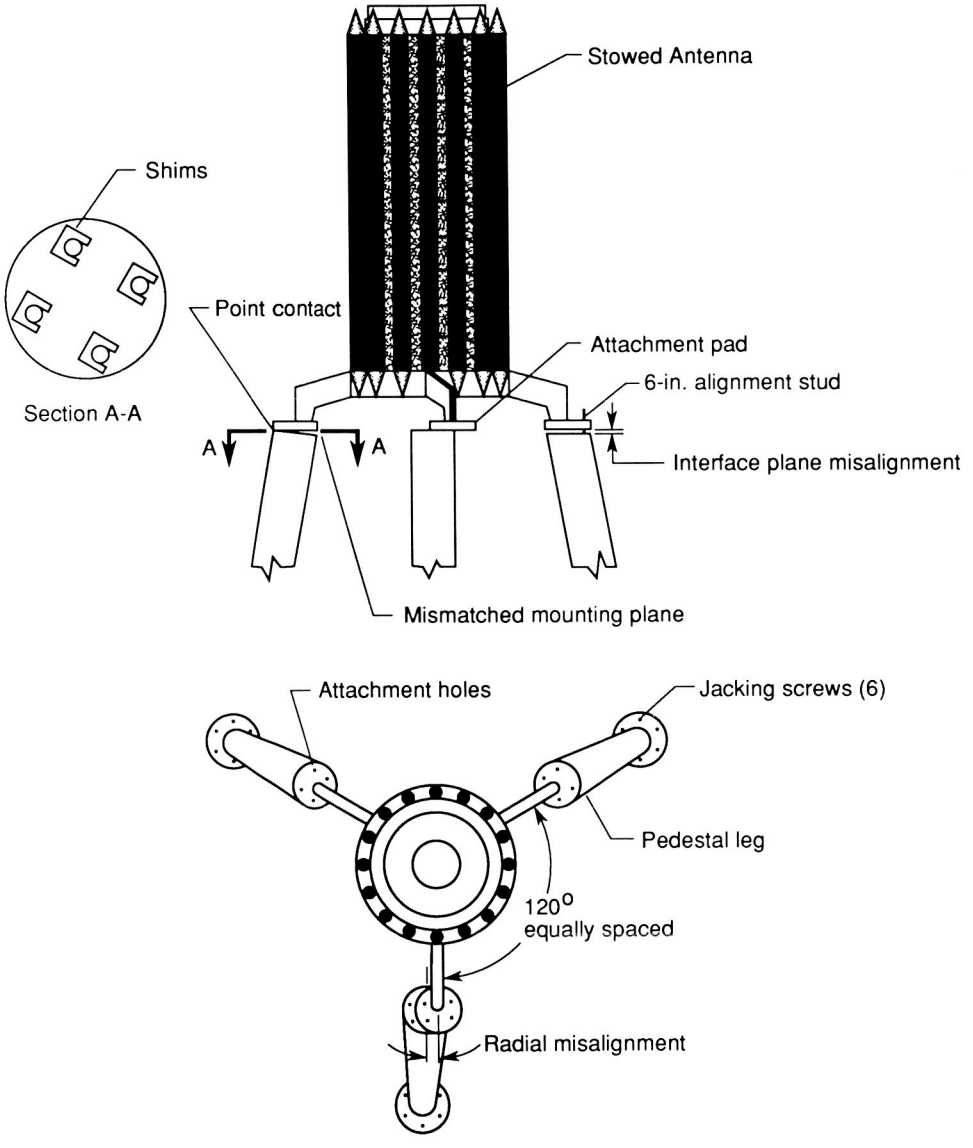

(b) Schematic of misalignment and solution.

Figure 16. Attachment pad misalignment during installation.

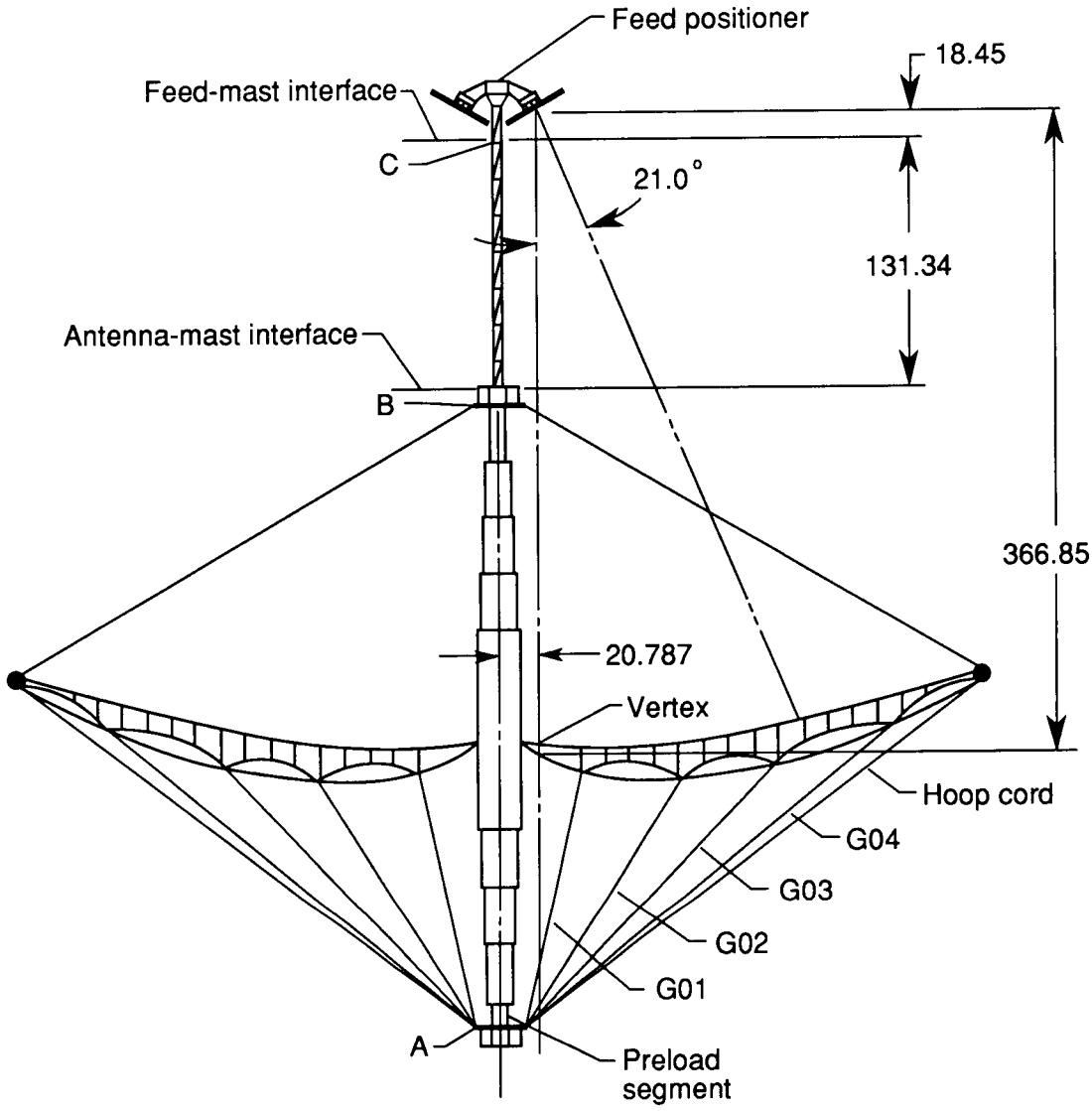

(a) Vertical alignment tolerance measurement points. Linear dimensions are in inches.

Figure 17. Alignment of antenna at MMA Near-Field Facility.

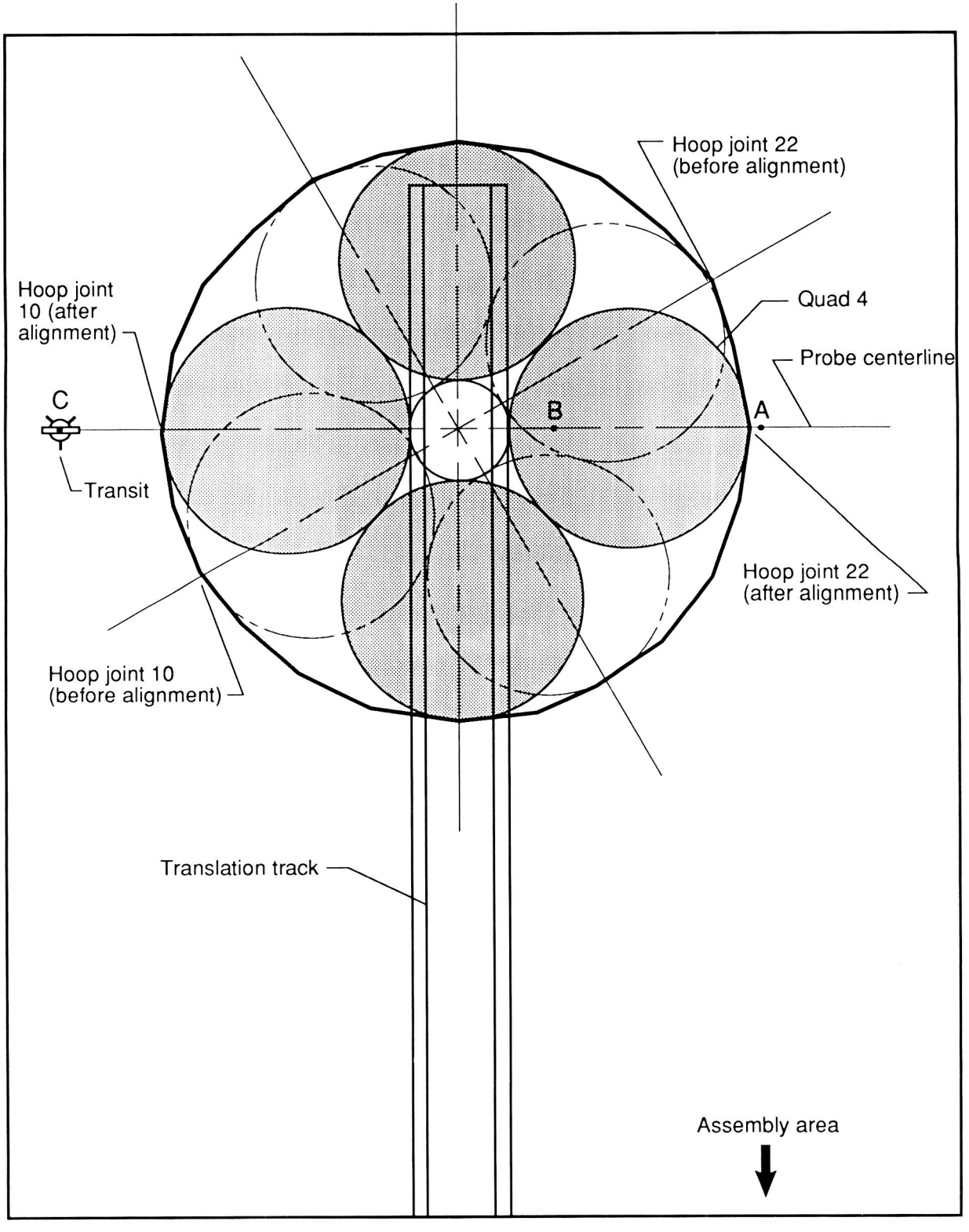

(b) Rotational alignment of antenna.

Figure 17. Concluded.

Figure 18. Hoop joint biases for 15-m antenna.

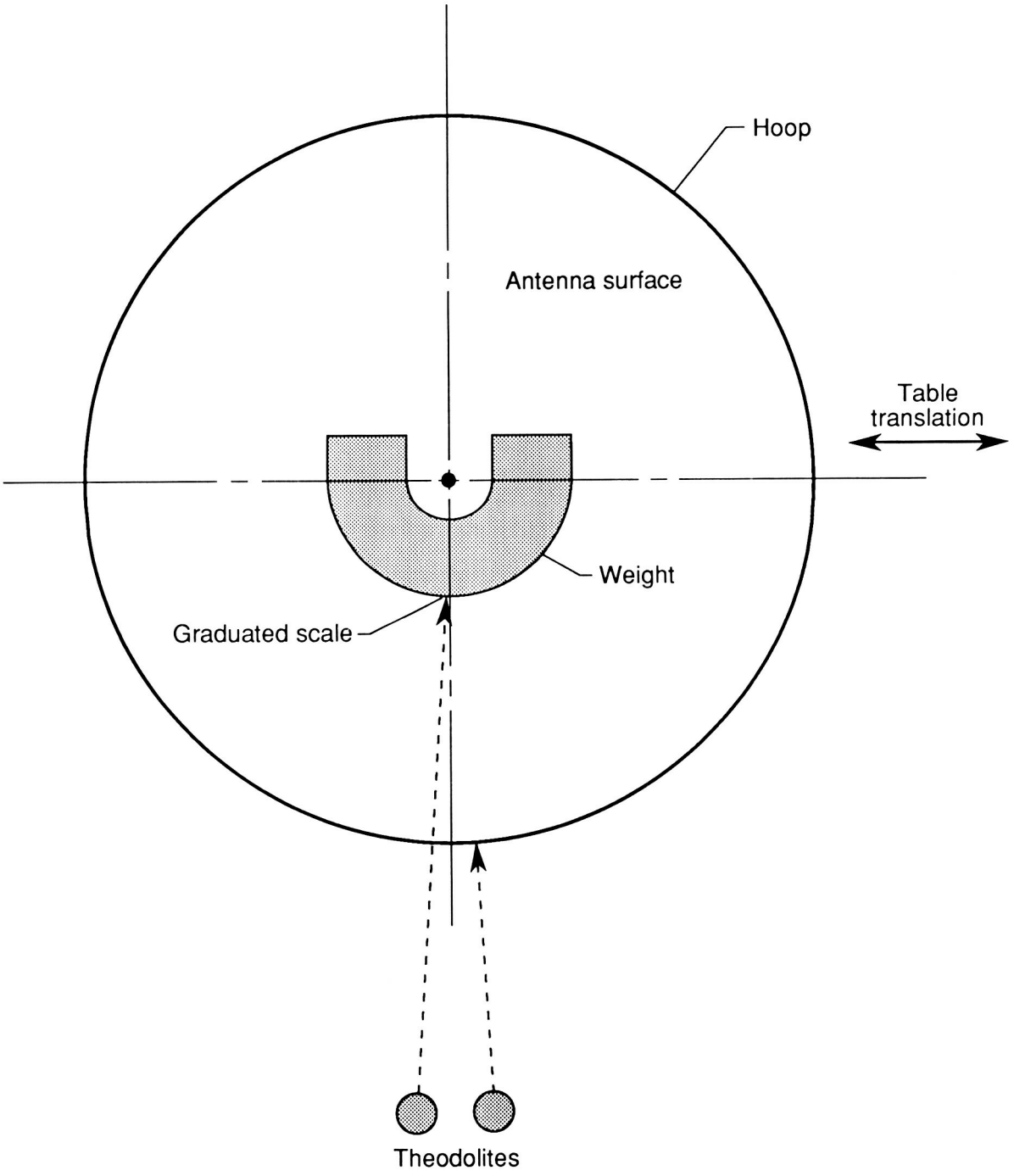

Figure 19. Proof test configuration for 15-m antenna.

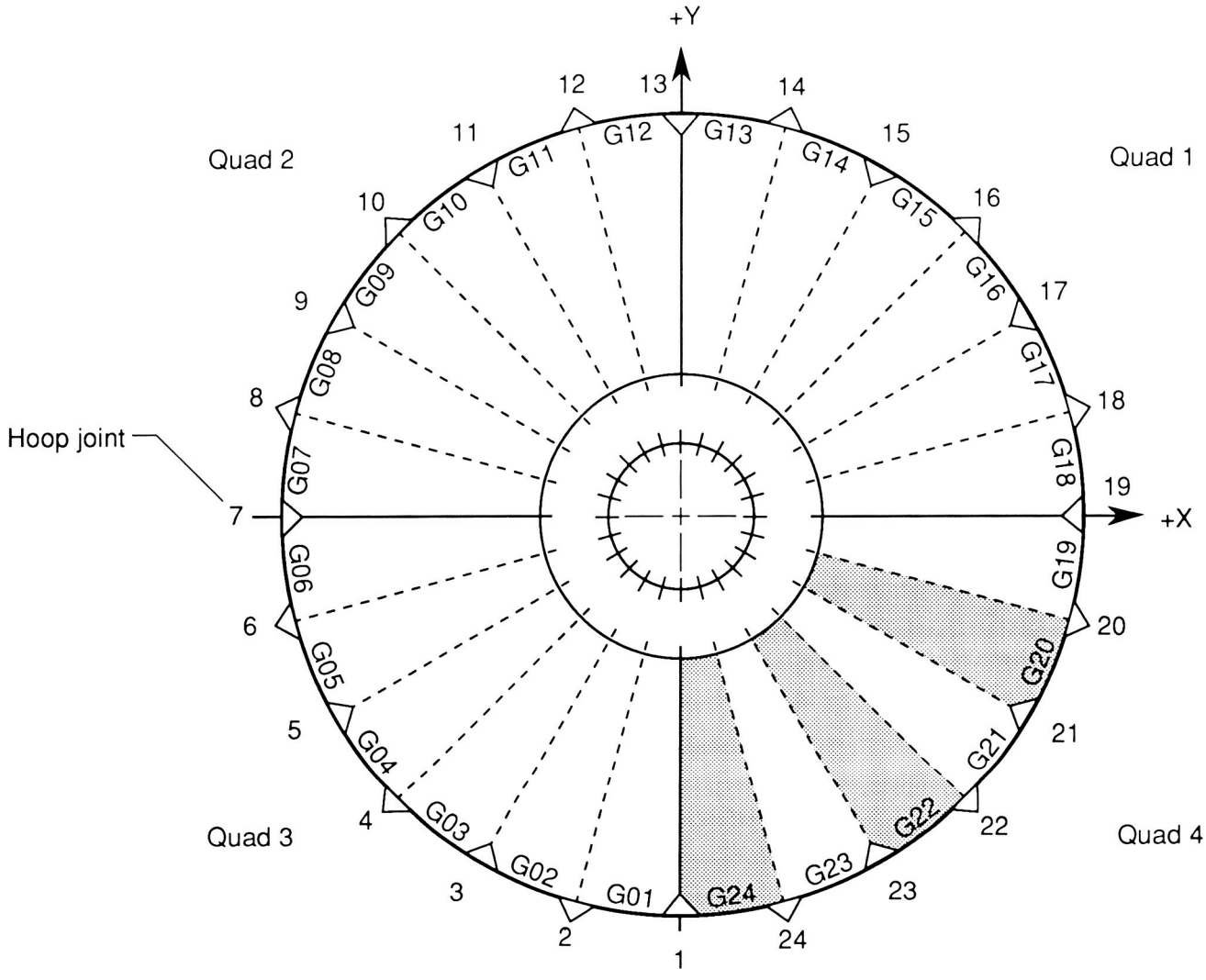

Figure 20. Schematic of 15-m antenna used for metric camera measurements.

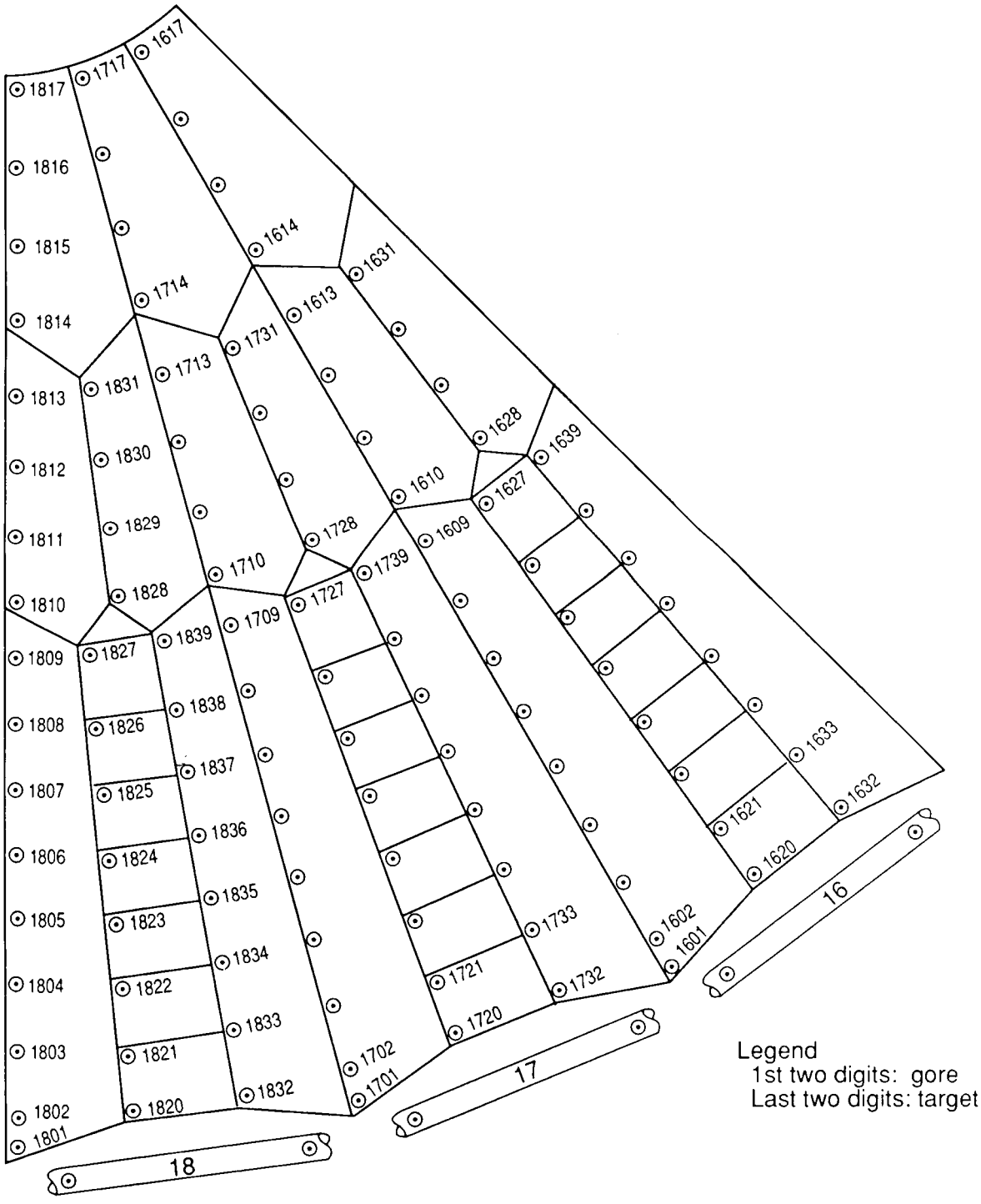

(a) Tie Points I set.

Figure 21. Metric camera targets.

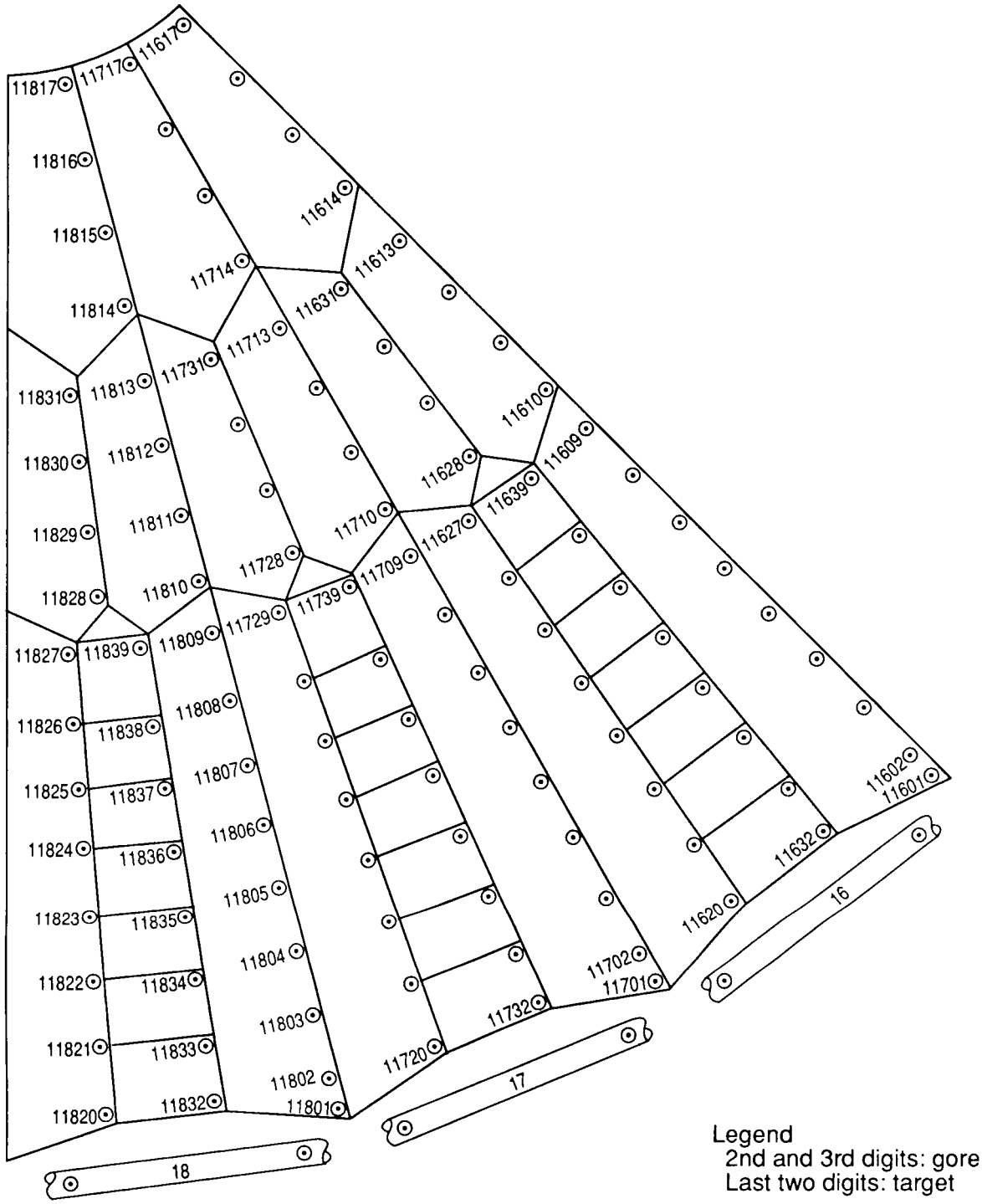

(b) Tie points II set.

Figure 21. Continued.

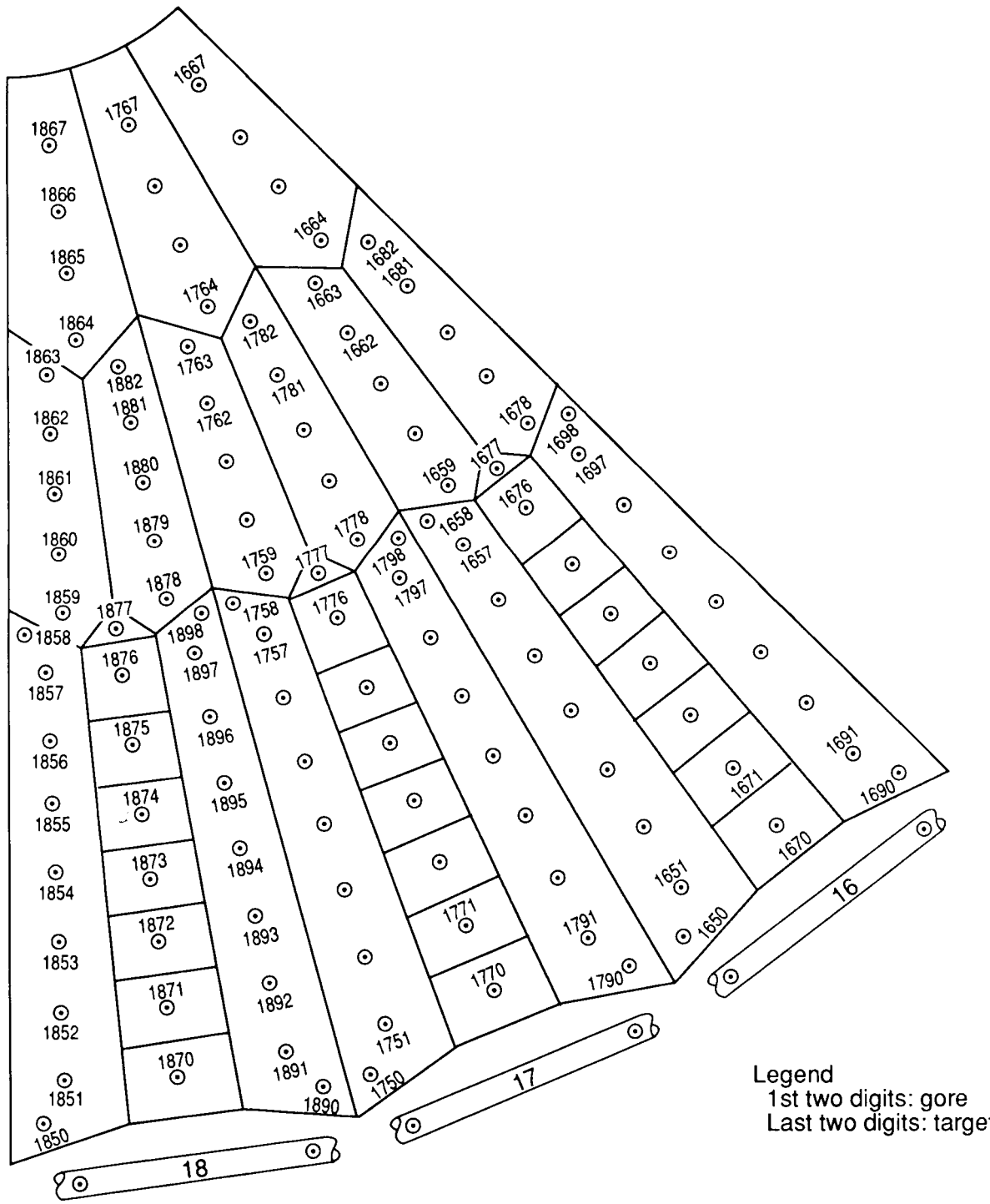

(c) Pillows I set.

Figure 21. Continued.

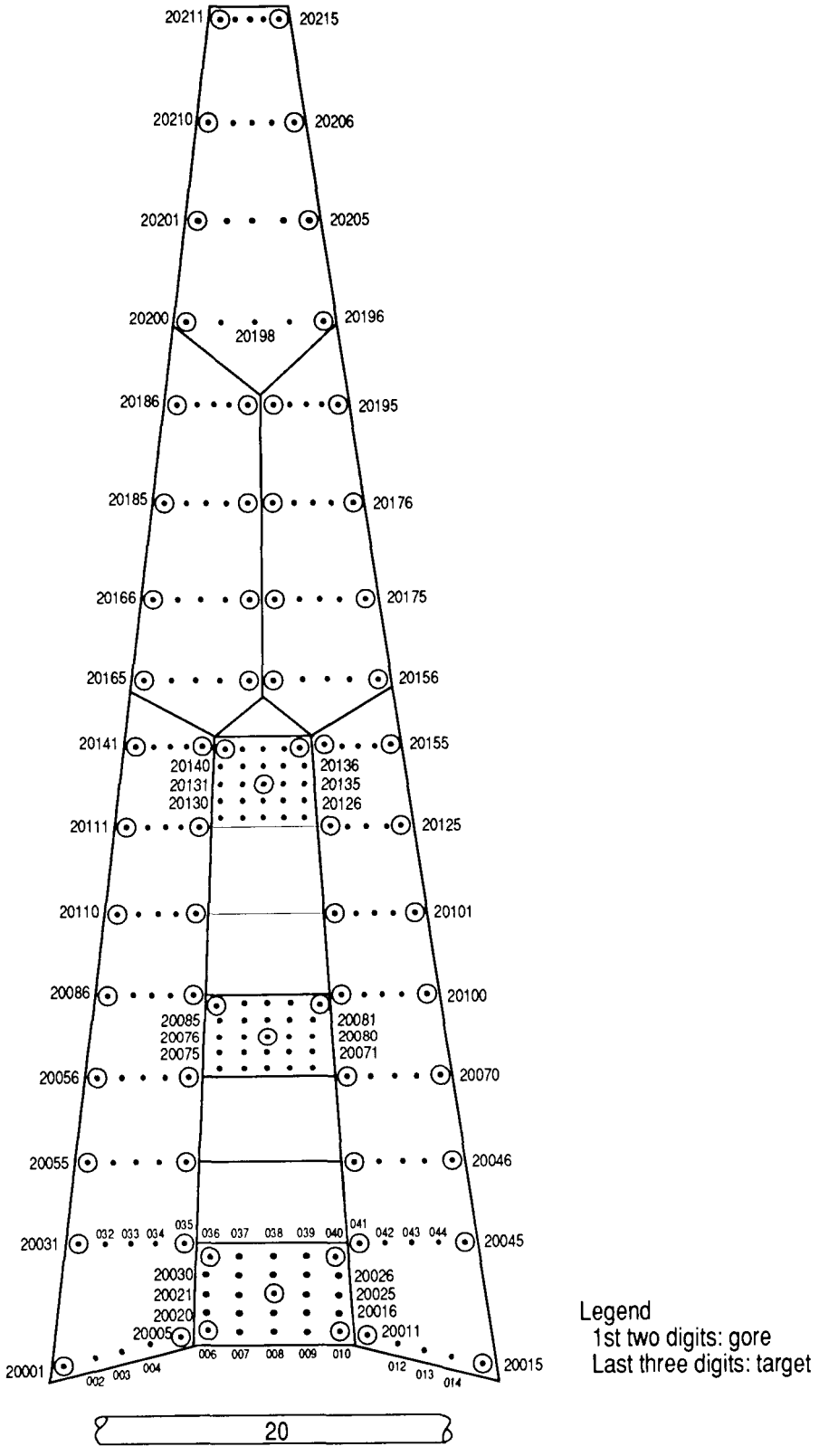

(d) Pillows II set. Only last three digits are given in some places.

Figure 21. Concluded.

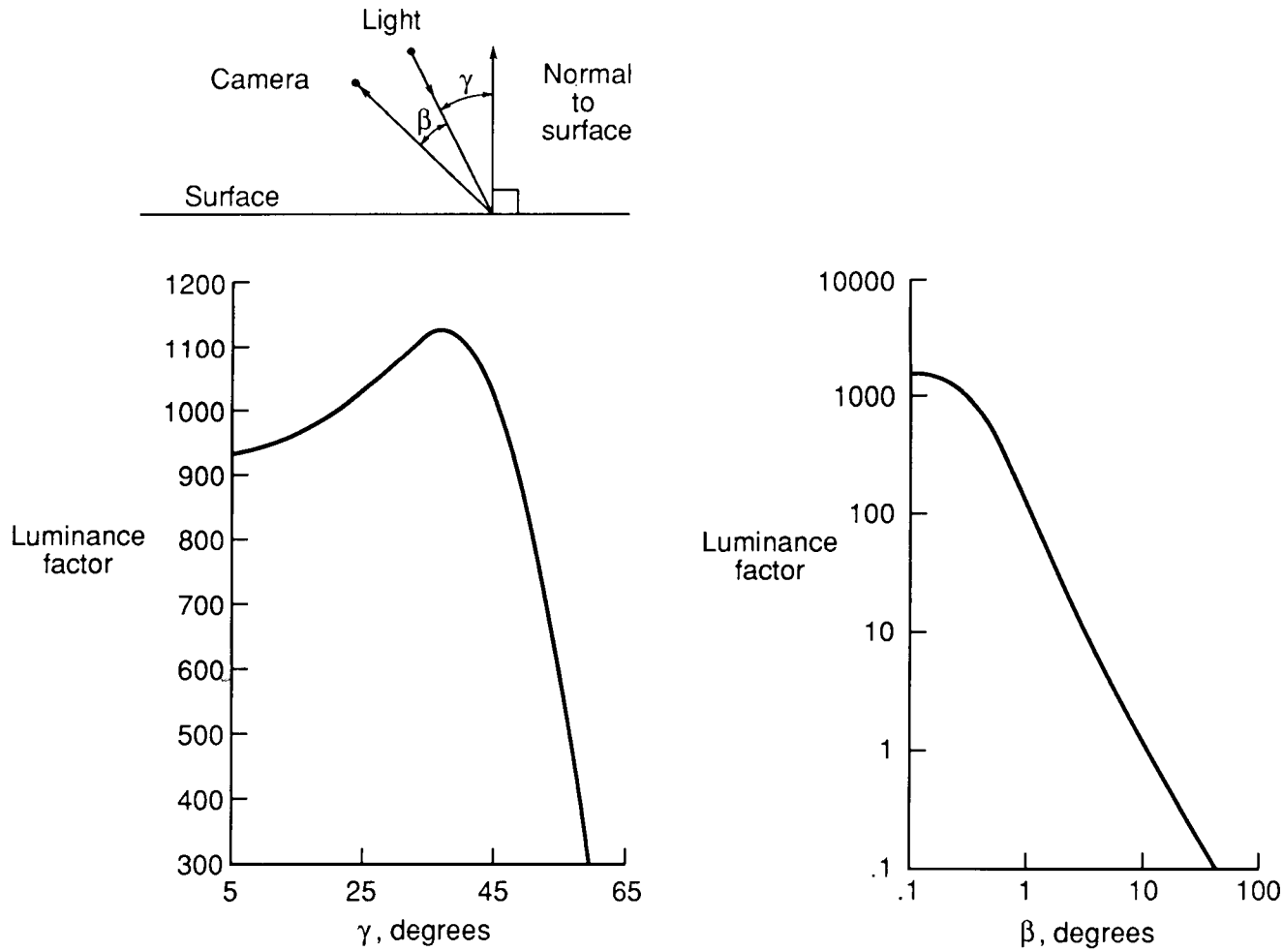

Figure 22. Luminance characteristics of retroreflective tape.

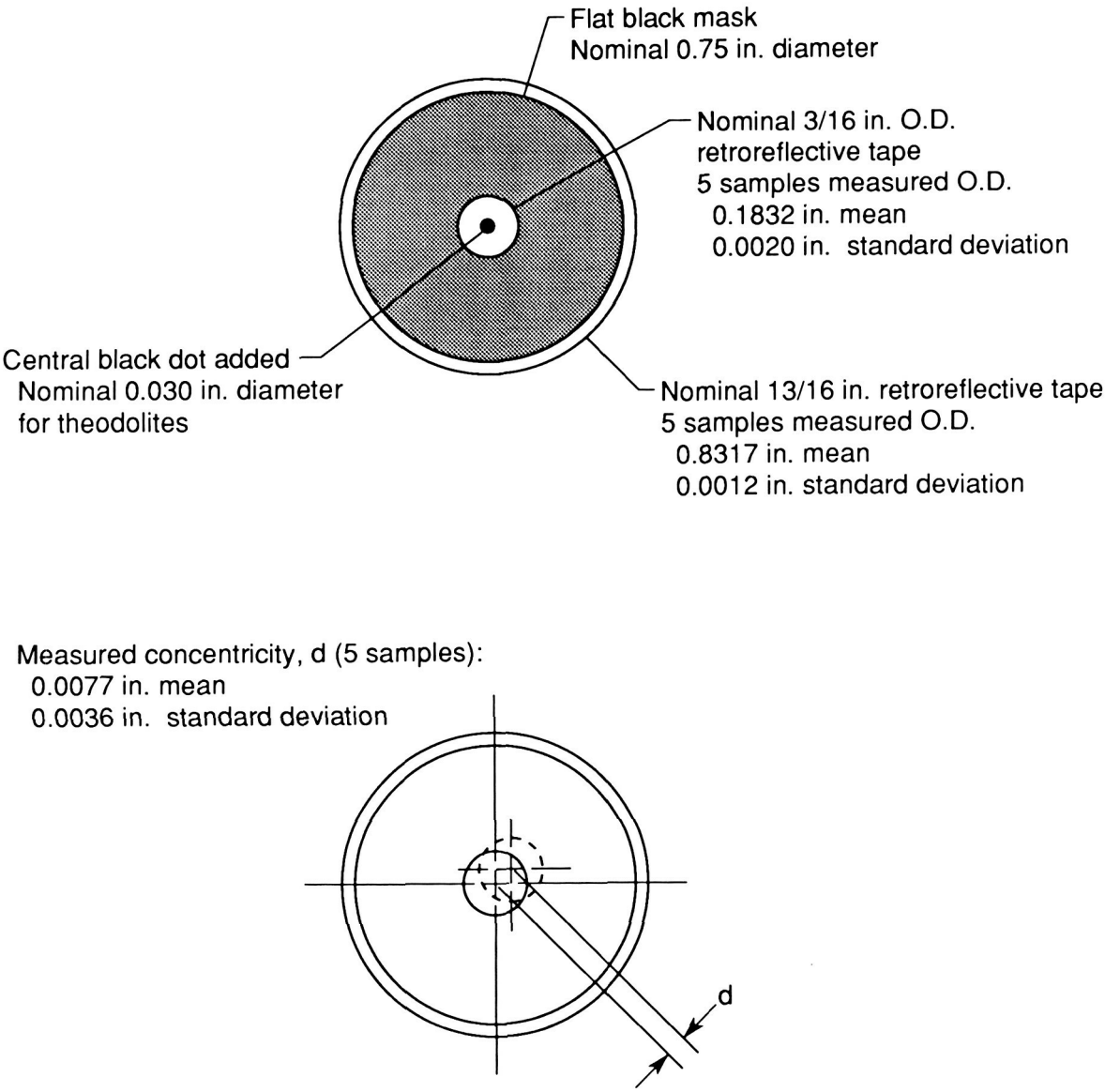

Figure 23. Retroreflective tape target fabrication details. All target materials were electrically nonconductive.

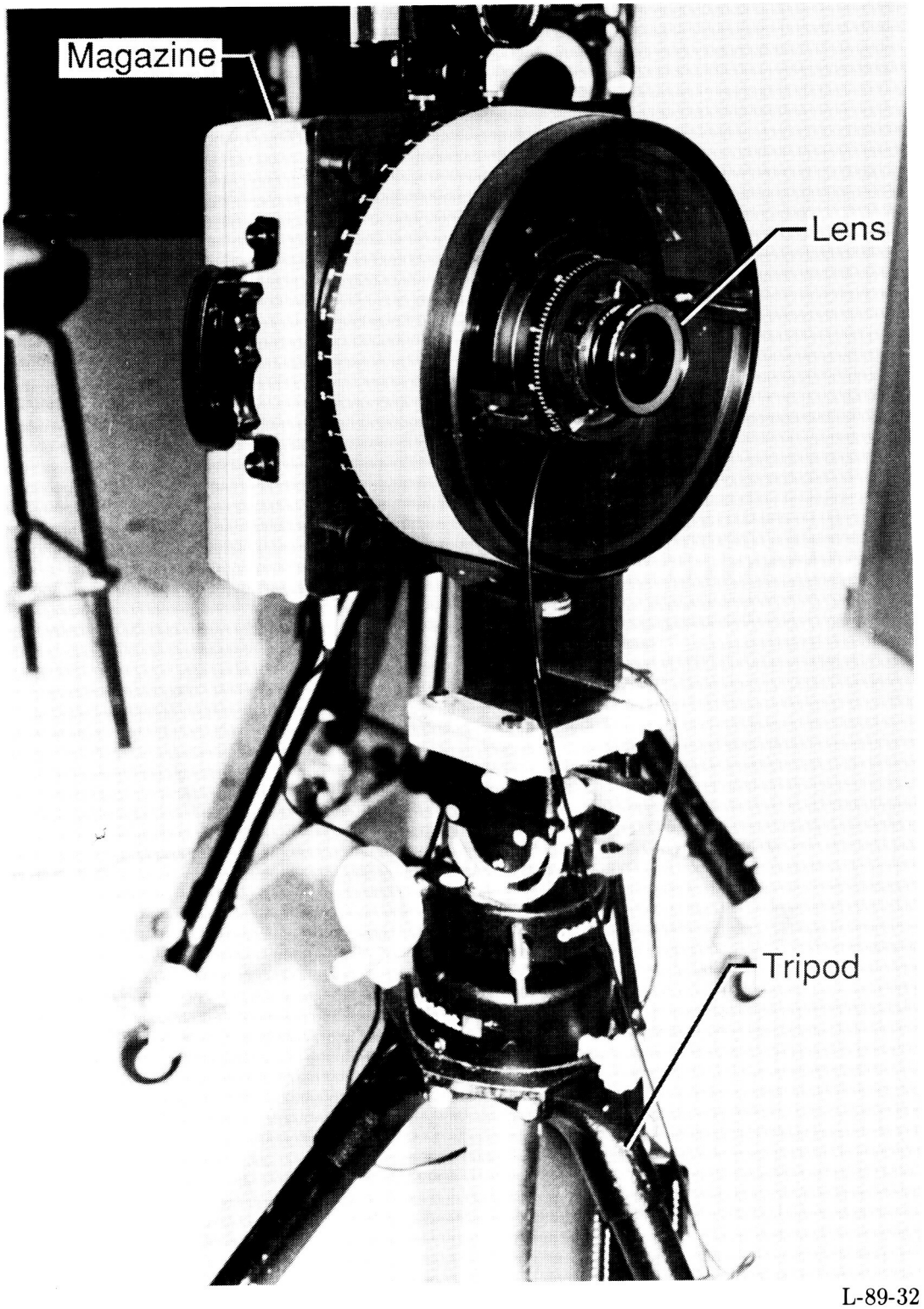

L-89-32

Figure 24. Metric camera.

ORIGINAL PAGE
BLACK AND WHITE PHOTOGRAPH

ORIGINAL PAGE
COLOR PHOTOGRAPH

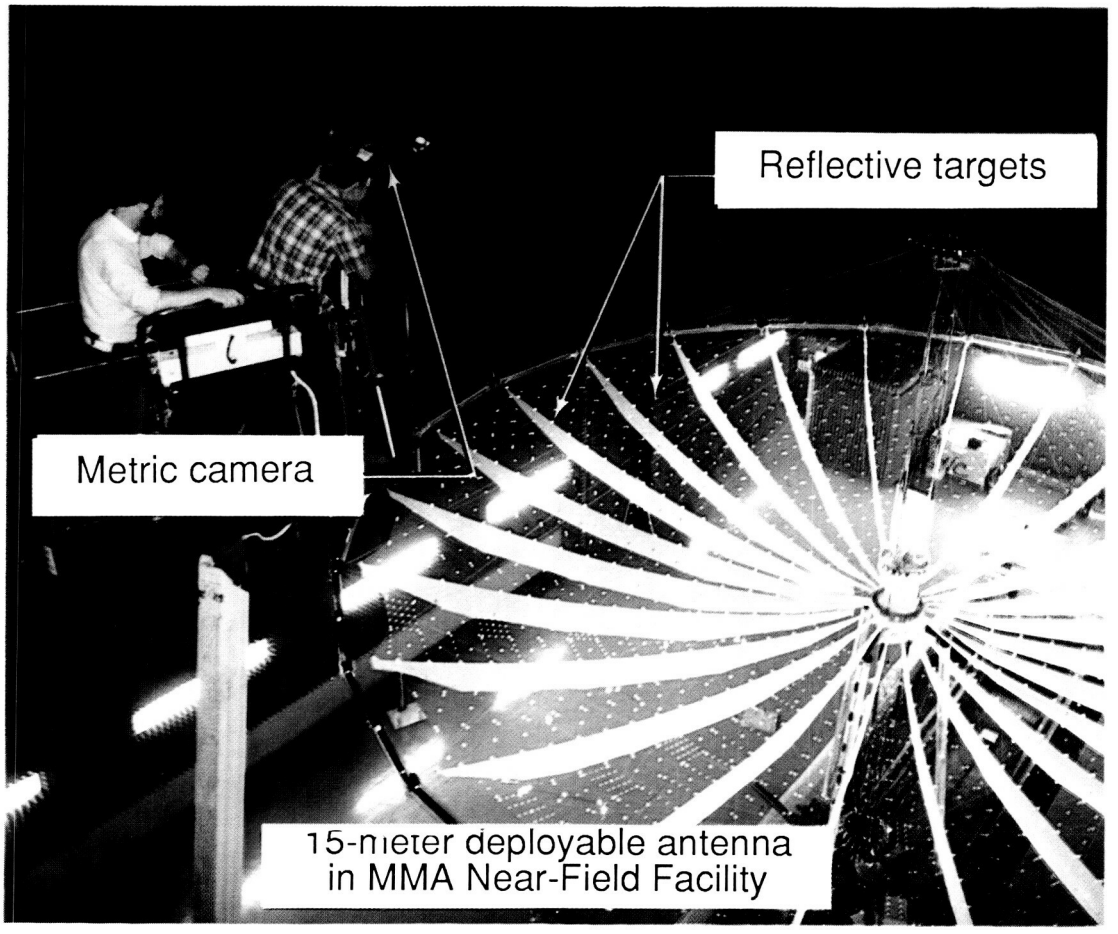

L-87-9758

Figure 25. Metric camera photographs being taken during 15-m antenna test program.

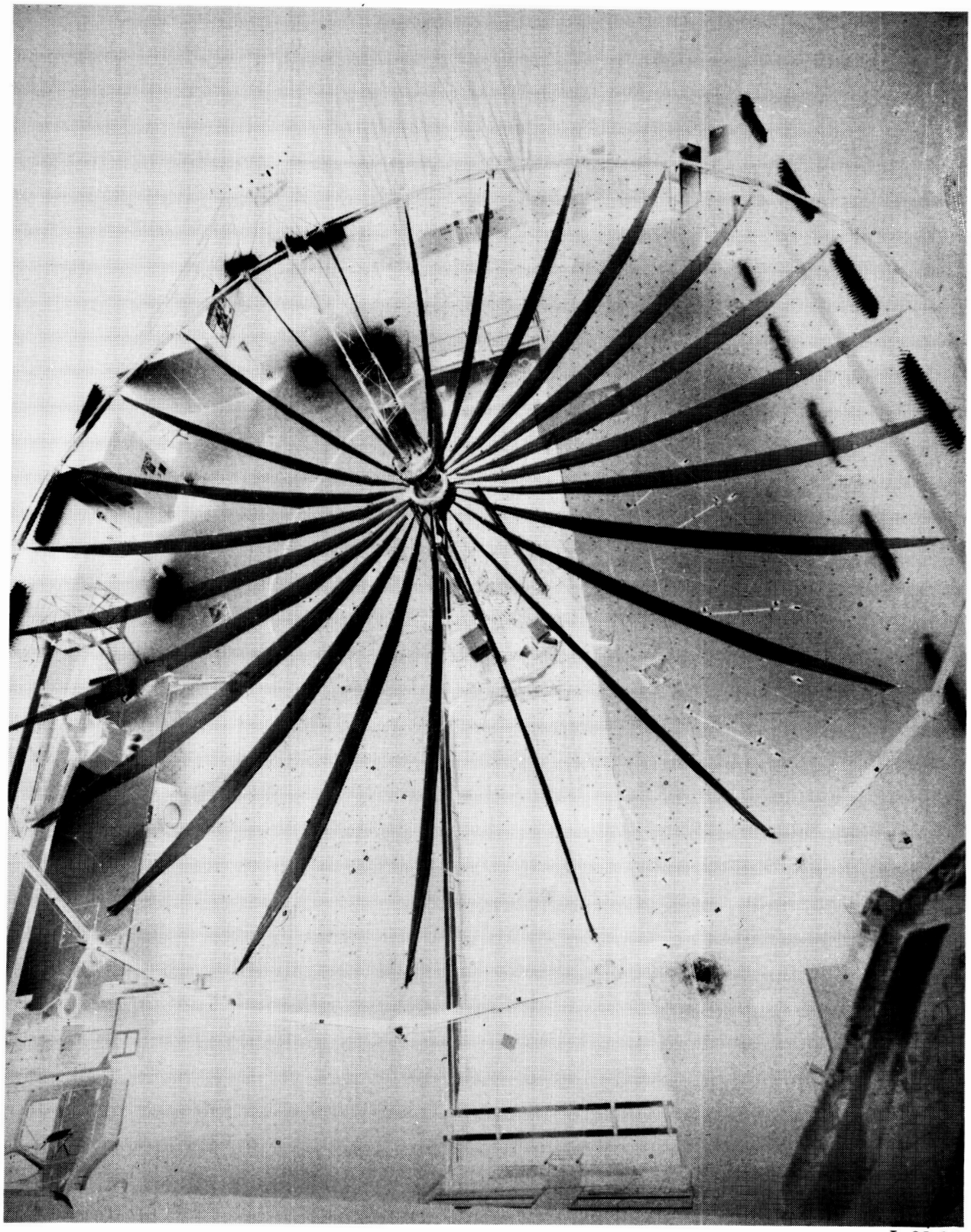

L-89-33

Figure 26. Metric camera photograph using a 10-sec time exposure (to enhance background).

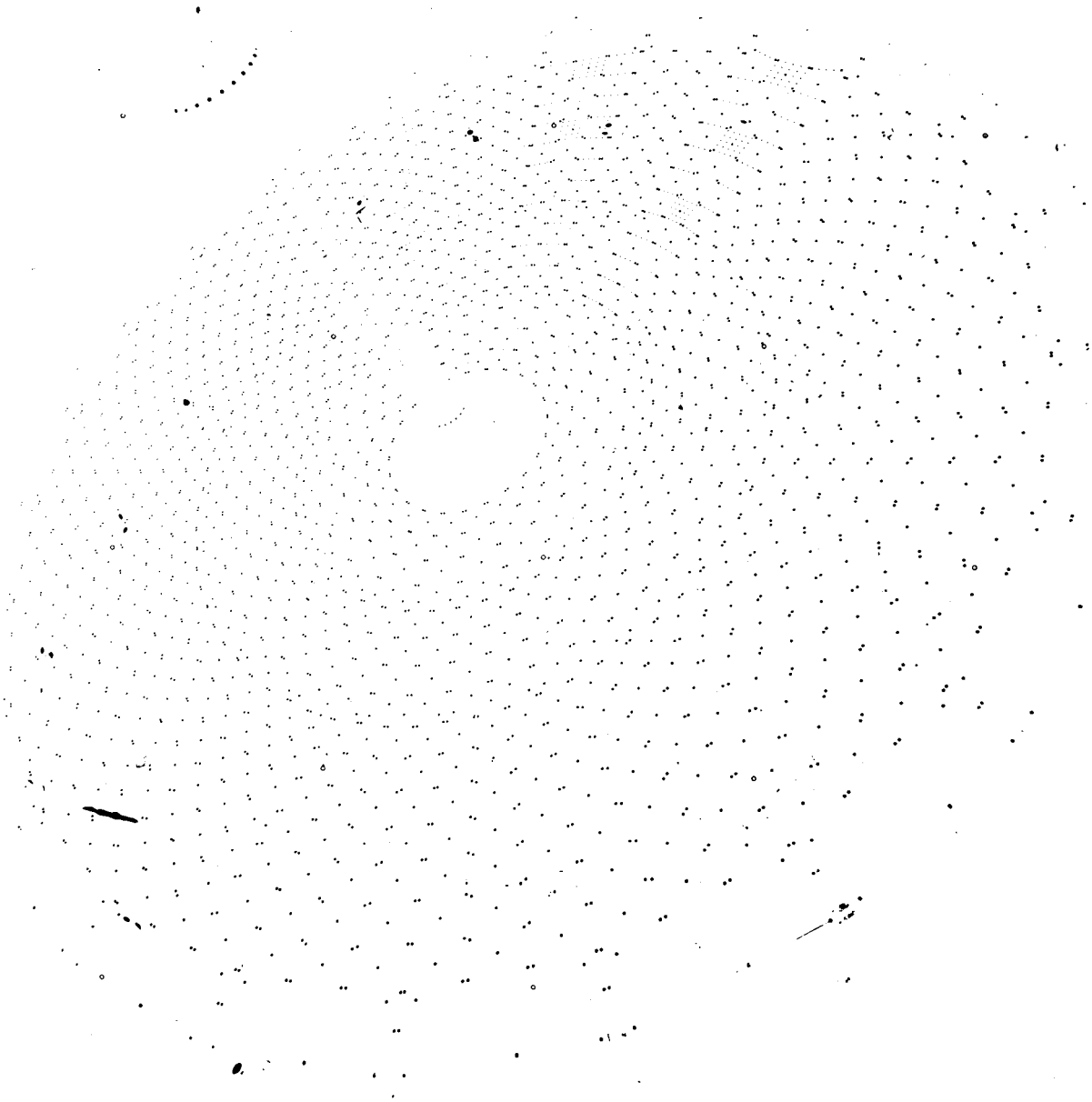

Figure 27. Metric camera photograph at 1/125 sec exposure (for mensuration).

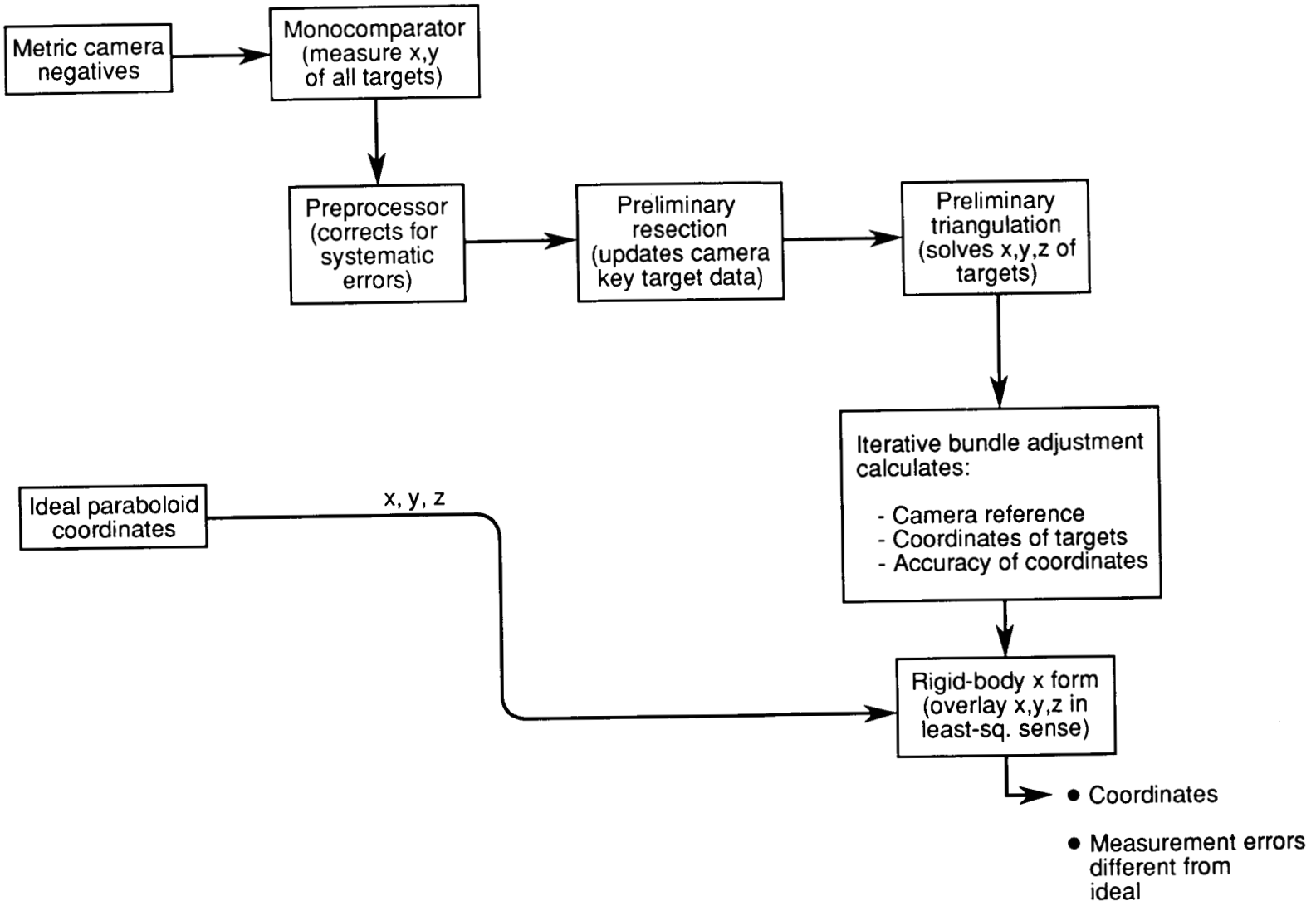

Figure 28. Processing of metric camera film data.

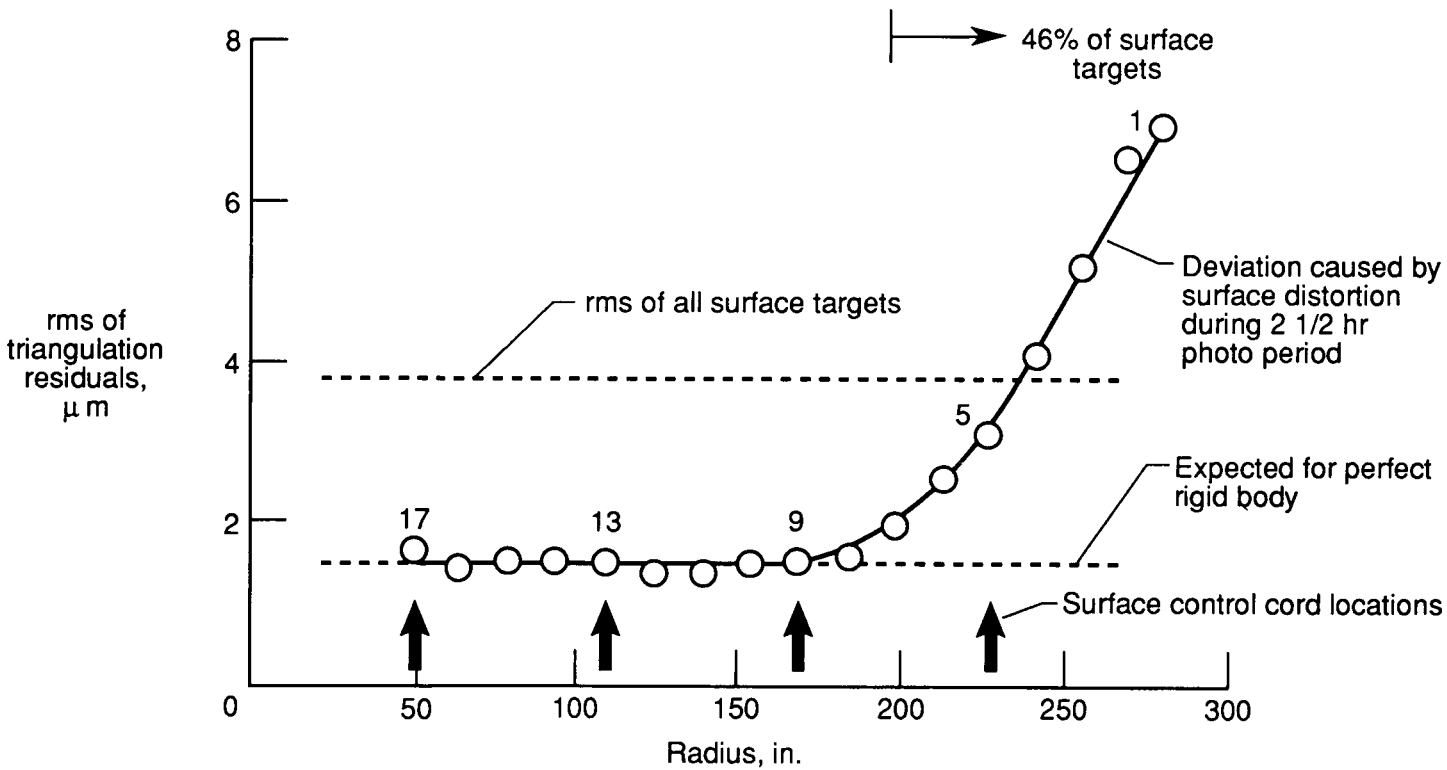

Figure 29. Effect of antenna torsional motion on metric camera triangulation residuals.

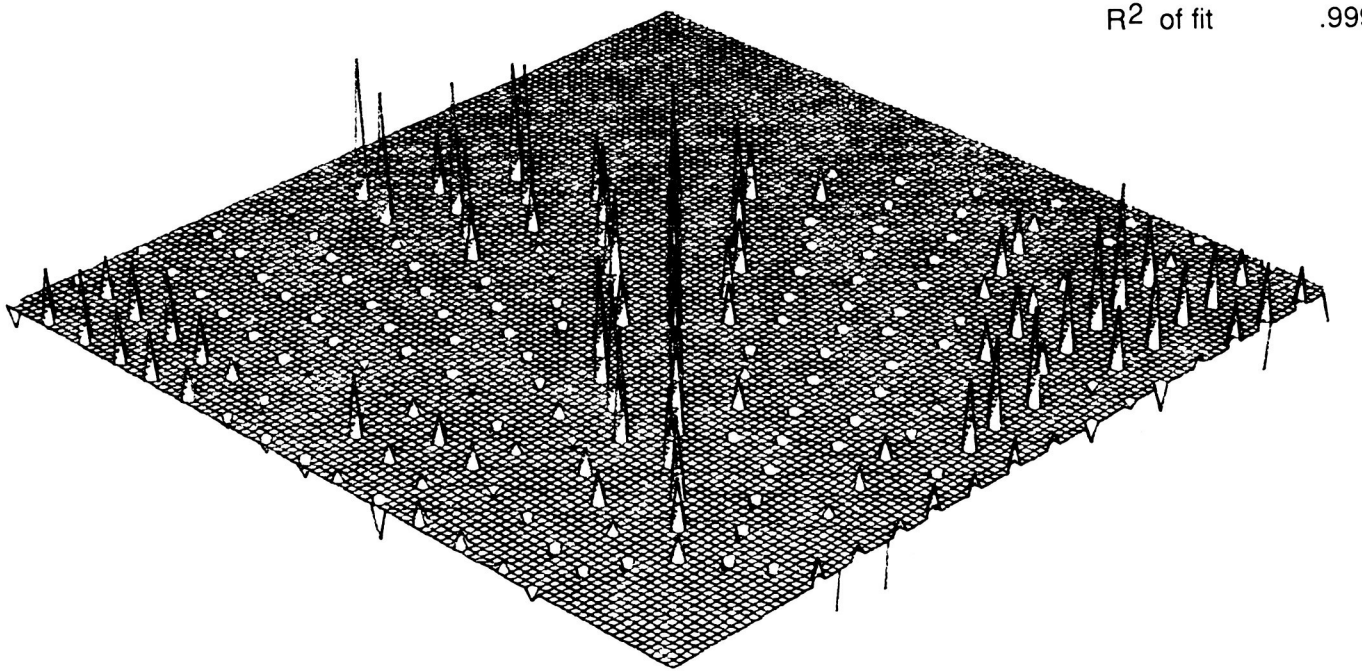

Figure 30. Plot of target z coordinates relative to best-fit paraboloid.

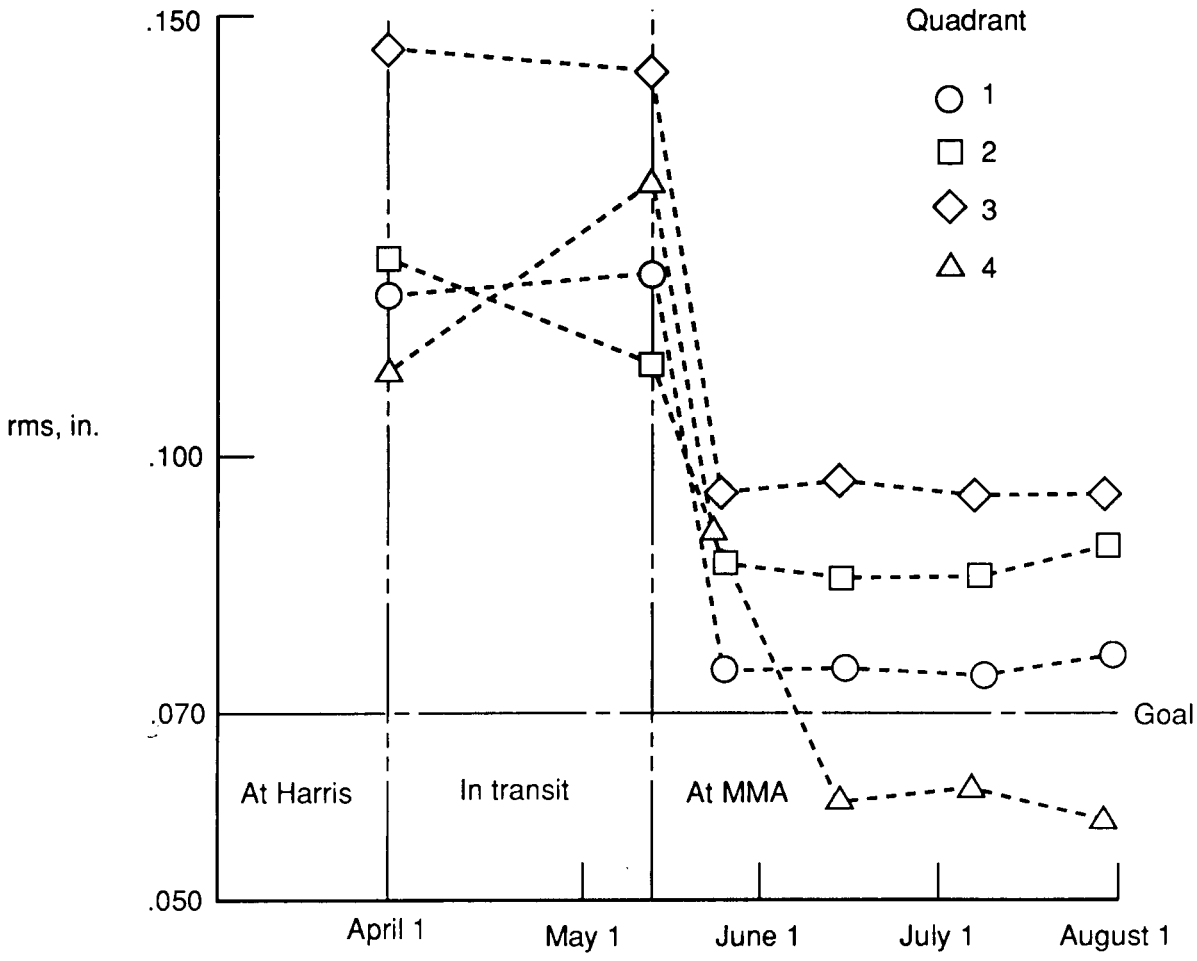

Figure 31. Surface error measurement history for 15-m antenna (effective surface only).

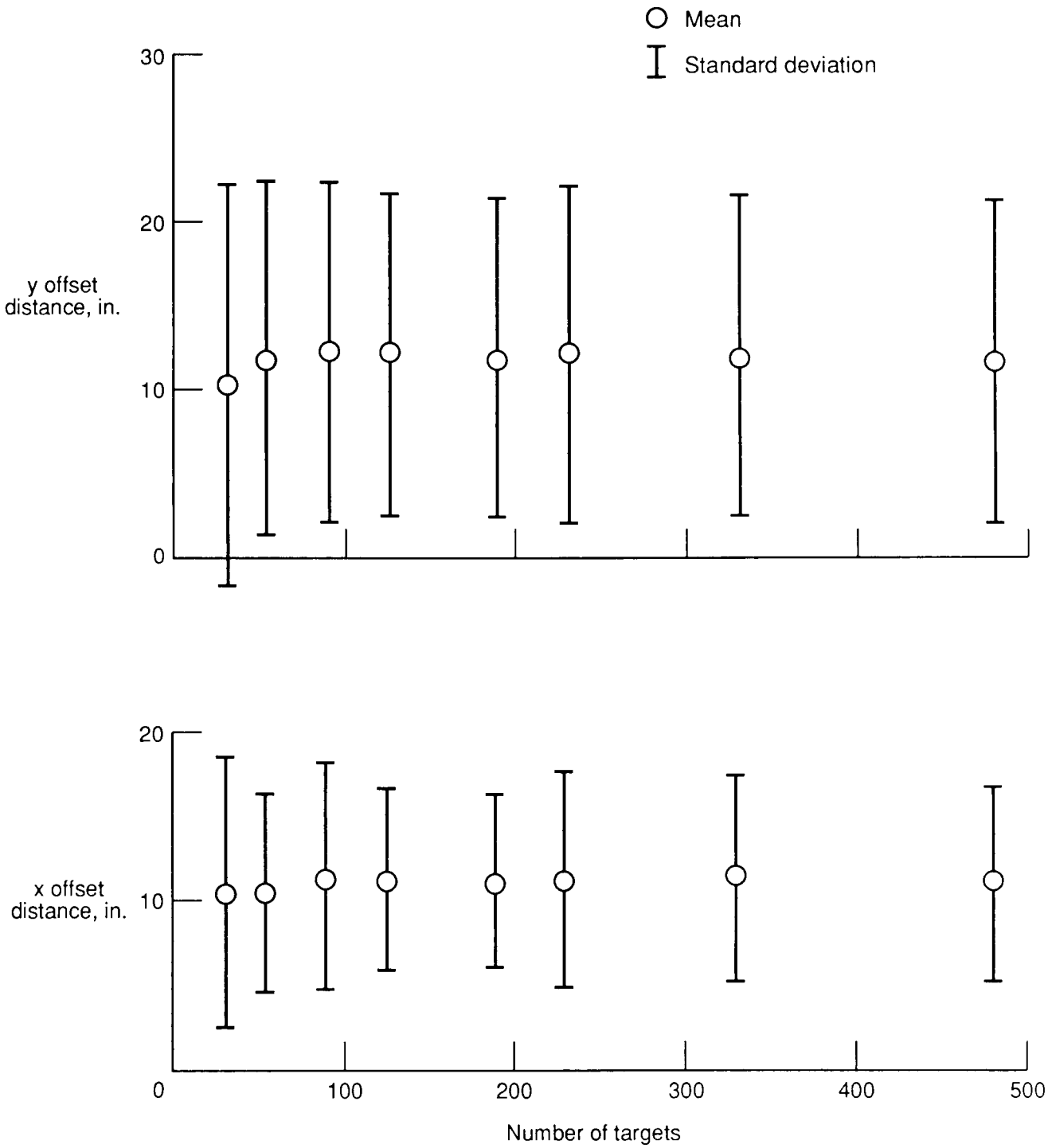

Figure 32. Monte Carlo simulation of effects of errors of Tie Points I and Pillows I on offset of focal point. Six seeds; 50-mil standard deviation target offset; 30-mil pillow height.

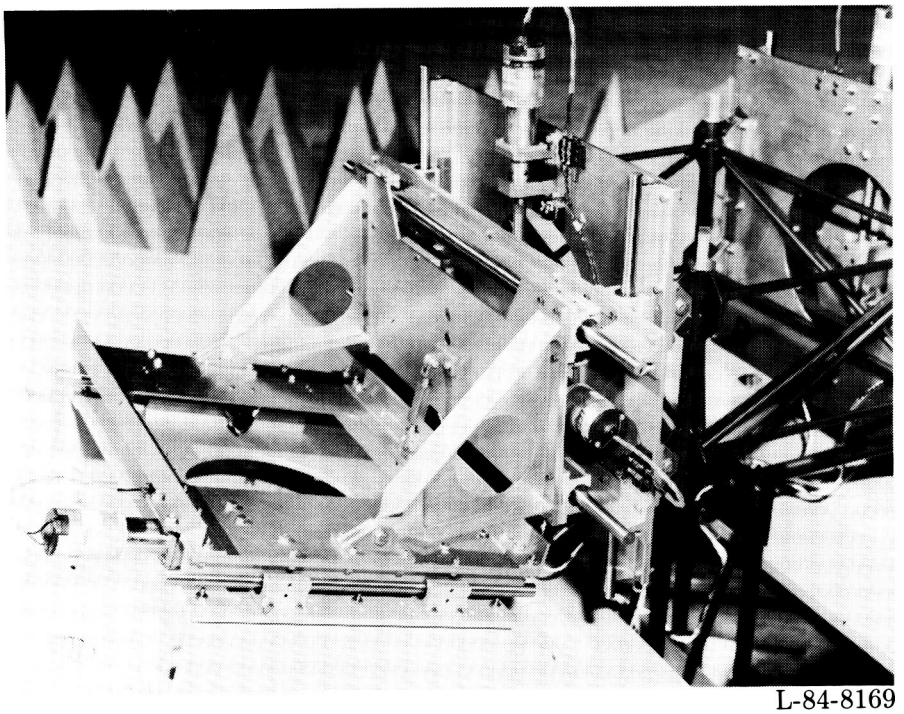

L-84-8169

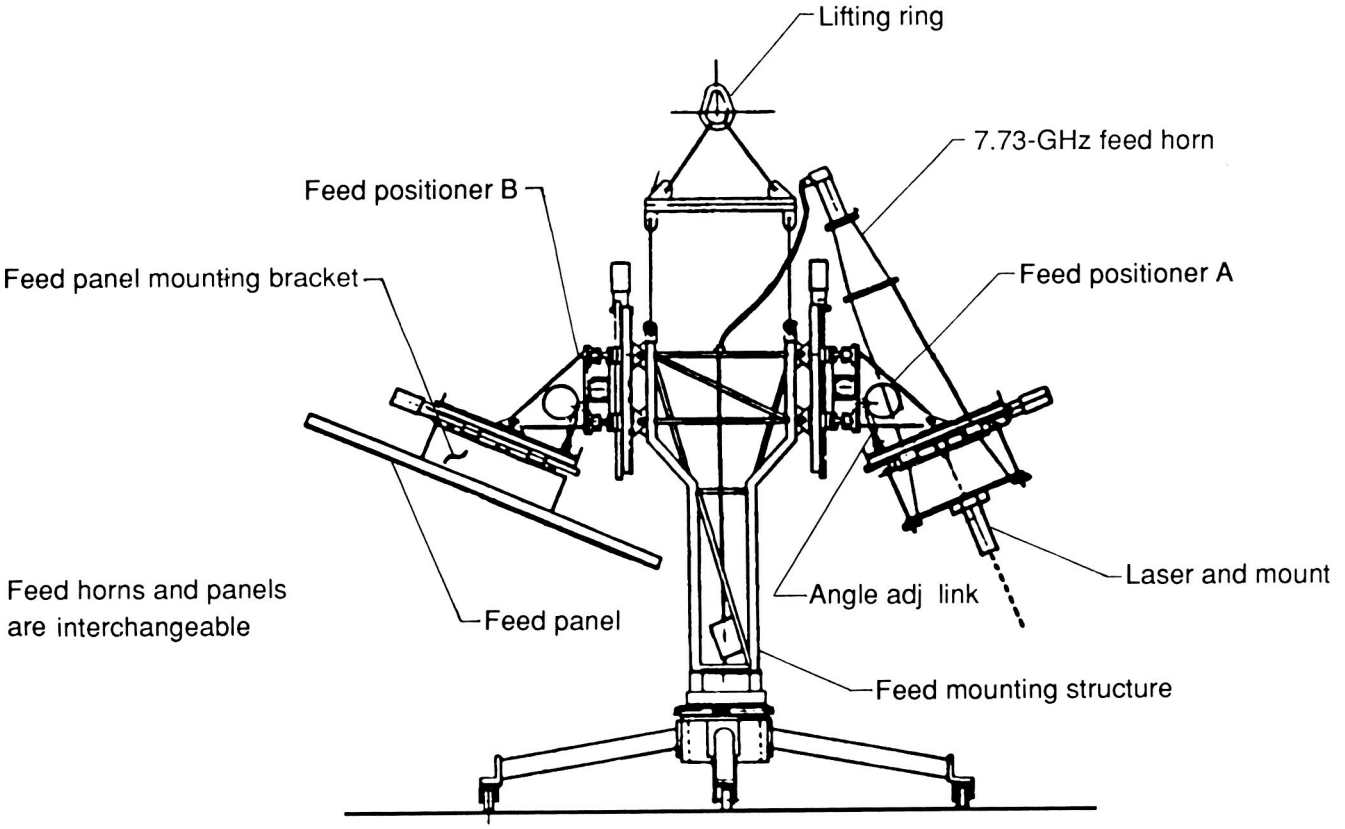

Figure 33. Feed adjustment bracket used for MMA 15-m antenna tests.

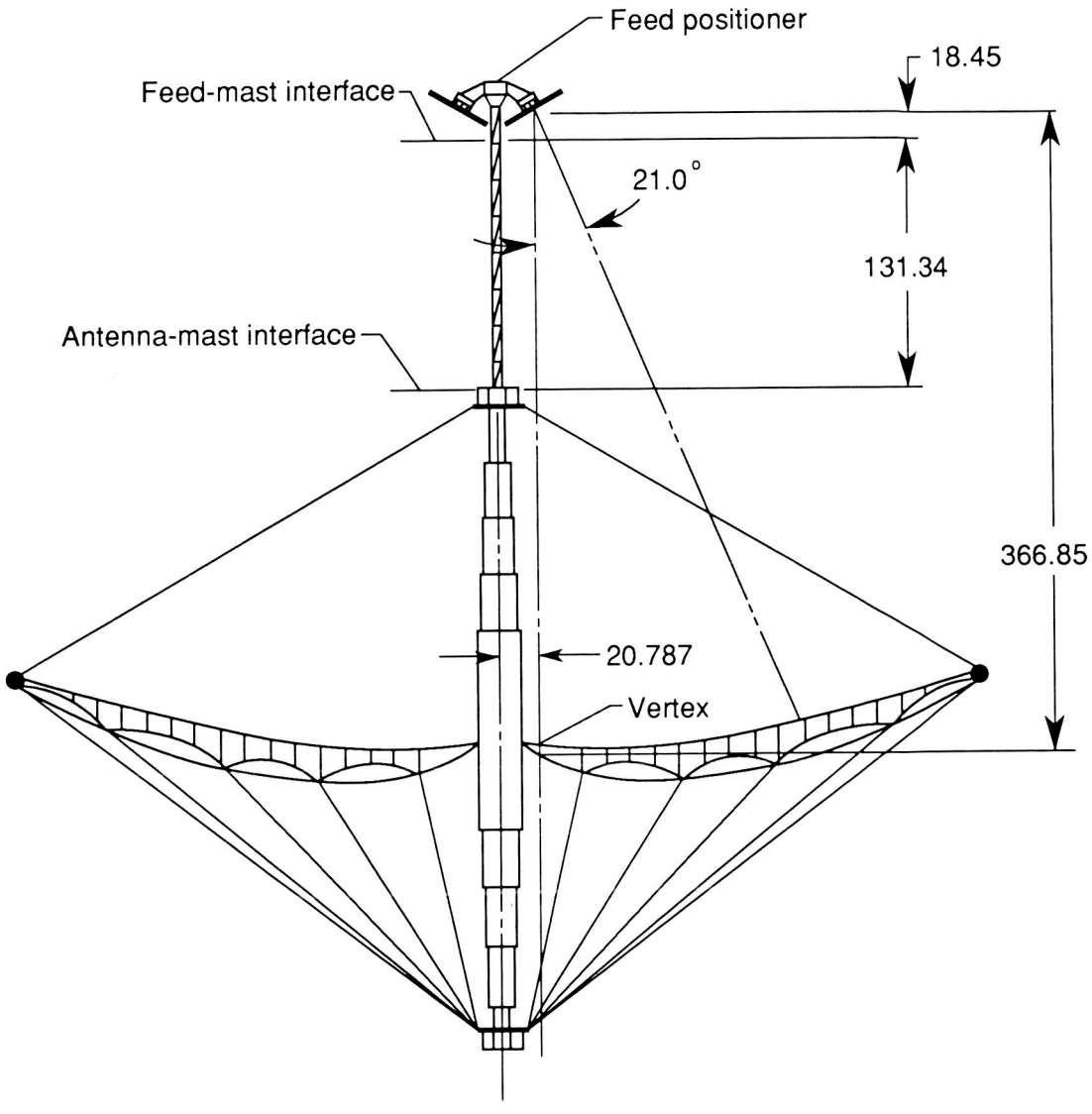

Feed mast weights

Freq, GHz	Weight, lb
2.27	220.8
4.26	196.9
7.73	146.4
11.60	137.6
2.225 (JPL)	209.4

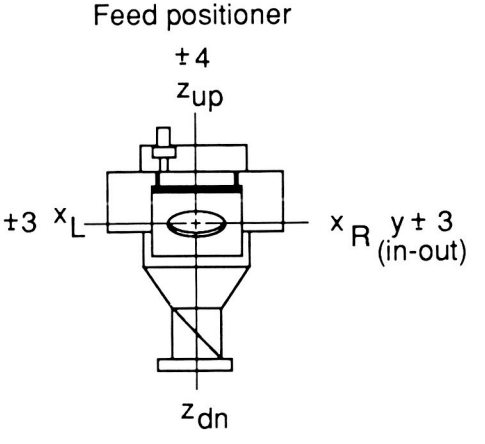

Figure 34. Orientation of feed positioner and mast on 15-m antenna. Linear dimensions are in inches.

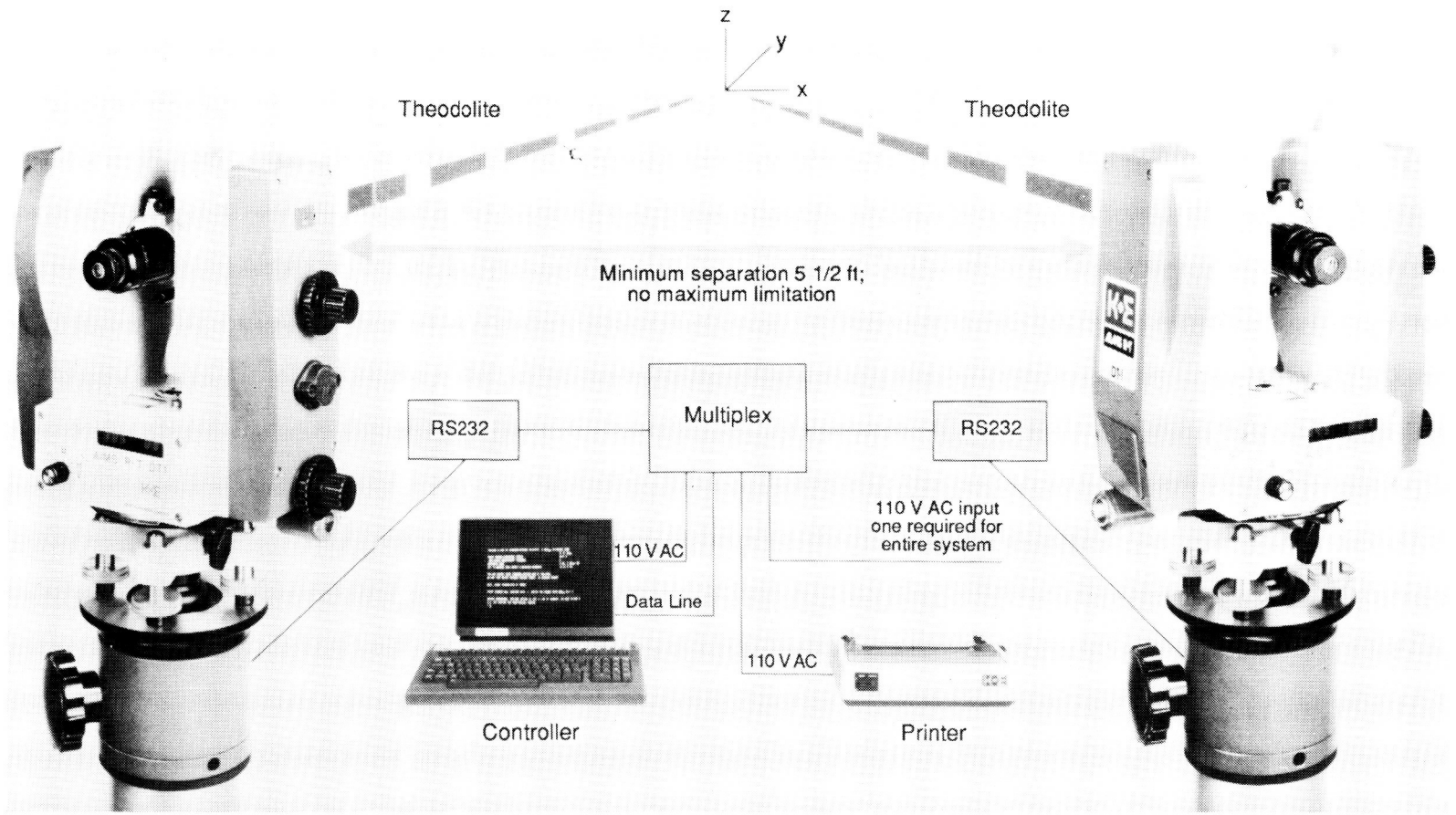

L-84-8789

Figure 35. Feed location measurement system with two theodolites.

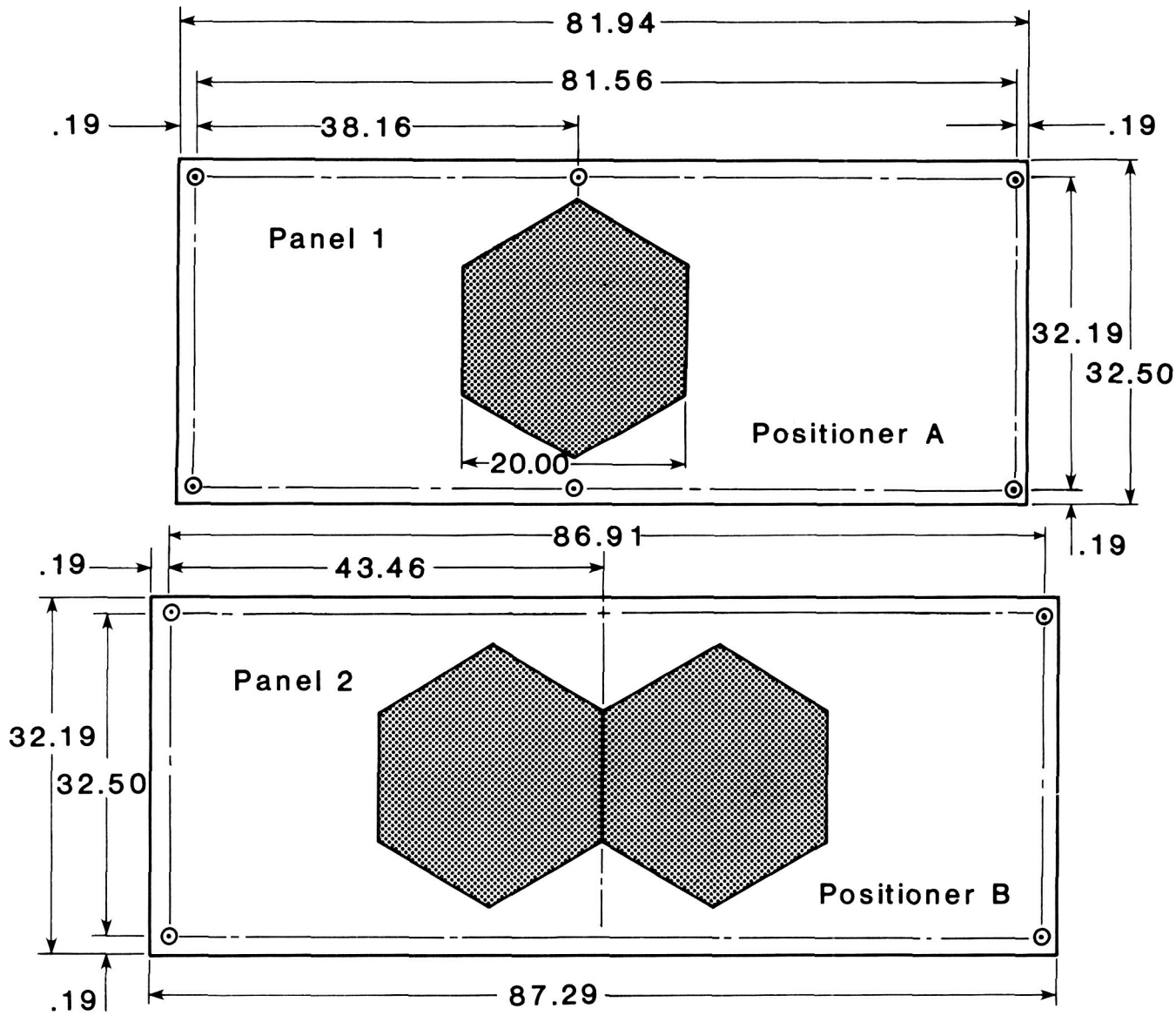

(a) Feeds for 2.27 GHz.

Figure 36. Feed and target locations. Dimensions are in inches.

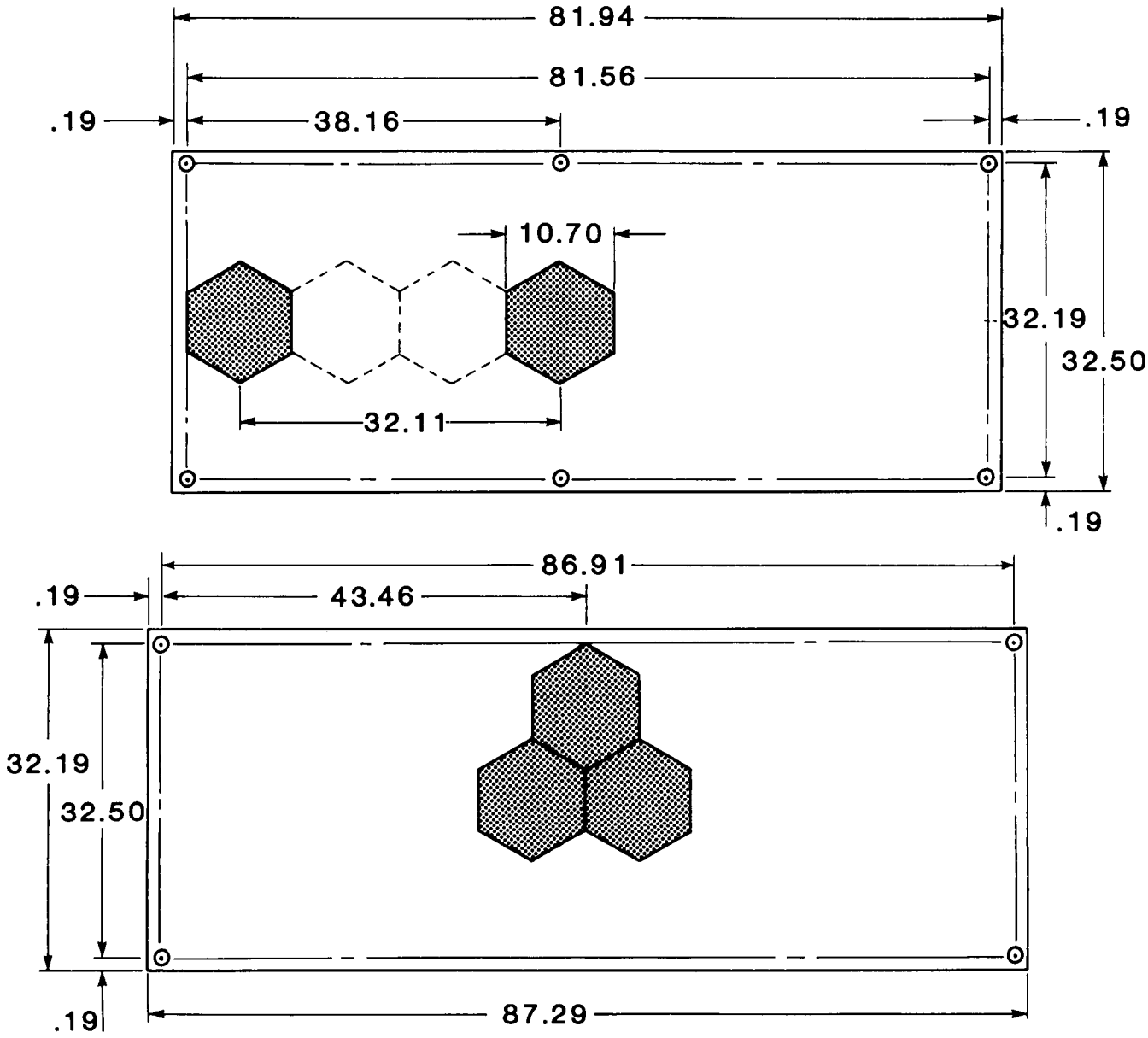

(b) Feeds for 4.26 GHz.

Figure 36. Continued.

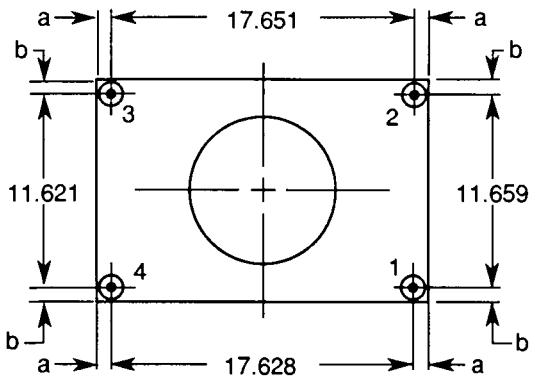

Positioner A

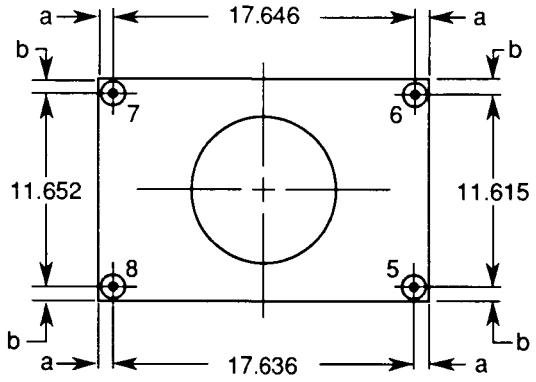

Positioner B

Target	a, in.	b, in.
1	0.172	0.170
2	0.163	0.171
3	0.186	0.181
4	0.200	0.198
5	0.196	0.194
6	0.166	0.191
7	0.188	0.176
8	0.168	0.172

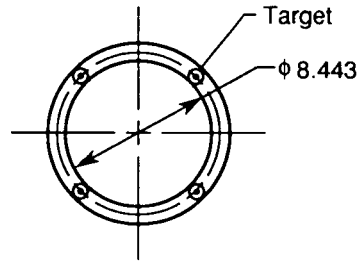

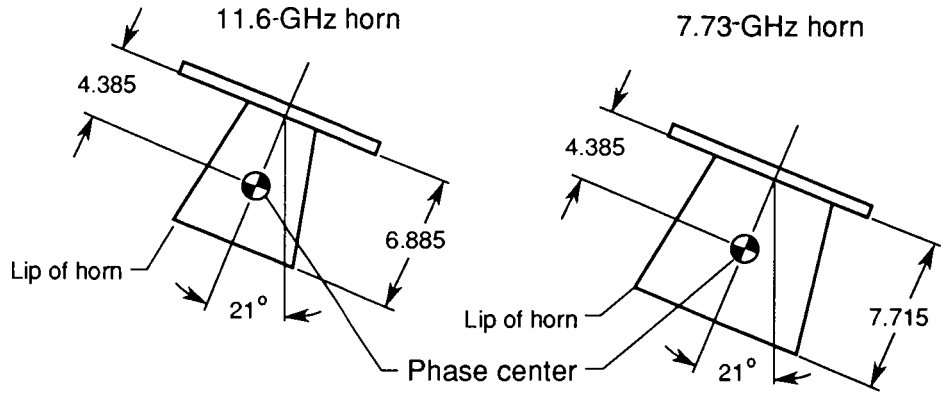

(c) Feeds for 7.73 GHz and 11.6 GHz.

Figure 36. Concluded.

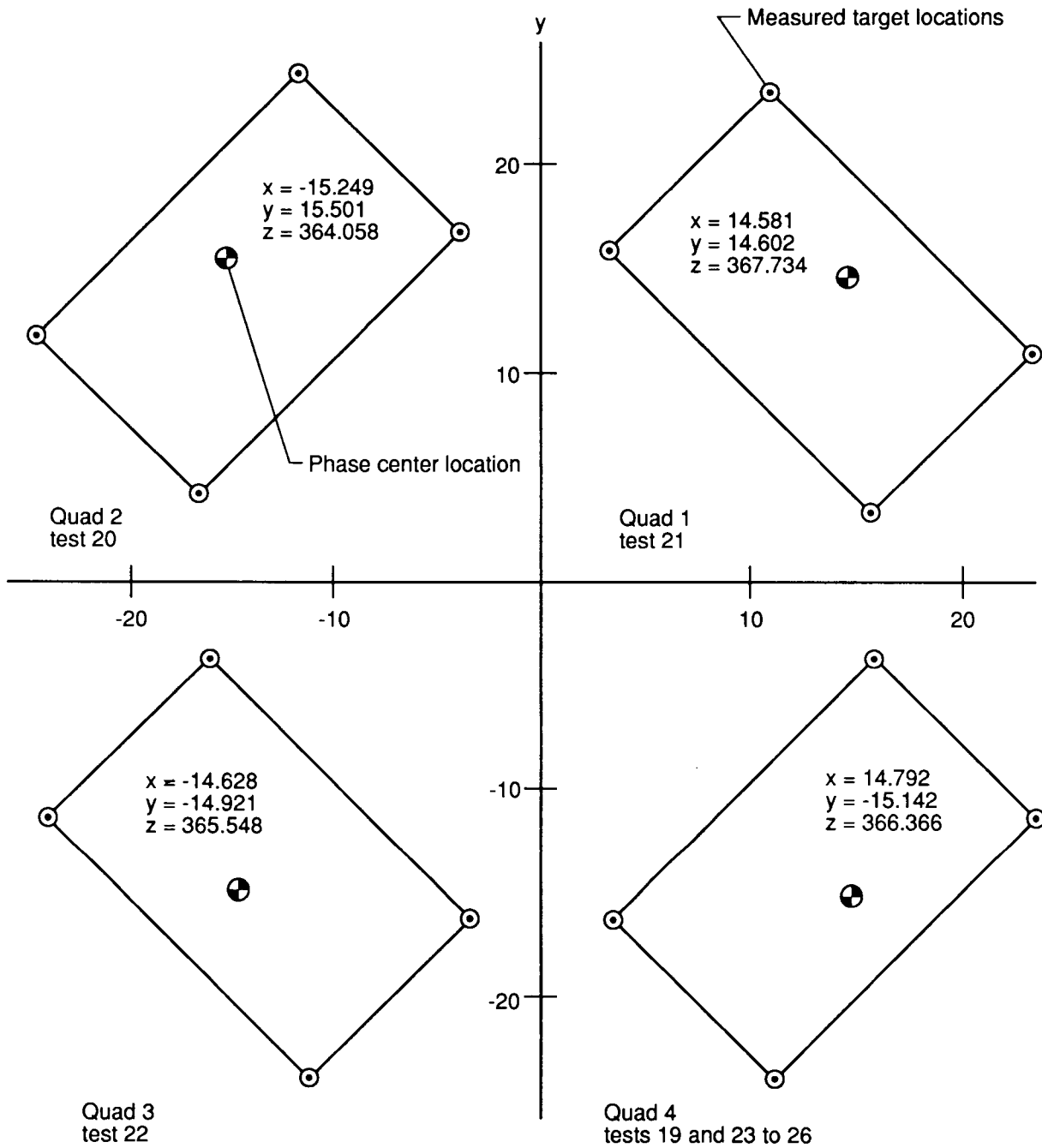

Figure 37. Metric camera feed measurement results for 7.73-GHz tests 19 through 26 on July 30, 1985.

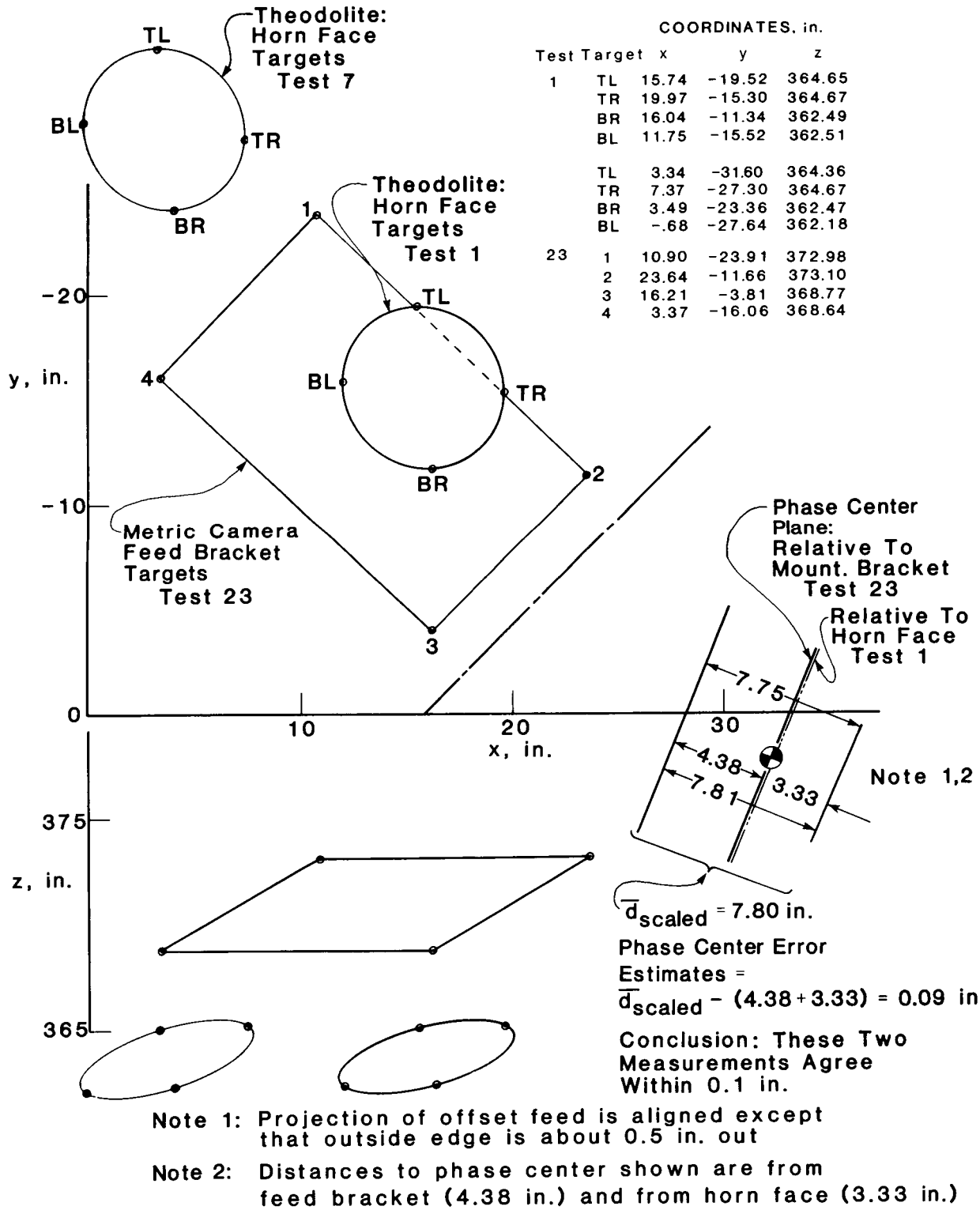

Figure 38. Comparison of 4.26 feed location measurements. Test 1 (June 5 theodolite data), test 7 (June 21 theodolite data), and test 23 (July 30 metric camera data); dimensions are in inches.

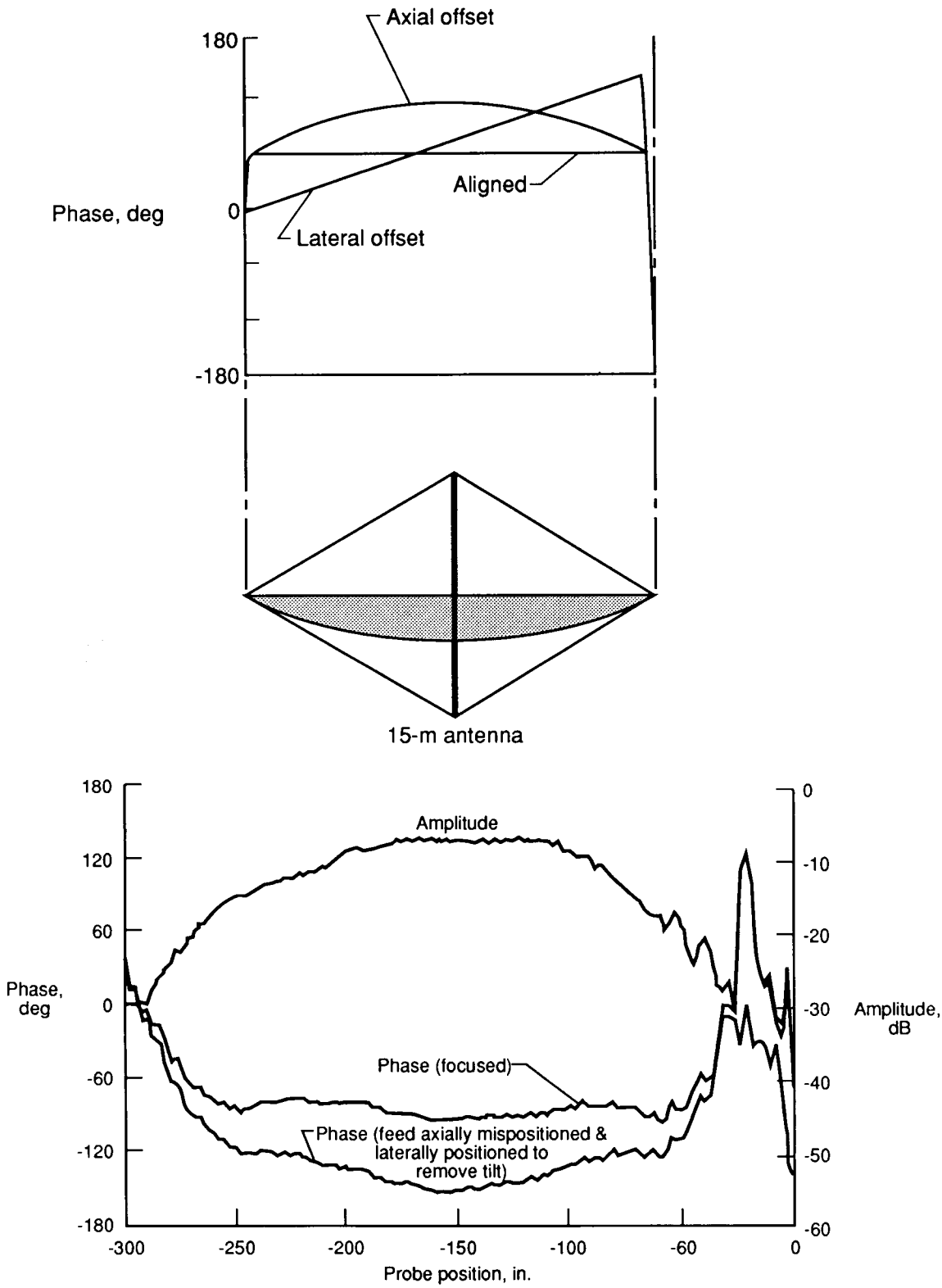

Figure 39. Typical phase trace across antenna aperture showing errors encountered due to feed misalignment.

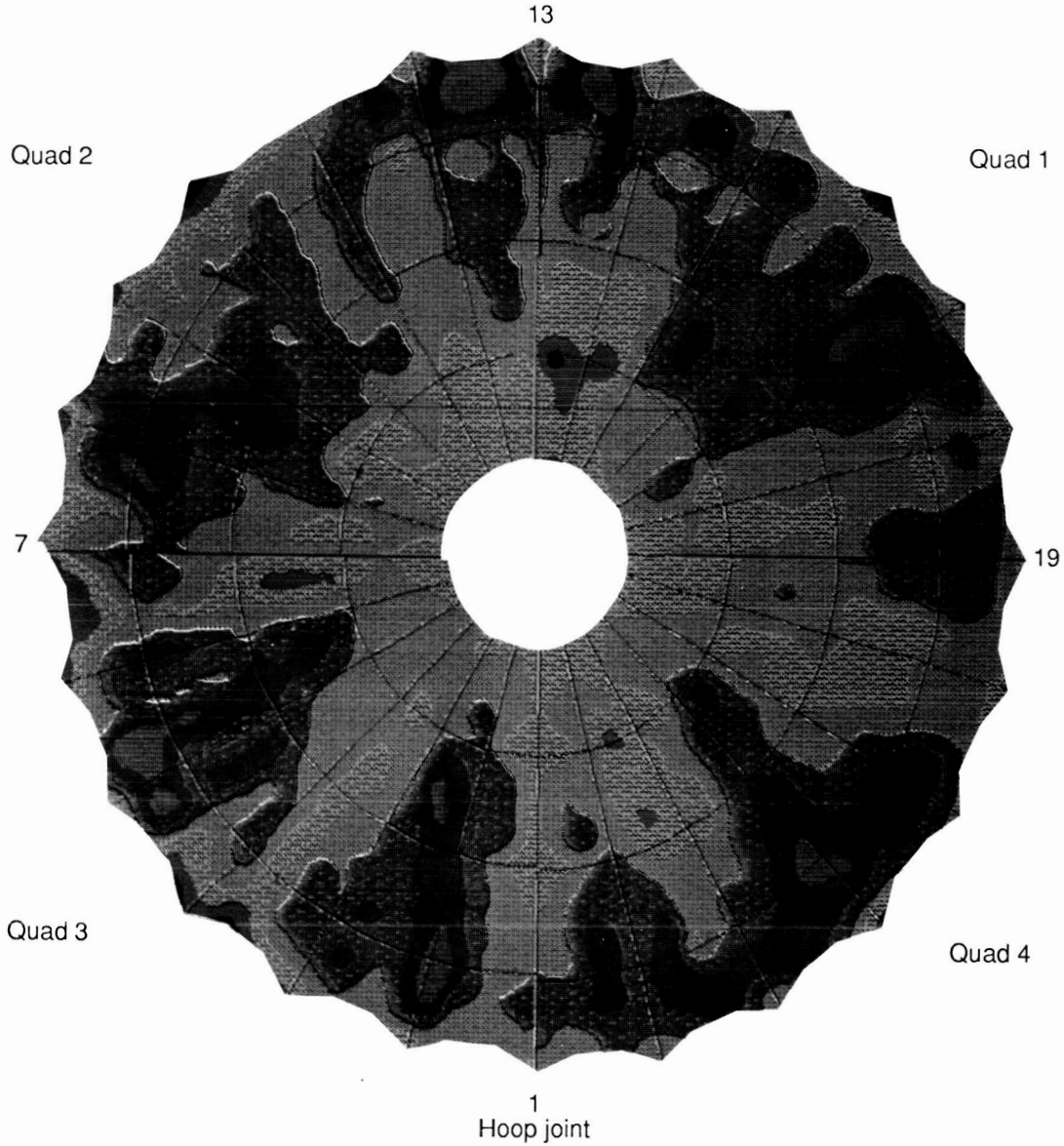

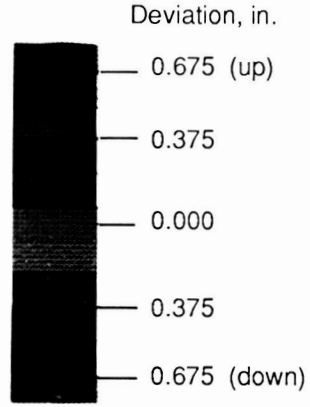

ORIGINAL PAGE
COLOR PHOTOGRAPH

Quadrant	rms error, in.	
	Ref: BFP	Ref: design
1	0.114	0.163
2	.107	.151
3	.145	.172
4	.108	.158

Figure 40. Contour plot of vertical surface errors measured by the metric camera during the second deployment at Harris, March 27, 1985.

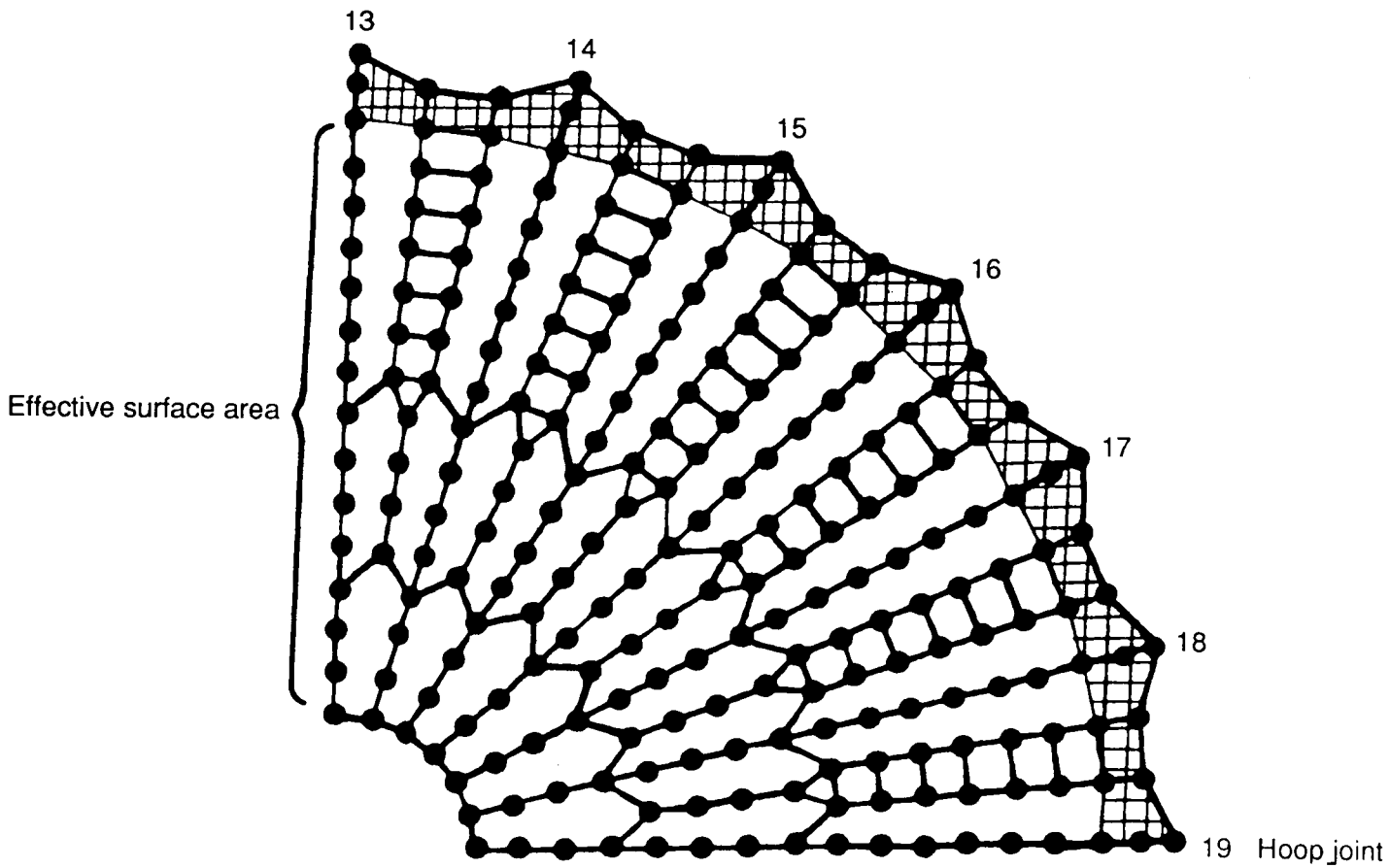

Figure 41. Surface target locations and definition of effective reflector surface area.

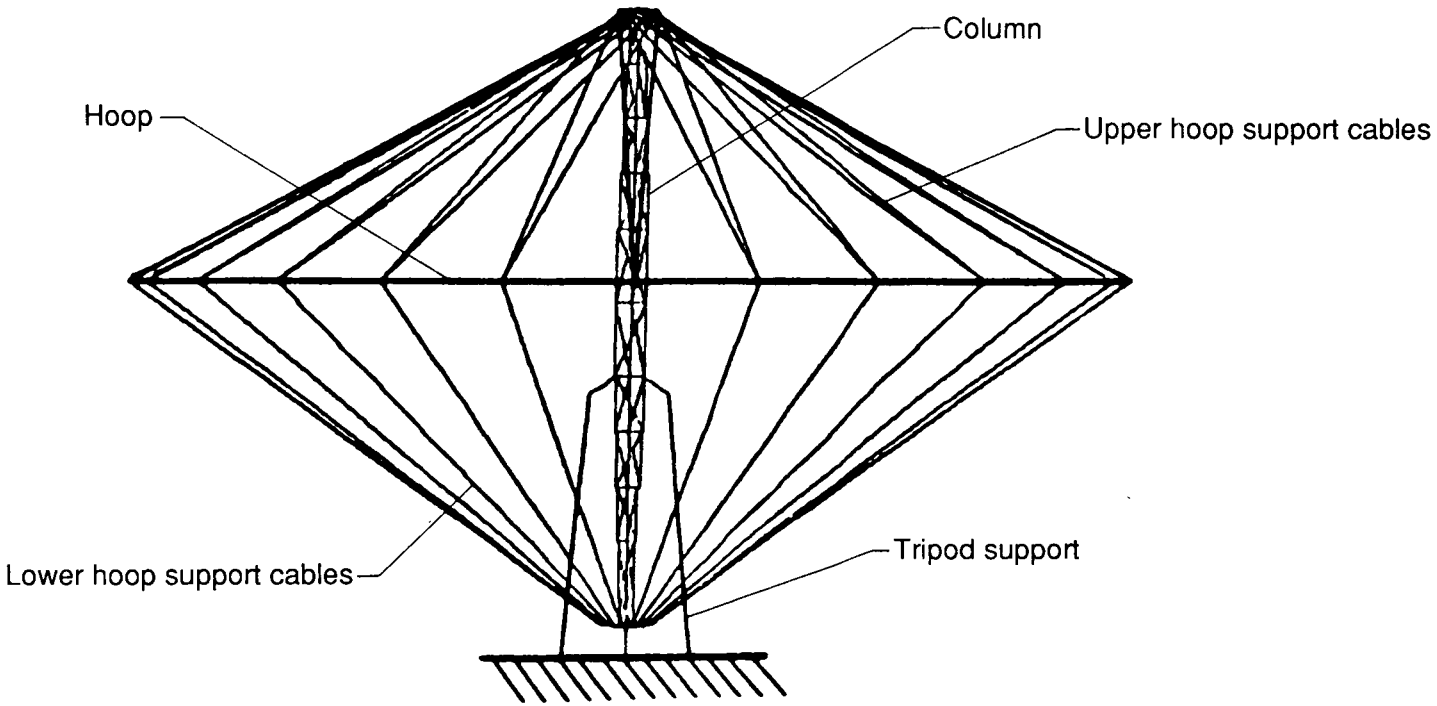

Figure 42. Elements of finite element analysis model without reflecting surface.

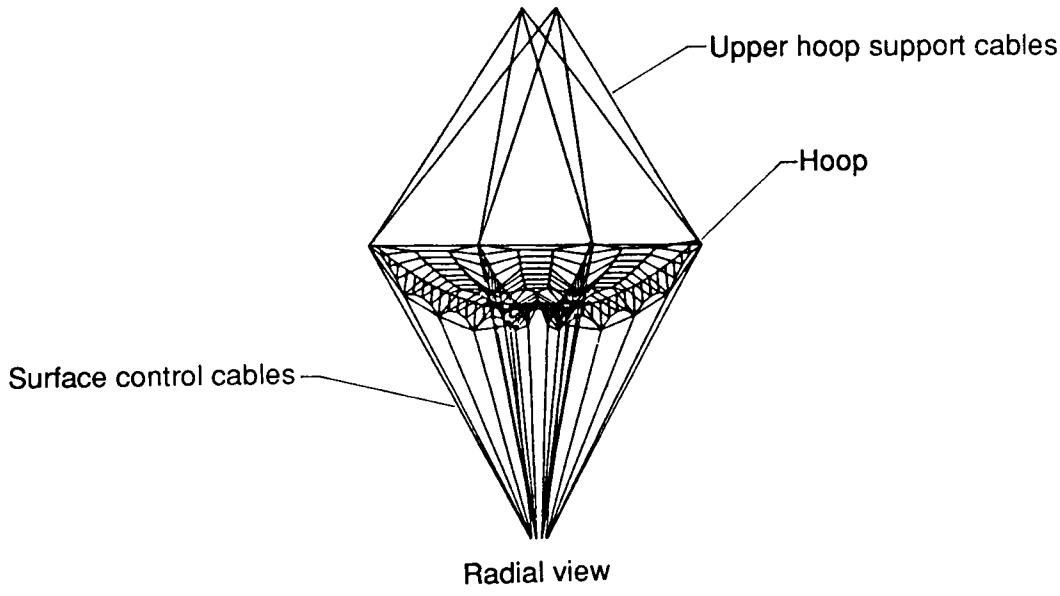

(a) Three-gore surface model.

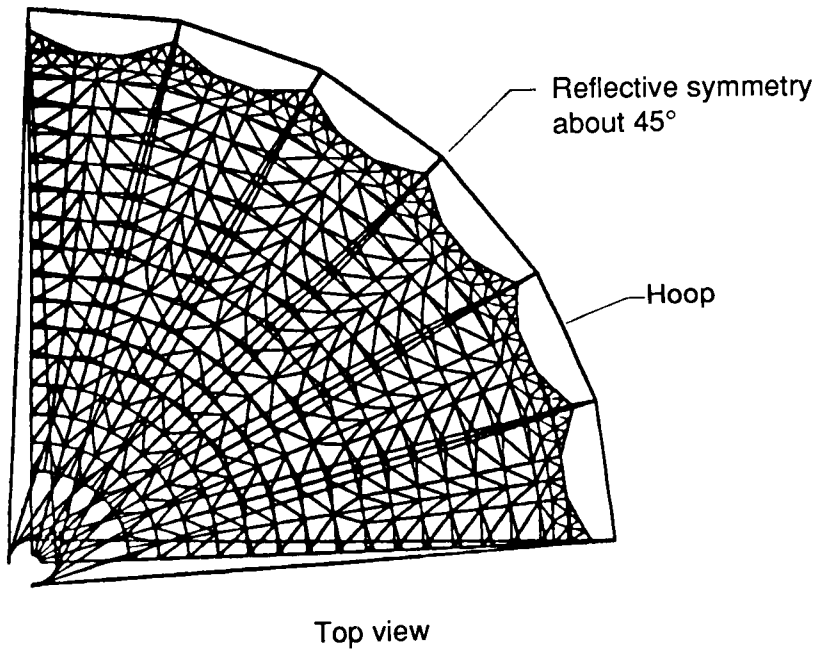

(b) Six-gore surface model.

Figure 43. Finite element surface model.

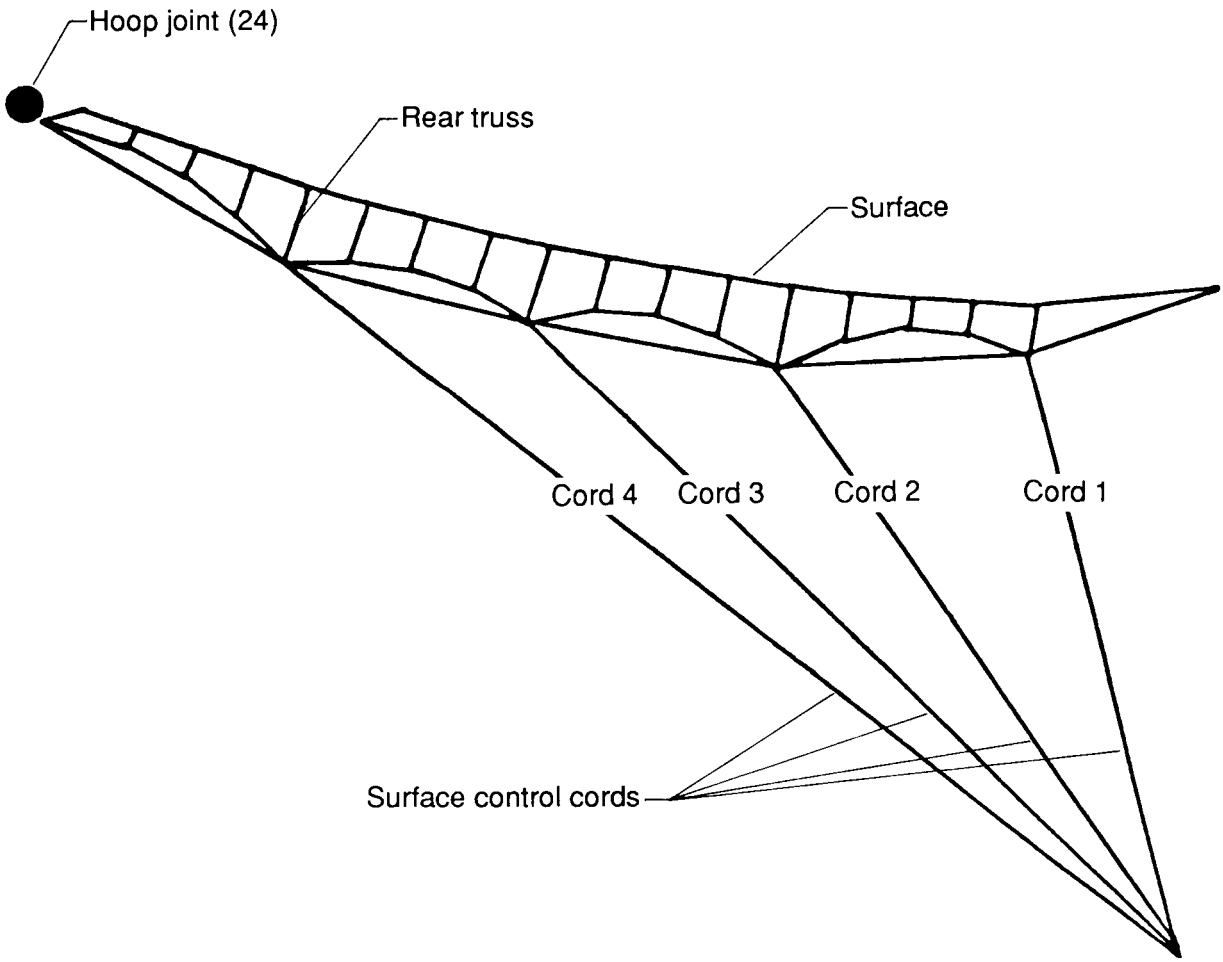

Figure 44. Surface shape control cable geometry (one gore only).

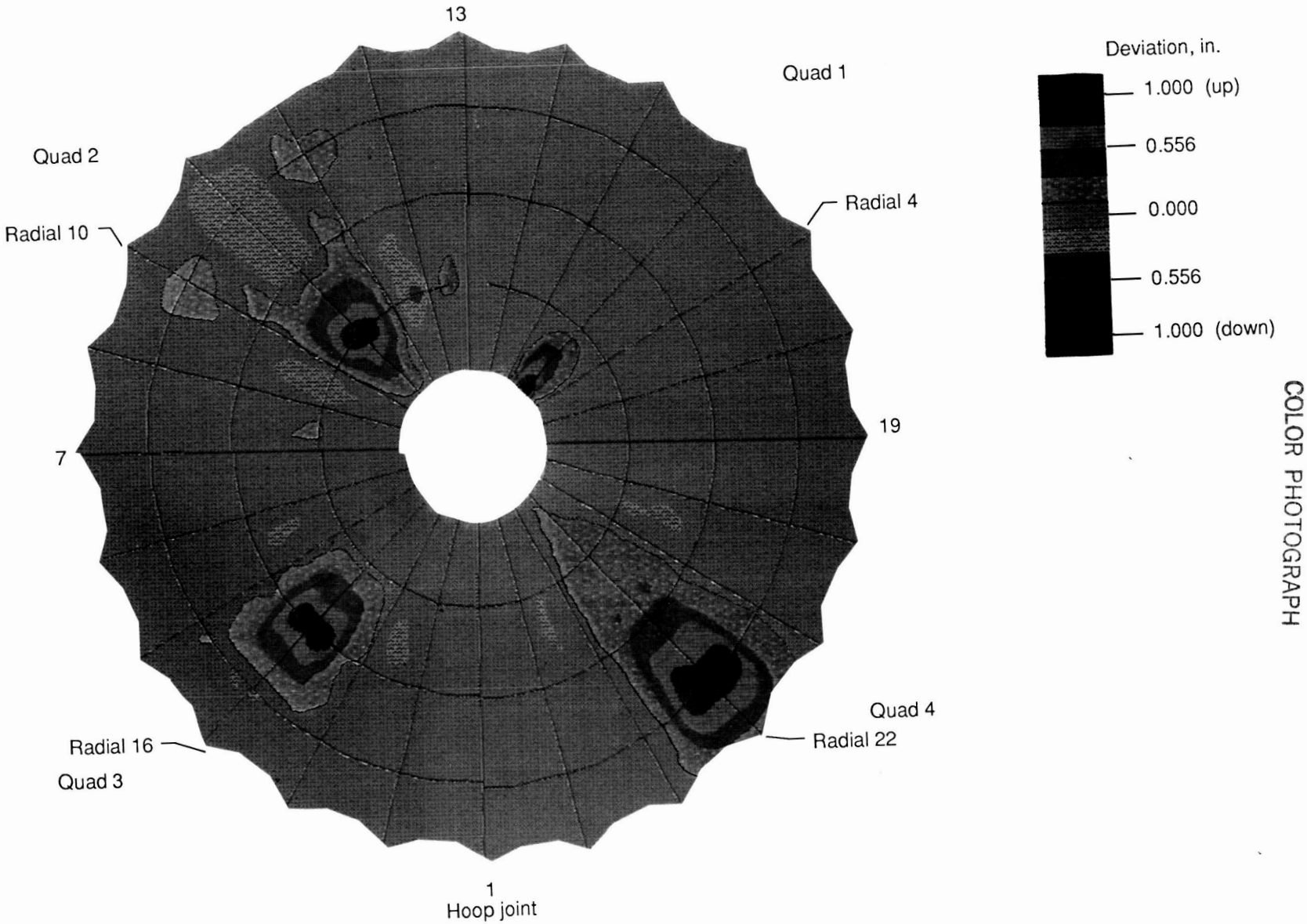

ORIGINAL PAGE
COLOR PHOTOGRAPH

Figure 45. Typical surface displacements resulting from control cable adjustments.

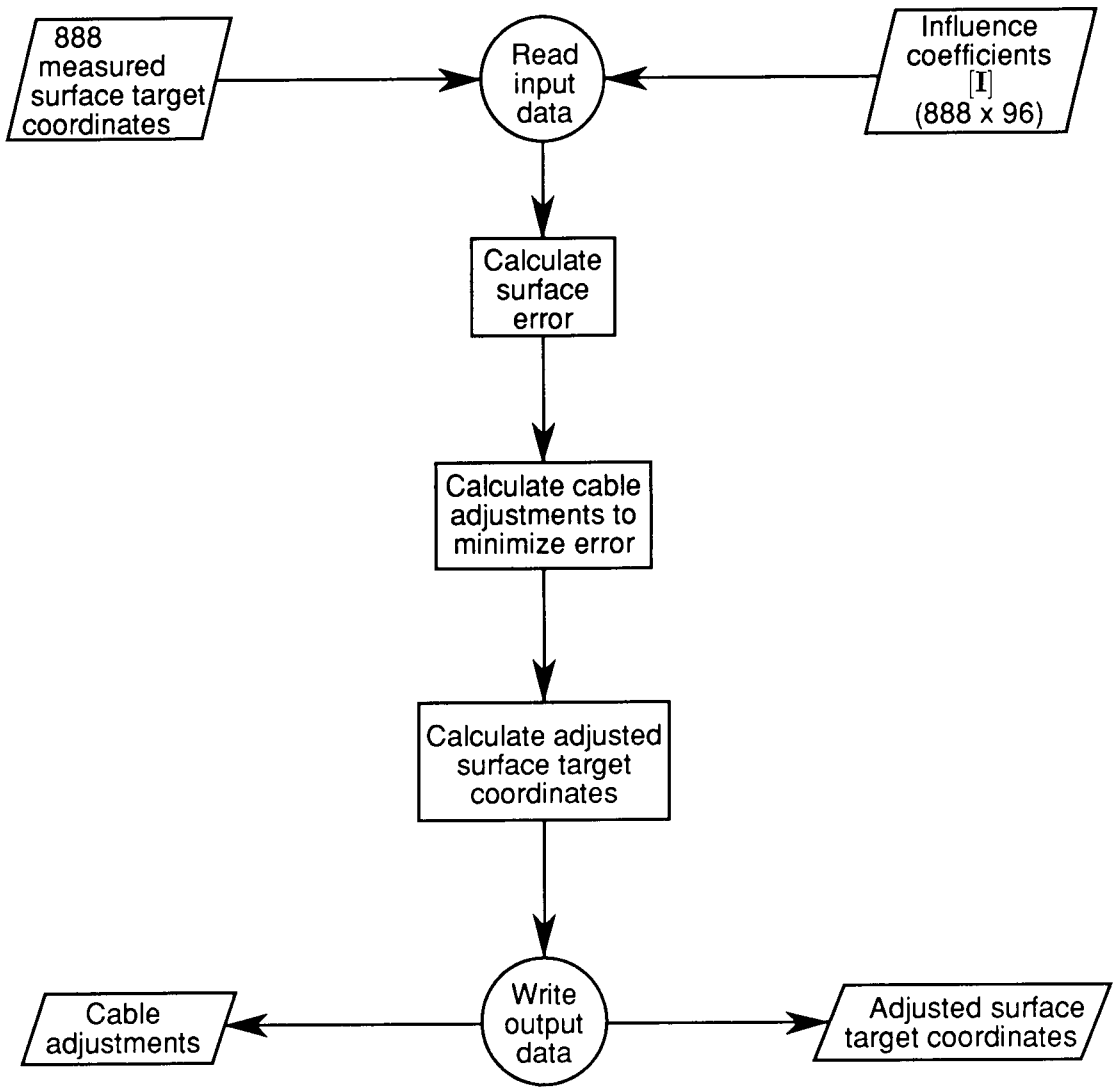

Figure 46. Flowchart of surface shape control algorithm.

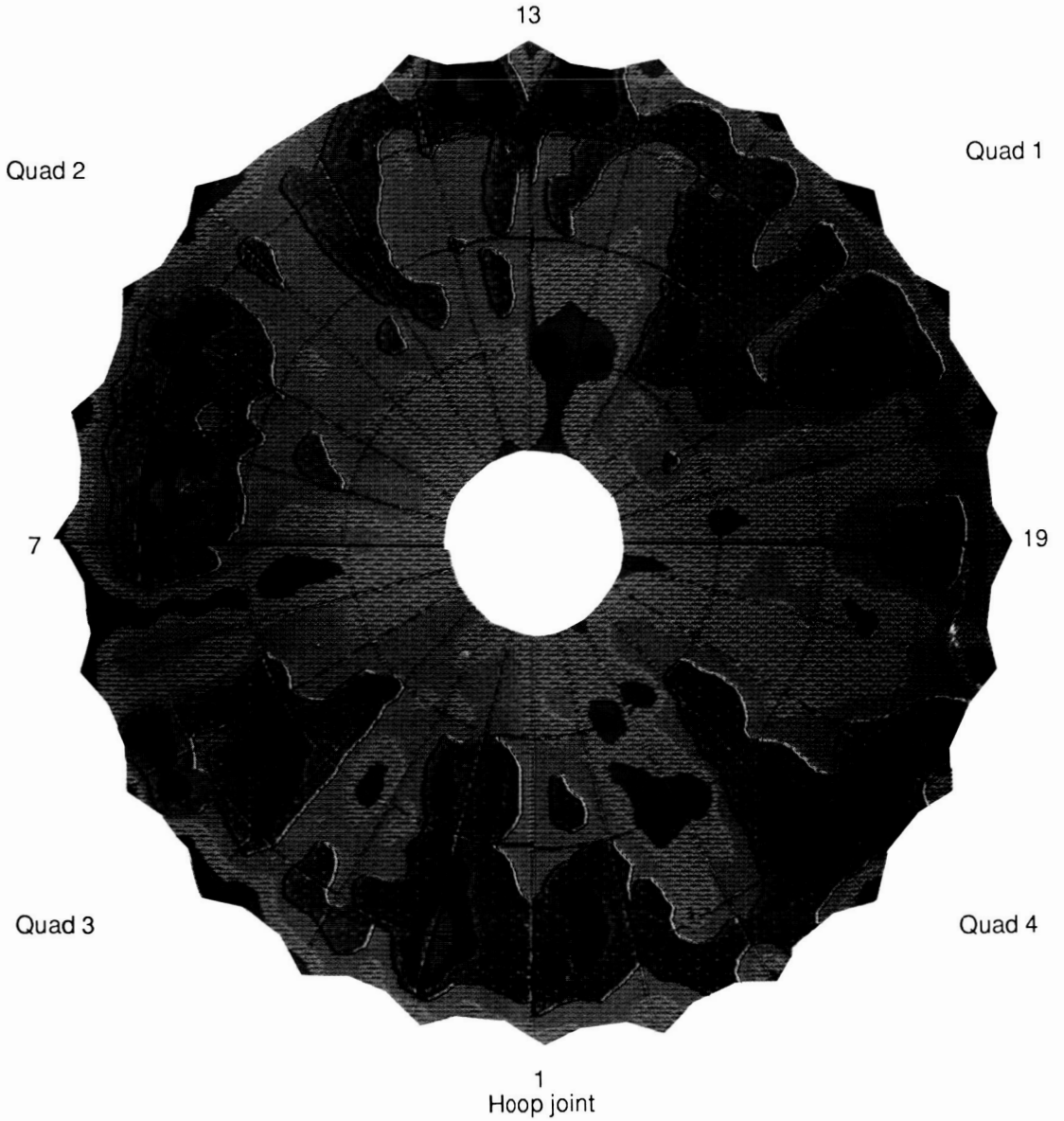

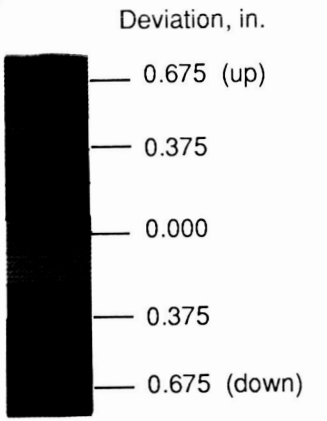

Quadrant	rms error, in.	
	Ref: BFP	Ref: design
1	0.117	0.155
2	.095	.136
3	.139	.162
4	.131	.169

ORIGINAL PAGE
COLOR PHOTOGRAPH

Figure 47. Surface error before control cable adjustment. Second measurement, May 16, 1985.

ORIGINAL PAGE
COLOR PHOTOGRAPH

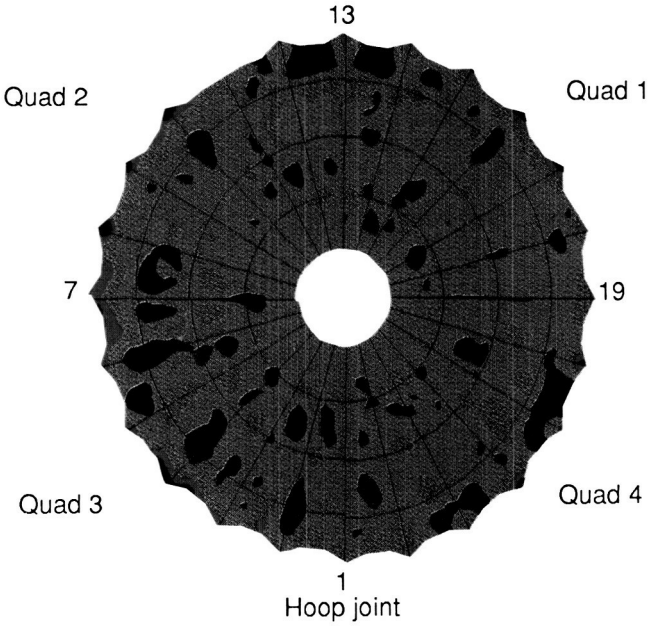

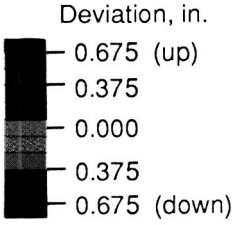

Quadrant	rms error, in.	
	Ref: BFP	Ref: design
1	0.076	0.072
2	.079	.081
3	.097	.098
4	.074	.073

(a) Predicted for 96 cables.

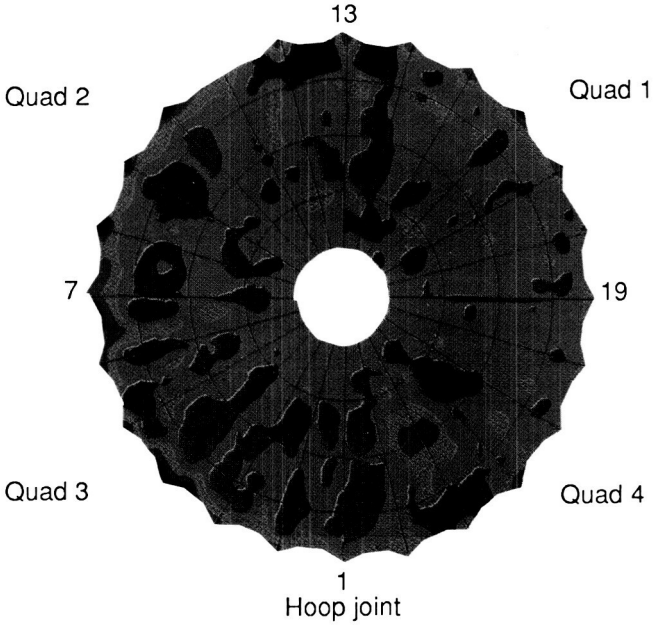

Quadrant	rms error, in.	
	Ref: BFP	Ref: design
1	0.075	0.078
2	.081	.091
3	.094	.105
4	.091	.096

(b) Measured for 85 cables, May 25, 1985.

Figure 48. Surface error after first control-cable adjustment.

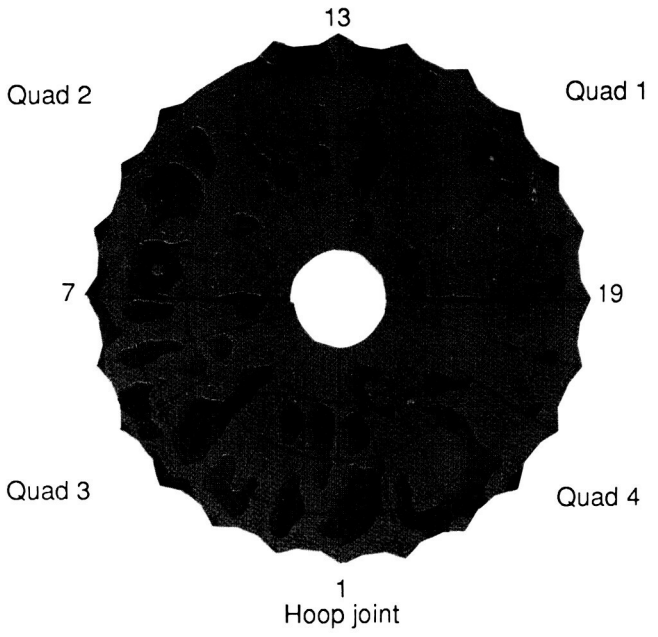

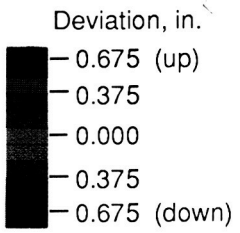

Quadrant	rms error, in.	
	Ref: BFP	Ref: design
1	0.072	0.073
2	.080	.088
3	.096	.102
4	.062	.072

(a) Predicted for 10 cables.

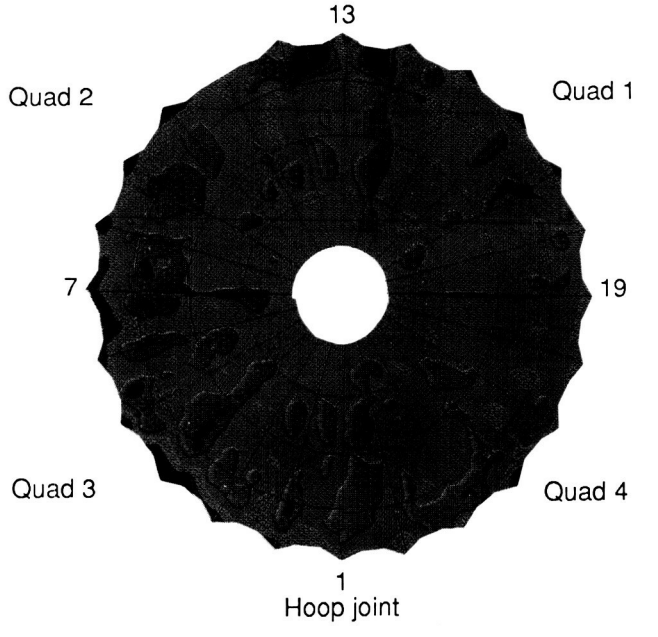

Quadrant	rms error, in.	
	Ref: BFP	Ref: design
1	0.075	0.076
2	.080	.089
3	.094	.101
4	.061	.071

(b) Measured for 10 cables, June 14, 1985.

Figure 49. Surface error after second control cable adjustment.

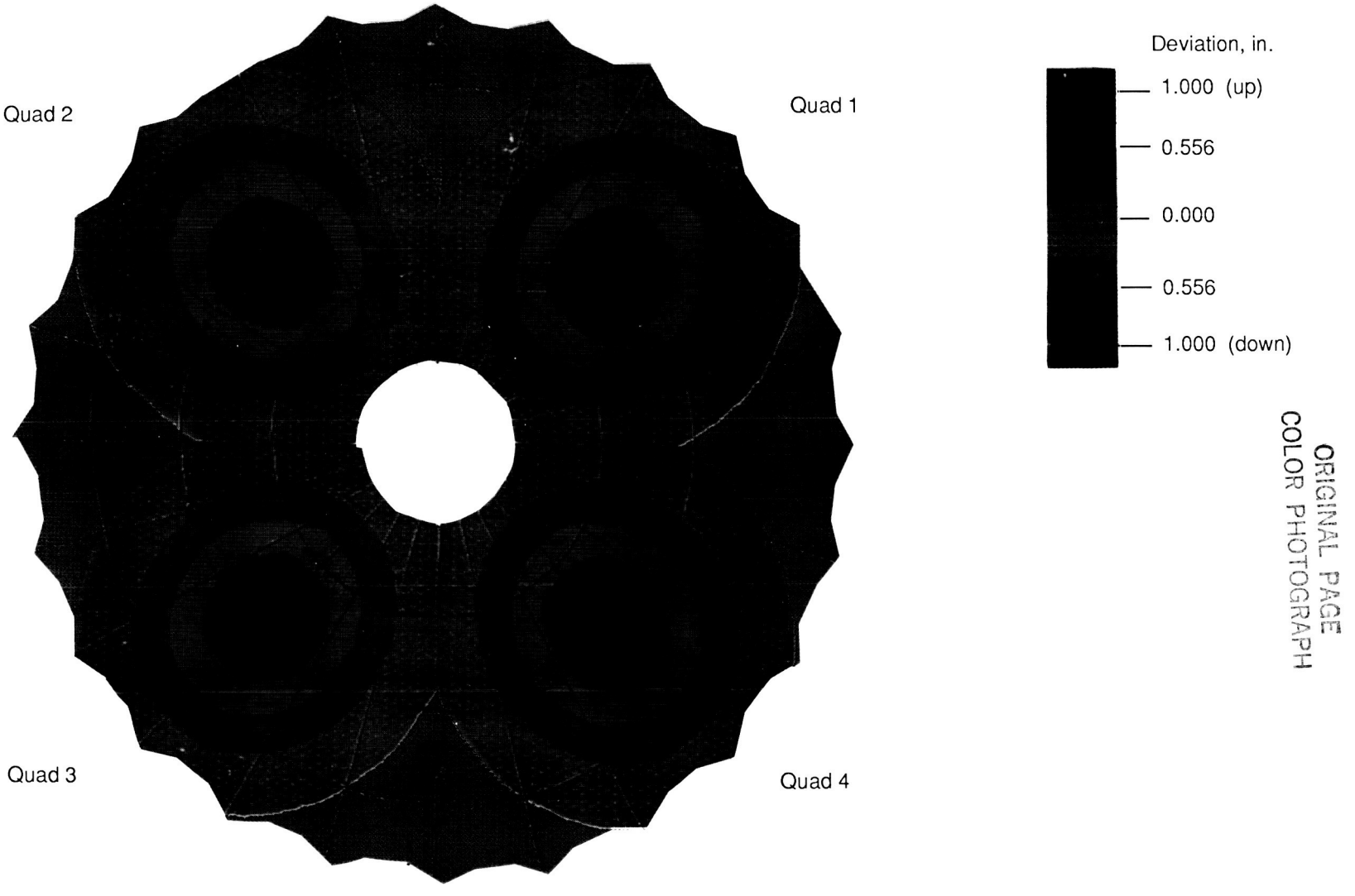

Figure 50. Feed illumination weighting pattern.

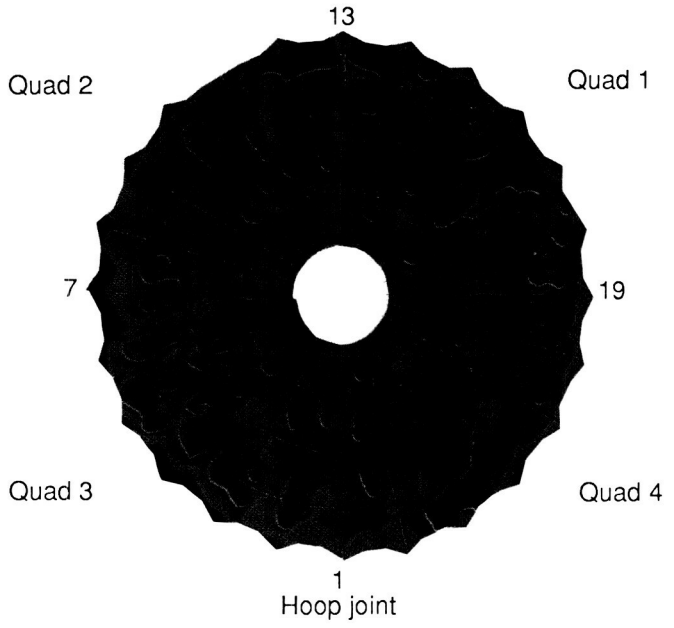

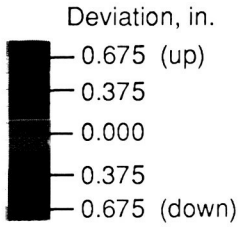

Quadrant	rms error, in.	
	Ref: BFP	Ref: design
1	0.072	0.075
2	.077	.087
3	.095	.101
4	.058	.059

(a) Predicted, weighted error for 33 cables.

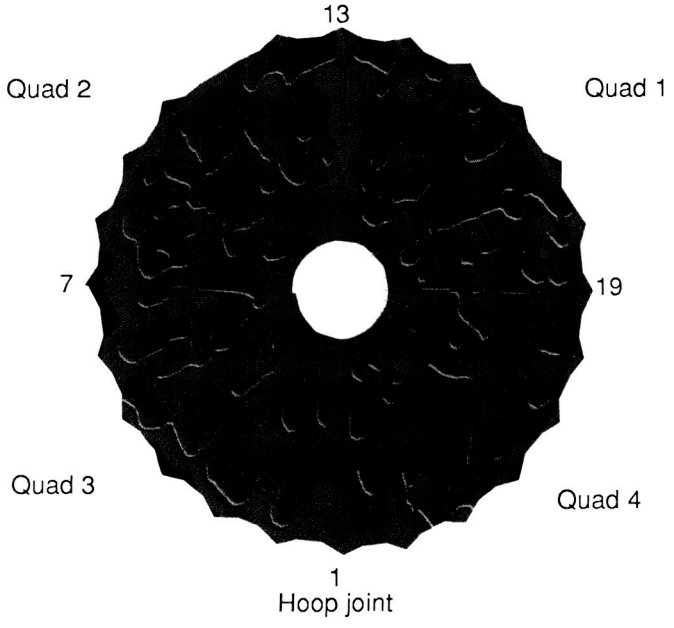

Quadrant	rms error, in.	
	Ref: BFP	Ref: design
1	0.074	0.083
2	.080	.094
3	.093	.106
4	.056	.060

(b) Measured, weighted error for 33 cables, July 30, 1985.

Figure 51. Surface error after third control cable adjustment.

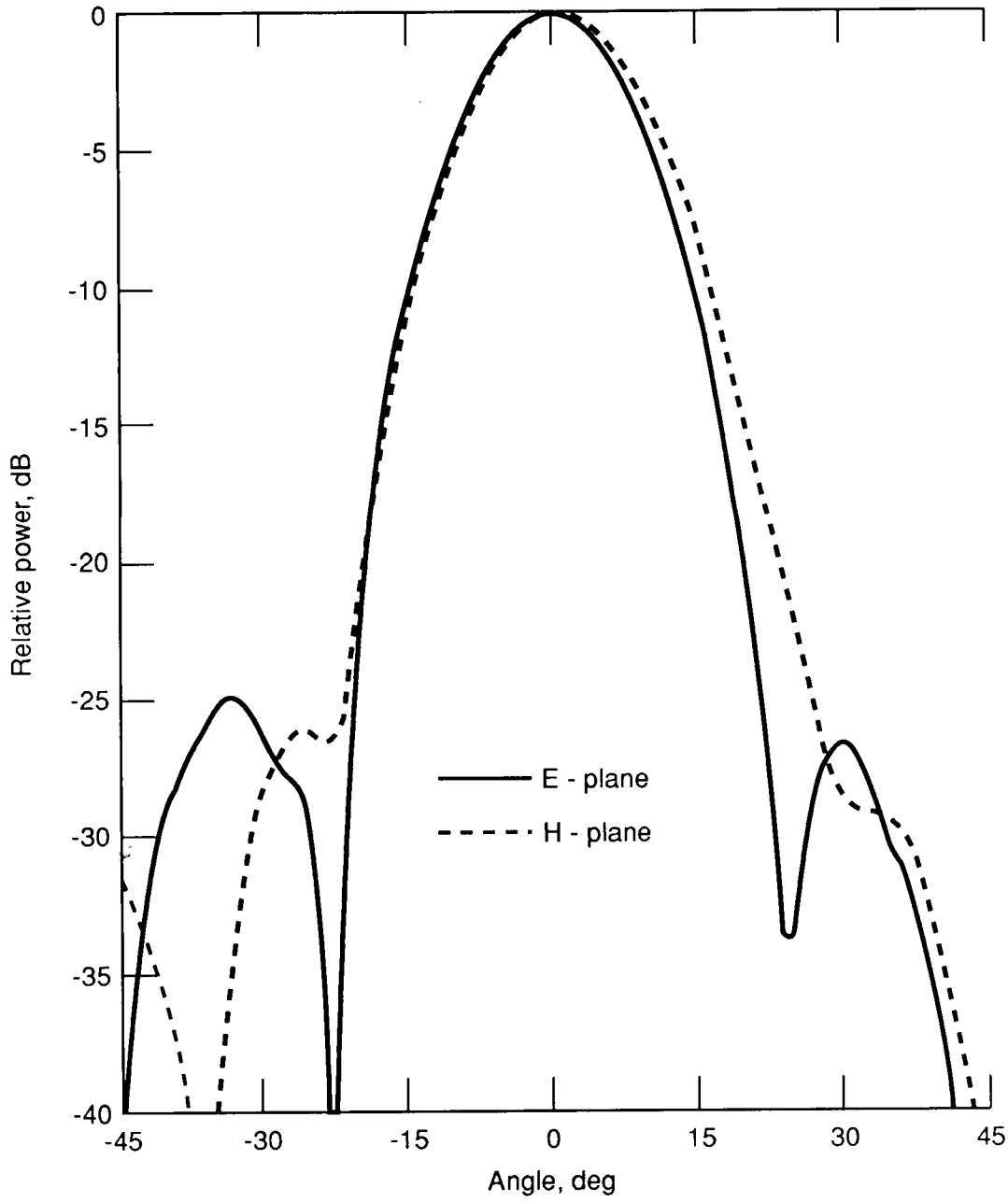

Figure 52. Measured radiation patterns of 2.27-GHz feed.

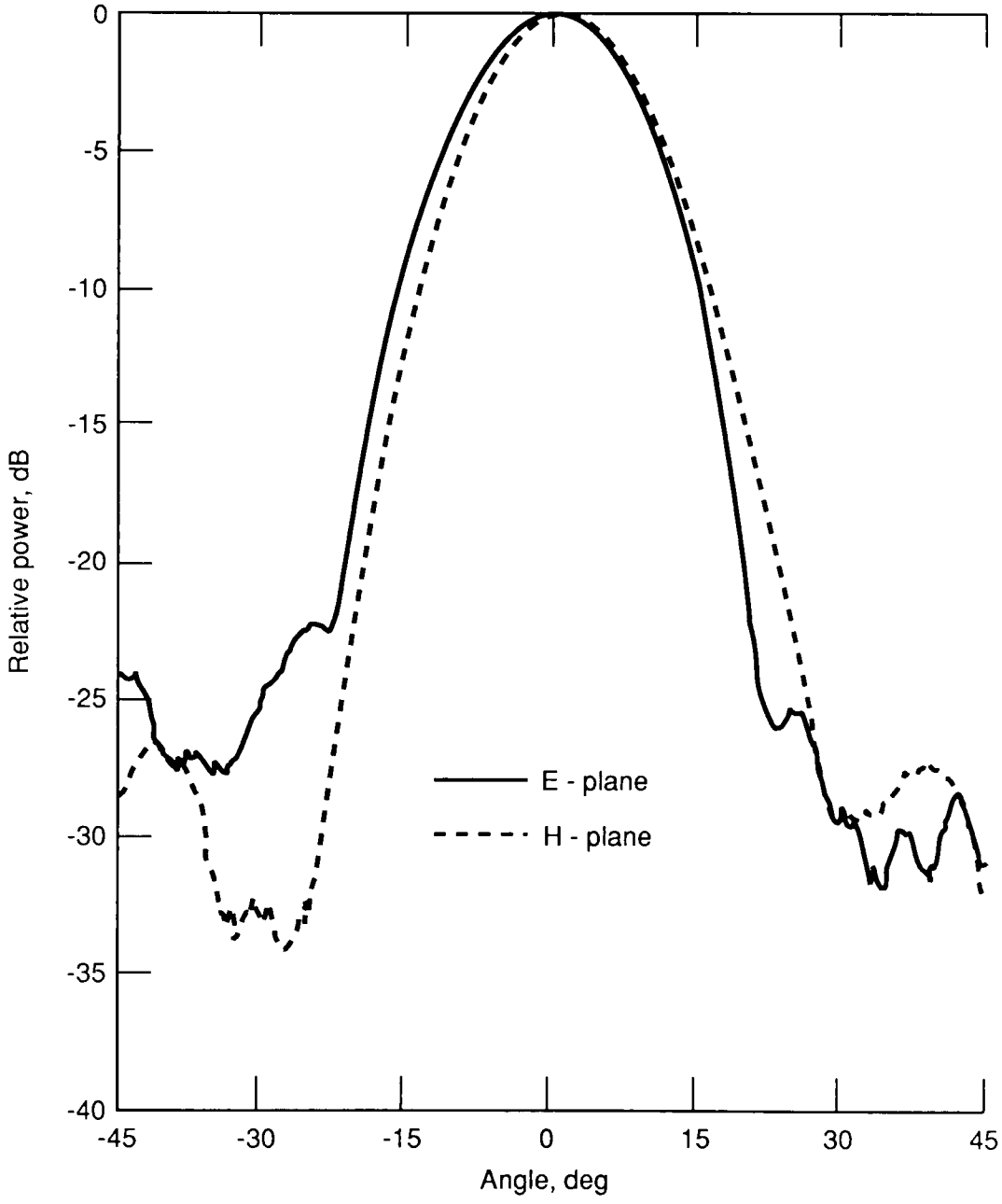

Figure 53. Measured radiation patterns of 4.26-GHz feed.

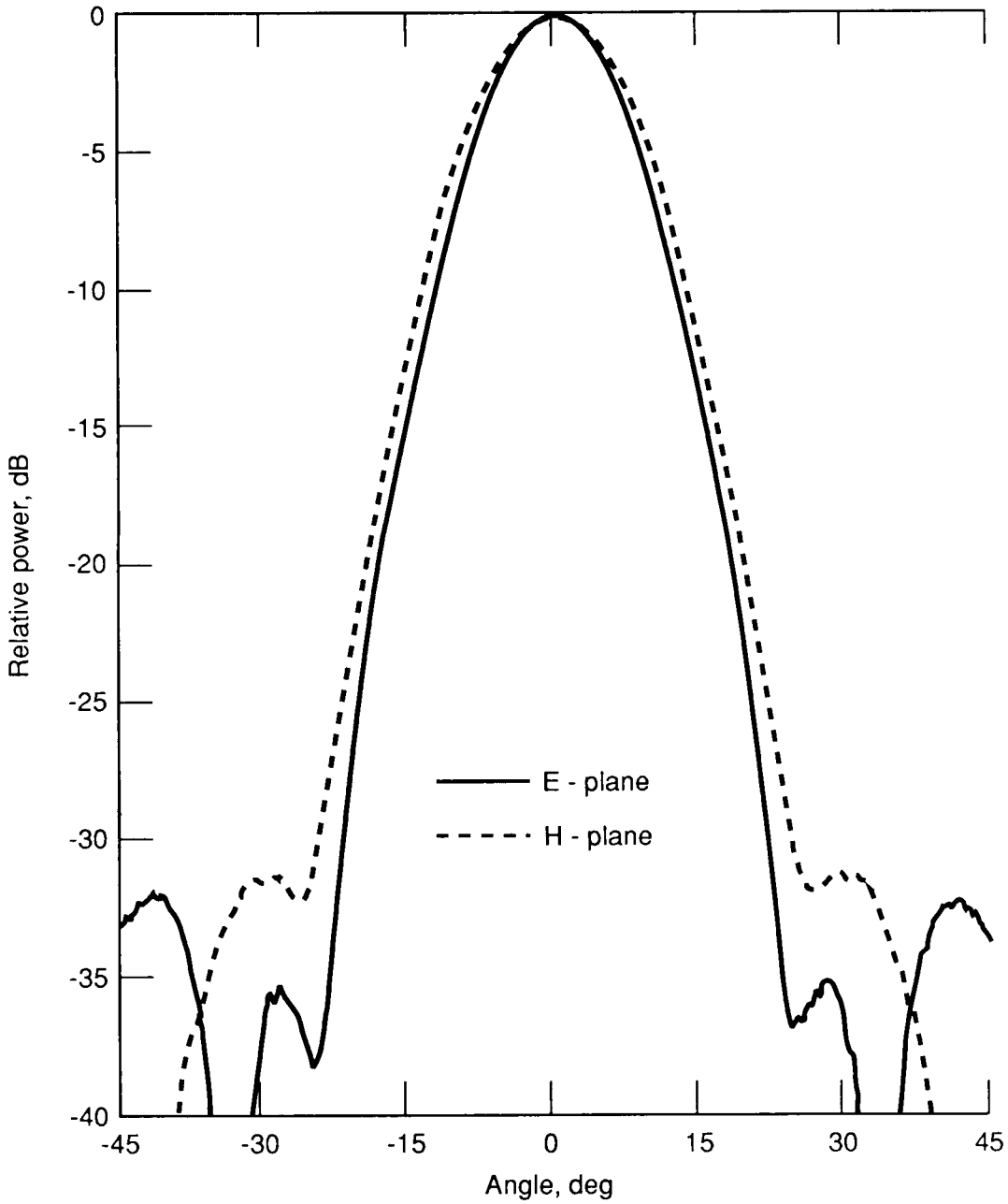

Figure 54. Measured radiation patterns of 7.73-GHz feed.

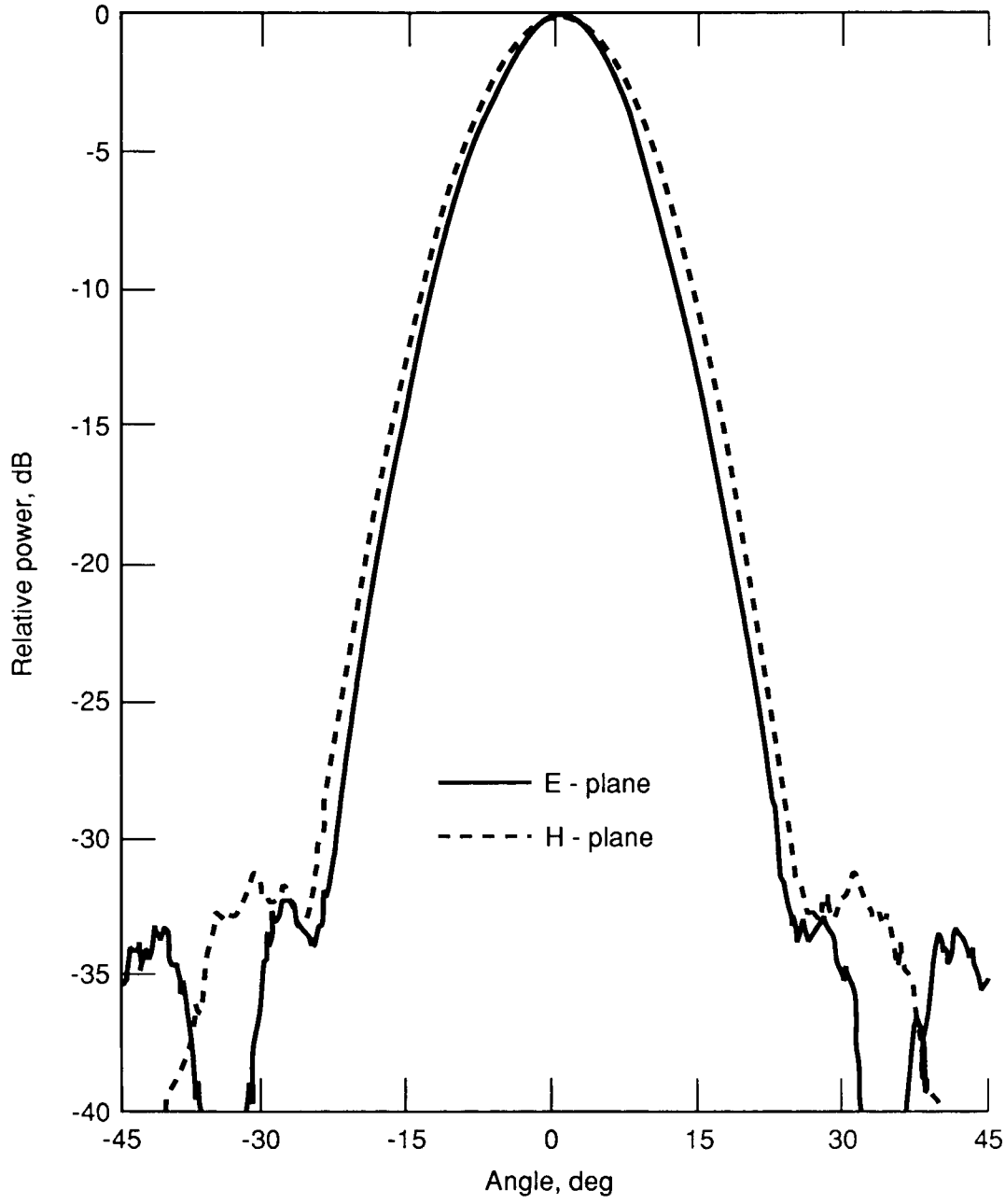

Figure 55. Measured radiation patterns of 11.6-GHz feed.

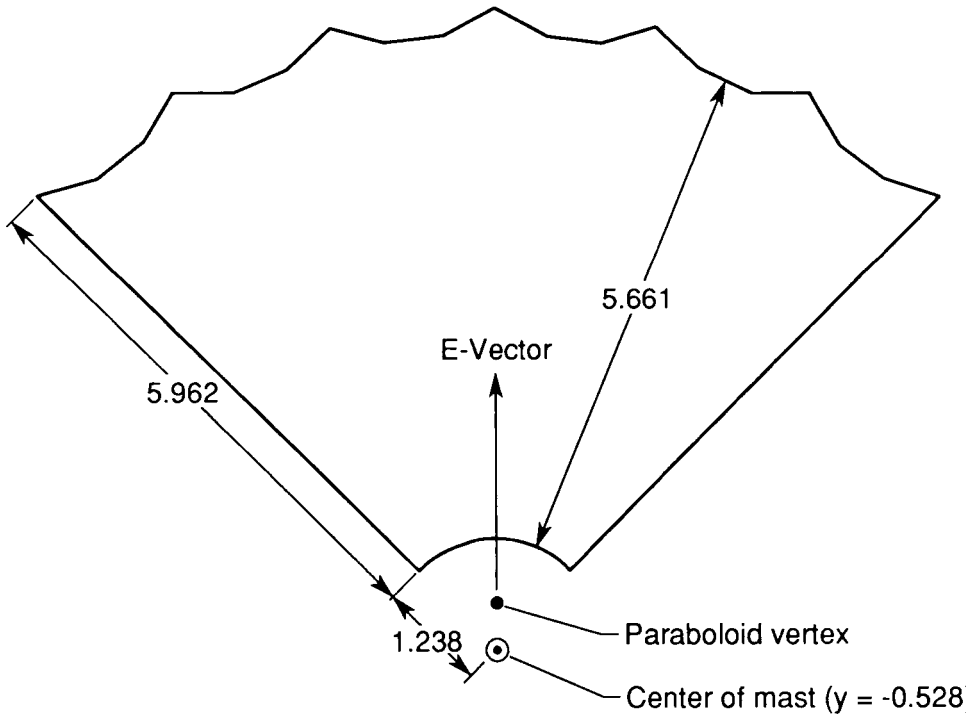

Figure 56. Geometry of aperture for one quadrant of hoop-column antenna. View is looking down on antenna; focal length, 9.318 m; dimensions are in meters.

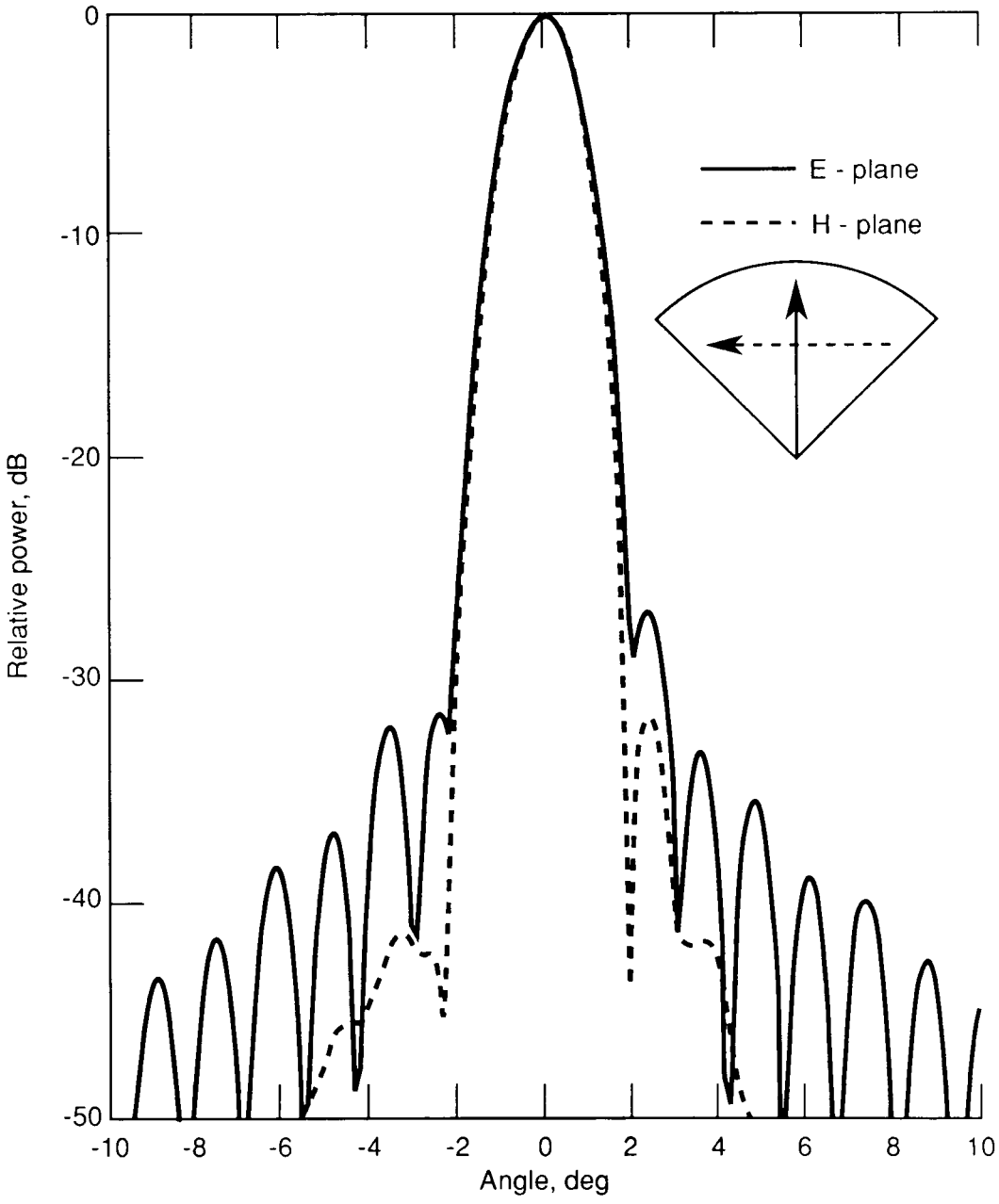

Figure 57. Calculated radiation patterns for one quadrant of hoop-column antenna with smooth surface at 2.27 GHz.

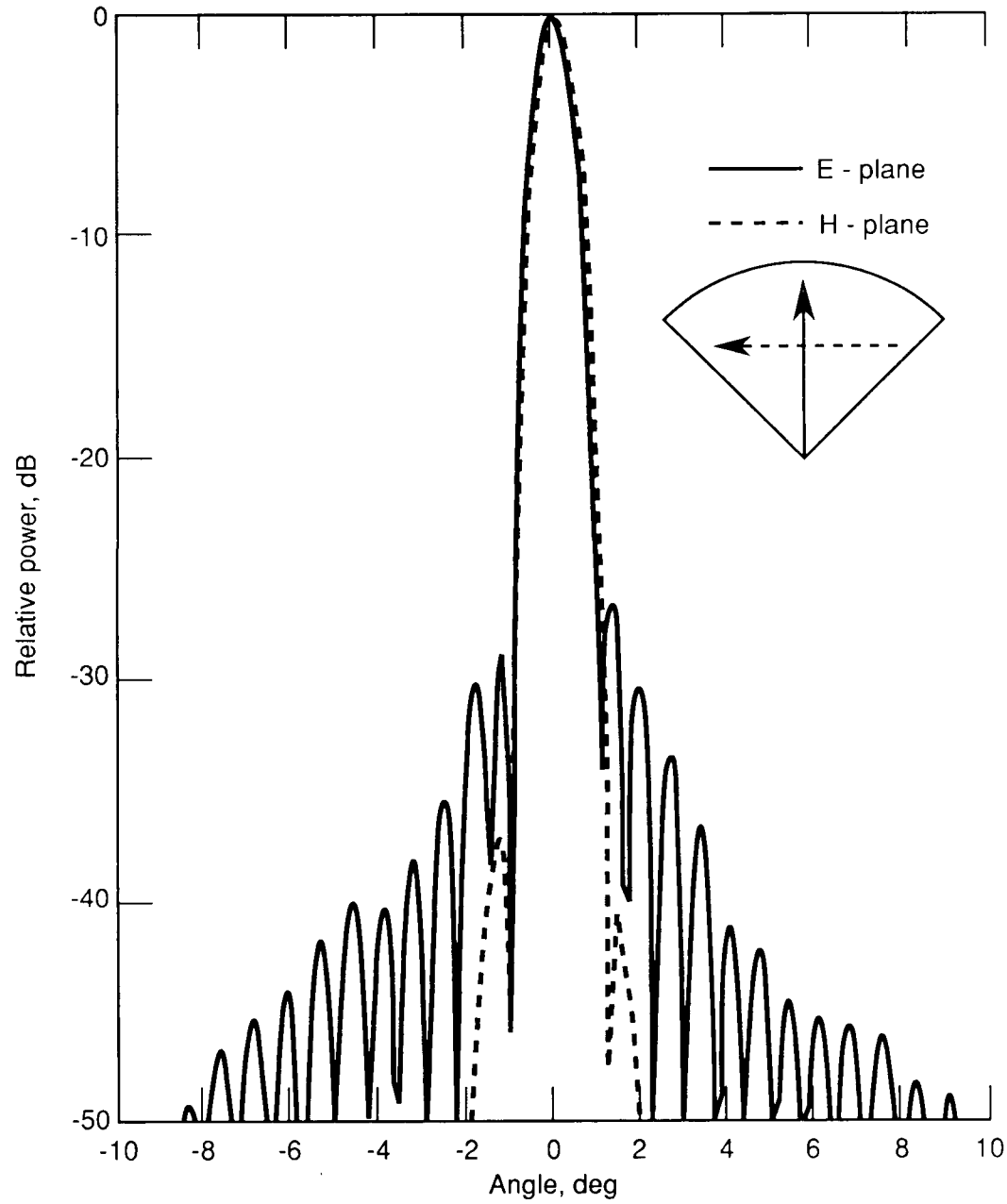

Figure 58. Calculated radiation patterns for one quadrant of hoop-column antenna with smooth surface at 4.26 GHz.

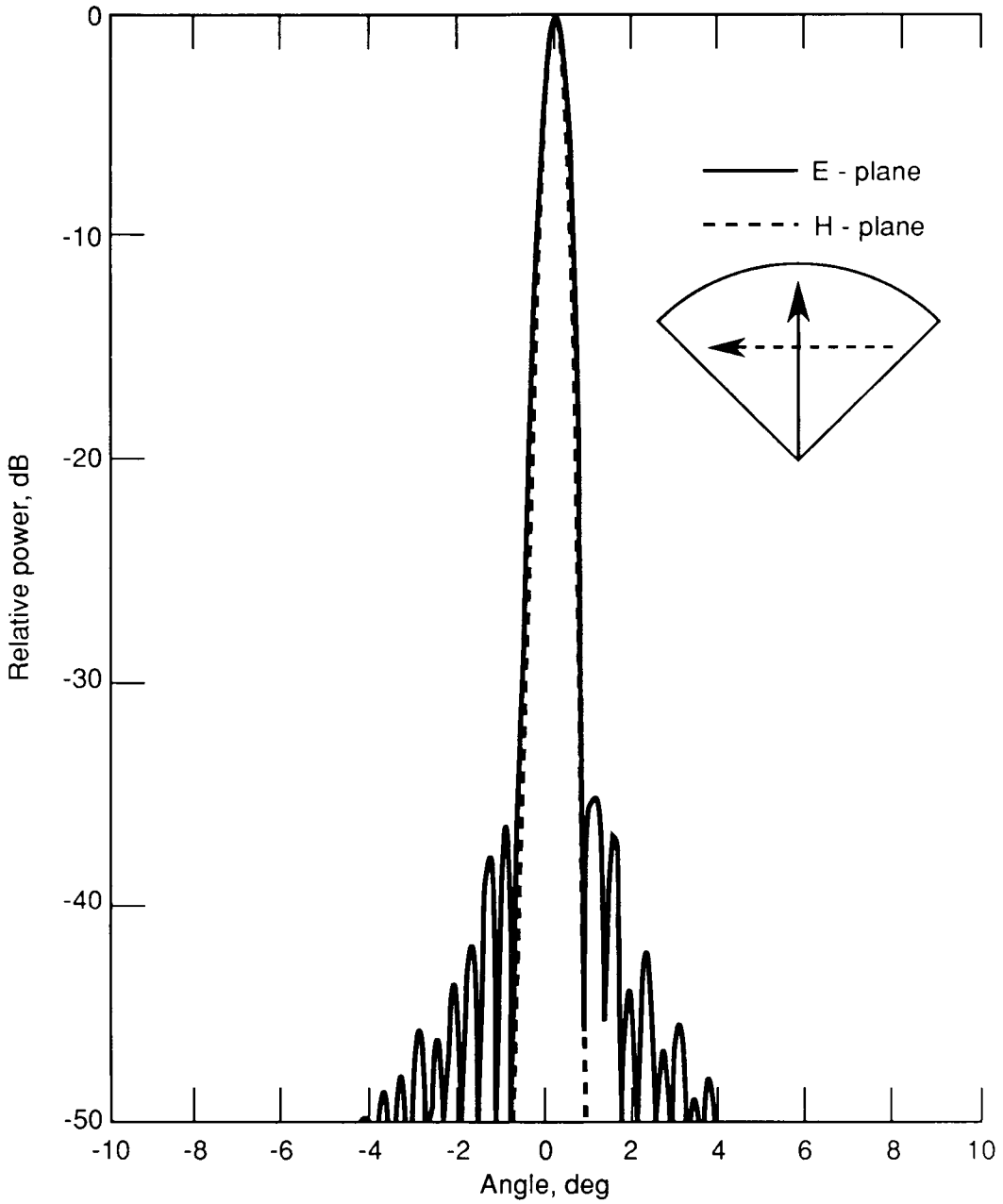

Figure 59. Calculated radiation patterns for one quadrant of hoop-column antenna with smooth surface at 7.73 GHz.

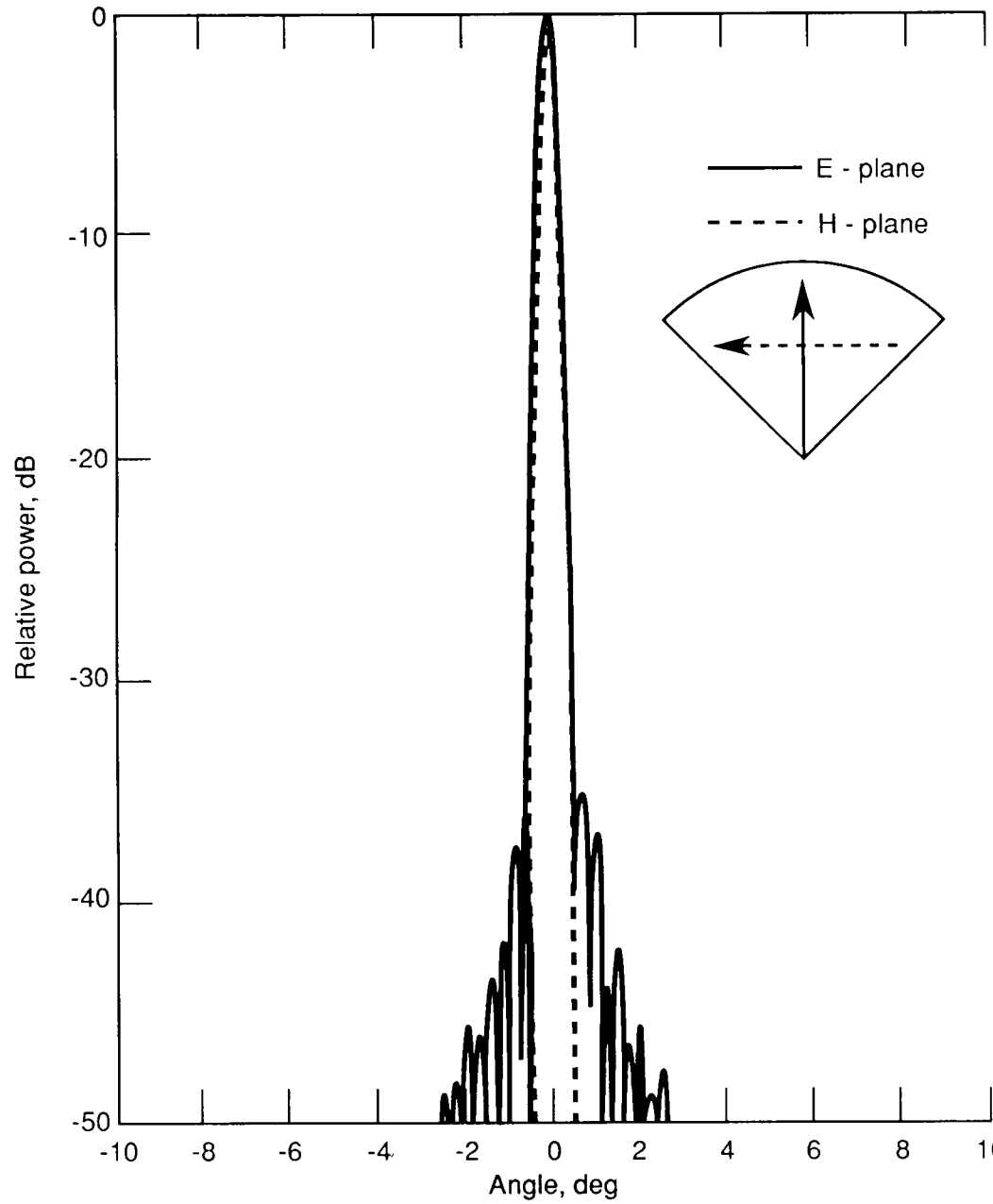

Figure 60. Calculated radiation patterns for one quadrant of hoop-column antenna with smooth surface at 11.6 GHz.

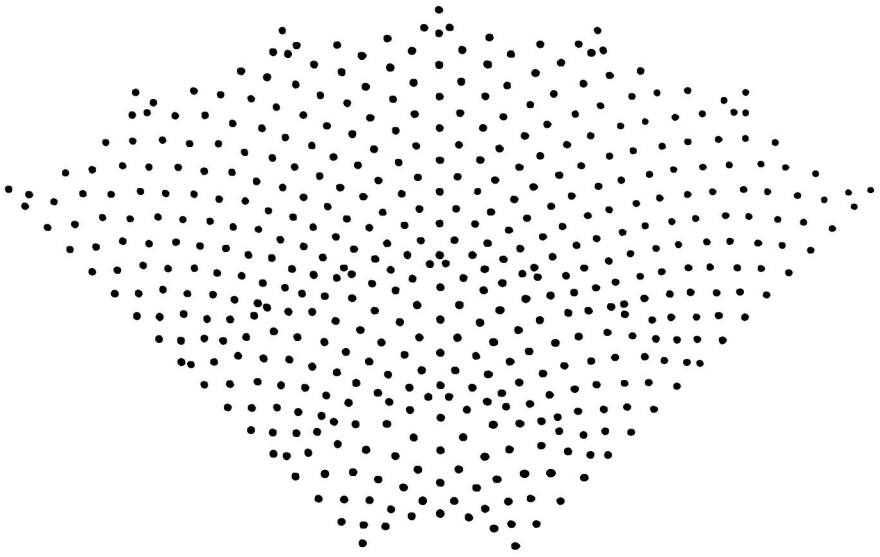

Figure 61. Surface target locations for one quadrant of hoop-column antenna. Tie Points I and Pillows I.

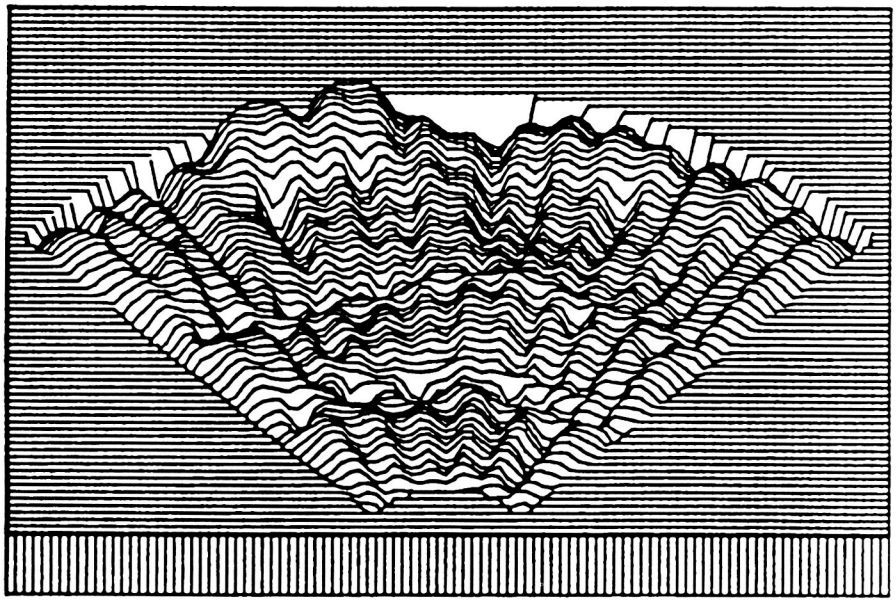

Figure 62. Fifth-order polynomial fit to residuals of best-fit paraboloidal surface defined by measured coordinates of surface targets for quadrant 4 of hoop-column antenna.

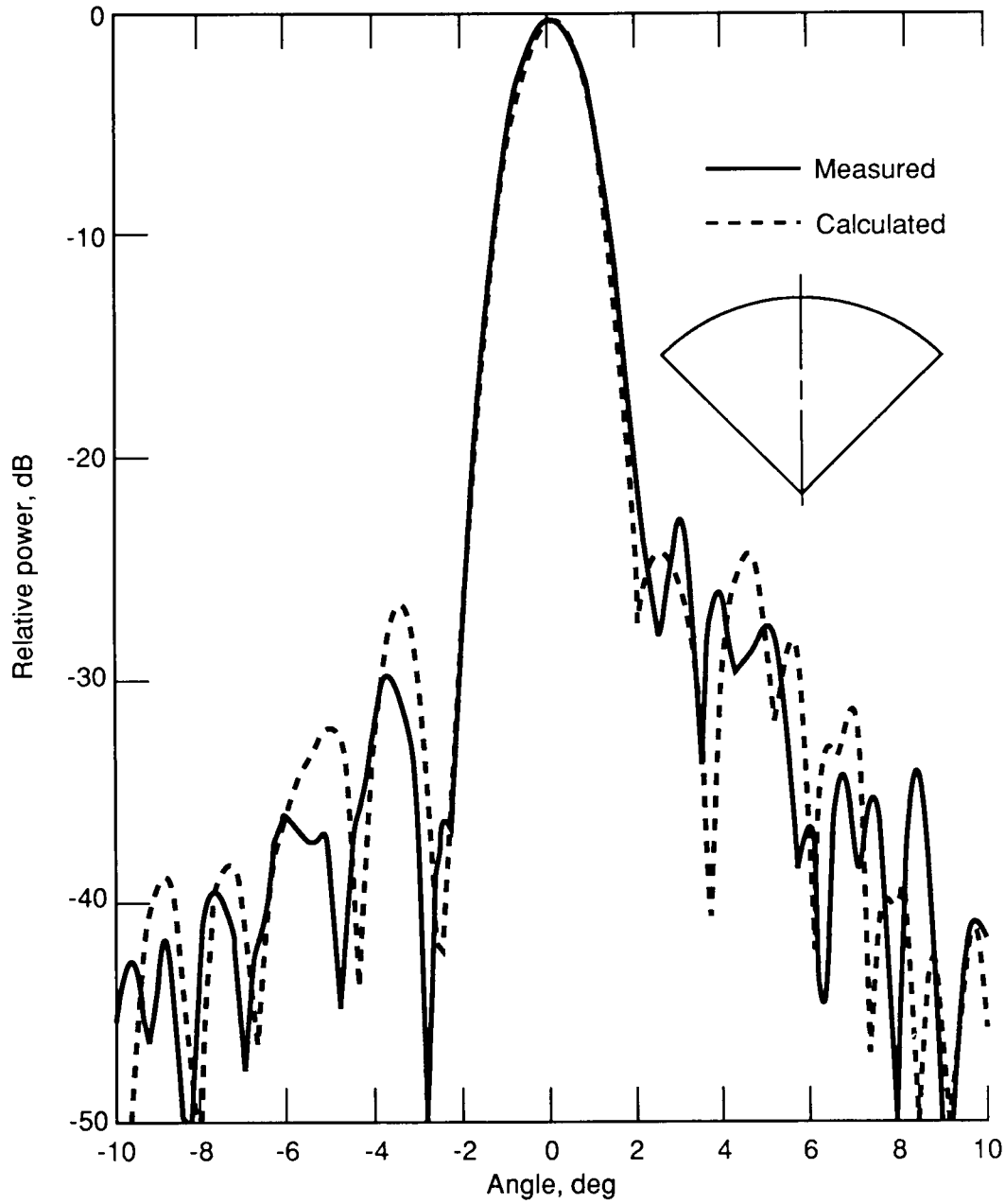

(a) E-plane.

Figure 63. Radiation pattern for quadrant 4 of hoop-column antenna with 2.27-GHz feed.

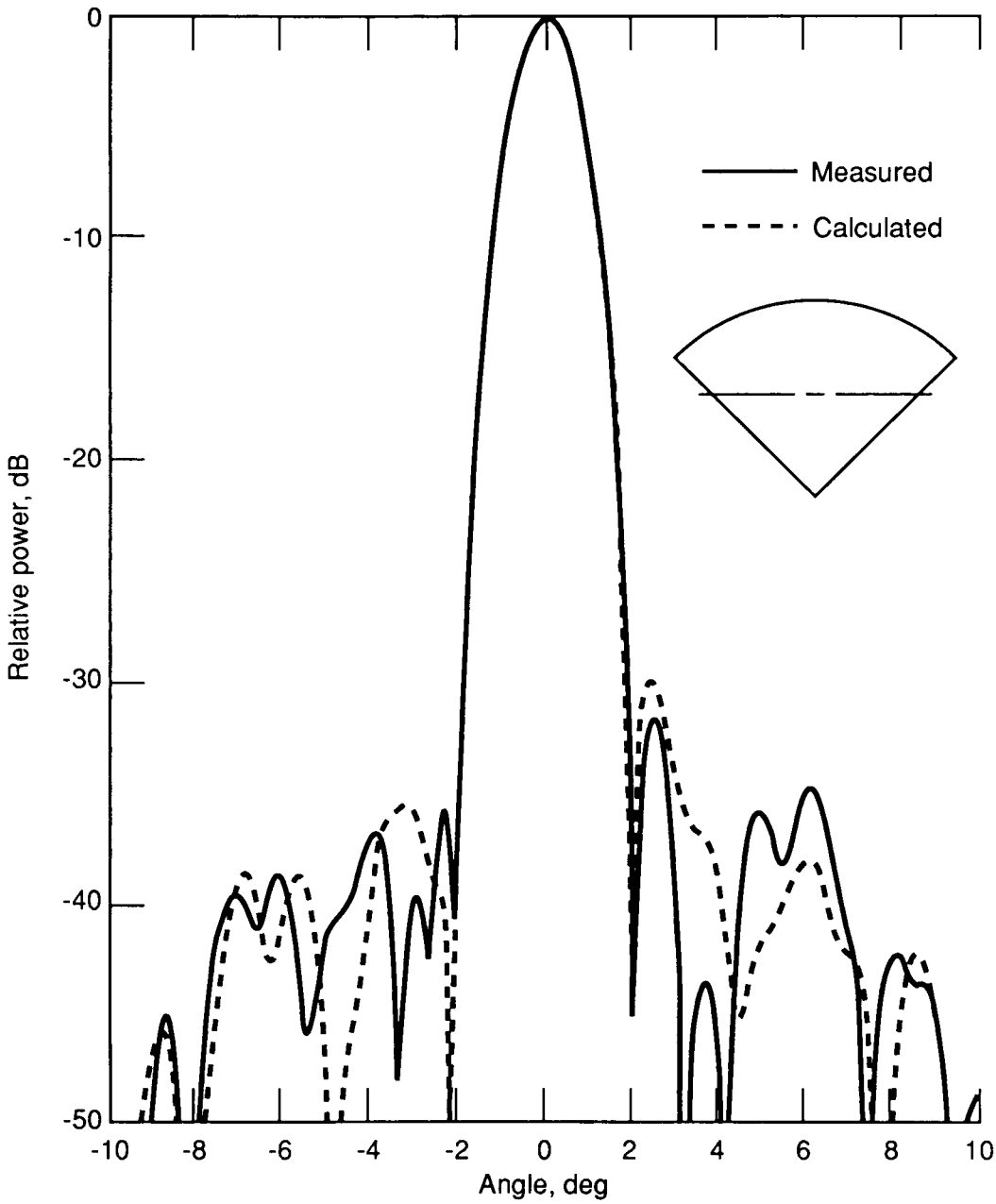

(b) H-plane.

Figure 63. Concluded.

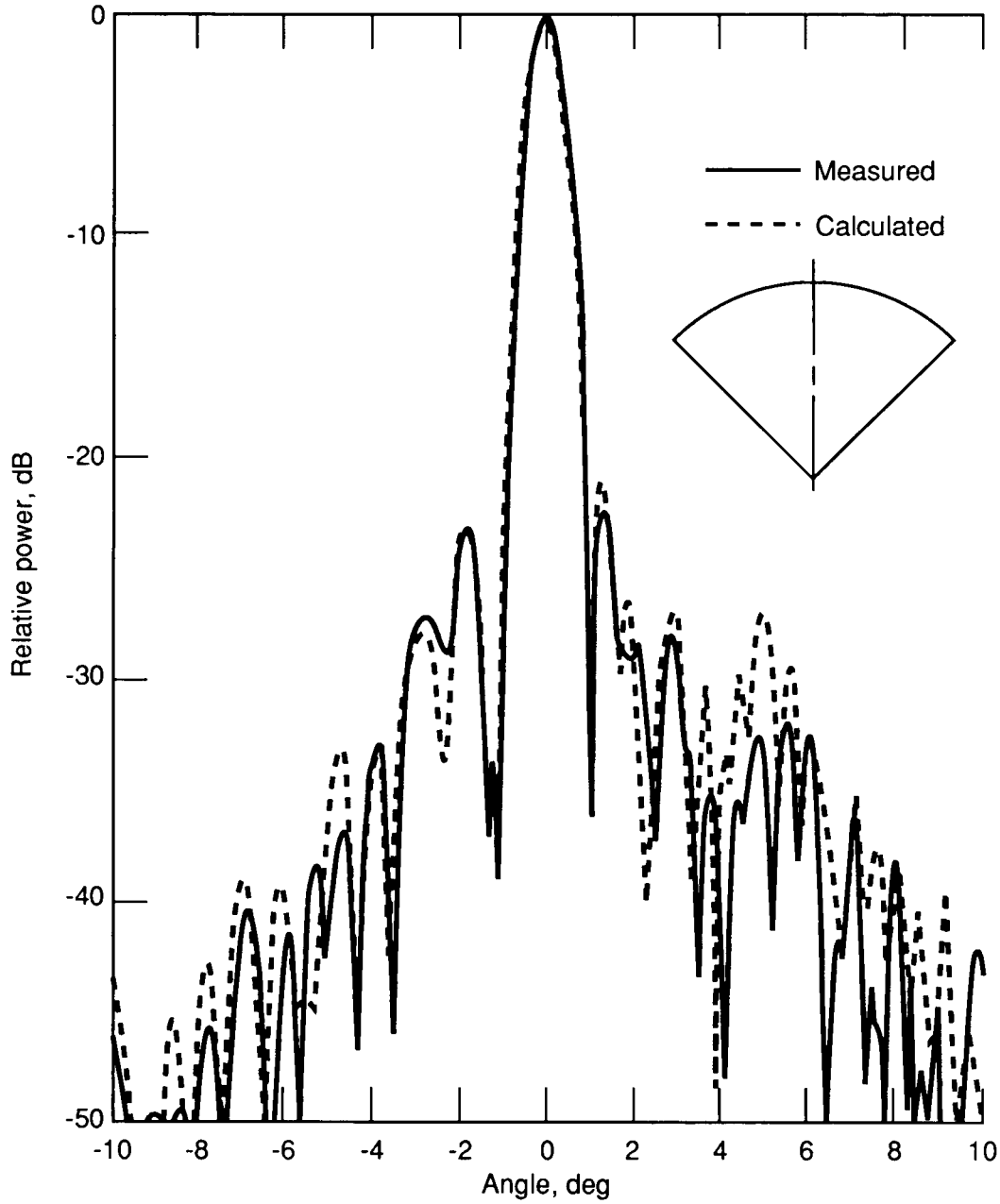

(a) E-plane.

Figure 64. Radiation pattern for quadrant 4 of hoop-column antenna with 4.26-GHz feed.

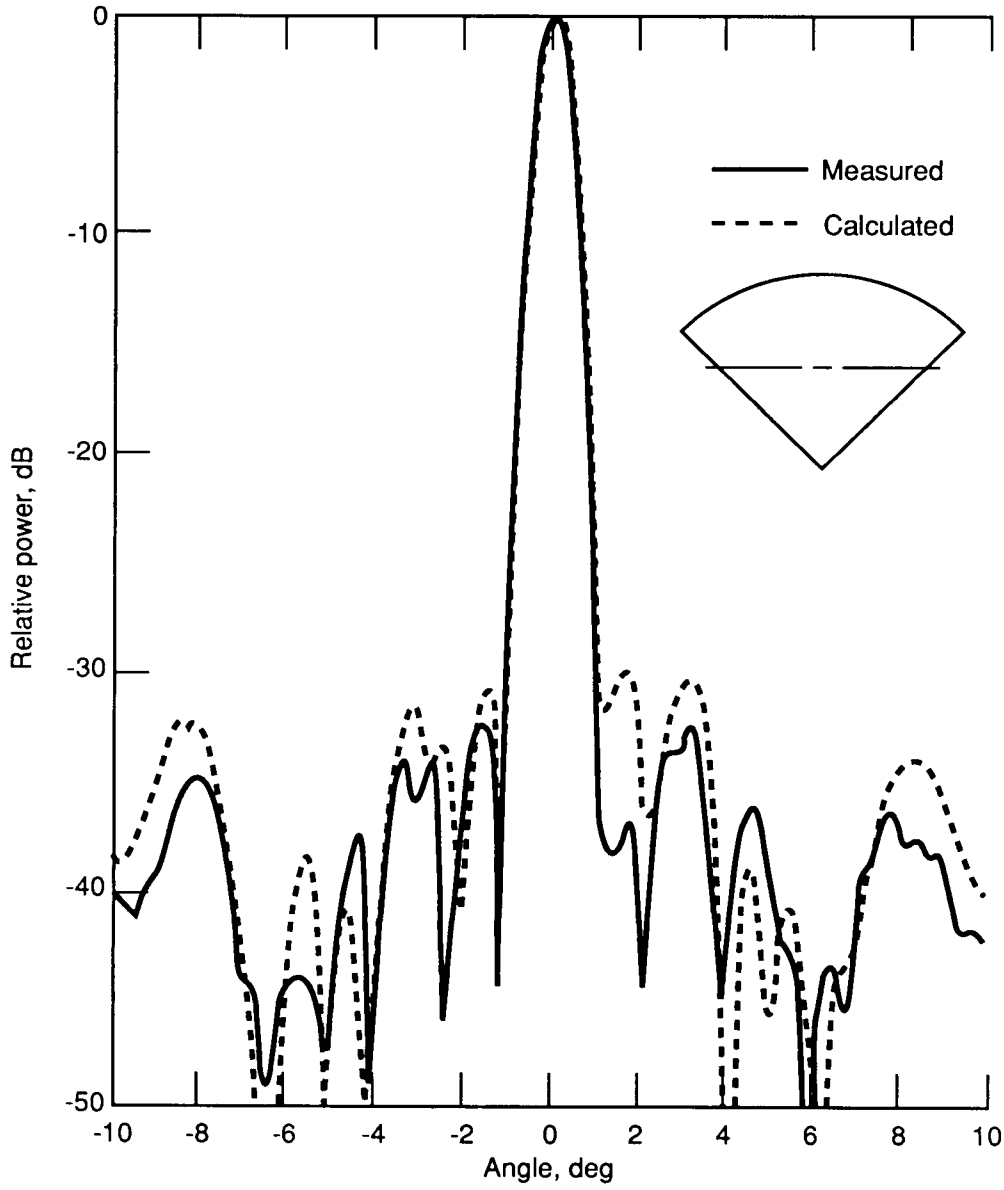

(b) H-plane.

Figure 64. Concluded.

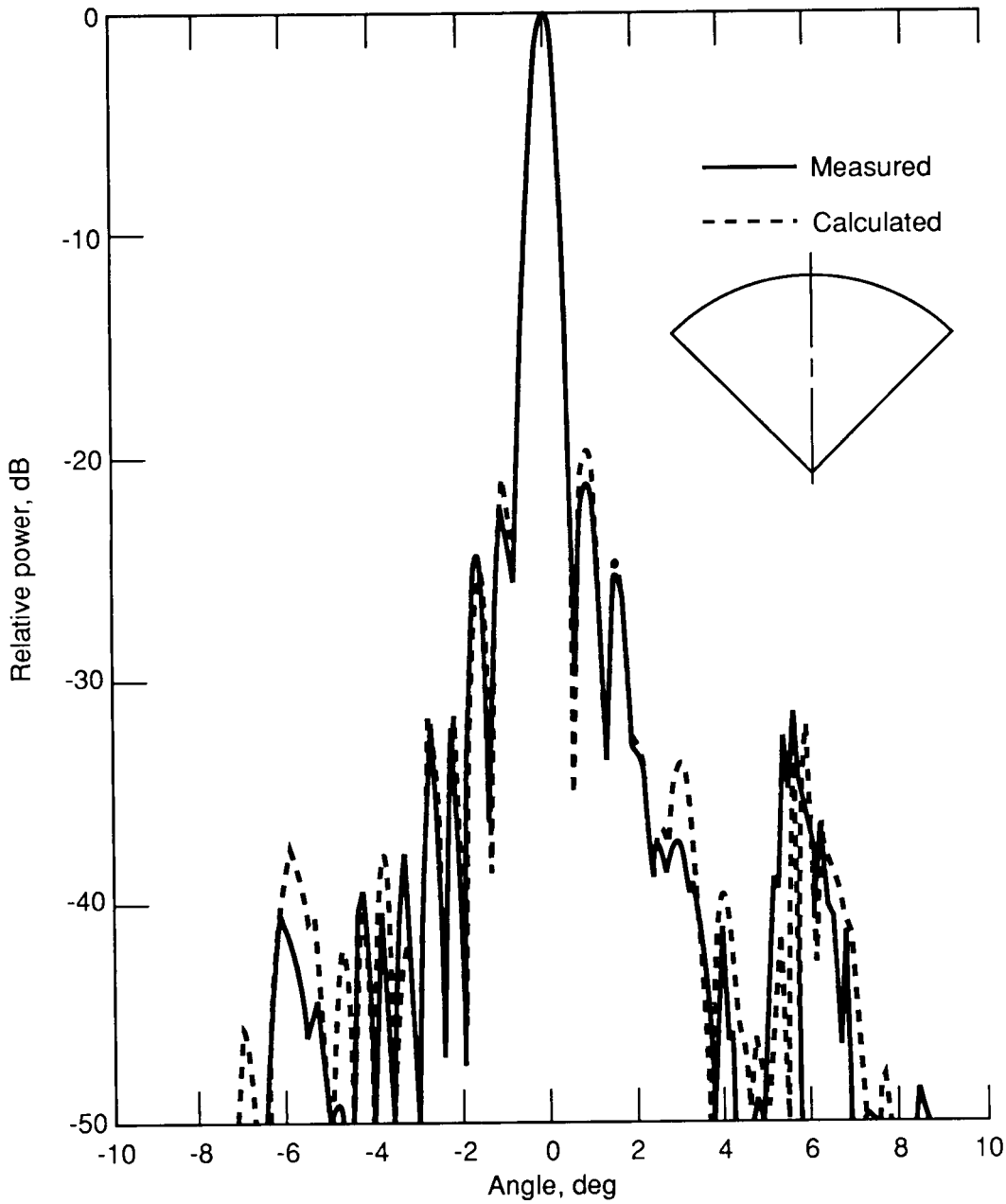

(a) E-plane.

Figure 65. Radiation pattern for quadrant 4 of hoop-column antenna with 7.73-GHz feed.

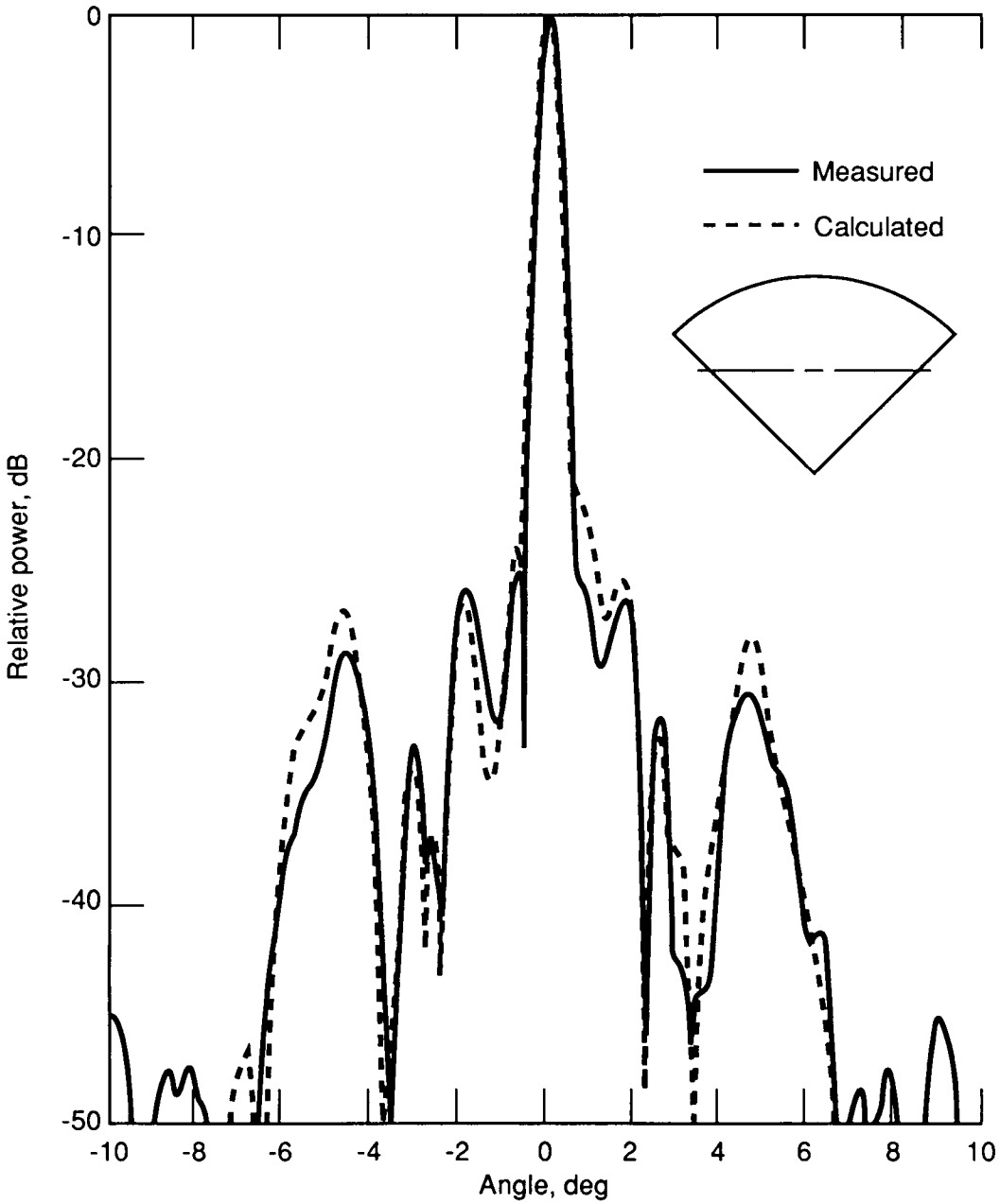

(b) H-plane.

Figure 65. Concluded.

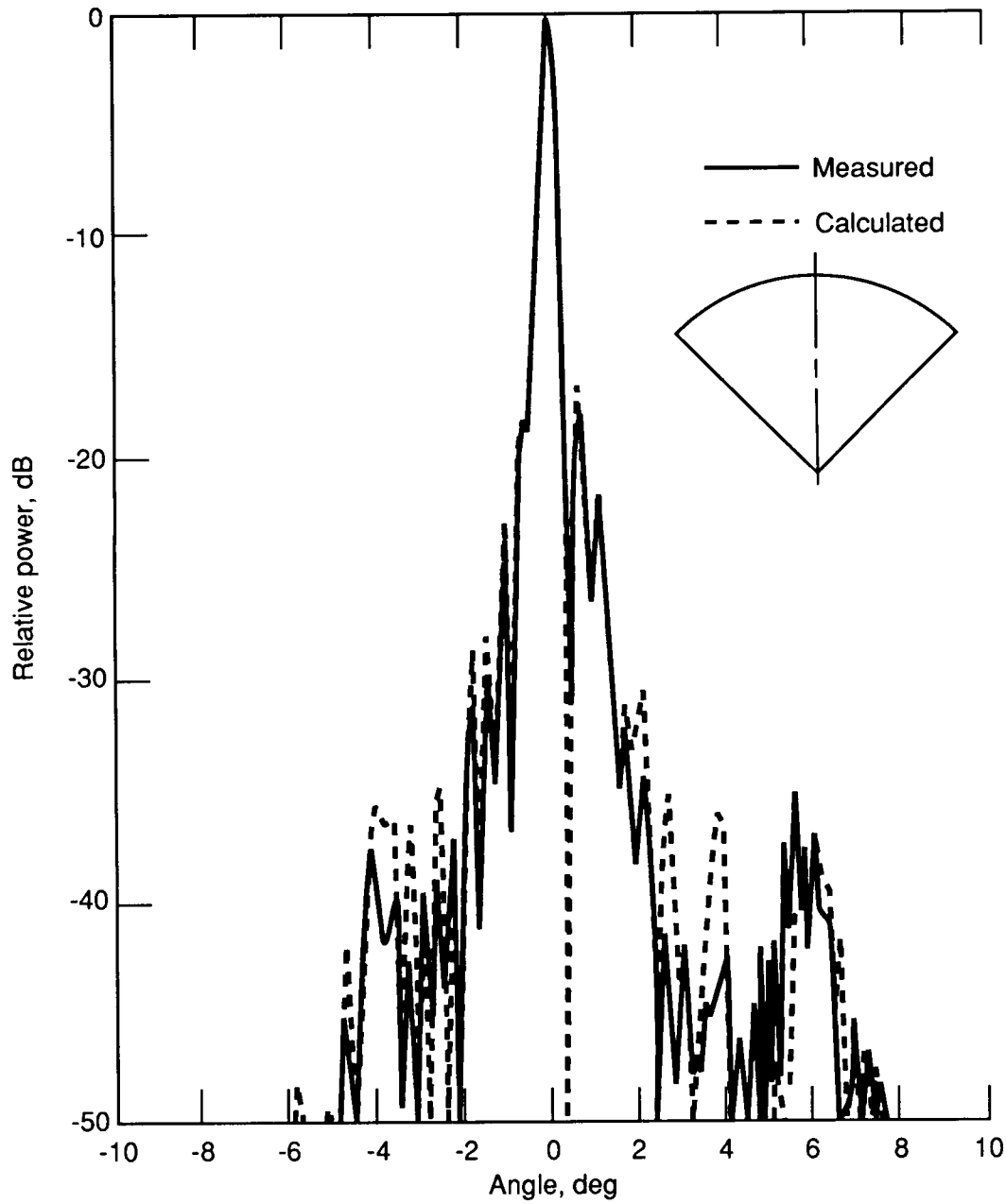

(a) E-plane.

Figure 66. Radiation pattern for quadrant 4 of hoop-column antenna with 11.6-GHz feed.

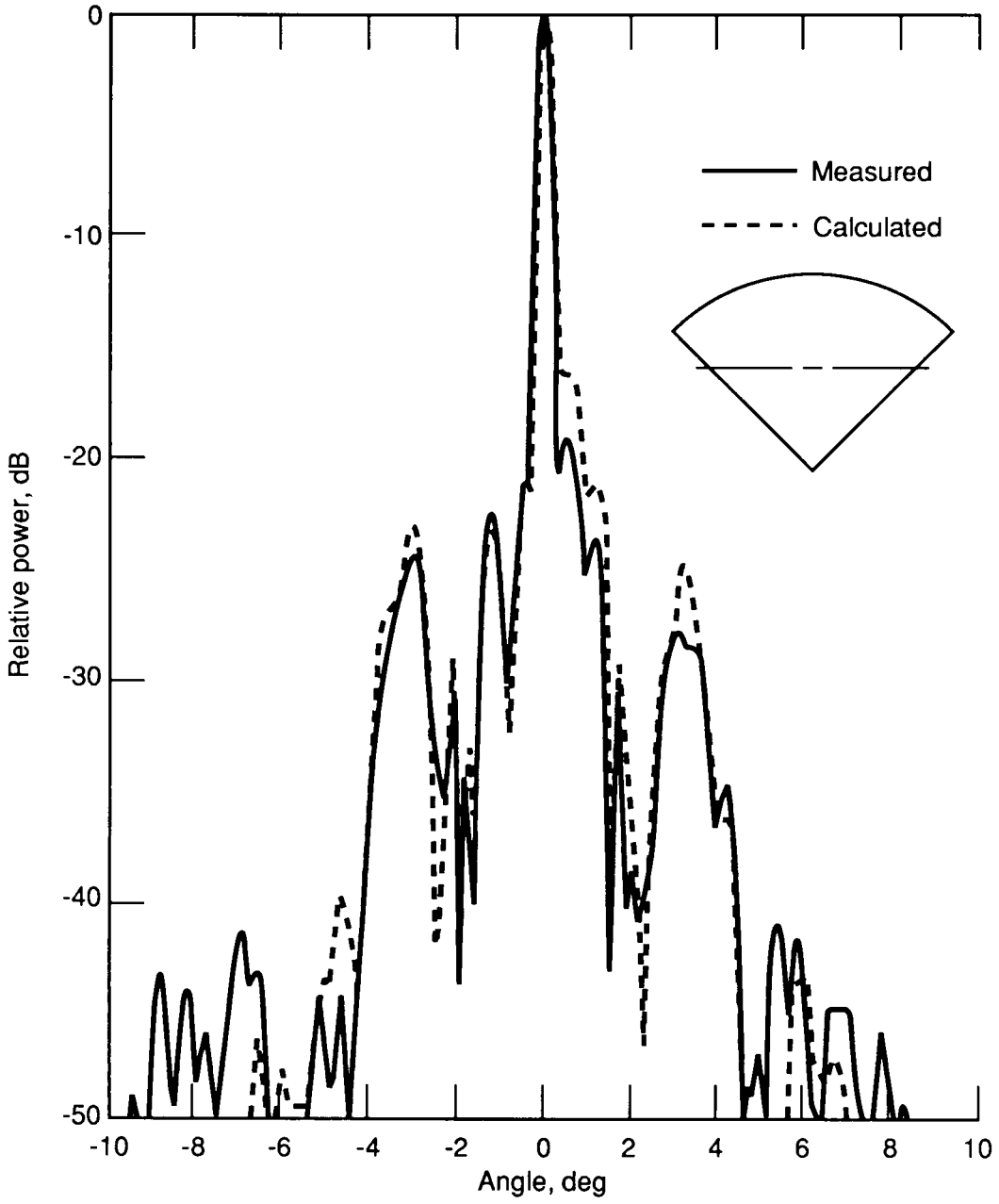

(b) H-plane.

Figure 66. Concluded.

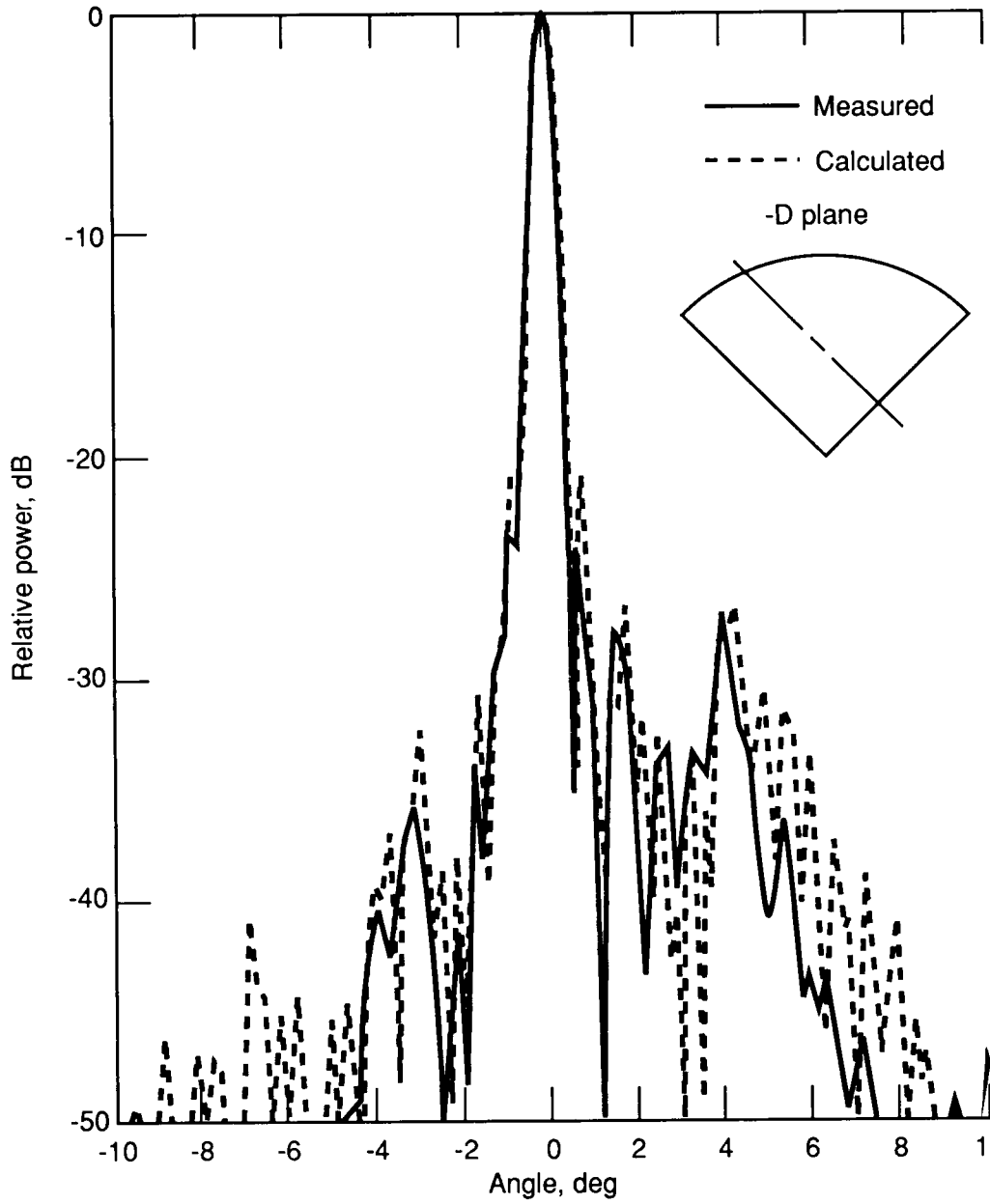

Figure 67. Radiation pattern at −45° for quadrant 4 of hoop-column antenna with 7.73-GHz feed.

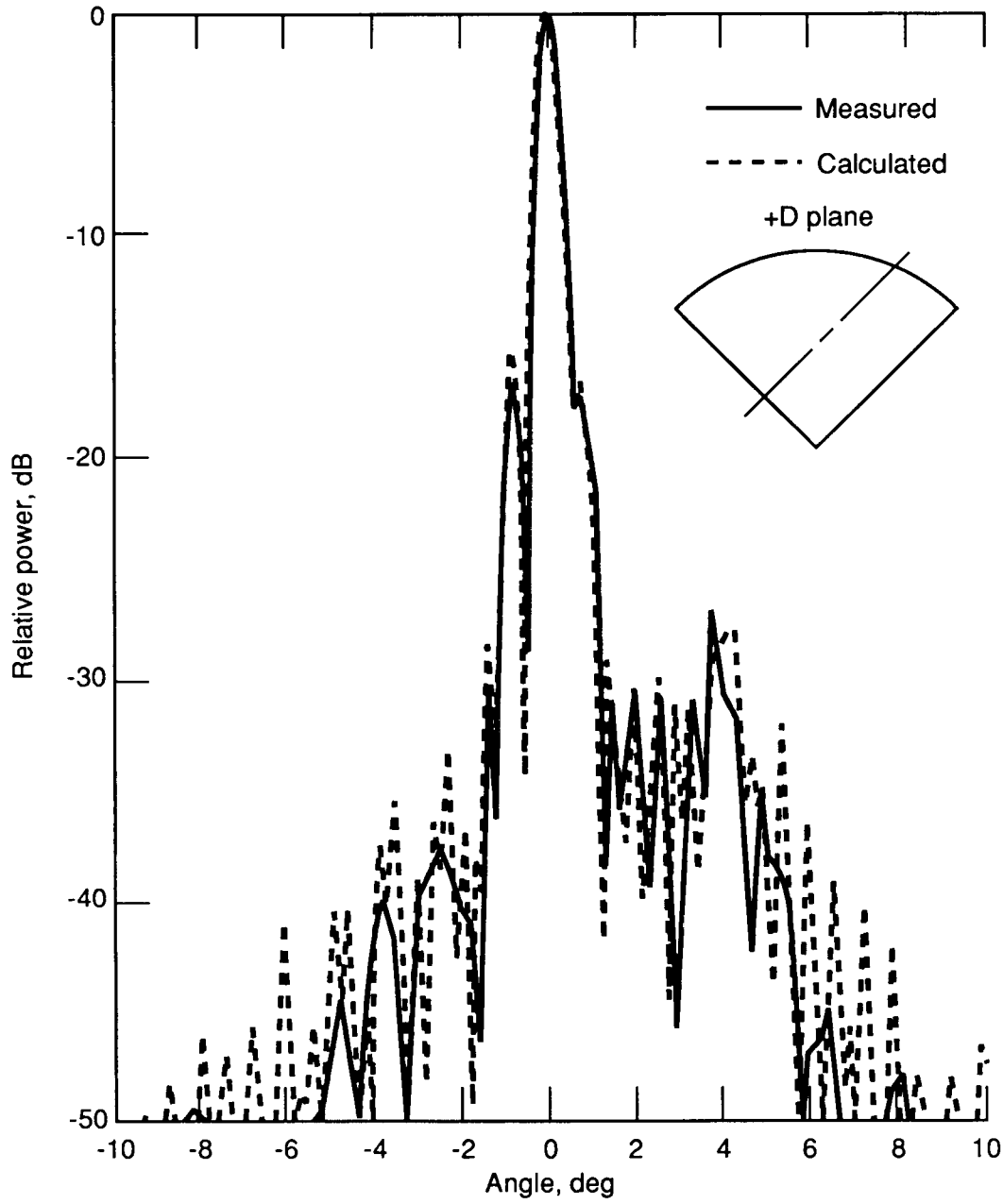

Figure 68. Radiation pattern at +45° for quadrant 4 of hoop-column antenna with 7.73-GHz feed.

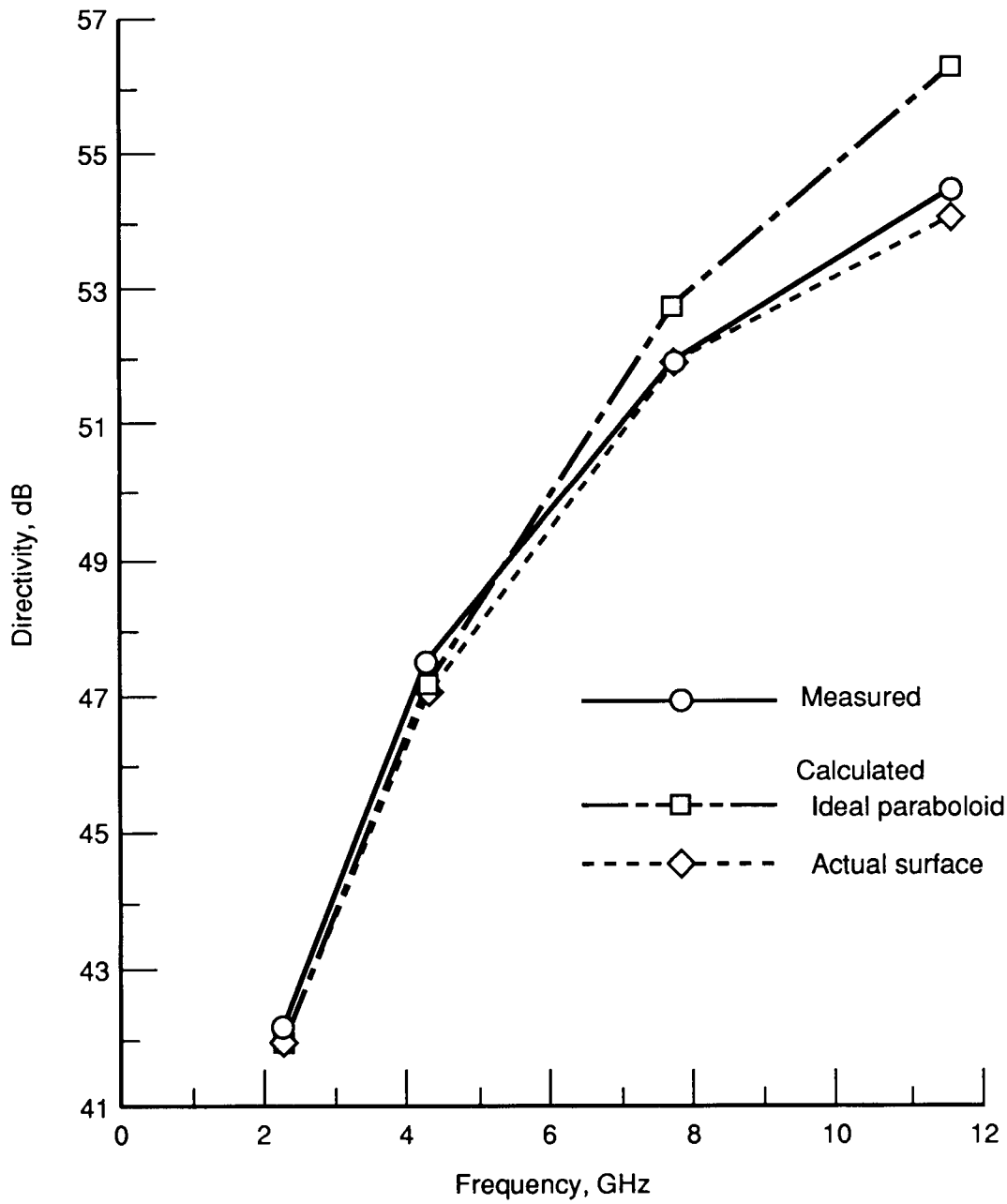

Figure 69. Directivity for hoop-column antenna measurements.

NASA
National Aeronautics and Space Administration

Report Documentation Page

1. Report No.	2. Government Accession No.	3. Recipient's Catalog No.
NASA TM-4073		

4. Title and Subtitle	5. Report Date
Near-Field Testing of the 15-Meter Hoop-Column Antenna	August 1989
	6. Performing Organization Code

7. Author(s)	8. Performing Organization Report No.
Lyle C. Schroeder, Richard R. Adams, M. C. Bailey, W. Keith Belvin, David H. Butler, and Thomas G. Campbell	L-16410

9. Performing Organization Name and Address	10. Work Unit No.
NASA Langley Research Center Hampton, VA 23665-5225	506-44-21-03
	11. Contract or Grant No.

12. Sponsoring Agency Name and Address	13. Type of Report and Period Covered
National Aeronautics and Space Administration Washington, DC 20546-0001	Technical Memorandum
	14. Sponsoring Agency Code

15. Supplementary Notes

16. Abstract

A 15-m-diameter antenna was tested at the Martin Marietta Near-Field Test Laboratory, May–August 1985, to verify that dimensional tolerances for acceptable performance could be achieved and to verify structural, electromagnetic, and mechanical performance predictions. This antenna utilized the hoop-column structure, a gold-plated molybdenum mesh reflector, and 96 control cables to adjust the reflector conformance with a paraboloid. The dimensional conformance of the antenna structure and surface was measured with metric camera and theodolites. Near-field pattern data were used to assess the electromagnetic performance at five frequencies from 2.225 to 11.6 GHz. The reflector surface was adjusted to greatly improve electromagnetic performance with a finite element model and the surface measurements. Measurement results show that antenna surface figure and adjustments and electromagnetic patterns agree well with predictions.

17. Key Words (Suggested by Authors(s))	18. Distribution Statement
Large space deployable antenna Mesh reflector offset feeds Metric photogrammetry Near-field measurements Surface adjustment	Unclassified—Unlimited Subject Category 15

19. Security Classif. (of this report)	20. Security Classif. (of this page)	21. No. of Pages	22. Price
Unclassified	Unclassified	129	A07

NASA FORM 1626 OCT 86

NASA-Langley, 1989

For sale by the National Technical Information Service, Springfield, Virginia 22161-2171